DOTTORATO DI RICERCA IN SCIENZE DELLA TERRA

Università degli Studi di Firenze

FRANCESCO MUGNAI

INTEGRATION OF REMOTE SENSING SYSTEMS AND WIRELESS SENSOR NETWORKS IN SELF-ADAPTIVE AND MULTI-PARAMETRIC PLATFORM FOR LANDSLIDE MONITORING

settore scientifico disciplinare: GEO-05

Tutor: Dott. Nicola Casagli

Coordinator: Prof. Federico Sani

XXII Ciclo

Firenze, 31 Dicembre 2010

A Pazienza, perchè tutto è possibile con lei.

A Costanza, tanto immobile quanto tenace equilibrista.

A Sara, che più di ogni altro concetto, evento od interesse,
mi riempie il volto, il petto e la coscienza, ed è, e possiede,
l'origine di quelle doti stesse, e della sua bellezza.

Contents

List of Figures

Abstract

The aim of this doctoral thesis is to demonstrate the effectiveness of an integrated use of monitoring systems to control situations characterized by serious environmental problems. Within this work the attention was focused on the processes of slope instability Figure 2.3 on page 19; different environmental contexts were also presented as possible applications. The main essentially intuitive idea of this thesis, is that instrumentation is able to provide quality information if it's run by a monitoring equipment correctly calibrated, depending on the scenario, and the activeness of the phenomenon, and on the specific purposes of intervention. As a complementary activity methods of correction and interpretation of the signal, collected in real time by different types of instrumentation were also tested and deferred. An attempted to develop integration processes of monitoring results, through handling, filtering and integrating of multi-parametric measurements (precipitations, amount of released seismic energy, magnitude of surface deformation and deep slope failure, temperature variations) was also performed. The purpose was not just to estimate the magnitude of the examined phenomenon (in terms of speed, extent, and intensity), but also to refine a description of the process optimized for use in situations of an early warning system. The work of this thesis is rooted in contexts related to the landslide risk management for the Italian National Civil Protection. However, non-emergency contingencies were dealt to extend the application of the monitoring instrumentation and non conventional procedures also to applicative areas of ordinary character. Already in the 50s, early studies on risk perception were highlighted as a perceived danger is much more lively as the danger is known, otherwise the common trend was to think that it was God's fault, and thus it is something uncontrollable.

Monitors -oris, comes from Monera (Latin), which means is: to admonish, to advise, to inform. Monitoring in the strict sense is mostly considered as the activity of the measuring and quantifying changes in physical parameters regarding a particular portion of the environment, through the use of tools having sensorial functions. These functions go from the possibility of measuring temperature through physical contact with an instrument like the mercury thermometer, to the most advanced digital cameras, capable of providing remote sensing areal temperature data. The original meaning of monitoring , especially within geomechanical and geotechnical issues associated with high levels of risk, has begun a spontaneous evolution in recent years. A monitoring system expands from a single measurement apparatus (sensor) to the whole ubiquitous data acquisition system (sensor networks), and remote sensing (laser scanners, radar interferometry), up to became an operative structure for the management of complex control processes and integrated monitoring activities. To select the most appropriate instruments (laser scanners, radar interferometry, wireless sensor networks, accelerometers, tiltmeters, crack gauges, thermometers and piezometers) were taken into account the environmental context of their application, the technical characteristics concerning the quality and the type of measurements, the durability and its ability to communicate remotely.

Chapter 1

Introduction

1.1 Dissertation scope

The aim of this doctoral thesis is to demonstrate the effectiveness of an integrated use of monitoring systems to control situations characterized by serious environmental problems. Monitoring systems based on self-adaptive and multi-parametric platforms have been designed and tested. In particular we tried to define what are currently the most effective tools to be used in emergencies related to slope instability, and to understand if and how different monitoring systems can be integrated. Scripts, tools and other control mechanisms have been developed and used in various applications. The intent is to provide an efficient and versatile monitoring platform to be used as a powerful monitoring tool and as an early warning system useful in emergency issues related to landslide risk.

1.2 Definition of the problem

Although in the environmental field several applications are known about multi-parametric devices (probe for water quality, chemical and physical parameters) in the geotechnical field there are only a few applications. One of the main advantage of multi-parametric monitoring is the correlation of geo-indicators at the same time and site conditions with a significative cost reduction for the drilling activities and control units/transmission systems, especially when piezometric, inclinometric and extensometric measurements are required in the same area. Some experimental systems for monitoring landslides are technically very advanced, but the use of these technologies in early warning circumstances highlights some of their shortcomings. Tools for remote sensing as the Ground Based Interferometric Synthetic Sperture Radar (GBinSAR) is able to describe some environmental parameters with accuracies that were unthinkable until a few years ago; this instrument is able to work in very problematic environments, such as the slope of an active volcano. However these tools are not perfect. The application of some monitoring instruments in various case studies has shown that the systems are not always performing during early warning conditions, as resulting from a variety of applications reported in the chapters of this thesis. For every application I have been fortunate to have participated as an active member in both the design and installation of the instrumentd, as well as in the data interpretation. In this way I was able to figure out what were the possible shortcomings of the individual instruments and tried to suggest a method of integrated use of multiple tools to try to remedy the major drawbacks

Figure 1.1: A Rock avalance of 2 billion cubic meters in the Kokomeren Valley (Kyrgyzstan, August 2007). The term "rock avalanche", first proposed by McConnell and Brock (1) to describe the 1903 Frank Slide in Canada, is a simplification of the complex "rockslide-debris avalanche", proposed by Varnes (2). Large rock avalanches are rare. However, their destructive potential is great and thus, they are not negligible as a natural hazard.

1.3 Importance of the problem

Landslides are complex natural phenomena, of which we know many things, but many things are still unclear. Most probably, a geologist who has good experience on landslides, it understands that it is facing a very unstable or stable slope, only one visit is often more than enough. However, it is unlikely that such a simple description is sufficient to satisfy the authority clients, especially in cases of active slope instability processes, associated with a high degree of risk. In these cases there is often a need to adopt a system of early warning, with the main purpose to protect property and people from a potentially catastrophic event. A long-term prediction, or at least an alarm signal dispatched well in advance can be crucial for this purpose. To reach these results we may use some of the best monitoring tools, and often the most expensive, but since the landslides are complex phenomena in many cases it is necessary to control multiple parameters simultaneously. The acquisition of several parameters with very sophisticated instruments can be an effective solution, however, to give efficiency to the entire monitoring system in the contexts of early warning it is necessary to organize tools and data acquired.

1.4 Structure of the dissertation

This dissertation is divided in three parts. The first one is called “State of the art, tools and methods” anddescriptions of some types of instability processes affecting risk slopes and complex deep gravitational movements are reported. Furthermore are presented the main monitoring systems, instruments and sensors used within the applications described in the part II. For each one of these tools a brief description, some technical characteristics, and the application field are described. Within the Part II “Applications”, the landslide of Torgiovannetto (Italy), the city of Mdina (Malta) and Citadel (Gozo), and the Elba Island (Italy) represent the main sites of interest, both for the abundance of instruments used and for the affinity among them. For each location survey campaigns were carried out (geological, geomorphological, structural and laser scanners). Because of the complexity of the processes it was decided to expose an accurate description of each instability phenomenon as well as the geological, geomorphological and geomechanical characterization. In the third part, ”Data analysis and Results” are reported “Optimal zones/point instruments positioning ”method created by integrated use of Laser Scanner and WSN. Here are also shown the results of data analysis carried out by ad-hoc created Matlab scripts to automate certain processes of acquisition, filtering and calculation of acquired data. Relations between trigger factors and evolution of case study instability processes are presented. The results from WSN monitoring activity carried out in the Maltese arcipelago are also proposed and the relation between structures deformations, temperature and variation of the piezometric level has been analyzed. At the end some considerations on Self-adaptive and Multi-Parametric platform are proposed together with early warning activities acting on the presented monitoring systems.

Part I

- State of the art, tools and methods

Chapter 2

Rock slope instability processes overview

According to Varnes (1978) [113] there are six basic considered types of slope movement: Falls, topples, slides, lateral spreads, flows and complex movement. In this section we reported a brief description of instability processes which you will encounter in part II as we considered it important to provide an immediate reference to better introduce the reported applications that only deal with rock slope instability processes.

From an engineering point of view, 'rock' means a compact semi-hard mass of a variety of minerals. All the features, starting from ultra microscopic to macroscopic, which influence the strength and the deformation characteristics of rocks, can be called defects [2]. The load carrying capacity of rocks is influenced by these defects, and its decrease can cause a concentration of stresses in certain directions. These defects may be correlate to the composition of rock and his internal texture or they may due to tectonic stresses to which the rocks have been subjected during the course of history.

Rocks can also be weathered by different causes such as mechanical processes or chemical dissolution. Rock weathering is a process which causes alteration of the rock due to the action of water, carbon dioxide and oxygen. The effect of weathering is not limited to the surface, but extends deeper depending on the presence of channels which permit the flow of water and contact with the atmosphere.

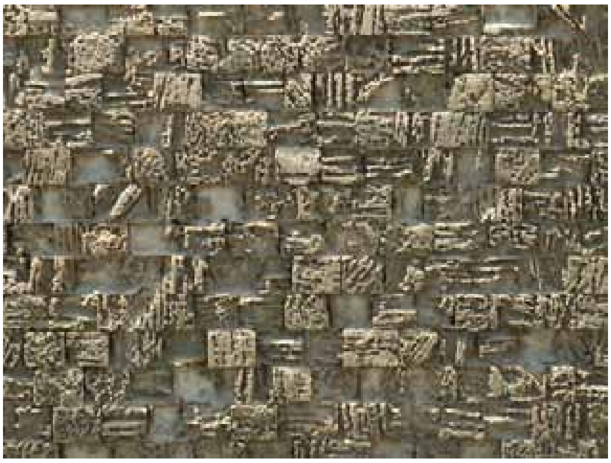

(a)

(b)

Figure 2.1: Chemical alteration of rock (a) and stone (b) along the Citadel walls (April, 2009).

Structural defects are commonly called discontinuity, their quantitative description is one of the main object of rock slope engineering.

Rock slope stability depends on the strength features of the rocks, the geometrical and strength features of the discontinuities and the presence of weathering action on the rock and rock defects.

A rock slope can be homogeneous or can be made up of a complex of rocks of different geological origins with a different sequence of sediments or be intruded by bodies of igneous rocks or partially metamorphosed. Different lithological units can have different strength, deformation and competence features.

The weathering of friable rock material, such as sandstone, or of closed fractured shales can be the cause of slope ravelling. When the slopes are faulted, fault zone can be subjected to slumping. A fault gauge behaves like a clay material, while a fault breccia behaves like debris composed of broken rock fragments varying in size from centimeters near the surface to several meters at a depth. Sedimentary rock depositional features can determine regular bedding and the principal weakness surfaces, present at the excavation faces, are the parallel bedding planes. Different types of mechanisms can cause the development of the forces that result in the jointing formation.

2.1 Rock-Fall

Rockfalls consist of free falling blocks of different sizes which are detached from a steep rock wall or a cliff Figure 2.2 on page 18. The block movement also includes bouncings, rollings and slidings with rock block fragmentation during the slope impacts. Unfavorable geology and climate are the principal causal mechanisms of rockfall Figure 2.3 on page 19, factors that include intact condition of the rock mass, discontinuities within the rock-mass, weathering susceptibility, ground and surface water, freeze-thaw, root-wedging, and external stresses. The pieces of rock collect at the bottom creating a talus or scree. Rocks falling from the cliff may dislodge other rocks and serve to create another mass wasting process, for example an avalanche [2].

Typically, rockfall events are mitigated in one of two ways: either by passive mitigation or active mitigation. Passive mitigation is where only the effects of the rockfall event are mitigated and are generally employed in the deposition or run-out zones, such as through the use of drape nets, rockfall catchment fences, diversion dams, etc. The rockfall still takes place but an attempt is made to control the outcome. In contrast, active mitigation is carried out in the initiation zone and prevents the rockfall event from ever occurring. Some examples of these measures are rock bolting, slope retention systems, shotcrete, etc. Other active measures might be by changing the geographic or climatic characteristics in the initiation zone, e.g. altering slope geometry, de-watering the slope, re-vegetation, etc.

The rock block fall movement is extremely rapid, more than 25-30 m/s, this type of process is active in the rock slope of Elba, Malta and Torgiovannetto Figure 2.4 on page 20.

However, the monitoring systems presented in this thesis are not appropriate to perform the monitoring activities on these processes. In particular, the block movements are too fast and their size is too small to be detected by the sensors used.

Figure 2.2: Main types of falls according to Hutchinson (1998). 1) Primary rock falls; 2) Secondary Stone falls.

Figure 2.3: Rock fall. Kokomeren Valley (Kyrgyzstan, August 2007)

(a)

(b)

(c)

Figure 2.4: Active rock fall processes in study cases. a) Provincial road in western sector of Elba island b) Eastern view of the barrier of Torgiovannetto landslide c) Underpinned outcorp along the boundary walls of Citadel (Malta).

2.2 Rock-Slide

A sliding movement is determined by unbalanced shear stress along one or more surfaces. These surfaces are visible or may be inferred by analyzing 'in situ' observations. Sliding surface determination is one of the most important problems in a landslide analysis. The figure Figure 2.5 on page 21shows some type of slide [2].

Hungr and Stephen G. Evans proposed 8 class or styles of failure: rock slump, rock collapse, translational rock block or wedge slide, structurally-defined compound slide, block slide with toe breakout (toe-constrained slide), compound slide, flexural toppling, block toppling.

Rock slide phenomena are active at the rock slope of Elba (rock collapse) and Torgiovannetto (translational rock block or wedge slide).

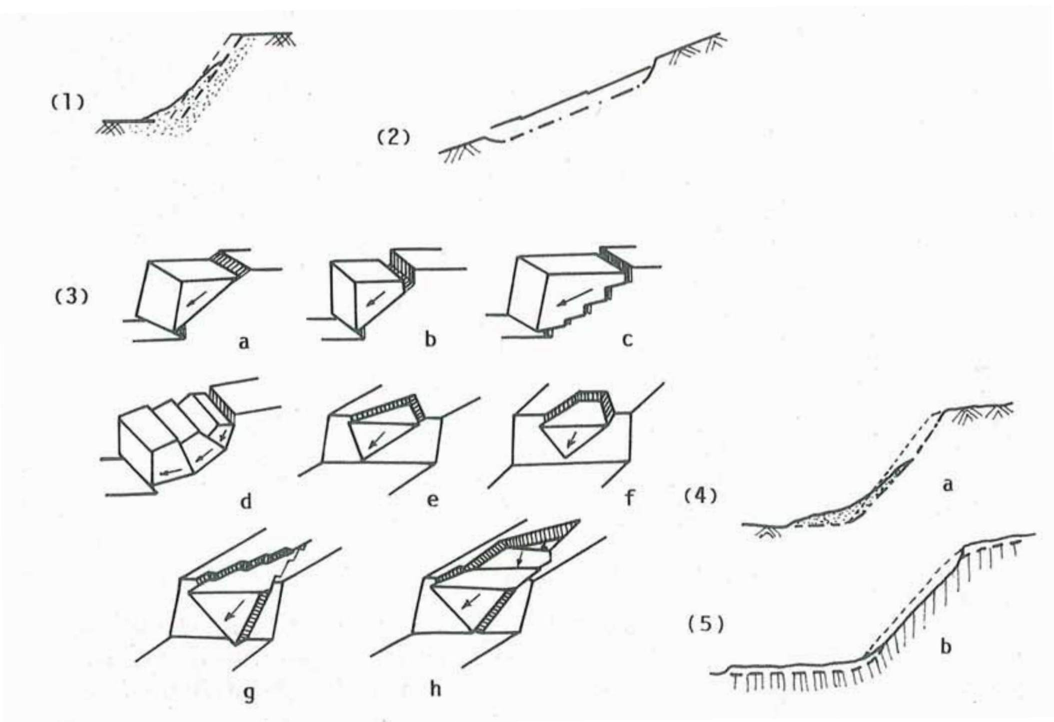

Figure 2.5: Principal types of sliding translations. 1) Sheet slides; 2) Slab slides; 3) Rock slides (a-d: 2-D phenomena); 4) Debris slides; 5) Sudden spreading failures (taken from[2]).

Figure 2.6: Rock slide, Kokomeren Valley (Kyrgyzstan, August 2007).

(a)

(b)

Figure 2.7: View of rock slides. a) Outcrop of Elba island b) Torgiovannetto landslide.

2.3 Rock Slab-Soft Substratum System

This type of movement is active in the rock slope of Malta. This geological setting consists of the superimposition of rock types with marked contrast in their geotechnical properties is one of the most critical geological environments for the stability of slopes [48].

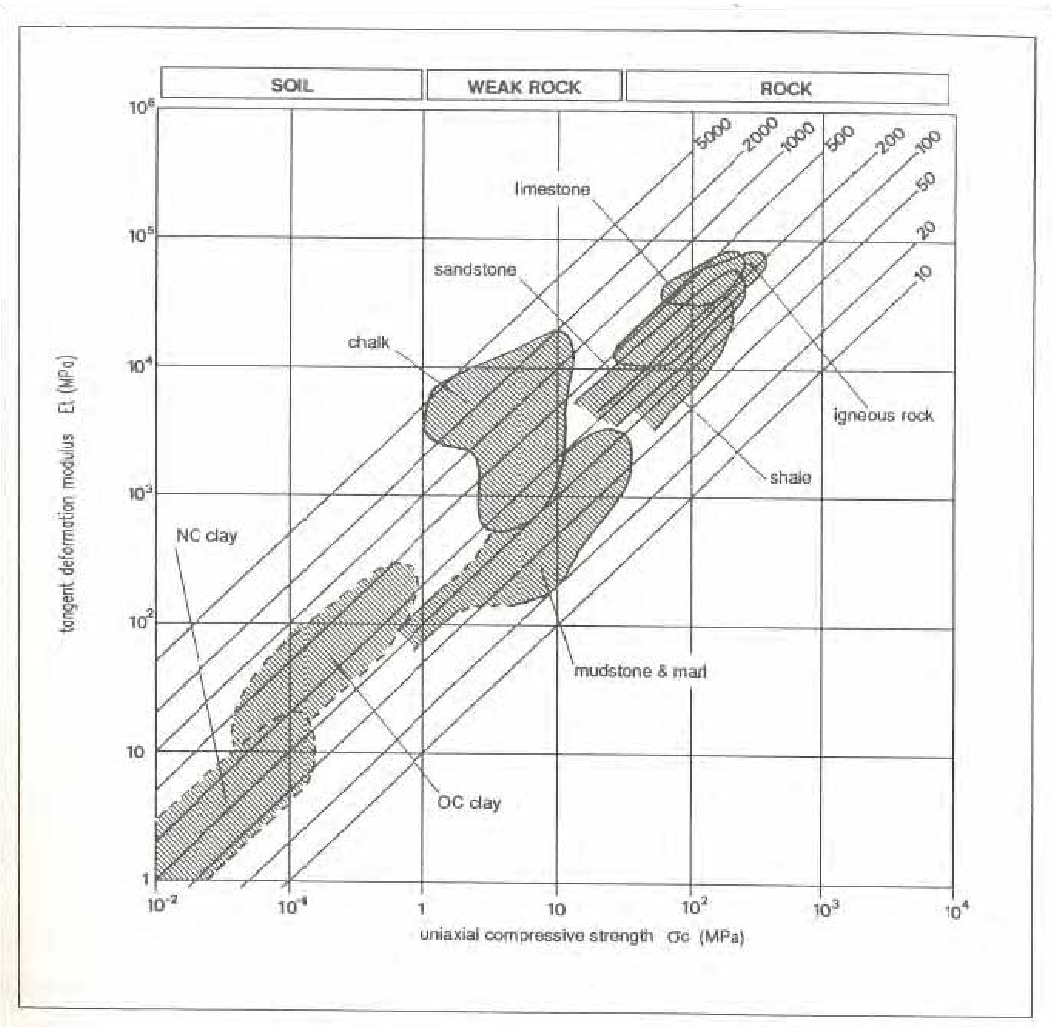

Figure 2.8: Deree's diagram (taken from [48])

The mechanical characteristics of the materials in the study area are, therefore, very different in terms of strength, stiffness and brittleness; this leads to typical geomorphological processes such as flow phenomena on the underlying ductile units and brittle ruptures involving the overlying rock masses. These cracks are often linked to huge sub-vertical joints, that isolate large blocks.

Associated with the slow – long term evolution of the rock slab – soft substratum system we often find small scale rapid instability phenomena, that may lead to dangerous rock falls. In fact, the rock mass slopes are very steep, sometimes overhanging, and there are several elements at risk over and around the cliff.

Figure 2.9: Rock Slab-Soft Substratum system on Gozo Island (Malta, May 2010)

Figure 2.10: View of Citadel from East (Malta, May 2010).

(a)

(b)

Figure 2.11: Instability mechanism on a Rock Slab-Soft Substratum system on Gozo island. (a) Rock fall and toppling. (b) Backward erosion on clay gully (Malta, May 2010).

2.4 Landslide Triggers

The therm "Landslide Trigger" refers to an external stimulus, such as intense rainfall, rapid snow-melt, seismic shaking, volcanic eruption, stream/coastal erosion, or natural dam failure, which causes an immediate or near-immediate in the form of Landslide activity. [3]

A deep earthquake releases energy that can reach the earth surface and cause serious damage to human buildings and activity.

Many case studies show rather close relation between rainfall and slope movements. The reaction time that elapses between rainfall event and slope movement are not always the same. Some types of landslides respond in an almost instantaneous manner (minutes or hours) others respond in a longer period, others are moving with impulsive acceleration.

The figure 2.12 shows the direct relation between rainfall and surface movement in Torgiovannetto landslide from July 2007 to April 2010.

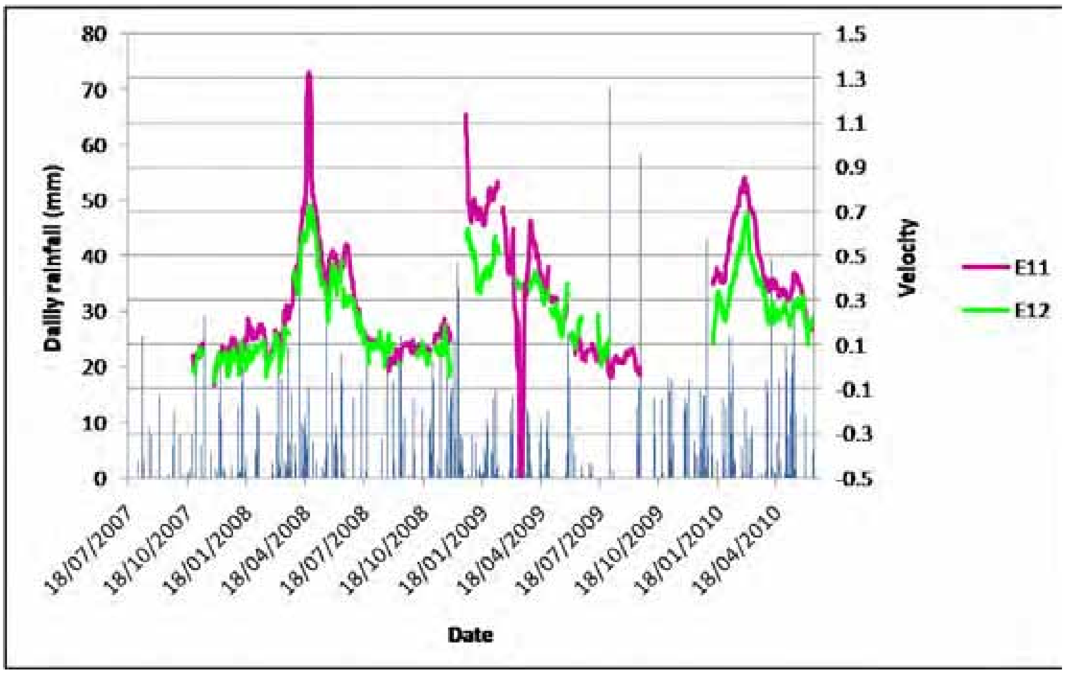

Figure 2.12: Moving averages of speeds calculated for the strain gauges E11 and E12 vs. daily precipitation.[4]

Some slope can be trigger by volcanic activities. In case of Stromboli, a morphological depression known as Sciara del Fuoco, is monitored by several tools (Interferometric Radar, accelerometers, tiltmeters). A comparison between the accelerogram Figure 2.13 on page 28, and the interferogram Figure 2.14 on page 28that include the moment in which there was an explosive event, it is clear that the movement of surface material Figure 2.15 on page 29was triggered by the event itself.

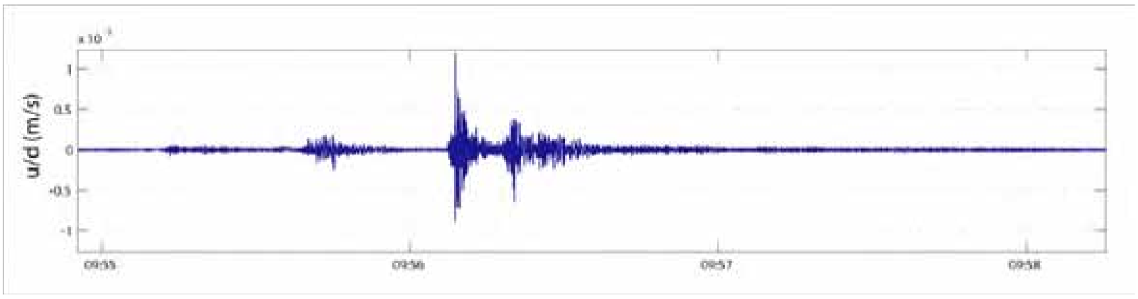

Figure 2.13: Seismic acceleration record of the event of 19_12_2010 (9:56:08).

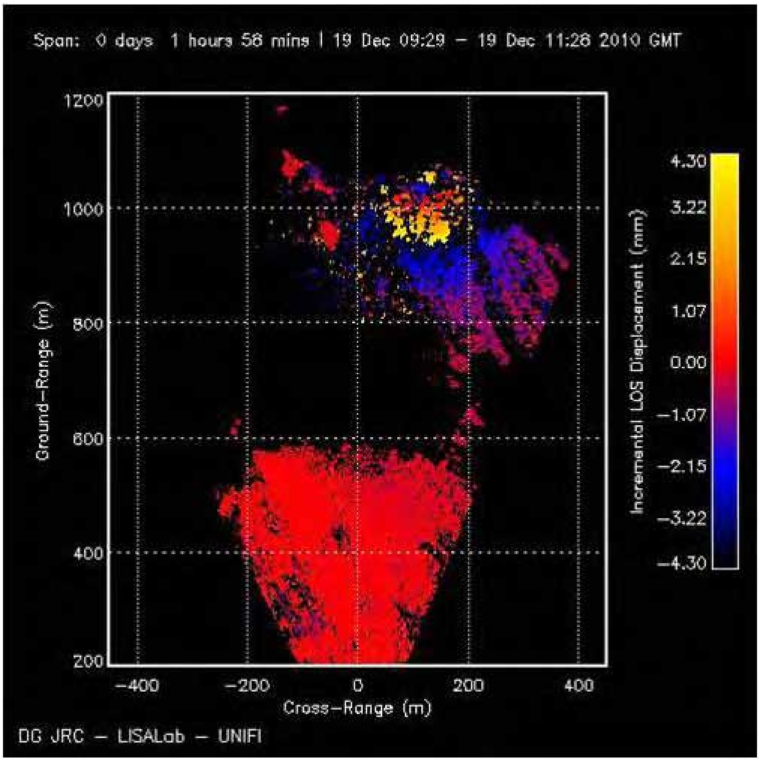

Figure 2.14: SAR interferogram between the hours of 19 December 2010 09:29 GMT (10:29 local time) and the hours of 19 December 2010 11:28 GMT (12:28 local time), time interval of 1 hour and 58 minutes.

Figure 2.15: Sciara del Fuoco during the eruption of March 2007.

The chart below shows how the radar-detected speed values of Stromboli Flank are increased by 2 orders of magnitude in conjunction with the explosive event.

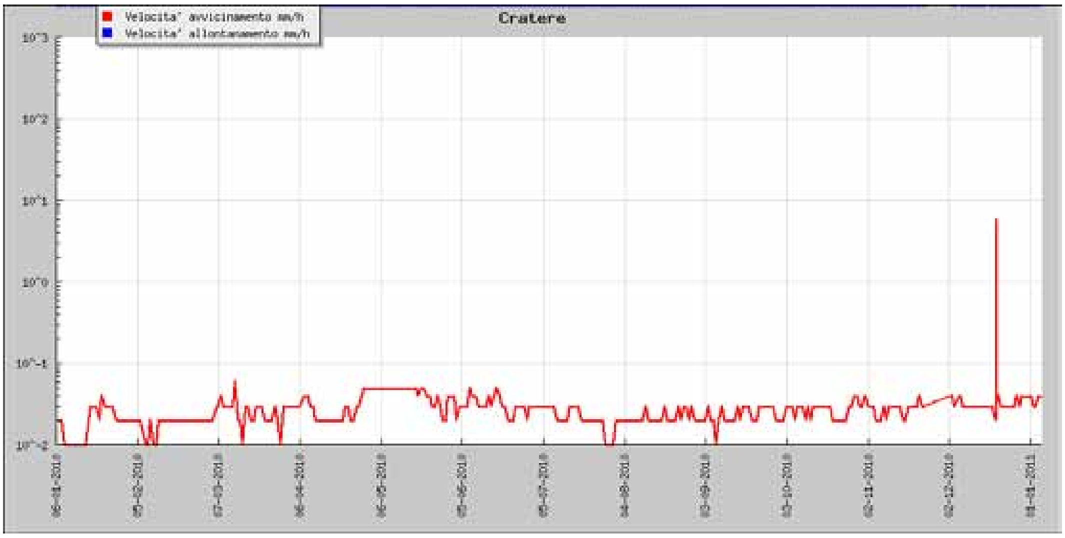

Figure 2.16: Diagram of the velocity-time of the crater from January 2010 to January 2011 . The speeds are reported in logarithmic scale in mm / h.

An effective trigger can also be represented by the increase of pore pressure in a Rock Slab-Soft Substratum System. In the city of Mdina some correlation between increases in pore pressure and movements recorded on structure of the walls were noticed. In particular some tilt variations measured by biaxial inclinometers installed in the walls seem to be related with increses in pore pressure recorded by pore pressure gauges (Vibrating wire piezometers).

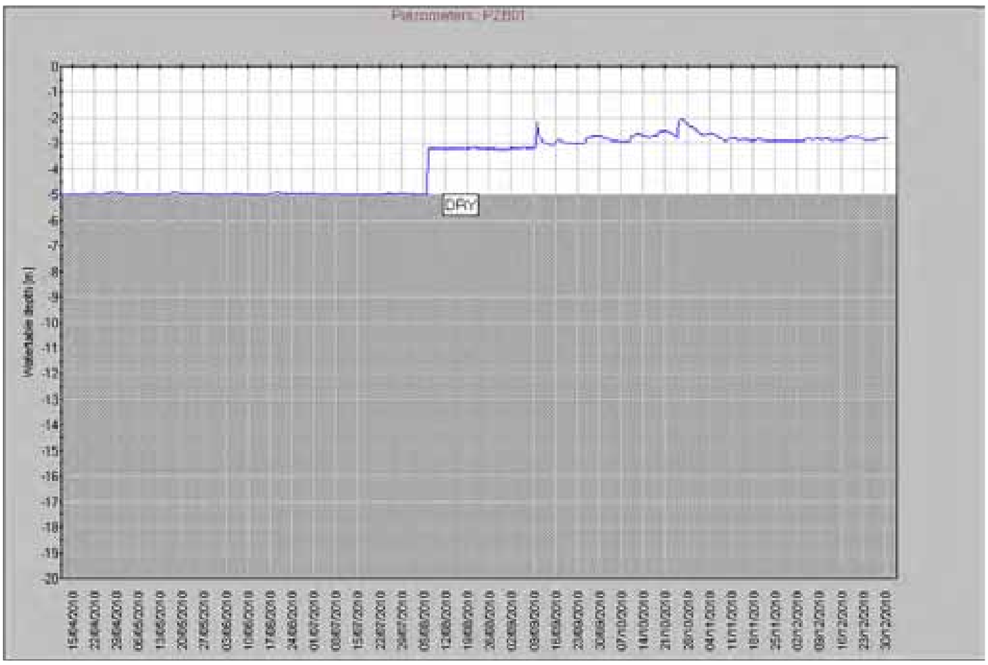

Figure 2.17: Piezometric data obtained from instrument PZB01 installed in Mdina (modified from [5]).

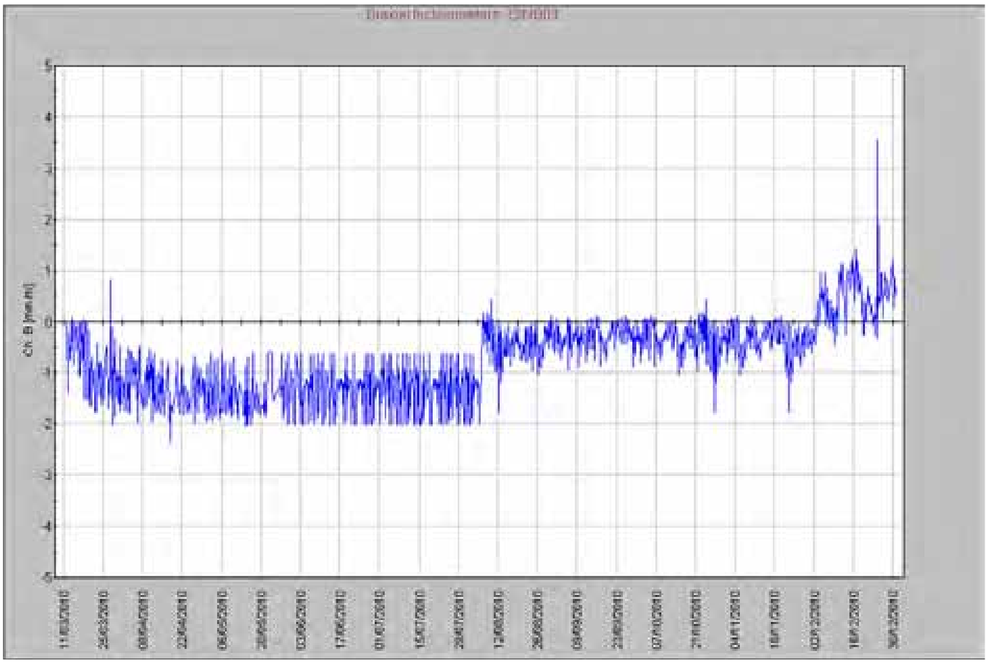

Figure 2.18: Inclinometric data obtained from instument BINB03 installed in Mdina (modified from [5])

Chapter 3

Employed monitoring tools

3.1 Wireless sensor networks

Last year I asked to Mauro Reguzzoni, the owner of Hortus S.R.L. and the installer and creator of the WSN installed in Torgiovannetto, what were his impressions on the sensor network after some months of use. This was his response:

"Wireless sensor networks are likely to have a great future even if they introduce critical issues which must be taken into account".

In recent years, advances in miniaturization; low-power circuit design; and simple, low power, yet reasonably efficient wireless communication equipment have been combined with reduced manufacturing costs to realize a new type of multifunctional sensor nodes that are small in size and communicate with each other through short radio distances [6]. These tiny sensor nodes consist of sensing, data processing and communication components and have deter- mined the birth of a new version of wireless networks named wireless sensor networks [7, 8, 9, 10, 11].

Due to the characteristics above described, in particular the short dimensions, the capability of processing and the use of wireless communications, WSN are suitable for a high number of applications [12]. It is possible classify them in appropriate categories:

- Military applications
- Environmental monitoring
  - Outdoor Monitoring - Application to Ecology
  - Outdoor Monitoring - Applications to agriculture
- Support for logistics
- Human-centric and robotic applications
- Human-centric applications
- Application to robotics

A WSN is composed of a large number of sensor nodes that are densely deployed either inside the phenomenon or very close to it. The position of sensor nodes can be predetermined to guarantee a uniformly sensing of a defined area or they can be randomly deployed in inaccessible terrains or in particular types of application as in disaster relief operations [10]. In this last case it is necessary to create a sensor networks protocols and algorithms that possess self-organizing capabilities.

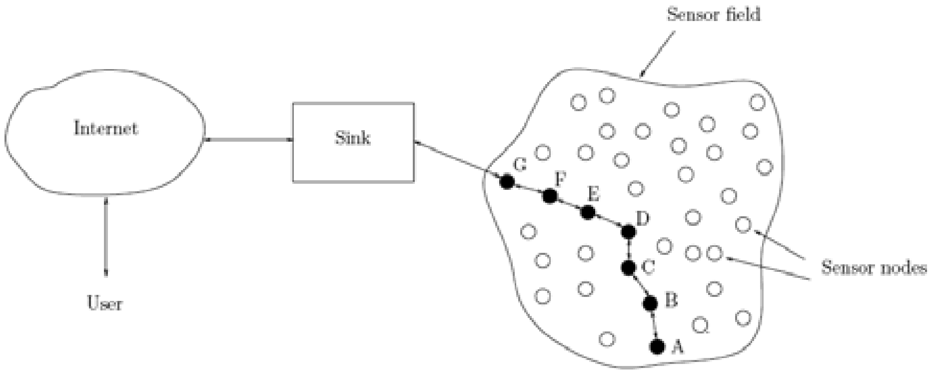

Figure 3.1: Typical wireless sensor networks scenario (Taken from [11]).

Typical application scenarios for WSNs Figure 3.1 on page 33 include a sink that acts as coordinator of the network and can trigger periodically the nodes, but especially collects the observations received by them and transmits the data to the user through wireless or wired link.

There are two main types of networks:

- Star network. Each sensor can transmit the observations directly to the sink.
- Mesh network. The nodes are positioned in a large area and the farther ones don't have a radio visibility with the coordinator.

In this case each node acts both as sensor and as router to forward the data of the neighbor nodes toward the sink. An important feature of sensor networks is the cooperative effort of sensor nodes. These instead of sending the raw data to the sink, use their processing capabilities to locally carry out simple computations and transmit only the required and partially processed data. WSNs are suitable for a wide range of applications in military, health, home, industry, agricultural and a lot of other fields, for instance in health, sensor nodes can be deployed to monitor and assist disabled or old patients. Realization of this and other sensor network applications require ad-hoc networking techniques. Although many protocols and algorithms have been proposed for traditional wireless ad hoc networks, they are not well suited to the features and applications requirements of sensor networks.

The main differences between these two types of networks are:

- The number of sensor nodes in a sensor network can be much higher than that in an ad-hoc network. These components are usually densely deployed.
- There is a high probability that sensor nodes can fail.
- In some cases the topology of a sensor network changes very frequently.
- Sensor nodes mainly use a broadcast communication, whereas most ad-hoc networks are based on point-to-point communications.
- Sensor nodes are limited in power, computational capacities, and memory.

3.1.1 Main features of Wireless Sensor Networks

The main factors that it is important to consider to planning or to design algorithms and protocols for this type of networks are:

- Fault Tolerance. It is important to consider that some sensor nodes may fail or can be blocked due to lack of power, or have physical damage or environmental interference. The failure of sensor nodes should not affect the overall task of the network. Fault tolerance is the ability to sustain sensor network functionality without any interruption due to sensor node failures.

- Scalability. The number of sensor nodes deployed in studying a phenomenon could be very high (of the order of hundred or thousand) for particular applications. Algorithms and protocols created for this type of networks must consider this aspect so as the high density that can range from few sensor nodes to few hundred in a region that can be less than 10m in diameter. Usually in those areas where there is a high density of nodes it is much easy to design energy-efficient algorithms, the great challenge is to design minimum-power-consumptions algorithms in that networks where there is a small redundancy of nodes.

- Costs. Since wireless sensor networks consist of a large number of sensor nodes, the cost of a single node is very important to justify the overall cost of the network. Obviously this cost has to be as low as possible. Actually the cost of a single wireless node is roughly 20 euros. The main producers are Texas Instruments, Crossbow, St Microelectronics, Zensys, FreeScale and others. With the development of technology the cost of a single node should be much less than 1 euro.

- Hardware Constraints. A typical structure of a sensor node is represented in Figure 3.2 on page 34. It is composed of four basic components: a sensing unit, a processing unit, a transceiver unit and a power unit. It is possible include additional components as a location finding system, a power generator and a mobilizer. Sensing units are usually composed of two subunits: sensors and analog-to-digital converters (ADCs). The sensors observe a determined phenomenon and produce the analog signals that are converted into digital form by the ADC, and subsequently are elaborated by the processing unit. This unit, which is generally associated with a small storage unit, manages the procedures both to extract information from the observations and for collaborate with the neighbor nodes in the mesh networks, in order to guarantee reliable communications with minimum power consumptions.

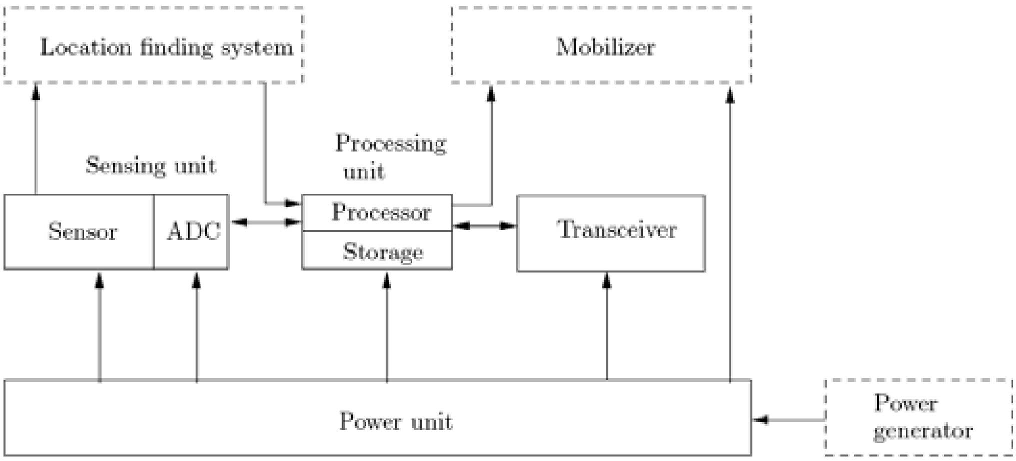

Figure 3.2: Units and subunits that composing a wireless sensor node (Taken from [11]).

A transceiver unit connects the node to the network. It contains the transmitter and receiver usually tuned on Industrial, Scientific and Medical (ISM) frequency bands (433MHz, 800MHz and 2:4GHz). Power units may be supported by power scavenging units such as solar cells. Additional subunits are useful to particular types of application. Most of the sensor network routing techniques and sensing tasks require knowledge of location with high accuracy. In these types of applications, it is important that a sensor node has a location finding system. A mobilizer can be useful to move sensor nodes in those applications where it is required to monitor a mobile phenomenon. All of these units and subunits it is important that are included into a small module.

- Environment. Sensor nodes are usually densely deployed either very close or directly inside the phenomenon to be observed. Therefore, they usually work unattended in a remote geographic areas. They may be working in the interior of large machinery, at the bottom of an ocean, in a biologically or chemically contaminated field, in a battlefield beyond the enemy lines, and in a home or large building. For some of these scenarios, sensor nodes are thrown for example by an airplane and assume random positions. It is important that they can auto- organize in order to create an efficient and reliable network. In scenarios accessible by man, nodes are positioned one by one in the sensor field to create a desired network topology.

- Transmission Media. In a mesh network, communicating nodes are linked by a wireless medium. These links can be formed by radio, infrared, or optical media. To enable global operation of these networks, the chosen transmission medium must be available worldwide. As above described, the three frequency bands actually utilized are 433MHz, 800MHz and 2:4GHz that are no licenses ISM bands. Another possible mode of inter-node communication in sensor networks is by infrared. Infrared communications is license-free and robust to interference from electrical devices. Moreover the transceiver are cheaper and easier to build. The big problem is that this type of transmission media require a line of sight between the sender and receiver (so as the optical media), that it is impossible to assure in environments as those described in the previous point.

- Power Consumption. Usually the wireless sensor node can only be equipped with a limited power source (in most cases two AA batteries). In some application scenarios, replenishment of power resources might be impossible. Sensor node lifetime, therefore has a strong dependence on battery lifetime. In a mesh network, each node plays the dual role of data originator and data router. The malfunctioning of a few nodes can cause significant topological changes and might require rerouting and reorganization of the network. Hence, power conservation and power management take an importance greater than reliability of communications. The main task of a sensor node in a sensor field is to detect events, perform quick local data processing, and then transmit the data. Power consumption can hence be divided into three domains: sensing, communication and data processing.

3.2 Laser Scanner

The main product of a long range laser scanning survey is a high resolution point cloud, obtained by measuring with high accuracy (millimetric or centimetric) the distance of a mesh of points on the object, following a regular pattern with polar coordinates [13].

The high acquisition rate (up to hundreds of thousands of point/s) allows to immediately obtain the detailed 3D shape of the object. Laser scanning data can be processed by true coloring point clouds from high resolution optical digital images,or by triangulat-ing points in order to create Digital Surface Models(DSM).

The tool we use is a LMS-Z420i, produced by Riegl Laser Instrument

Figure 3.3: Laser Scanner Tool - LMS-Z420i Opposite to the Canossa wall cliff (Taken from [102]).

I performed the first application of this instrument at Canossa, during my MSc thesis. The work was focused on the study of instability processes of the calcarenitic cliff over which the Canossa Castle was built in 940 BC . The Castle is an Italian National Monument, Especially Known as the seat of the Walk to Canossa, the meeting of Emperor Henry IV and Pope Gregory VII During the Investiture Controversy (1077).

Laser scanner measurements were performed in different locations and with different purposes during the four years following. The instrument was used in both Italian and international projects as Collagna, Torgiovannetto, Cardoso, Pitigliano, Elba Island (Italy) and Mdina, Gozo (Malta).

3.2.0.1 Technical data

The main technical data of the employed sensor are:

- Maximum range: 1000 m
- Beam divergence: 0.25 mrad
- Measurement accuracy: ± 5 mm

- Max scanning rate: 12000 pts/sec
- Min. angle step-width: Vertical: 0.008°, Horizontal: 0.01°.

3.2.0.2 Key features and potential uses.

A laser scanner survey is usually performed to obtain spatial information of the investigate area and surface. In most of our applications, the laser was used to reproduce three-dimensional models of rock masses. Once acquired the model it was used to perform stability studies, Kinematic analysis and reconstruction of geological structural sections [13].

Some common uses are the Evaluation of large scale deformational evolution by comparing point clouds acquired at different times, the generation of high resolution DEMs to correctly set up rockfall simulation models and numerical models and data collection in impervious areas (distances, block dimensions, joint orientation, block displacement).

When we face engineering geology problems in rock, it is fundamental to reconstruct the 3D geometry and the structural setting of the rock-masses, sometimes in inaccessible areas. An accurate description of the geometrical and mechanical properties of the material is specifically required, as the overall mechanical behavior of a rock mass depends on its structure, on the characteristics of discontinuities and on the properties of intact rock.

Traditional geomechanical surveys are performed in situ, either in one dimension (scanline method) or two dimensions (window method), and require direct access to the rock face for the collection of the relevant parameters [14]. ISRM [15] selected the following ten parameters for the quantitative description of discontinuities in rock-masses: orientation, spacing, persistence, roughness, wall-strength, aperture, filling, seepage, number of sets, and block size. For practical and safety reasons, traditional geomechanical surveys are often carried out on limited sectors of the rockmass, and usually they do not provide data for a complete reconstruction of the full variability of a rockmass. Nowadays, several techniques are available for retrieving high resolution 3D representations of land surface, such as digital photogrammetry [16, 17], laser scanning (terrestrial and aerial) [18, 19] and SAR-interferometry [20]. In addition, the increased computational performance of personal computers allows us to process large amounts of data in a relatively short time. The advantage of employing remote and high resolution surveying techniques for geomechanical purposes is based on the capability of performing both large scale [22, 21] and small scale [23, 24] analysis and to rapidly obtain information on inaccessible rock exposures. Sometimes, the features of interest can be very large [25], and they could actually remain unnoticed if only a small scale field survey is performed. On the other side, the observation of small details, such as discontinuity planes or traces and surface roughness, is a key element for the geomechanical characterization of the rock mass. In order to perform correct analysis from a statistical point of view, we need, therefore, to investigate a portion of the rock face as wide as possible. The capability of capturing small details depends primarily on the resolution and on the accuracy of the survey method.

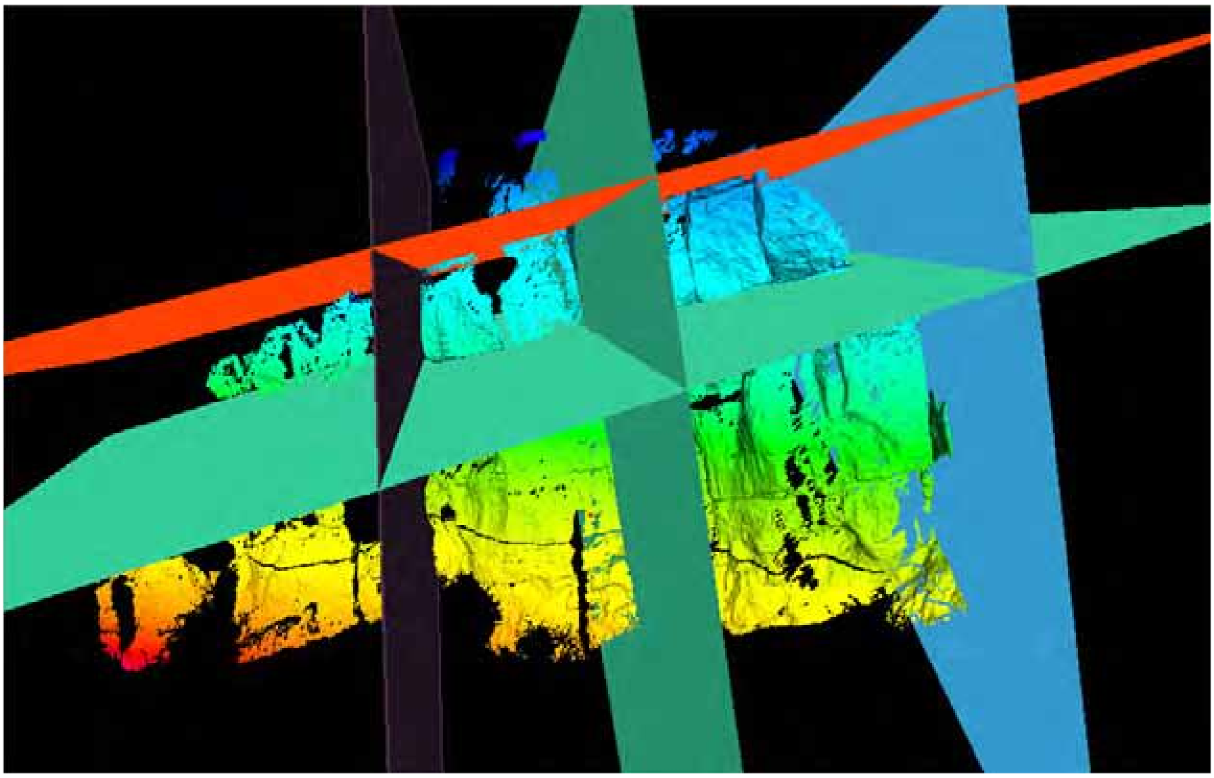

Figure 3.4: Joint orientation of Canossa cliff, obtained from point clouds analysis (taken from [102]).

3.3 Interferometric RADAR

3.3.1 Introduction

The word Radar is the acronym of Radio detection and ranging. Radar is an active instrument, which measures the echo of scattering objects, surfaces and volumes illuminated by an electromagnetic wave internally generated belonging to the microwave portion of the electromagnetic spectrum. It was born just before the second world war for detecting and ranging target for non-civilian scopes. In this case the requested spatial resolution was not so challenging for the technology available that time. The opening of new technological frontiers in the fifties, including the satellites and the space vehicles, demanded a better spatial resolution for application in geo-sciences remote sensing (RS). Synthetic aperture radar (SAR) technique was invented to overcome resolution restrictions encountered in radar observations from space and generally to improve the spatial resolution of radar images. Thanks to the development of this peculiar technique, the radar observations have been successfully refined, offering the opportunity of a microwave vision of several natural media. Nowadays SAR instruments can produce microwave images of the earth from space with resolution comparable to or better than optical systems and these images of natural media disclosed the potentials of microwave remote sensing in the study of the earth surfaces. The unique feature of this radar is that it uses the forward motion of the spacecraft to synthesize a much longer antenna, which in turn, provides a high ground resolution. The satellite SEASAT launched in 1978 was the first satellite with an imaging SAR system used as a scientific sensor and it opened the road to the following missions: ERS, Radarsat, ENVISAT, JERS till the recent TerraSARX and Cosmo-SkyMED. The measurement and interpretation of backscattered signal is used to extract physical information from its scattering properties. Since a SAR system is coherent, i.e. transmits and receive complex signals with high frequency and phase stability, it is possible to use SAR images in an interferometric mode. The top benefit from microwave observations is their independence from clouds and sunlight but this capability can weaken by using interferometric techniques. Among the several applications of SAR images aimed at the earth surface monitoring, in the last decades interferometry has been playing a main role. In particular, it allows the detection, with high precision, of the displacement component along the sensor–target line of sight. The feasibility and the effectiveness of radar interferometry from satellite for monitoring ground displacements at a regional scale due to subsidence [26], earthquakes and volcanoes[36, 35] and landslides [37, 38] or glacier motion [27, 39] have been well demonstrated. The use of Differential Interferometry based on SAR images (DInSAR) was first developed for space-borne application but the majority of the applications investigated from space can be extended to observations based on the use of a ground-based microwave interferometer to whom this chapter is dedicated. Despite Ground based differential interferometry (GBInSAR) was born later, in the last years it became more and more diffused, in particular for monitoring landslides and slopes.

3.3.2 Ground Based SAR interferometry

3.3.2.1 The landing of a space technique

After this introduction the first following sections of this chapter resume SAR and Interferometry techniques basics, taking largely profit from some educational sources from literature [32, 33, 34, 26]. The following sections are devoted to the GBInSAR Figure 3.5 on page 40and to three case studies as examples of application of the technique.

It is possible to acquire SAR images through a portable SAR to be installed in stable area. The motion for synthesizing the SAR image is obtained through a linear rail where a microwave transceiver moves regularly. Ground-based radar installations are usually at their best when monitoring small scale phenomena like buildings, small urban area or single hillsides, while imaging from satellite radar is able to monitor a very large area. As for satellite cases GBinSAR radar images acquired at different dates can be fruitful for interferometry when the decorrelation among different images is maintained low. In ground based observations with respect to satellite sensors there is the necessity of finding a site with good visibility and from where the component of the displacement along the LOS is the major part. Recent papers have been issued about the feasibility of airborne [40], or Ground Based radar interferometry based on portable instrumentation as a tool for monitoring buildings or structures [28], landslides [30, 29] glaciers [31]. On the other hand satellite observations are sometimes not fully satisfactory because of a lengthy repeat pass time or of changes on observational geometry. Satellite, airborne and ground based radar interferometry are derived from the same physical principles but they are often characterized by specific problems mainly due to the difference of the geometry of the observation. A number of experimental results demonstrated its effectiveness for remote monitoring of terrain slopes and as an early warning system to assess the risk of rapid landslides: here we briefly recall three examples taken from recent literature. The first is the monitoring of a slope where a large landslide is located. The second deals with an unstable slope in a volcanic area where alerting procedures are a must. Finally an example of a research devoted to the interpretation of interferometric data collected through a GB SAR system to retrieve the characteristics of a snow cover is discussed.

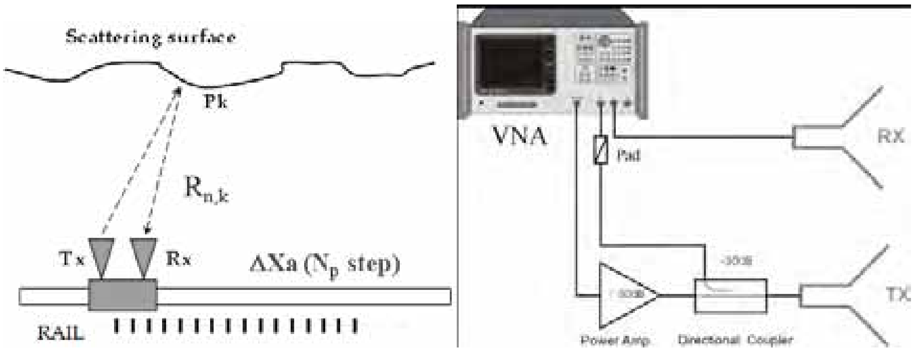

Figure 3.5: A) Basic scheme of the RF section of the C band transceiver based on the Vectorial Network Analyser VNA. B) GB SAR acquisition through a linear motion.

3.3.2.2 The GBInSAR instrumentation

Despite the use of the same physical principle, the satellite and ground based approaches differ in some aspects. In particular radar sensors of different kinds are usually employed mainly because of technical and operational reasons. While satellite SAR systems due to the need of a fast acquisition are based on standard pulse radar, continuous wave step frequency (CWSF) radar are usually preferred in ground based observations. The Joint Research Center (JRC) has been a pioneer of this technology and here the first prototype was born. The first paper about a GB SAR interferometry experiment dates back to 1999 [108], reporting a demonstration test on dam financed by the EC JRC in Ispra and the used equipment was composed of a radar sensor based on Vectorial Network Analyser (VNA), a coherent transmitting and receiving set-up, a mechanical guide, a PC based data acquisition and a control unit. After some years a specific system, known as GBInSAR LiSA, reached an operative state and became available to the market by Ellegi-LiSALab company which on June 2003 obtained an exclusive license to commercially exploit this technology from JRC. The use of VNA to realize a scatterometer, i.e. a coherent calibrated radar for RCS measurement, has been frequently used by researchers [41] as it easily makes a powerful tool for coherent radar measurements available. The basic and simplest schematic of the radio-frequency set-up used for radar measurements is shown in fig.4 together with a simple scheme of the GBSAR acquisition. Advanced versions of this set-up have been realized in the next years to improve stability and frequency capabilities [42, 43].

Figure 3.6: GBinSAR installed in a shelter on the Shara del Fuoco (Stromboli Volcano, March 2007).

Figure 3.7: GBinSAR during monitoring activities at Torgiovannetto (April 2007).

This apparatus is able to generate microwave signals at definite increasing frequencies sweeping a radio-frequency band. This approach apparently different from that of the standard pulse radar owns the same physical meaning because a temporal pulse can be obtained after Fourier anti transforming the frequency data (the so called synthetic pulse approach). The rapid grow of microwave technology occurred in the last years encouraged the development and realization of different instruments [44]; recently ground based interferometer with a non-SAR approach has been designed with similar monitoring purposes. Data are processed in real time by means of a SAR processor. An algorithm combines the received amplitude and phase values stored for each position and frequency values, to return complex amplitudes [45]. The optimization of focusing algorithms has been recently updated by Reale et al, 2008; Fortuny, 2009. To reduce the effect of side lobes in range and azimuth synthesis [46], data are corrected by means of a window functions (Kaiser, Hamming etc), for range and azimuth synthesis). The attainable spatial resolutions and ambiguities are related to radar parameters through the relation shown in Table 1. The accuracy of the measured phase is usually a fraction of the operated wavelength: by using centimeter wavelengths millimeter accuracy can be attained. As previously introduced, the phase from complex images can suffer from the ambiguity due to the impossibility of distinguishing between phases that differ by 2π. Single radar images are affected by noise and related interferometric maps must be obtained through an adequate phase stability between the pair of images: only pairs whose coherence loss can not affect the accuracy of the interferometric maps are usable. This task is of major difficulty when the considered time period is of the order of months. A detailed analysis to the possible causes of decorrelation in the specific case of GBInSAR observations gathering many images per day for continuous measurements has been discussed by some researchers [109] while for campaigns carried out on landslides moving only few centimeters per year, when the sensor is periodically installed at repeated intervals several months apart over the observation period, a novel method has been proposed [43].

Range resolution	$\Delta Rr = \frac{c}{2B}$
Azimuth resolution	$\Delta Raz = \frac{\lambda_c}{2L_x} \cdot R$
Non ambiguous range (m)	$R_{na} = \frac{c}{2\Delta f}$

Table 3.1: Calculated resolution available from a CWSF radar observation; B radio-frequency bandwidth, λc in vacuum wavelength, f frequency step, Lx rail length, R range, c light velocity.

The used apparatus , an Interferometric Ground-based Imaging Deformeter Linear Synthetic Aperture, namely InGrID-LiSA, is composed of a continuous-wave step-frequency (CW-SF) radar, a 3.0 m long linear rail and two antennas that move on it at steps of 5 mm forming a synthetic aperture. The microwave transmitter produces, step-by-step, continuous waves at 1601 discrete frequency values, sweeping the bandwidth from 17.0 and 17.1 GHz (Ku band). The receiver acquires the in-phase and the quadrature components of the microwave signal backscattered by the target thus providing its amplitude and phase. Range and cross-range synthesis of complex images is obtained by coherently summing signal contributions relative to different antenna positions and different microwave frequencies. As radar images are obtained through sampling techniques, frequency and spatial steps have to be selected in order to avoid ambiguity in range and cross-range [47].

3.4 Vibrating Wire Instruments

Vibrating-wire sensors have been used in a number of instruments built for measurement of the density and viscosity of fluids up to high pressure and in wide temperature ranges. These instruments are based on a rigorous theoretic model describing the mechanics of oscillation of a wire.

The Embedded wire, which is held under tension, is read by an excitation/reading coil. Any change in the strain (tension) on the wire causes the resonant frequency of the wire to alter and is directly proportional to strain changes.

Some instruments wihch compose the applied sensor networks (Tiltmeter, biaxial inclinometers, extensimeters, piezometers.) are based on the vibrating wire principle briefly reported here.

$f = \frac{\nu}{2L} = \frac{1}{2L} \cdot \sqrt{\frac{T}{\mu}}$
f =frequency
L=length
T= wire tension,μ= density of material.

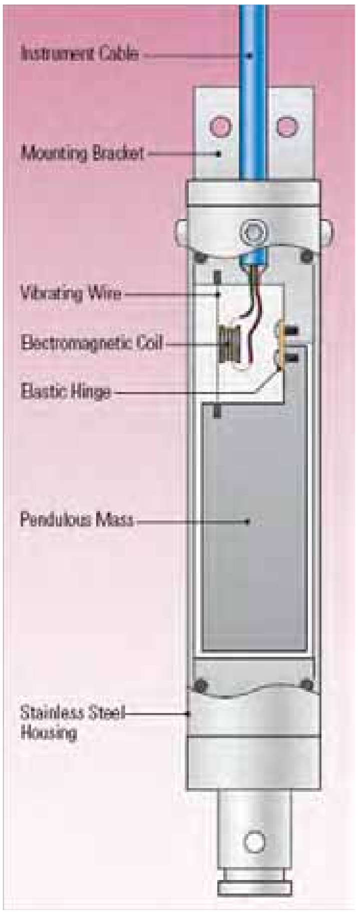

Figure 3.8: Vibrating wire tiltmeter scheme (taken from [114]). [67]

Part II

Applications

4 application sites are presented below, the laser scanner tool and wireless sensor networks have been used in an integrated way in this applications to create effective monitoring systems.

Integration of these two instruments returned satisfactory results. The laser scanner was used to return a three-dimensional reconstruction of the study area, to calculate in an expeditious manner the volume of unstable mass, their geometric structure and kinematic mechanisms with the highest hazard index.

The walls crack pattern was identified by running the laser scanner survey in Mdina, furthermore the movement main direction of blocks and the magnitude of the deformation were assessed. points of application of monitoring tools (bi-axial strain gauges and inclinometers) and the calibration of these have been defined by this information.

The design and installation of the monitoring system on Citadel (Gozo) was instead characterized by few financial resources. 8 Exstensimeter, 4 biaxial inclinometer and 3 piezometers were installed to monitor all the bastion walls. This equipment was inadequate to monitor the entire perimeter of the walls, it should have been at least double. It was therefore important to determine whether there were areas most affected by slope instability processes, so that the instruments will be installed only where it is needed only in areas of high instability. The laser scanner survey was used for this purpose, in particular the crack pattern of the rock mass underlying walls was reconstructed through the analysis of 3D point cloud. A kinematic analysis of rock mass was afterward performed using the characterization of the crack pattern.

In this way the parts of rock mass affected by mechanisms associated to the highest kinematic index where located on the rock mass. This knowledge, together with the spatial setting of fractures, were exploited to determine the location for installation of instruments.

All the applications listed below are, or have been in the past, monitored with remote monitoring systems within this PhD activity. The closest installed systems is in to Torgiovannetto (Assisi) at a distance of 130 Km from head quartiers, the farthest one is installed in Mdina (Malta) 908 Km.

Figure 3.9: Real time monitored sites within this PhD Thesis work. (modified from [78]) .

Chapter 4

Monitoring activities on the walled cities of Mdina (Malta)

In this chapter we describe the results of the geological and geotechnical surveys carried out in the island of Mdina and Gozo, Malta 4.1, on the slopes underlying Citadel by the Department of Earth Sciences of the University of Florence, within a restoration project financed by the European Regional Development Fund.

4.1 Mdina

The maltese archipelago consists of three inhabited islands, Malta Gozo and Comino, and some small uninhabited islands. It is located in the central Mediterranean sea at: Latitude: 35°48'28" - 36°05'00" North Longitude: 14°11'04" – 14°34'37" East The study area is located in the central - western sector of the island 4.2, where the ancient capital of Malta is built on a relief constituted of the Upper Coralline Limestone Unit .

Figure 4.1: Satellite view of Maltise arcipelago, cities of Mdina and Citadel. (modified from [78])

Figure 4.2: Aerial view of Mdina. (modified from [78]).

4.1.1 Geological settings

The Geological setting of Malta is mainly represented by marine sedimentary limestone rocks. These materials are geologically quite young, with the oldest rock dating back only to the Tertiary period. All exposed rocks were deposited during the Oligocene and Miocene periods of geological time dating back to some 30 to 35 million years ago. The most recent deposits are the quaternary deposits which are found in minor quantities and are of terrestrial origin. The resultant rock formations are relatively simple, consisting of five basic layers. Thus, the rock succession of the Maltese Islands takes the form of a simple-layered cake 4.3. Each rock layer has distinct characteristics such as thickness and hardness, due to their formation under different conditions.

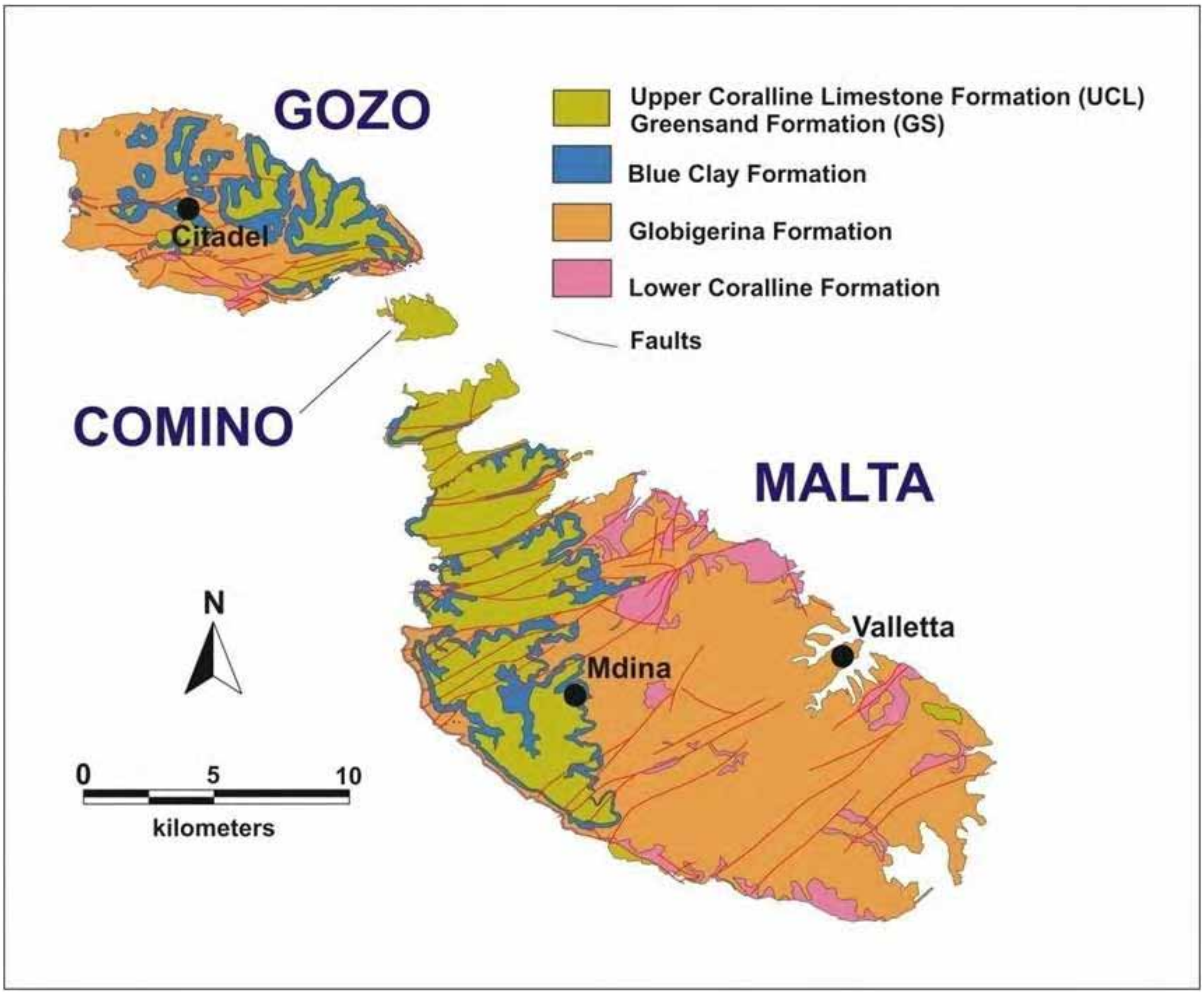

Figure 4.3: Geological Map of Malta (modified from [103]).

In particular, from the oldest to the youngest, we can find the following units:

Lower Coralline Limestone (Eocene - Oligocene) (LCL) Biogenic whitish limestone laid down between 30 and 25 million years ago. The maximum outcropping thickness is in the vertical cliffs near Xlendi, Gozo (about 140 meters high). The presence of tests of coralline algae suggest deposition in a shallow gulf environment; many bivalves and gastropods are also present. It's the oldest exposed rock in Malta. Globigerina Limestone (Low.-Midd. Miocene) (GL): Marly-globigerina-limestone, which represents more than 70% of the island's outcrops; it is the second oldest rock in Malta. This formation has considerable variations in thickness, ranging from 23 meters near Fort Chambray (Gozo) to 207 meters around Marsaxlokk (Malta), it's subdivided into three units (Lower, Middle and Upper Globigerina Limestones). Common fossils are bivalves, gasteropods and sea urchins, especially in to the pebble beds.

Blue Clay (Tortonian) (BC): Clay and marly clay, overlying the Globigerina Limestone formation. It erodes easily when wet and forms taluses which flow out over the underlying rock. Variations in thickness are considerable ranging from 75m at Xaghra, Gozo to nil in eastern Malta, where Upper Coralline Limestone rests directly on Globigerina Limestone. Deposition of the Blue Clay may have occurred in an open muddy water environment with water depths up to 150m for the lower part of the formation. Green Sand (Upp.

Miocene) (GS): It consists of bioclastic sandstones rich in glauconite deposited in a warm sea. Unweathered sections are green but are oxidised to an orange colour when exposed. The deposit attains a maximum thickness of 11m in localized depressions at Il-Gelmus in Gozo, but elsewhere is less than 1m thick.

Upper Coralline Limestone (Upp. Tortonian – Low. Messinian) (UCL): Biogenic whitish limestone; it's the youngest Tertiary formation in the islands reaching a thickness of approximately 160m in the Bingemma area, Malta. Local tectonic activity appears to have resulted in the brief emergence of the formation above the sea. The strata are very similar to the lowest stratum in the Maltese Islands. It is also named because of the abundance of the Coralline fossil algae species. It resembles the Lower Coralline Limestone 10 both on chemical and paleontological grounds, indicating deposition in shallow waters. The transition from the underlying greensands is gradual, sometimes merging into red and black granular sandstone, or red and white coralline rich limestone, which passes into a white calcareous sandstone compact, soft or porous but always rich in organic remains. Though some layers are completely crystalline and have lost traces of the organisms from which they originated, other portions are highly fossiliferous containing casts of shells and other organisms. These rocks are sporadically overlain by terrestrial, aeolian and alluvial deposits laid down following the emergence of the Maltese Islands above sea level. Much of the central and south-eastern portion of the island comprises outcrops of Globigerina Limestone while the northern and north-western regions are characterized by highlands on which upper coralline limestone is the dominant outcrop. The geology of Gozo is more varied than that of Malta, with more frequent outcrops of Blue Clay being a characteristic feature. A detailed geological survey has been performed over the study area. We employed a GPS system to define geologic contacts and outcrops as accurately as possible and a NW-SE tunnel, crossing the relief in the south western sector of the city, has also been inspected. The resulting geological maps are presented in (4.3). Anthropic debris with different thickness is also present at the base of the structures. However, we decided not to include it in the map, as we still lack information about the extension of this material in sectors other than the Vilhena Palace area, and we want to enhance the plurimetric contact between UCL and BC formations. For each study area, geologic cross-sections have also been drawn (4.5- 4.9).

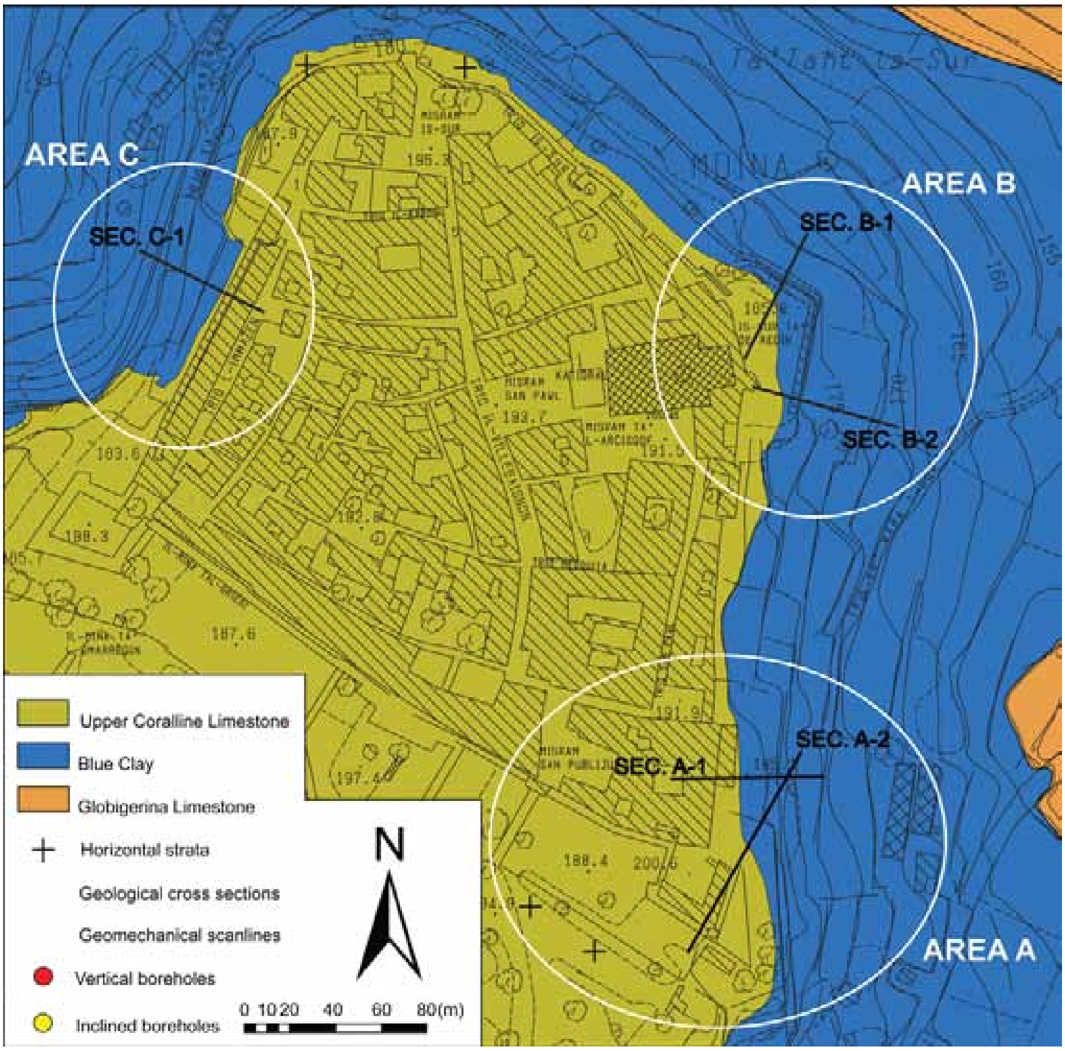

Figure 4.4: Geological Map of Mdina, elaborated according to geological survey and borehole investigation.

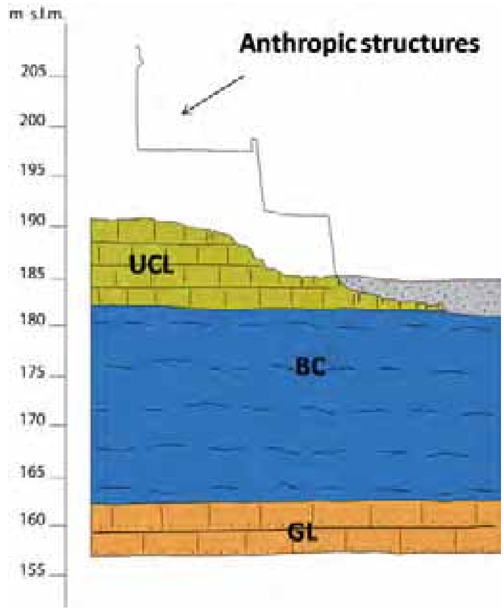

Figure 4.5: Geological cross-section A_1 (UCL: Upper Coralline Limestones; BC: Blue Clay; GL: Globigerina Limestones).

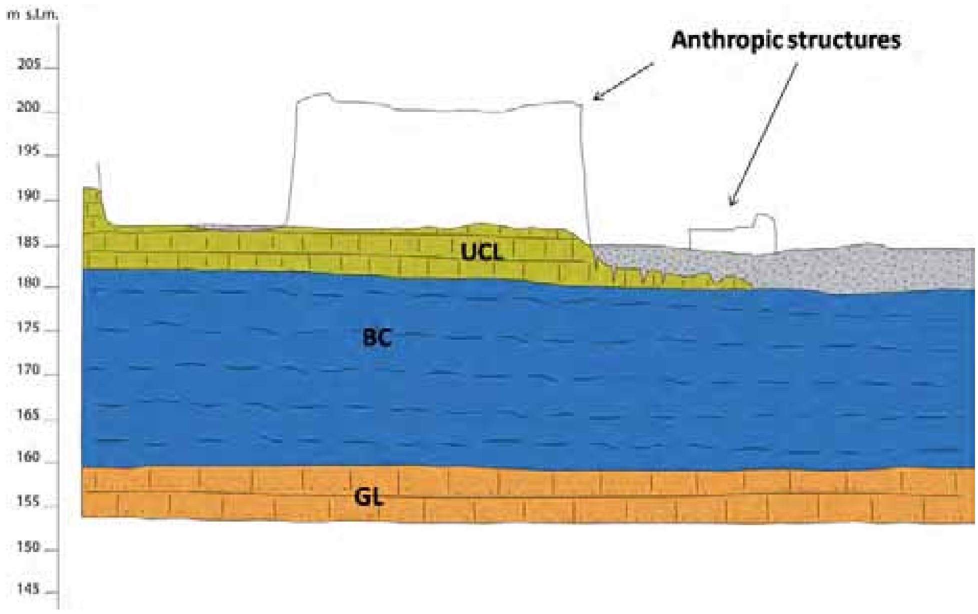

Figure 4.6: Geological cross-section A_2 (UCL: Upper Coralline Limestones; BC: Blue Clay; GL: Globigerina Limestones).

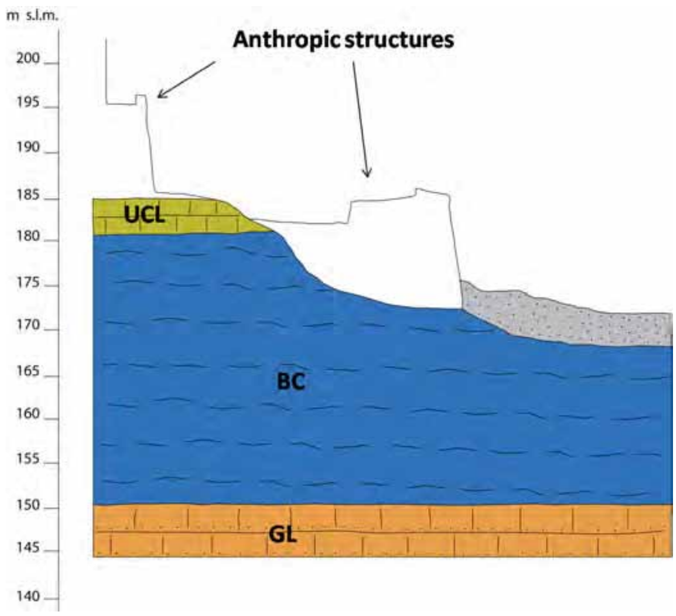

Figure 4.7: Geological cross-section B_1 (UCL: Upper Coralline Limestones; BC: Blue Clay; GL: Globigerina Limestones).

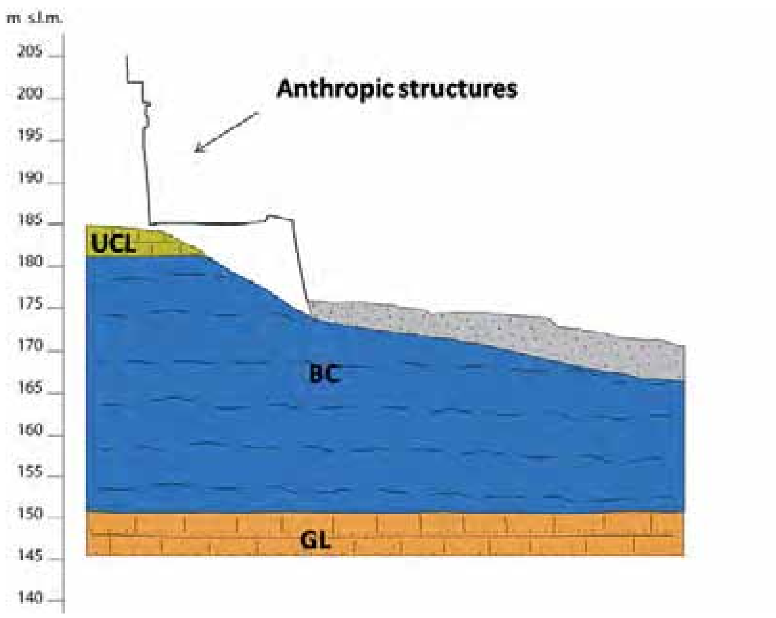

Figure 4.8: Geological cross-section B_2 (UCL: Upper Coralline Limestones; BC: Blue Clay; GL: Globigerina Limestones).

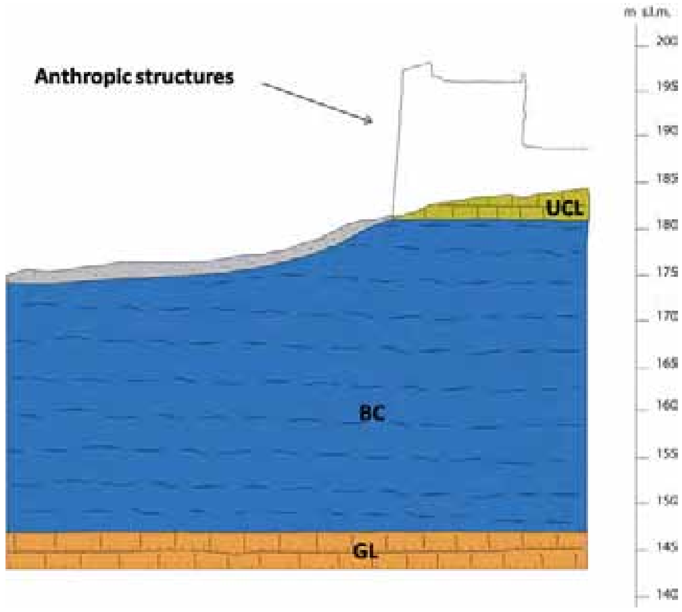

Figure 4.9: Geological cross-section C_1 (UCL: Upper Coralline Limestones; BC: Blue Clay; GL: Globigerina Limestones).

4.1.2 Geomorphologic setting

No mountains and a flat landscape are the main features of Malta. The highest point is at Ta' Zuta on Dingli Cliffs which is 253 m above sea level. The topography is mainly modeled by erosion of different rocks types (cake layered) and normal faults. Sheer cliffs are formed by Lower Coralline Limestone on the coast, and limestone-platform plateaux inland, massive cliffs and limestone-platform are formed also by Upper Coralline Limestone which are hardly affected by active karsism. Blue clays form cone screes over the underlying rocks. The island is cut by normal faults, there are two main directions: NW-SE and NE-SW. The geological setting of the study area shows the superimposition of a stiff and brittle limestone plate (UCL), on a thick Blue Clay unit. The superimposition of rock types with marked contrast in their geotechnical properties is one of the most critical geological environments for the stability of slopes (4.10). The mechanical characteristics of the materials comprising the rock slab – soft substratum systems are very different in terms of strength, stiffness and brittleness; this leads to typical geomorphological processes, such as flow phenomena on the underlying ductile units and brittle ruptures involving the overlying rock masses. The latter are often linked to huge sub-vertical joints that isolate large blocks.

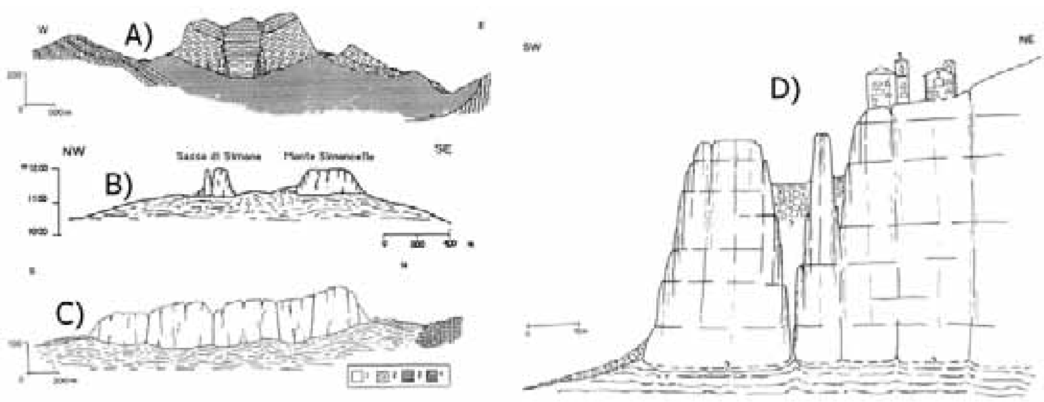

Figure 4.10: Examples of rock slab – soft substratum systems from Northern Apennines – Italy. A) Mt. Fumaiolo; B) Sasso di Simone – Mt. Simoncello; C) La Verna; D) Detail of La Verna relief, beneath the Monastery(modified from [48].

4.1.3 Hydrogeologic settings

The hydrogeologic characteristics of the study area are affected by the superimposition of the Upper Coralline Limestone and Green Sand layers on the Blue Clay layer. In fact these materials are characterized by very different hydraulic conductivities. The upper layer is characterized by very high primary (Green Sand) and secondary (UCL) hydraulic conductivity. The large aperture of discontinuities found in the UCL formation, due to tectonics, differential movements of rigid blocks (mainly in the external sectors of the plate) or dissolution phenomena, are able to produce hydraulic conductivities of the order of m/s. This contrasts with the Blue Clay permeability, which constitutes therefore an impermeable barrier. Water usually infiltrate through the permeable UCL and then exits after flowing on the impermeable Blue Clay layer (4.11). This can produce very intense weathering along specific flow directions, particularly in soft rocks like UCL. In confirmation of this behavior, many hydrofoil plants (like canes) grow along the boundaries of the study areas in correspondence with the UCL – BC contact; however this kind of process could be less significant in urban areas like Mdina, where the surface has impermeable artifacts and the feeding area of the aquifer is quite small.

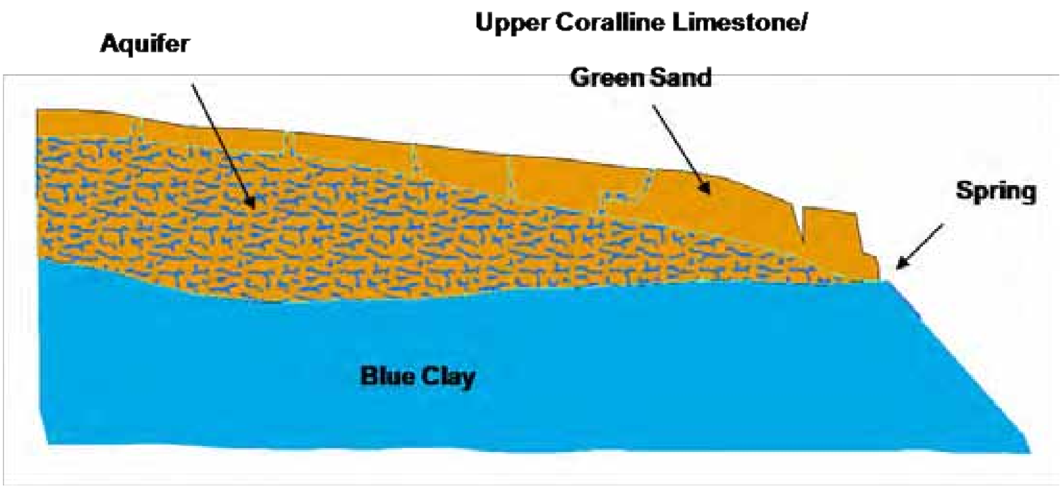

Figure 4.11: Water infiltration scheme.

Figure 4.12: Canes along the Cathedral bastion boundaries, Area B (February 2008).

4.1.4 Geotechnical Settings

Mdina, the former capital of Malta, is an old city located in the centre of the island. It is built on the top of a 5–6 meters thick rigid limestone plate (Upper Coralline Limestones) (4.3) overlying a thick clayey layer (Blue Clay) [50]. Over the years, the city has been influenced by many cultures. In 1693 it was extensively damaged by the Val di Noto (Sicily) earthquake [51], and most of the buildings and bastions were constructed after-wards [49]. The geological setting of the area is responsible for the occurrence of several damages on many buildings and bastion walls located in the perimetral sectors of the city [53, 52].

The geological setting of Mdina area dominated by the superimposition of a stiff and brittle limestone plate, belonging to the Upper Coralline Limestone Formation, on a clayey layer of the Blue Clay Formation. The mechanical characteristics of the materials comprising the rock slab – soft substratum system are very different in terms of strength, stiffness and brittleness, leading to typical morphological processes such as ductile phenomena in the underlying unit and brittle ruptures within the overlying rock masses. The latter are often linked to major joints that isolate large blocks. The bastion and buildings in the investigated areas were built in different periods and are founded both on the rock slab and on the clayey unit. The damage to the bastions and buildings is therefore associated to differential movements produced by different mechanical behavior of the underlying materials or UCL block displacements. In fact the UCL rock mass is quite thin; this leads to rock fragmentation, located mainly along the plate borders. Furthermore, in the study areas this process is enhanced by the presence of unfavorably orientated discontinuity sets with respect to instability mechanisms.

4.1.5 Carried out surveys

4.1.5.1 Geomechanical survey

The mechanical properties of the rock mass and discontinuities were derived from geomechanical survey data. The survey was carried out according to ISRM (International Society for Rock Mechanics) [15] suggested methods.

Intact rock properties In order to state the UCL intact rock tensile and compressive strength a number of point load tests have been performed, following ISRM (1985) suggested methods. With this test a rock sample is broken in tension by applying a vertical and punctual load.

The standard Point Load Index ($I_{s(50)}$) is defined:

$$I_s(50) = \frac{P}{D^2}$$

where P is the applied force at failure (in N) and D = 50mm is the diameter of a standard core.

For other core sizes the $\frac{P}{D^2}$ is retained, and can be multiplied by a size correction factor F:

$$I_s(50) = \frac{FP}{D^2}$$

where F = $\left(\frac{D}{50}\right)^{0.45}$ For shapes other than cores, an equivalent core diameter (D_e) is calculated:

$$D_e^2 = \frac{4WD}{\pi}$$

where W is the mean sample width and D is the sample height in the direction of loading. Thus, the standard index can be obtained:

$$I_s(50) = \frac{FP}{D_e 2}$$

The point load index value ($I_{s(50)}$) can be used to derive intact rock tensile (σ_t) and compressive (σ_c) strength by means of empirical equations:

$$\sigma_t = -1.3 I_{s(50)}$$

$$\sigma_c = 1.3 m I_{s(50)}$$

where

$$m = \frac{\sigma_c}{\sigma_t}$$

In accordance with ISRM (1985) suggested methods, 10 tests were carried out on irregularly shaped UCL samples (4.1); the Is(50) value is obtained by excluding the two highest and lowest values and averaging the remaining.

The calculated value is: Is(50) = 2.14 MPa

By considering a value of m = 8 for the UCL intact rock:

$$\sigma c = 22.3\text{MPa}.\ 23\sigma t = -2.8\text{MPa}.$$

These values are higher than those obtained by other studies [54]. It is possible that rock strength characteristics vary considerably in space; moreover the employed method is also different. New tests are scheduled once the monitoring program will be carried out and new samples will be available.

sample	D (mm)	W1 (mm)	W2 (mm)	W medio (mm)	P (N)	F	De ^2	Is 50 (Mpa)	σ_t (Mpa)	σ_c (Mpa)
1	41	107	102	104.5	7000	1.192	5457.962	1.529	1.99	15.90
3	45	90	88	89	7000	1.174	5101.911	1.611	2.09	16.75
7	44	94	95	94.5	8000	1.184	5296.815	1.788	2.32	18.60
5	52	94	95	94.5	10000	1.229	6259.873	1.964	2.55	20.42
8	46	89	91	90	9000	1.183	5273.885	2.019	2.62	20.99
2	43	103	95	99	10000	1.190	5422.93	2.195	2.85	22.83
9	46	92	97	94.5	11000	1.196	5537.58	2.376	3.09	24.71
6	46	86	90	88	11000	1.177	5156.688	2.511	3.26	26.11
4	47	79	90	84.5	12000	1.172	5059.236	2.780	3.61	28.91
10	49	97	104	100.5	15000	1.230	6273.248	2.941	3.82	30.59
						media		**2.14**	**2.78**	**22.28**

Table 4.1: Point load test results for the UCL formation. D: sample height; W: sample width; P: load at failure; F: size correction factor; Is50: point load index. The excluded values are highlighted.

4.1.5.2 Geomechanical characterization of discontinuities

Quantitative characterization of discontinuities ISRM (1978) suggested methods were employed for the quantitative description of discontinuities in rock masses[15]. In order to collect geometrical and mechanical properties of discontinuities, a geomechanical survey based on the scanline method was performed. Unfortunately, due to the poor surface of UCL outcrops, we were able to trace only two scanlines, located near the Vilhena Palace area (4.13).

Figure 4.13: Geomechanical survey: Scanline 1 (December, 2007).

For each scanline (varying from 35 to 45m in length) we filled a form by investigating all crossing discontinuities. The scanline locations are reported in 4.3 and the scanline 1 form is shown in

The complete form of geomechanical characterization of discontinuities and the synthesis form are reported in Appendix 1.

Discontinuity sets Discontinuities do not occur at completely random orientations, but for specific mechanical reasons. They have therefore a certain degree of clustering around preferred orientations associated with the formation mechanisms. For these reasons it is convenient to consider groups of parallel or sub-parallel discontinuities, generating a so called set. With the aim of identifying the major sets, discontinuity orientation data have been plotted on a stereographic projection (lower hemisphere). By observing 4.14, four main sets can be identified (dipdir/dip):

Jn1: 272/75° 27

Jn2: 104/76°

Jn3: 314/81°

Jn4: 075/76°

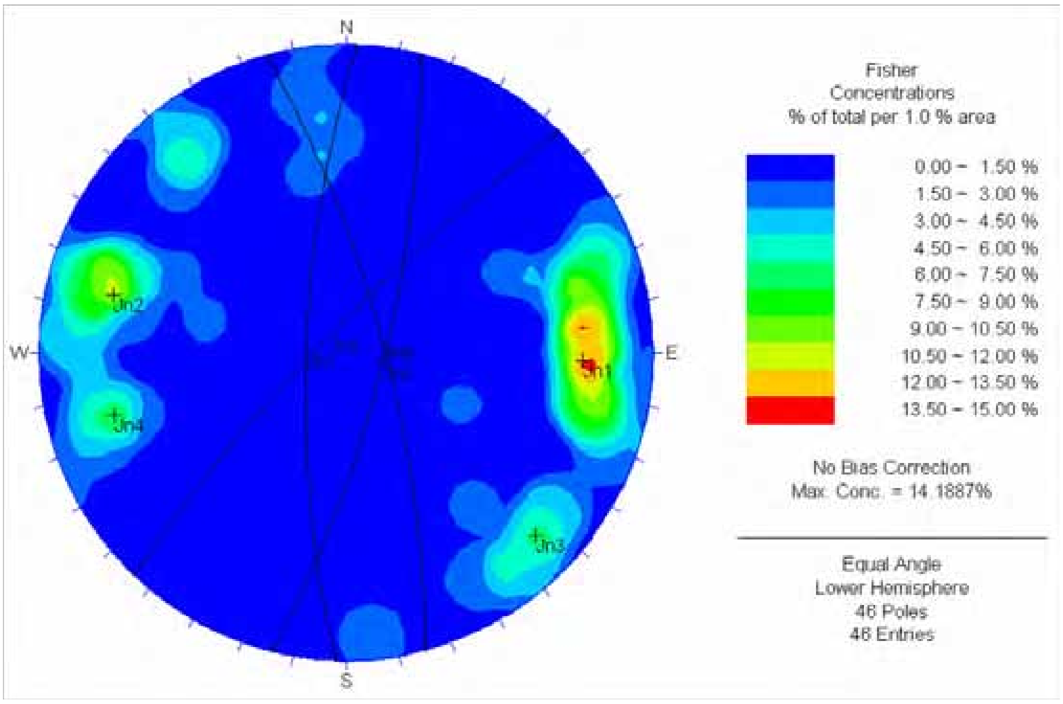

Figure 4.14: Stereographic projection and discontinuity set selection.

As we collected systematic data only in the aforementioned location (4.13), in order to extend the rock mass mechanical properties to the other study areas, we took some random discontinuity orientation measurements, which partially confirmed the spatial distribution of the identified discontinuity sets. With the execution of boreholes, during the monitoring program, we'll be able to identify local discontinuities and to better adapt the geostructural model to the specific site.

4.1.5.3 Mechanical properties of discontinuities

All rock masses contain discontinuities such as bedding planes, joints, shear zones and faults. At shallow depth, where stresses are low, failure of the intact rock material is minimal and the behavior of the rock mass is controlled by sliding on the discontinuities. In order to Analise the stability of this system of individual rock blocks, it is necessary to understand the factors that control the shear strength of the discontinuities which separate the blocks.

Since natural discontinuities do not have a perfectly smooth surface, their shear resistance will be affected by wall strength, surface roughness and normal stress. The empirical Barton criterion [55] describes discontinuities behavior with the following analytical expression:

$$\tau = \sigma_n \tan\left[\phi_r + JRC \cdot \log\left(\frac{JCS}{\sigma_n}\right)\right]$$

where JRC is the joint roughness coefficient, JCS is the joint wall compressive strength σn is the normal stress and φr is the residual friction angle. The joint roughness coefficient JRC is a number that can be estimated by comparing the appearance of a discontinuity surface with standard profiles published by Barton & Choubey (1977) and varies within the range from 0 to 20, increasing with wall surface roughness. JCS can be estimated using the Schmidt hammer; the rebound resulting from the impulse given to the rock wall by a spring loaded mass is given in a numerical range from about 10 to 60. In order to determine the joint wall compressive strength we applied the following relation:

$log(jcs) = 0.00088 \cdot \gamma \cdot R_{corr} + 1.01$

Regarding residual friction angle, Barton & Choubey (1977) suggest that φrcan be estimated from:

$\phi_r = \left(\phi_b - 20^{\circ}\right) + 20^{\circ}\left(\frac{r}{R}\right)$

where r is the Schmidt rebound number on wet and weathered fracture surfaces, R is the Schmidt rebound number on dry unweathered surfaces and $\varphi b$is the basic friction angle. The basic friction angle was determined with tilt tests executed on artificially sawn discontinuity surfaces. The obtained value for the UCL formation is: $\varphi b = 32.3°$. In the case of small scale laboratory specimens, the scale of the surface roughness will be approximately the same as that of the profiles illustrated. However, in the field the length of the surface of interest may be several meters or even tens of meters and the JRC value must be estimated for the full scale surface.

Barton & Bandis (1982) proposed the scale corrections for JRC defined by the following relation:

$JRC_n = JRC_0\left(\frac{L_n}{L_0}\right)^{-0.02\times JRC_0}$

where JRC_0, and L_o (length) refer to 100 mm laboratory scale samples and JRC_n, and Ln refer to in situ block sizes.

Because of the greater possibility of weaknesses in a large surface, it is likely that the average joint wall compressive strength (JCS) decreases with increasing scale. Barton & Bandis (1982) proposed the scale corrections for JCS defined by the following relation:

$JCS_n = JCS_0\left(\frac{L_n}{L_0}\right)^{-0.03\times JRC_0}$

where JCS_0, JRC_0 and L_o (length) refer to 100 mm laboratory scale samples and JCS_n, and Ln refer to in situ block sizes. JRC, JCS, JRC_n and JCS_n values for each discontinuity set are reported in the synthesis form. Most of the stability analysis are expressed in terms of the Mohr-Coulomb parameters. However it has been demonstrated that the relation between shear strength and normal stress is more accurately represented by a non-linear relation. Therefore it is necessary to devise some means for estimating the equivalent cohesive strengths and angles of friction from such relation. To solve this problem we can define the instantaneous cohesion ci and the instantaneous friction angle $\varphi i$for a normal stress σn.

These quantities are given by the intercept and the inclination, respectively, of the tangent to the non-linear relation between shear strength and normal stress (4.15).

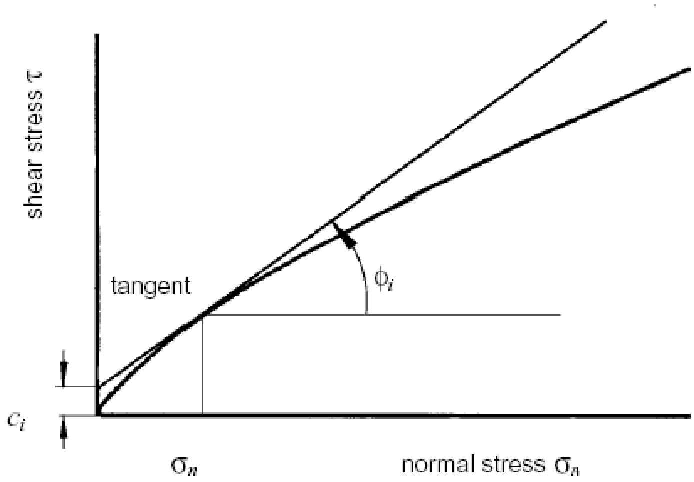

Figure 4.15: Instantaneous cohesion $(ci)$and friction angle $(\varphi i)$for a non linear failure criterion [114].

For each discontinuity set, mean cohesion and friction angle were determined, considering a normal stress interval between 0 and 0.4 MPa. 4.16 deals with shear resistance parameter determination for discontinuity set Jn1. Mohr Coulomb equivalent parameters for all sets are reported in

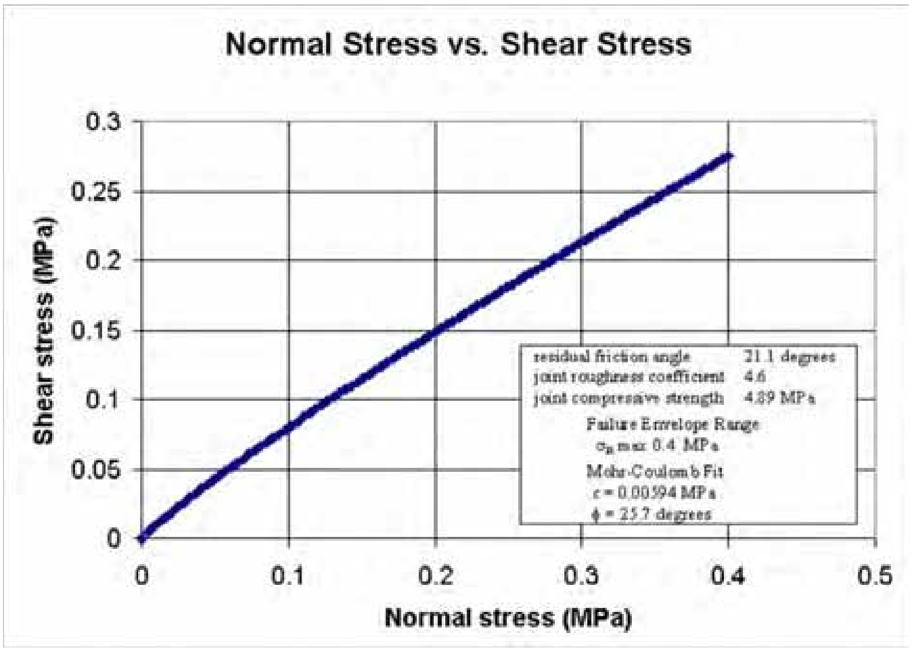

Figure 4.16: Barton non linear relation between shear and normal stress, and Mohr Coulomb equivalent parameters determination for discontinuity set Jn1.

Rock mass characterization

4.1.5.4 Rock mass classification

Several authors have developed rock mass classification schemes, which consider some of the key rock mass parameters and assign numerical values based on the class within which these parameters lie. This approach provides a shortcut to the main rock mass properties, and provides direct guidance for engineering design.

The rock mass has been classified based on the two main classification methods: the Rock Mass Rating (RMR) system [56], and the Q system [57]. The following six parameters are used to classify a rock mass using the RMR system:

1. Uniaxial compressive strength of rock material.
2. Rock Quality Designation (RQD).
3. Spacing of discontinuities.
4. Condition of discontinuities.
5. Groundwater conditions.
6. Orientation of discontinuities.

In applying this classification system, the rock mass is divided into a number of structural regions and each region is classified separately. The ratings for the first five parameters listed are summed to yield the basic Rock Mass Rating for the study area (RMRb).

Finally the Rock Mass Rating is adjusted by including the sixth parameter regarding the influence of the direction of discontinuities (RMRc). reports parameter ratings for the UCL rock mass, according to RMR system [56]. The obtained basic Rock Mass Rating is RMRb = 58 typical of fair rock;

however, considering a very unfavorable discontinuity orientation for building foundations , the corrected rating is: RMRc = 33.

The other employed classification (tuneling Quality Index, Q) has been proposed by Barton et al. (1974) for the determination of rock mass characteristics and tunnel support requirements. The numerical value of the Q index varies on a logarithmic scale from 0.001 to a maximum of 1000 and is defined by:

$$Q = \left(\frac{RQD0{,}1}{Jn}\right) \times \left(\frac{Jr}{Ja}\right) \times \left(\frac{Jw}{SRF}\right)$$

where RQD is the Rock Quality Designation; Jn is the joint set number; Jr is the joint roughness number;Ja is the joint alteration number; Jw is the joint water reduction factor; SRF is the stress reduction factor.

.

The resulting value is: $Q = 0.11$

typical of very poor-extremely poor rock masses.

4.1.5.5 Rock mass properties

Rock mass geomechanical characteristics depend both on intact rock properties and discontinuity net properties. One of the most widespread criteria for obtaining estimates of the strength of jointed rock masses is the Hoek & Brown criterion [6, 110]. It is based upon an assessment of the interlocking of rock blocks and the condition of the surfaces between these blocks. The generalized Hoek & Brown criterion [111] is expressed in terms of principal stress as:

$$\sigma_1' = \sigma_3' + \sigma_{ci} \cdot \left(m_b \frac{\sigma_3'}{\sigma_{ci}} + s\right)^a$$

where σ_{ci} is the compressive strength of the intact rock, m_b is a reduced value of the material constant m_i and is given by :

$$m_b = m_i \cdot \exp \cdot \left(\frac{GSI-100}{28-14D}\right)$$

s and a are constants for the rock mass given by the following relation:

$$s = \exp \cdot \left(\frac{GSI-100}{9-3D}\right)$$

$$a = \frac{1}{2} + \frac{1}{6}\left(e^{\frac{GSI}{15}} - e^{\frac{20}{3}}\right)$$

D is a factor which depends upon the degree of disturbance to which the rock mass has been subjected by blast damage and stress relaxation. It varies from 0 for undisturbed in situ rock masses to 1 for very disturbed rock masses. GSI is the Geological Strength Index, introduced by Hoek (1994) and Hoek et al. (1995). With this system it is possible to estimate the reduction in rock mass strength for different geological conditions This system is suited for blocky rock masses and for heterogeneous rock masses such as flysch [58]. UCL rock mass parameters are presented in the synthesis form (4.17).

SCHEDA DI SINTESI PER LA DESCRIZIONE DELL' AMMASSO ROCCIOSO (DST - UNIFI)

DATI GENERALI

N. Scheda: 1_2	Località: Mdina	Stazione: Mdina - UCL
N. Foto:	Rilevatore: Gigli, Leoni, Mugnai	Data rilevamento: 10/12/2007

AFFIORAMENTO		**MATERIALE ROCCIA**			
Tipo (1):	2	Formazione:	**Upper Coralline Limestone**		
Immersione [°]:	30	Litologia:	Calcareniti organogene	Co lore:	Bianco
Inclinazione [°]:	85	Granulometria:		Tessitura:	
Altezza [m]:	4	Resistenza (3):	R2	Indice di Point Load [MPa]:	2.1
Larghezza [m]:	100	Note:			

LINEE DI STENDIMENTO

N.	orientazione		lungh.	No.disc.	freq.	RQD	Note
	α	β	L	N	λ=N/L	100(0.1λ+1)exp(-0.1λ)	
	[°]	[°]	[m]	[-]	[1/m]	[%]	
1	120	0	45	32	0.71	99.8	
2	120	0	35.5	14	0.39	99.9	

FAMIGLIE DISCONTINUITA'

	orientazione		spaziatura			persistenza				apert.	rugosità		resistenza			degrad.	riempim.		filtrazione	
sigla	α	β	x	θ	X=x|cosθ|	Tx	Td	Tr	L	e	JRC	JRCn	R	JCS	JCSn	r/R	tipo	resist.	tipo	portata
(2)	[°]	[°]	[m]	[°]	[m]	[%]	[%]	[%]	[m]	[mm]	[-]		[-]	[MPa]		[-]	(5)	(3)	(4)	[l/min]
JN1	272	75	4.1	31	3.51	58	7	35	1.3	9.8	11.1	4.60	14.4	18.34	4.89	0.44			U1-U2	
JN2	104	76	7.5	21	7.00	60	10	30	1.6	15.3	12.8	4.63	13.1	17.4	3.79	0.52			U1-U2	
JN3	314	81	5.6	17	5.38	88	6	6	1.6	15.6	14.6	4.58	18.5	21.66	3.81	0.71			U1-U2	
JN4	75	76	11.3	46	7.81	50	0	50	1.5	21.4	13	4.63	16.7	20.13	4.28	0.47			U1-U2	

DATI DI SINTESI SULLE FAMIGLIE DISCONTINUITA'

Sigla della famiglia:		**JN1**	**JN2**	**JN3**	**JN4**
angolo di attrito di base	ϕ_b (tilt test) [°]	32.3	32.3	32.3	32.3
angolo di attrito residuo	$\phi_r = (\phi_b\text{-}20)+20r/R$ [°]	21.1	22.7	26.5	21.7
angolo di attrito di picco	$\phi_p = 2\ JRC + \phi_b$ [°]	41.5	41.6	41.5	41.6
permeabilità	$k = (g\ e^3) / (12\ \nu\ X)$ [m/s]	0.22	0.42	0.58	1.03

PROIEZIONE STEREOGRAFICA

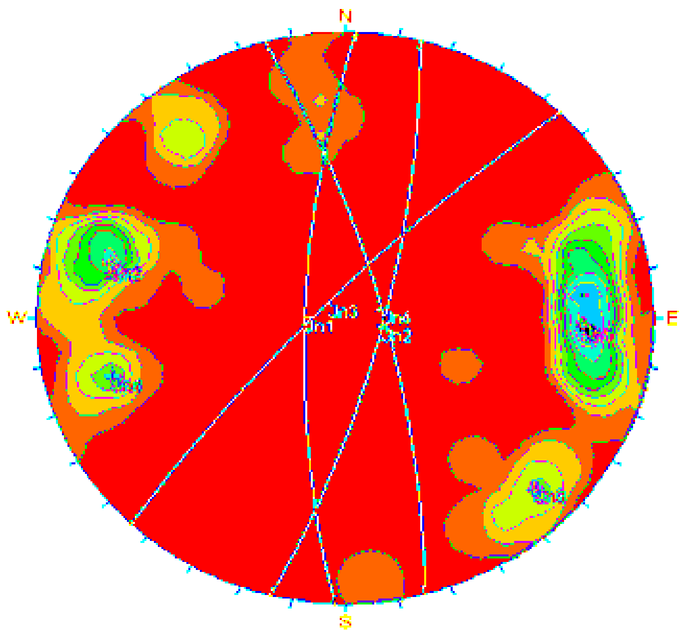

AMMASSO ROCCIOSO	
N. Famiglie	4
Degradaz. (6):	W3
Struttura (7):	I
Dim. blocchi (m3) (Palmstrom):	155.60
Lato blocco (cubico) m	5.29
indice Jv=Σ(1/X$_i$) [1/m3]	0.6
RQD=115-3.3Jv [%]	100.0
Classificazione di Bieniawski	
resistenza della roccia intatta	3
indice RQD	20
spaziatura delle discontinuità	20
condizioni delle discontinuità	0
acqua sotterrenea	15
RMR di base non corretto	58
RMR di base modificato	58
aggiustamento	-15
RMR corretto	43
Classificazione di Barton	
indice RQD	100
N. famiglie discont. Jn	15
N. rugosità discont. Jr	1
N. alterazione discont. Ja	8
Fattore riduz. tensioni SRF	7.5
Fattore riduz. acqua Jw	1
Q=(RQD/Jn)(Jr/Ja)(Jw/SRF)	0.11
Parametri geomeccanici	
GSI	55
m_i (roccia intatta)	8
σ_c (roccia intatta) [MPa]	22.3
m_b	1.604
s	6.7E-03
a	0.504
c [MPa]	0.248
phi	57
sigt [MPa]	-0.094
sigcm [MPa]	3.9
E [GPa]	6.3

(1) affioramento	**(3) resistenza**	**(4) filtrazione**	**(5) riempimento**	**(7) struttura**
1 - naturale	S1 - molto molle (<25kPa)	*Senza riempimento*	0 - assente	B - a blocchi
2 - scavo sup.	S1 - molto molle (<25kPa)	U1 - chiusa/secca	1 - coloraz. superficiale	L - lastriforme
3 - scavo sotteraneo	S2 - molle (25-50kPa)	U2 - aperta asciutta	2 - terra coesiva	C - colonnare
(2) tipo discont.	S3 - moder. consist. (50-100kPa)	U3 - aperta tracce flusso	3 - terra granulare	I - irregolare
BG - stratificazione	S4 - consistente (100-250kPa)	U4 - aperta umida	4 - cementazione	F - frantumato
JN - giunto	S5 - molto consistente (250-500kPa)	U5 - aperta bagnata	7 - calcite	**(8) dimens. blocchi**
FL - faglia	S6 - estem. consistente (>500kPa)	U6 - flusso continuo	8 - clorite, talco, gesso	*dimensione max :*
FR - fessura	R0 - estrem. debole (<1MPa)	*Riempimento*	9 - altro (specificare)	1 - molto grandi (>2m)
FS - fissilità	R1 - molto debole (1-5MPa)	F1 - asciutto	**(6) degradazione**	2 - grandi (0.6-2m)
ST - stilolite	R2 - debole (5-25MPa)	F2 - umido	W1 - inalterata	3 - medi (0.2-0.6m)
SC - scistosità	R3 - moder. resistente (25-50MPa)	F3 - bagnato	W2 - decolorata	4 - piccoli (0.06-0.2m)
CL - clivaggio	R4 - resistente (50-100MPa)	F4 - tracce dilavamento	W3 - moder. altrer. (<50%)	5 - molto piccoli (<0.06m)
FO - foliazione	R5 - molto resistente (100-250MPa)	F5 - localmente dilavato	W4 - fortem. alterata (>50%)	
VN - vena	R6 - estrem. resistente (>250MPa)	F6 - complet. dilavato	W5 - completam alterata	

Figure 4.17: UCL rock mass synthesis form.

Since most geotechnical software is still written in terms of the Mohr-Coulomb failure criterion, it is necessary to determine equivalent angles of friction and cohesive strengths for 34 each rock mass and stress range. This is done by fitting an average linear relation to the curvilinear criterion for a particular stress range of interest. Mohr Coulomb equivalent parameters c e φ 4.18 were obtained for low stress conditions by using roclab software [104].

Finally, the rock mass modulus of deformation is given by [111]:

$$E_m\,(GPa) = \left(1 - \frac{D}{2}\right) \cdot \sqrt{\frac{\sigma_{ci}}{100}} \cdot 10$$

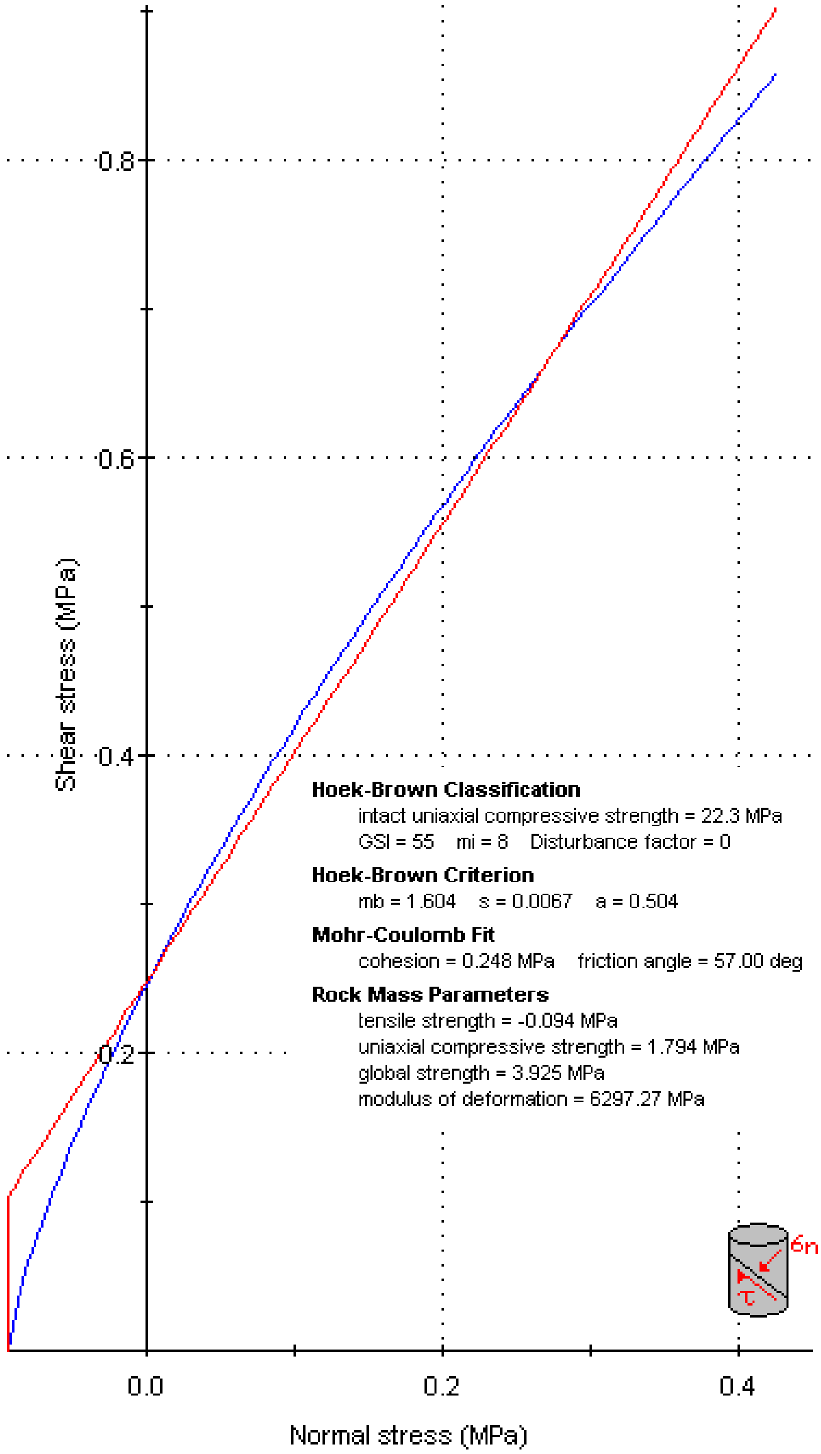

Figure 4.18: UCL equivalent Mohr Coulomb parameters (taken from [**?**]).

4.1.5.6 Kinematic analysis

By observing the crack distribution in the study areas (9.79.89.9), we can assert that it is mainly caused by differential movements due to different mechanical characteristics of the underlying materials. In addition, rigid block displacements along pre-existing or new discontinuity planes can occur. In fact, the shear resistance of discontinuities is much lower than the intact rock strength. Thus, the presence of unfavorably oriented discontinuity sets would enhance deformational mechanisms on the UCL slab, leading to major cracks on the overlying buildings and bastions. 4.19 shows the stereographic projection of discontinuity poles from the geomechanic survey with the local orientation of the UCL plate in the study areas. To quantify this attitude of the UCL rock mass we can make use of kinematical analysis principles. Although kinematical analysis applies to sub aerial slopes, we can extend this concept to a buried rock plate, such as the UCL rock mass underlying the town of Mdina. The aim of this study is to demonstrate that damages on buildings and ground displacements observed in the study areas are enhanced by the presence of unfavorable discontinuity sets, riving the UCL plate. It is important to remark that the geostructural survey was performed near the Vilhena Palace area and, although random measures suggest a possible extendibility of identified sets over the entire area, they have to be integrated with borehole discontinuity information. For this reason, while this analysis is reliable for Vilhena Palace area, results for Cathedral and Magazines areas must be taken with care. The term kinematic refers to the study of movement, without reference to the forces that produce it. This kind of analysis is able to establish when a particular instability mechanism is kinematically feasible, given the geometry of the slope and discontinuities.

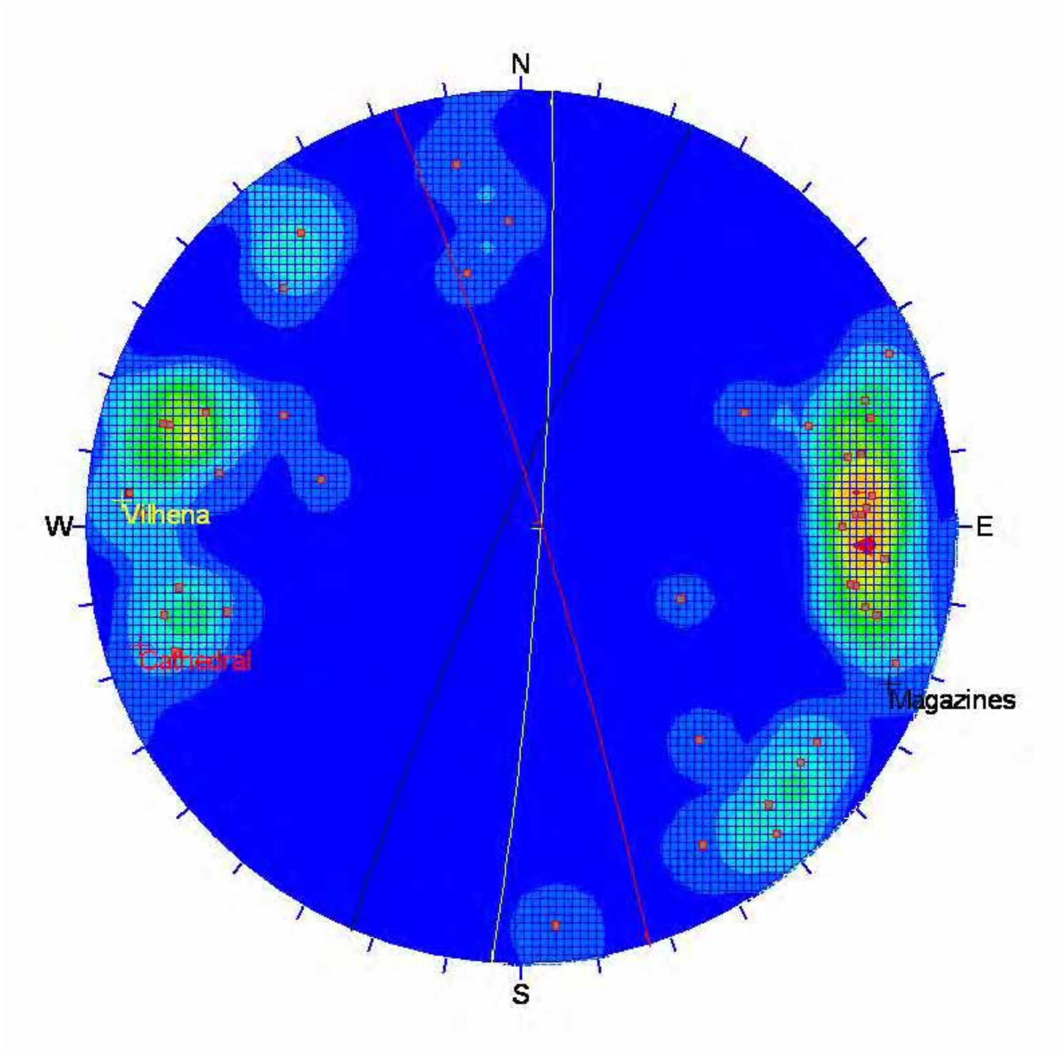

Figure 4.19: Study area orientations and identified discontinuity planes.

The main instability mechanisms investigated with this approach are (4.20):

- plane failure [95];
- wedge failure [95];
- block toppling [59];
- block toppling and sliding; • flexural toppling [95][96].

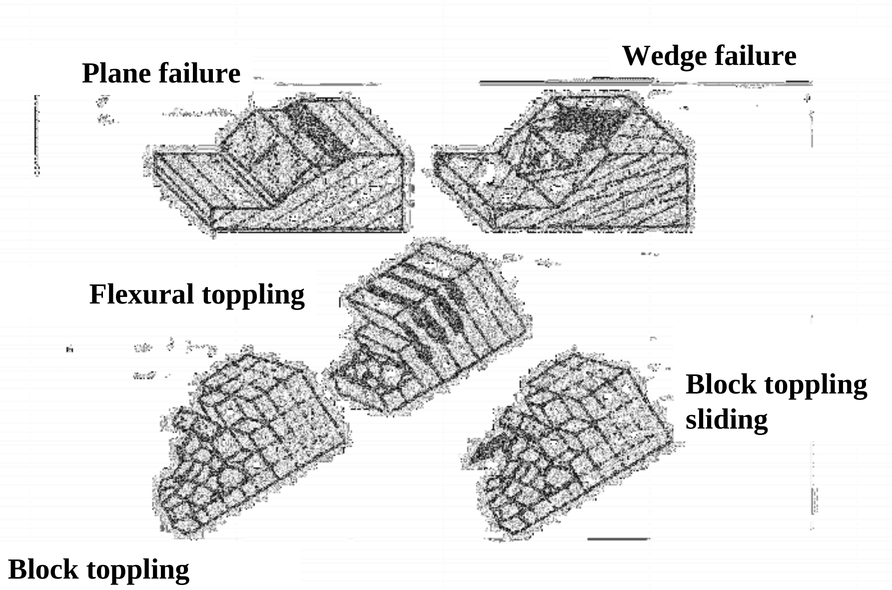

Figure 4.20: Instability mechanisms in rock slopes (taken from [48].

Quantitative kinematic analysis Casagli & Pini (1983) [60]introduced a kinematic hazard index (indice di pericolosità cinematica) for each instability mechanism. These values are calculated by counting poles and discontinuities falling in critical areas:

Npf = number of poles satisfying plane failure conditions;

Iwf = number of intersections satisfying wedge failure conditions;

Nbt = number of poles satisfying block toppling conditions;

Ibt = number of intersections satisfying block toppling conditions;

Nft = number of poles satisfying flexural toppling conditions.

The kinematical hazard index are calculated as follows:

$C_{pf} = 100\times(\frac{N_{pf}}{N})$ for plane failure;

$Cwf = 100\times(\frac{I_{wf}}{I})$ for wedge failure;

$Cbt = 100\times(\frac{N_{bt}}{N})\times(\frac{I_{bt}}{I})$ for block toppling;

$Cts = 100\times(\frac{N_{pf}}{N})\times(\frac{I_{bt}}{I})$ for block toppling and sliding;

$Cft = 100\times(\frac{N_{ft}}{N})$ for flexural toppling.

By using a specific software [60] we can load a great number of discontinuities with different friction angles. Intersection lines are calculated automatically (4.14) together with the equivalent friction angle, based on the intersecting planes friction angles and the shape of the wedge [60].

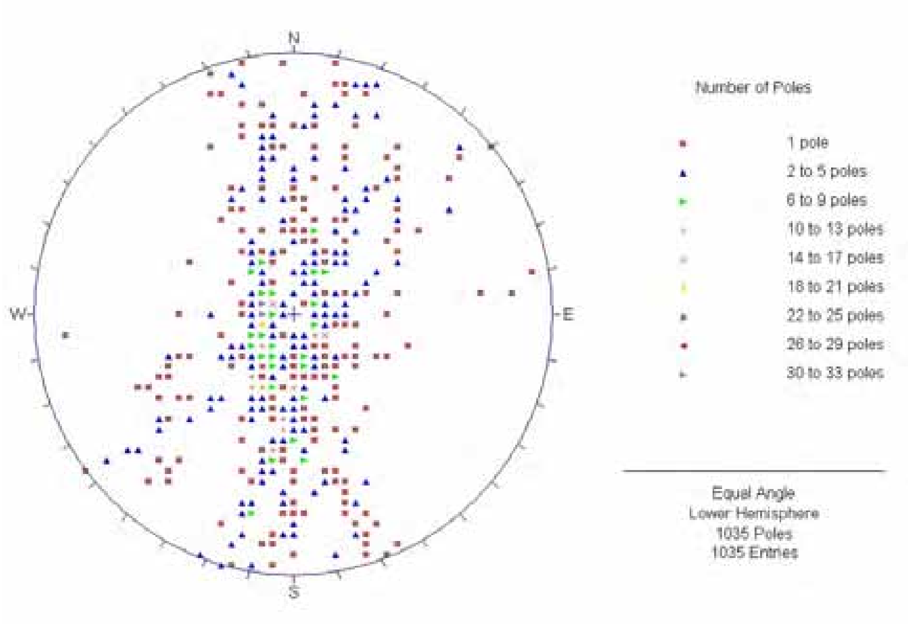

Figure 4.21: Stereographic projection of the intersection lines between observed discontinuity planes.

The employed quantitative approach considers a fixed slope dip; the kinematic hazard index for each instability mechanism is then calculated by varying the slope dip direction from 0 to 360°. Given a certain slope dip, it is therefore possible to identify the most unfavourable slope orientations for the main instability mechanisms. The results of the analysis are presented in 4.22, where the kinematic indexes are plotted for each slope dip direction; yellow rectangles indicate the dip direction range for each study area. All the study areas are associated with slopes oriented unfavourably with respect to instability mechanisms, with high kinematic hazard indexes (ranging from 20% to 35%).

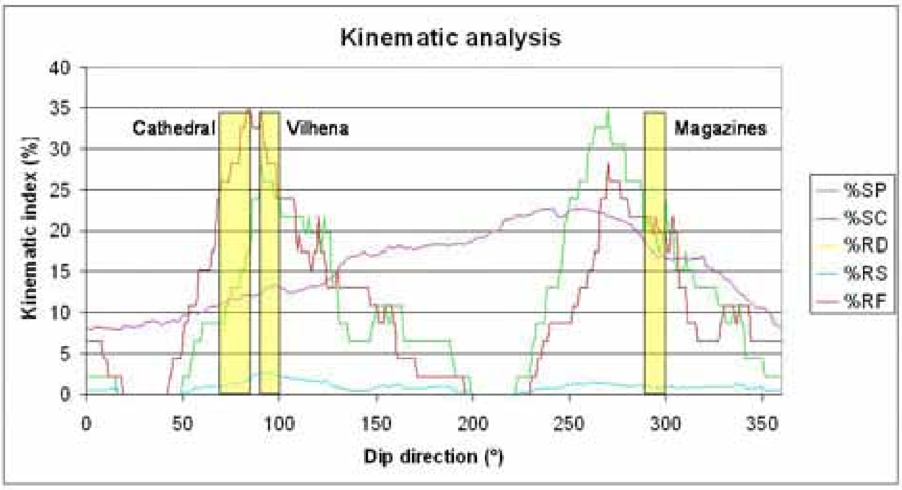

Figure 4.22: Constant dip quantitative kinematical analysis. Yellow rectangles indicate the dip direction range for each study area. (SP: plane failure; SC: wedge failure; RD: block toppling; RS: block toppling and sliding; RF: flexural toppling).

4.1.6 Laser Scanner Survey

The Laser Scanning technique is more and more used for instability analyses in cultural heritage sites [61, 62, 63, 64], as it allows to obtain, in a short time, a detailed and high accuracy 3-D representation of both the ground and the structures built on it. We applied this technique in order to reconstruct the 3-D model of some areas of the city of Mdina, which are experiencing serious instability problems.

Thanks to the high resolution of the point cloud we have been able to draw an accurate 3-D map of cracks, the main displacement vectors of the structures and to identify the associated instability mechanisms. Acknowledgements. This study has been performed within the “Service Contract for the provision of geotechnical engineering consultancy and project management services in relation with the consolidation of the terrain underlying the bastion walls and historic places of the city of Mdina, funded by the ERDF for Malta and carried out by a consortium led by Politecnica Ingegneria e Architettura for the MRRA, Works Division, Restoration Unit, Floriana, Malta [19].

Laser Scanner survey of the study areas, in order to build a 3D digital model of both the structures and the slopes of the intervention areas. A long range 3d laser scanner (RIEGL LMSZ410-i) has been employed (4.23). In order to cover completely the intervention areas several surveys from different scan positions were performed. The different point clouds were subsequently linked to a project reference system with the aid of reference points, whose coordinates were defined by using a gps device. Three different projects were built, according to the number of the study areas. Area A was covered by 26 different scan positions, and area B and C by, respectively by 12 and 18 scan positions. A total of more 200 million points and 250 high resolution digital images were taken.

Figure 4.23: Laser Scanner Tool - LMS-Z420i during a Scanning on Mdina bastion walls (November, 2007).

During the campaign, which took place from November 21st to December 8th, detailed geologic, and geomechanical surveys were also carried out, with the aim of correlating local stratigraphy (obtained from past and future geognostic and geophysical surveys) and soil - rock mass geotechnical characteristics with overlying structures, damaged areas and instability phenomena. All the gathered information will be subsequently integrated within a GIS platform.

After the campaign we have been processing all the acquired data 4.274.284.294.244.254.26 and performing laboratory analyses (point load and tilt tests) on the collected samples.

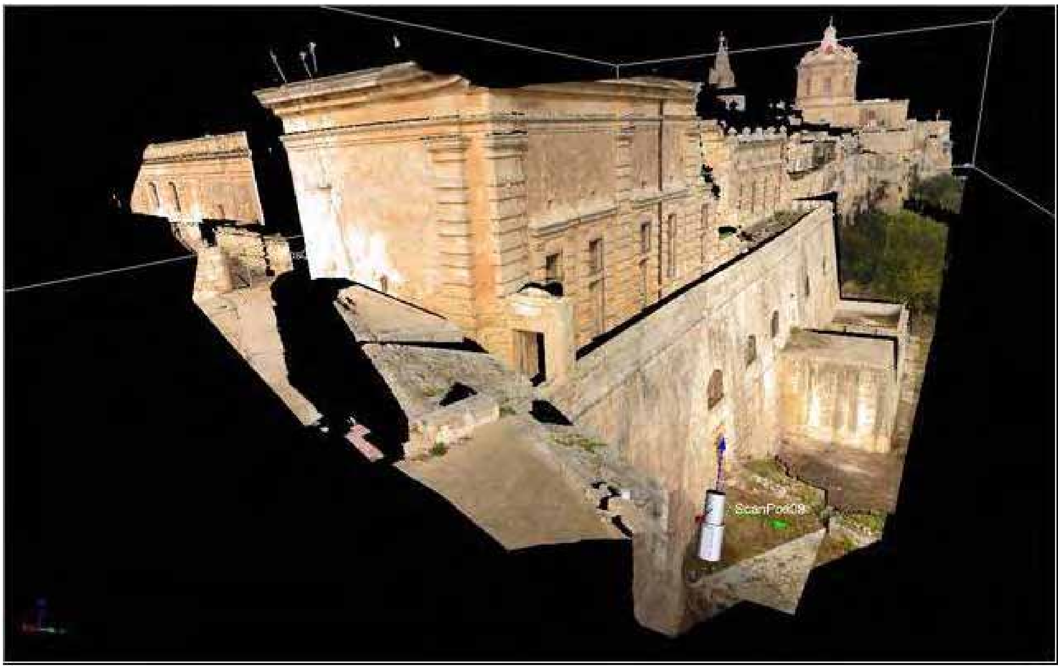

Figure 4.24: Area A: scan position 09 - true colored point cloud.

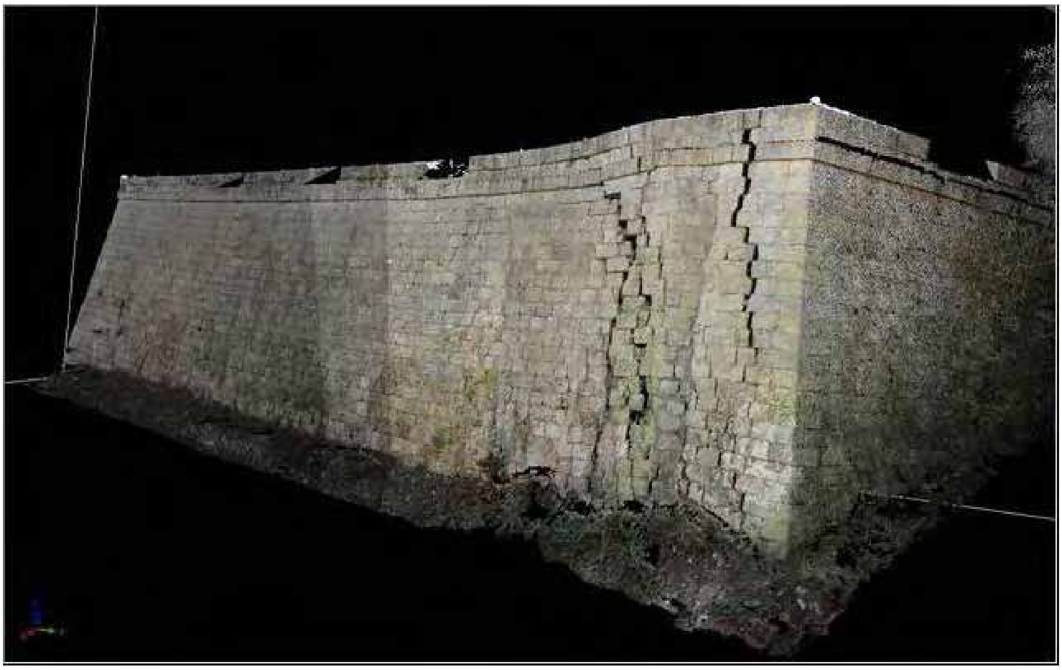

Figure 4.25: Area B: scan position 10 - true colored point cloud.

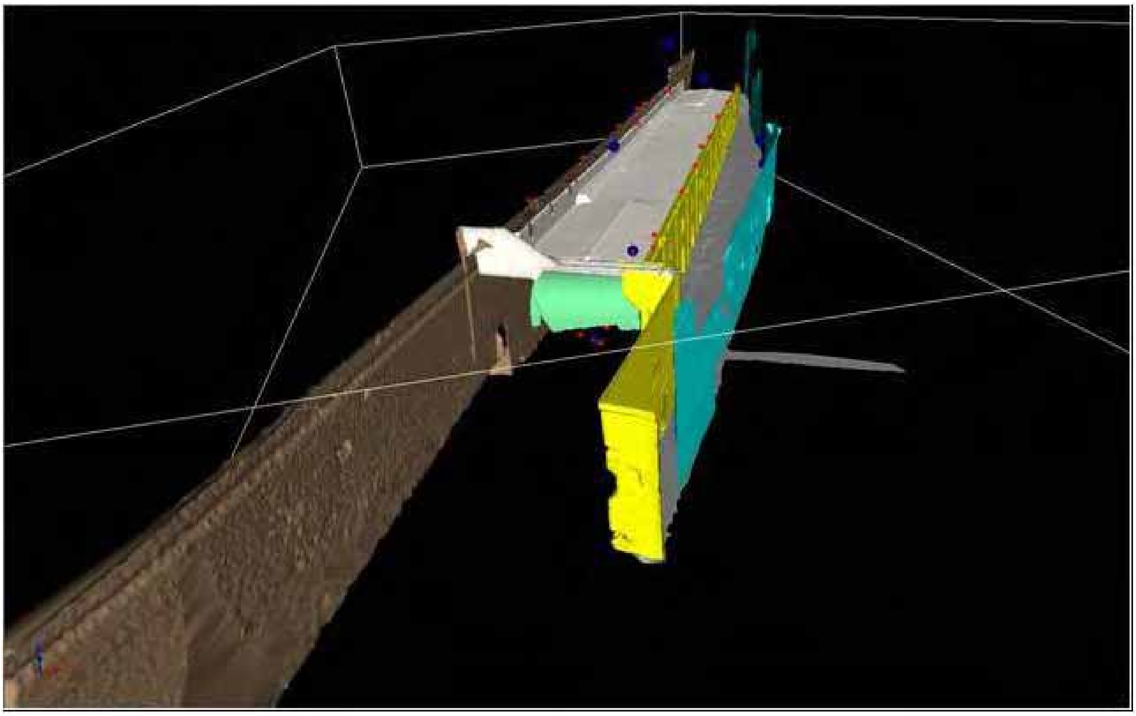

Figure 4.26: Area C: triangulated surface from the different point clouds. Blue and red dots represent respectively the scan positions and the reflectors.

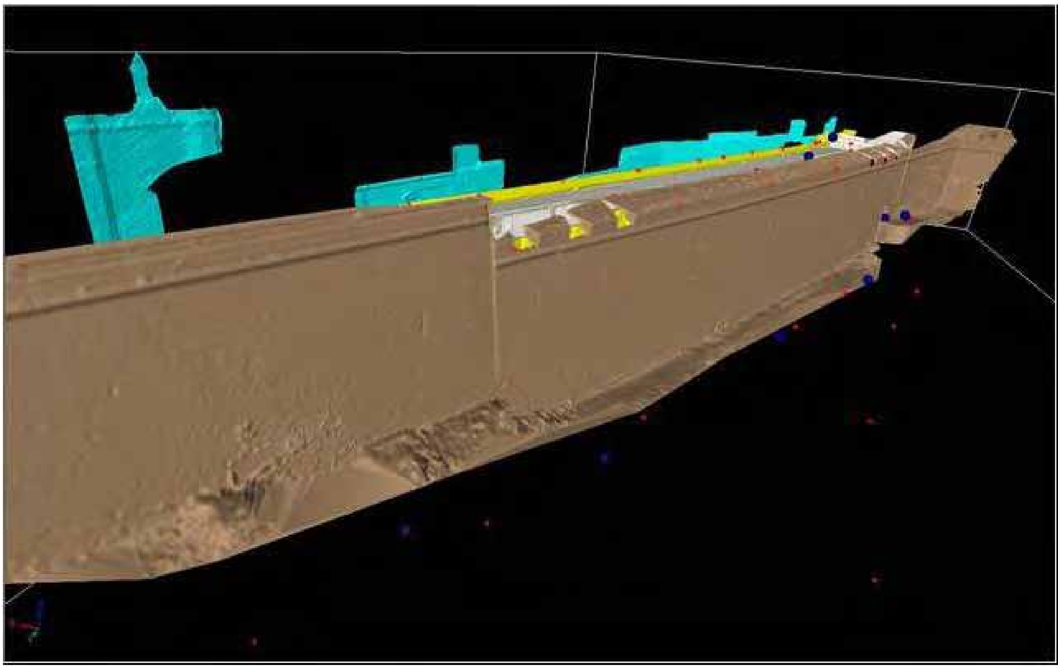

Figure 4.27: Area C- (Back view): triangulated surface from the different point clouds. Blue and red dots represent respectively the scan positions and the reflectors.

Figure 4.28: Intensity coloured point cloud of the roof of the Magazine Curtain.

Figure 4.29: Area C. True coloured point cloud of the Magazine Curtain.

4.1.7 Monitoring System - Wireless Sensor Network -

The network design We have developed the monitoring project as a result of a collaboration with the Politecnica Ingegneria e Architettura. The monitoring system is designed to be installed within a city environment. He must therefore have a low visual impact and yet be widely disseminated in the ravines, roads, walls and gardens. The choice was therefore directed to the use of a network of wireless sensor network placed inside a prototype monitoring platform for structural instability in urbanized environments with hydrogeological problems.

The monitoring system was installed in Mdina (Malta) within the contract for the ground investigation works and the monitoring system regarding the bastion walls. The system has delivered by GDTest in all of its sections according to the specifications of the project we produced.

The city of Mdina has been divided into three areas to facilitate the time schedule of work and to separate the activities of study and restoration work at the design stage. The first includes the Vilhena Palace and the entire area enclosed by the outer wall (Zone A), the second includes the Despuig Bastion and the walls of the cathedral (Zone B) - and finally, the third area includes warehouses and the outer walls (Zone C) .

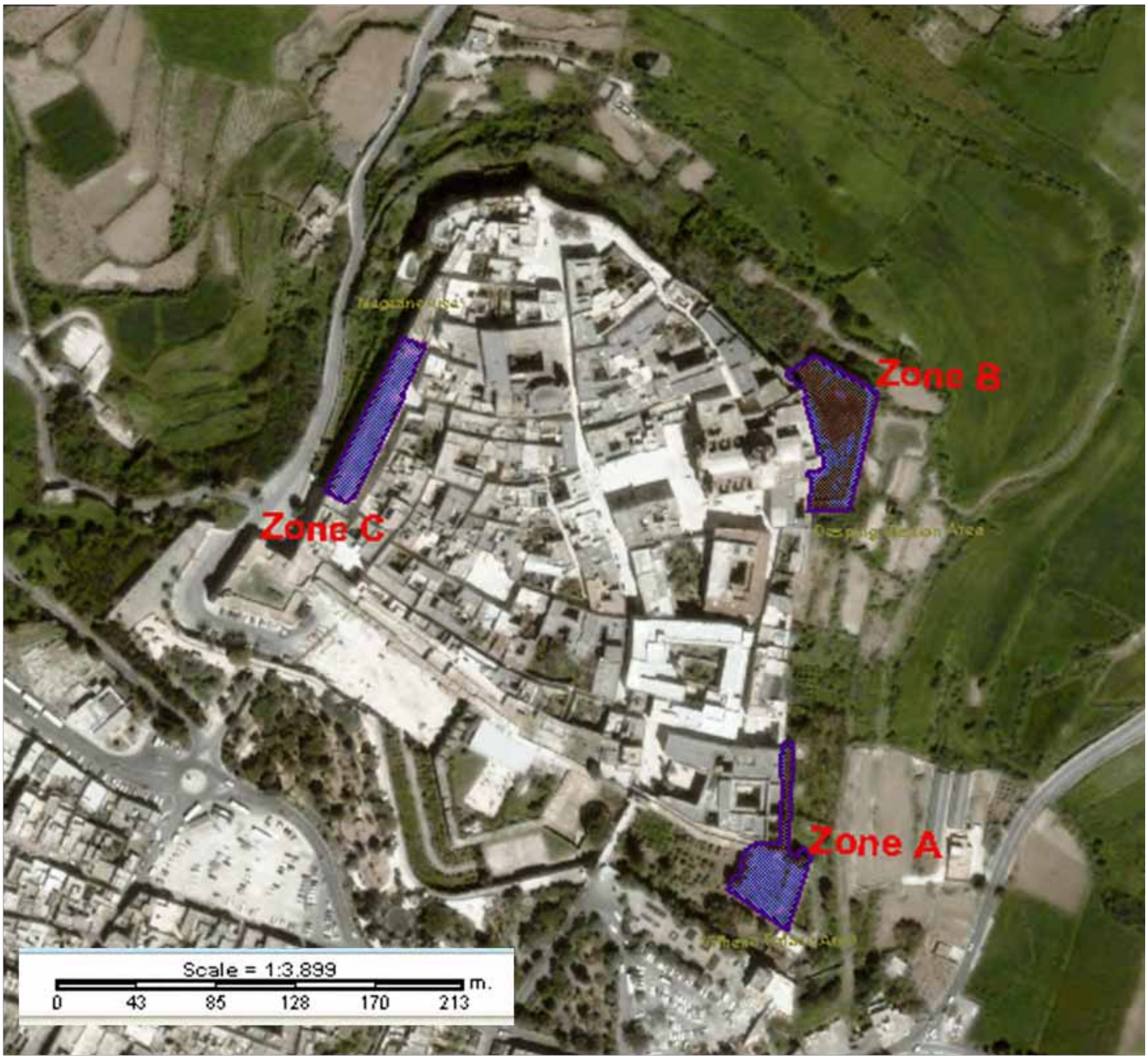

Figure 4.30: Localizzation map of the three zone A-B-C (modified from [5]).

4.1.7.1 System's Description

Every system's section is now perfectly functioning, after an initial period of testing and fining.

The system's sections are:

- Communication system
- Sensors
- Web-page interface

Communication system The installed monitoring system ueses a Wireless Datalogging System (WDS) developed by RIBES Tecnologie. WDS is a new system of monitoring data management developed for an

automatic acquisition of any type of geotechnical electrical instrument, collected in a central wireless unit.
The WDS is set up by 2 apparatus:

- A Local Transmitter Unit (LTU), with a two-channel unit 4.42.
- A Radio logger Acquisition Unit (RAU) for the wireless data collection.

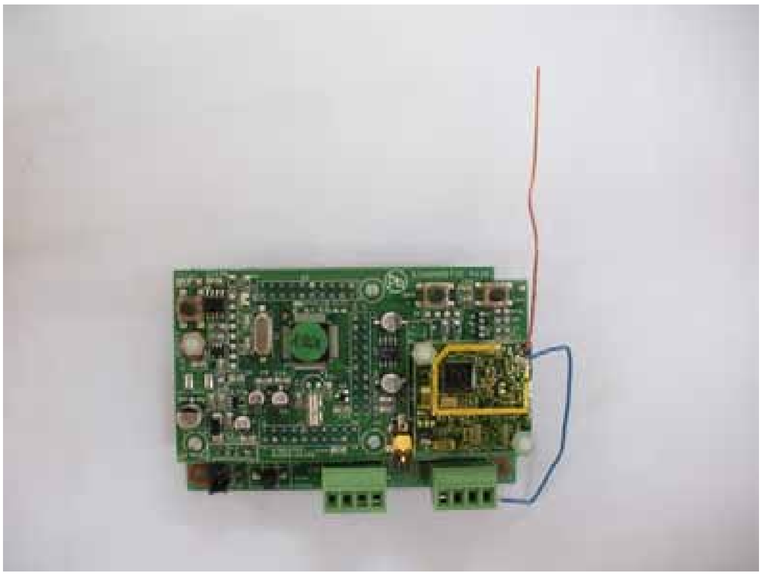

Figure 4.31: Loca Transmitter Unit (LTU).

(a) Radio Acquisition Unit (RAU).

(b) Visualizzation screen mounted on RAU.

(c) GPRS module installed on RAU.

Figure 4.32: Components of Radio Aquisition Unit (RAU).

For the WDS system there is also a repeater LTU, useful when the LTU are too far from the RAU. The LTU collected the samples data from very different type of vibrating wire electrical instruments (for example crack gauges, piezometeres, tiltmeters, etc.). The LTU can be wired to two different instruments, and its position is adopted to make easy manual readings and to facilitate the maintenance and a better radio transmission too. The LTU are equipped with a long duration battery that allow a collections data until six month long, in function of type of sensors, frequency of readings and environmental conditions. The frequency of readings can be programmed and the unit can store until 700 data readings that will be wire-less transmitting to the RAU. The RAU can be static type: installed inside a box with IP65 (completely waterproof) and supplied by the 220 V. The RAU can also be of portable type, when it's necessary to go near the instruments. For a complete monitoring system a RAU can collected of 100 LTU unit (200 instruments) that are installed at very different distances, and can collected until 150.000 data. The RAU can be wired in Ethernet modality by a dedicated switch, so the data goes to a computer in an office directly. The data collected are organized in numeric files named for every LTU installed, the data transmission can be automated by a dedicated server to control and publish on a Web-GIS portal.

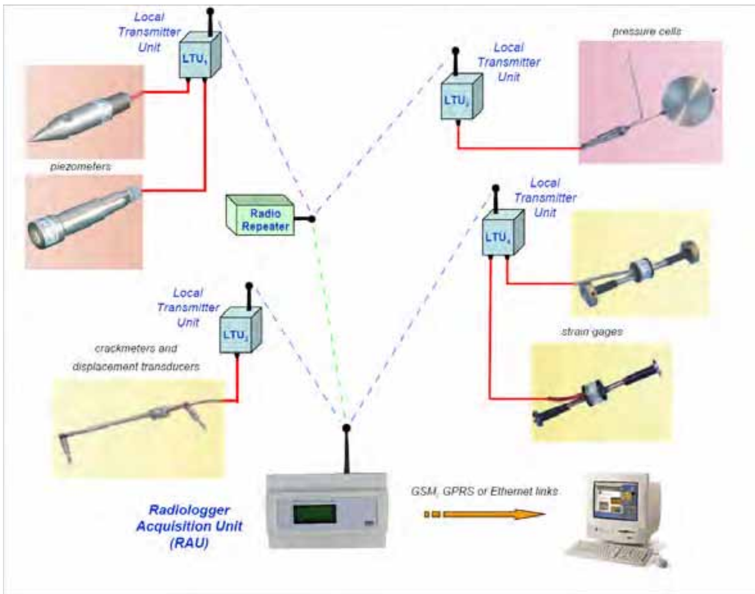

Figure 4.33: Scheme of the Wireless datalogging system (WDS), (taken from [65]).

Sensors

Piezometers (PZ): Appropriate groundwater measuring stations were installed in order to obtain data on the magnitude, variation and distribution of the heads of groundwater and pore pressures in the ground: we have installed n. 2 piezometers in this area.

The model used is a Encardio Rite (MODEL EPP-30V-XX).

Figure 4.34: Image of a installed Pore pressure gauge “Piezometer”, (taken from [100]).

The piezometer, also known as pore pressure meter, is used to measure pore water pressure in soil, earth/rock fills, foundations and concrete structures. It provides significant quantitative data on the magnitude and distribution of pore pressure and its variations with time. It also helps in evaluating the pattern of seepage, zones of potential piping and the effectiveness of seepage control measures undertaken. Proper evaluation of pore pressure helps in monitoring the behavior after construction and indicates potentially dangerous conditions that may adversely affect the stability of the structure.

Principle of operation

The Encardio-rite pore pressure meter basically consists of a magnetic, high tensile strength stretched wire, one end of which is anchored and the other end fixed to a diaphragm which deflects in some proportion to the applied pressure. Any deflection of the diaphragm changes the tension in the wire, thus affecting the resonant frequency of the vibrating wire.

The resonant frequency with which the wire vibrates can be accurately measured by a vibrating wire readout unit.

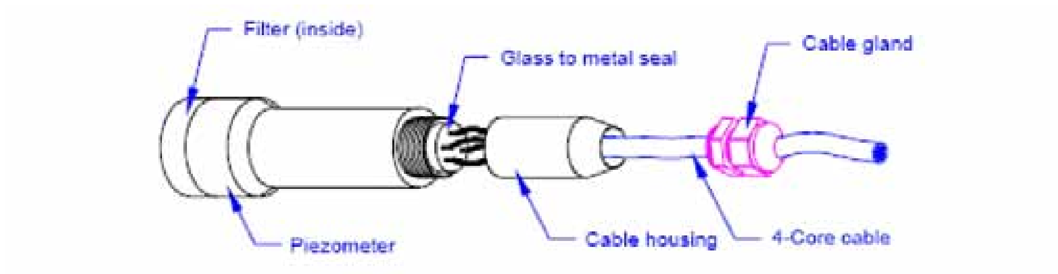

Figure 4.35: Piezometer technical scheme (taken from [100]).

Crack gouges(CG) In order to measure the relative movements of the cracks on the walls (opening and sliding) in the three areas. The main cracks were detected by the a crack pattern survey. The sensors were installed across the main cracks and wherever will be notice active displacements and will be connected to automatic wireless readout LTU.

The model EDJ-31/34V vibrating wire crack cauge from GEOKON, is suited for measurement of displacement/movement across joints. The model EDJ-31/34V vibrating wire crack cauge consists of a long cylinderical body. The central portion comprises of a metallic bellow that permits expansion or contraction. One end of the cylinder is provided with M12 threads which screw the meter through a flexible link into model EDJ-35V steel socket which is anchored and buried perpendicular to the contraction joint in a block of concrete. The steel socket is shown at the right in the picture on previous page. The flexible link reduces the possibility of damage to the crack cauge in case of a small lateral movement. The other end of the cylinder comprising of an end flange and cable joint housing is embedded in the concrete block on the other side. Thus the crack cauge is embedded across the joint, half on each side so as to be stretched when the joint opens and vice versa.

Figure 4.36: Crack gauge installed on a wall of Mdina, Area C..

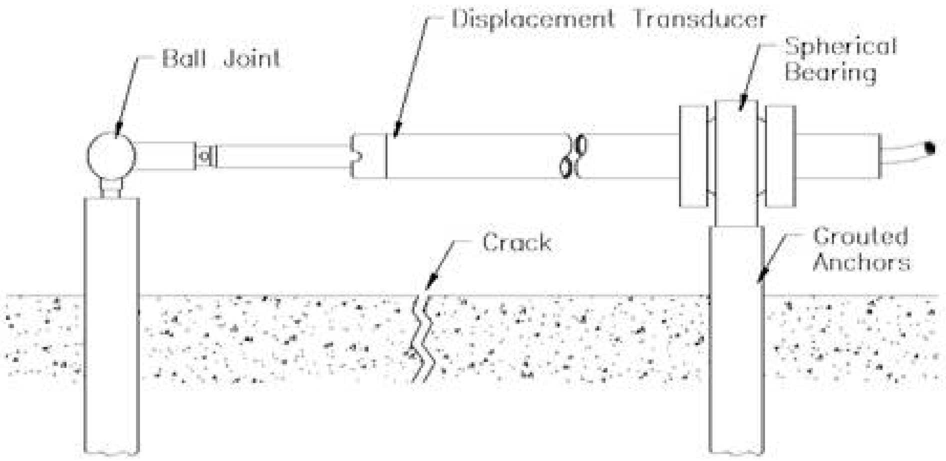

Figure 4.37: Crack Gauge MODEL EDJ-31/34V vibrating wire (taken from [100]).

Biaxial Inclinometer(BIN) They were installed on the masonry structures or on rock wedges in order to monitor tilt variations of x-y axis. The sensors are been connected to automatic wireless readout units LTU. The selection of location was been performed after a crack pattern survey.

The Model 6350 Tiltmeter is designed for attachment to structures, on either a vertical or horizontal surface by means of an adjustable bracket, and for the subsequent measurement of any tilting that may occur. When at rest, in a vertical configuration, a pendulous mass inside the sensor, under the force of gravity, attempts to swing beneath the elastic hinge on which it is supported but is restrained by the vibrating wire. As the tilt increases or decreases the mass attempts to rotate beneath the hinge point and the tension in the vibrating wire changes, altering its vibrational frequency. This frequency is measured using the Geokon Model GK-401, GK-403 or GK-404 Readout Box, or the Micro-Datalogger, and is then converted into an angular displacement by means of calibration constants supplied with the sensor. Advantages and Limitations Vibrating wire tiltmeters combine a high range with high sensitivity, and very high calibration accuracy. They have excellent long-term stability and their temperature dependence is close to zero. The sensor output is a frequency, which can be transmitted over long cables, and renders the sensors less susceptible to the effects of moisture intrusion. Biaxial measurements can be achieved by mounting the sensors in pairs, each member oriented at 90 degrees to the other. Damping fluid may be added to the sensor to counteract the effect of any vibrations of the structure. In-built shock absorbers protect the sensor from shock loading.

(a)

(b)

Figure 4.38: Vibrating Wire Tiltmeter "Geokon, Model 6350" installed on the Mdina walls (taken from [114]). a) Monoaxial configuration b) Biaxial configuration.

Thermo hygrometers and Pluviometer. An electrical thermoigrometer and a pluviometer have been installed on the top of the Stendardo Tower. All these sensors have been connected to the main automatic data acquisition system.

4.1.7.2 The three Areas

The whole instrumentation has been installed in the three areas A-B-C following both the directions provided by the project plan and the ones taken after field inspections.

A Area Instrumentation set in the area:

- N° 22 Crack gauges
- N° 5 Biaxial inclinometers

- N° 2 Piezometers

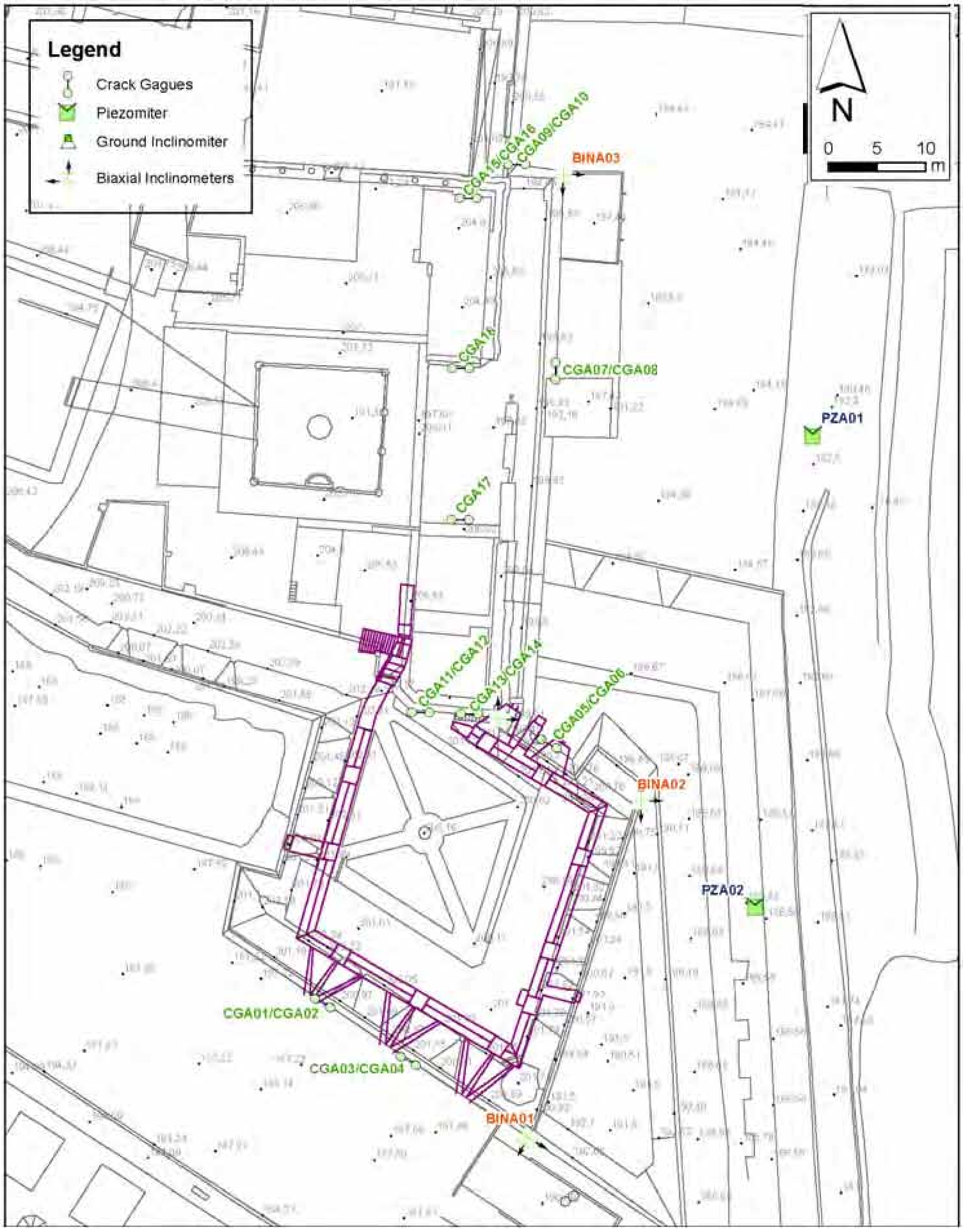

Figure 4.39: Location map of the instruments of the A Area.

B Area Instrumentation set in the area:

- N° 14 Crack gauges
- N° 3 Biaxial inclinometers
- N° 3 Piezometers

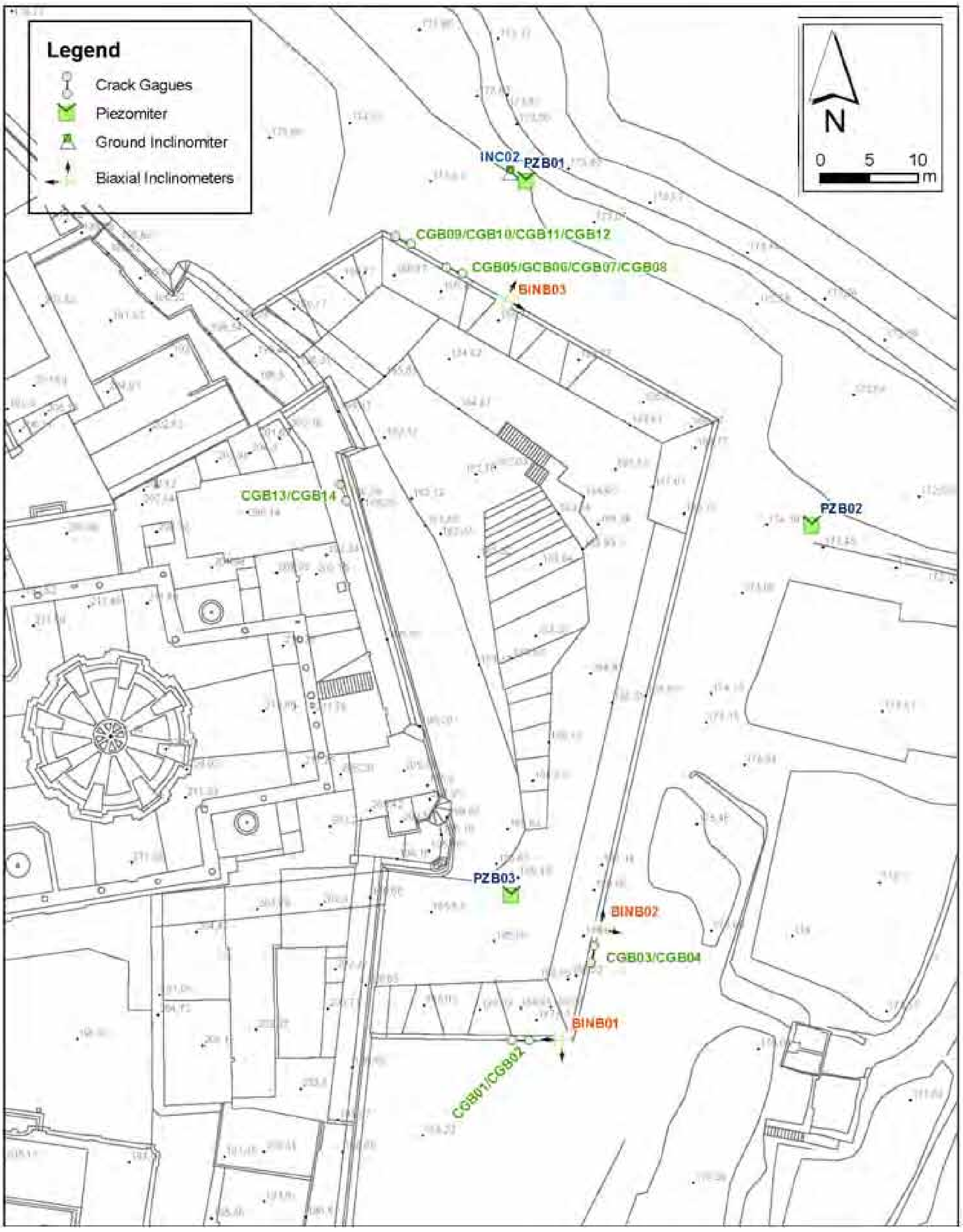

Figure 4.40: Location map of the instruments of B Area.

C AREA Instrumentation set in the area:

- N° 20 Crack gauges

- N° 4 Biaxial inclinometers
- N° 3 Piezometers

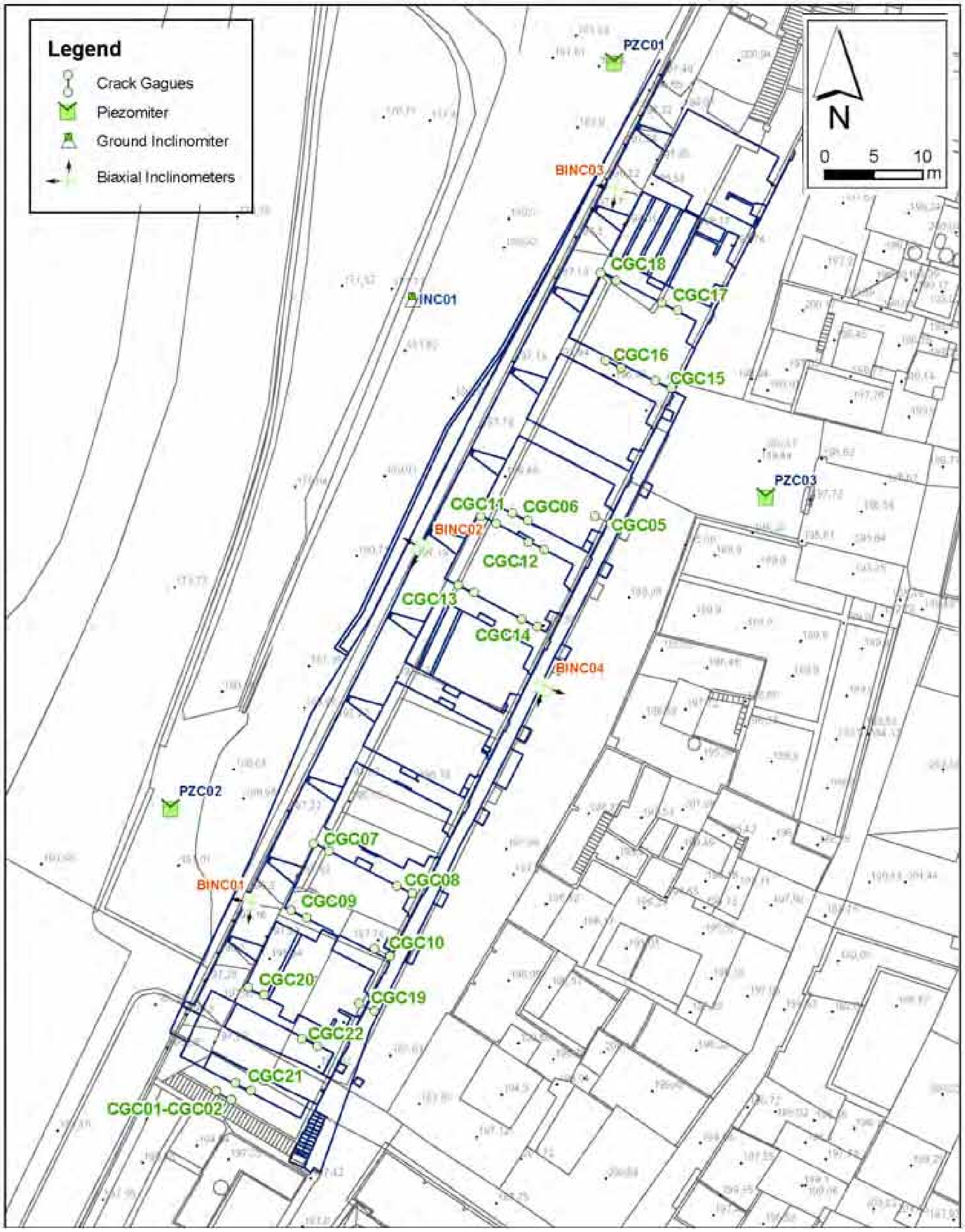

Figure 4.41: Location map of the instruments of C Area.

- Peripheral data logging and TX/RX units LTU. N°14 LTU were been cabled with short length connections to the sensors. LTU are two channels data logger lower power consumption so they are powered by alkaline batteries. LTU are programmable readout units able to power and read the vibrating wire sensors, to record locally up to 700 readings and to transmit, by radio frequency (wireless network), all the acquired data to a central radio logger.

Figure 4.42: Local Transmitter Unit (LTU) (November, 2010).

- Radio Repeater Unit (RRU) The RRU is a special unit that can be used to guarantee the wireless network operation if some of the LTU are not well recovered. In all the three areas were installed n°4 RRU.

- Datalogging and data transmission system. In the Torre dello Stendardo are been located the central server and the accessories as required in the Technical Specifications of the Tender. The layout of the data logging and transmission system is based on a wireless local network (Wireless Data logging System – WDS) constituted by the following elements:

  1. Torre dello Stendardo Radio logger Acquisition Unit (RAU). It is been installed on the roof of the tower and it is communicating by wireless network with the LTUs and by GPRS with the main WEB-GIS server. RAU is able to call and check the functionality of the LTU with programmable frequency, to download data, and to change LTU's setup as required.
  2. Server room: inside the tower is been installed a prefabricated room (data rack room) complete of air conditioner, electrical 230 V switchboards, lamp and all the security electrical accessories. Inside the room there is the computer connected to the RAU, complete of LCD monitor and a printer, and a battery for an hour of autonomy. The computer is directly connected via internet to the Main Web Server.
  3. In the Magazzini Area there is another RAU for the instruments in the area, it is installed on a pile in the middle of the area and powered by photovoltaic panel.

Figure 4.43: Server Room located inside the tower of the standard (March, 2010).

Figure 4.44: Solar panel to provide the RAU power supply (taken from [5]).

4.1.7.3 Communication system

The communication system assures the coverage of the entire area of interest. Most of the area has been covered by wireless connection whereas, for those sectors where this has not been possible, cable connection has been use. All of the sensors are recorded in real time.

The communication system assures the coverage of the entire area of interest. Most of the area has been covered by wireless connection whereas, for those sectors where this has not been possible, cable connection has been used. All of the sensors are recorded in real time. All data are collected in a central server located in Torre dello Stendardo (Mdina), thus they are available for visualizing and processing.

4.1.8 Web Gis Interface

Main Web Server is the central data management and controls unit which manages RAU and LTU units and provides the WEB-GIS based interface for data consultation, analysis and downloading. The data management software is been the GD Test own made GDMS based on WEB-GIS platform. The web interface is available for:

- project public viewing;
- authorized only data viewing;
- automatic raw data upload;
- manual raw data upload;
- automatic data elaboration results upload;

- manual data elaboration results upload;
- manual document and pictures upload;
- automatic alarm popup;
- remote control of Mdina Central Server and its accessories.

Figure 4.45: Web GIS Interface (provided by [5])

The front/end interface allows the site map navigation with different menu options (zooms, windows selections, distance measurements,). An additional technical description of the GDMS is given in the datasheet annexed at par. "Technical Specifications of Instruments". By clicking with the selection pointer the object symbols on the map it will be possible to visualize the dynamic graph of the reading recorded in the database and all the relevant documents correlated (pictures, borehole stratigraphic description, calibration and test certificates, Installation and Maintenance sheets, etc.).

WEB-GIS system will be able to manage alert/alarm conditions due to the following warning situations:

1. defined thresholds overcoming by the sensors
2. power supply failure
3. environment conditions
4. data transmission failure
5. In case of warning conditions a real time advice will be transmitted by e-mail and by SMS to the authorized users.

The web-page provides whole data recorded by the instruments of the monitoring system through a smart and intuitive interface as shown in 4.46.

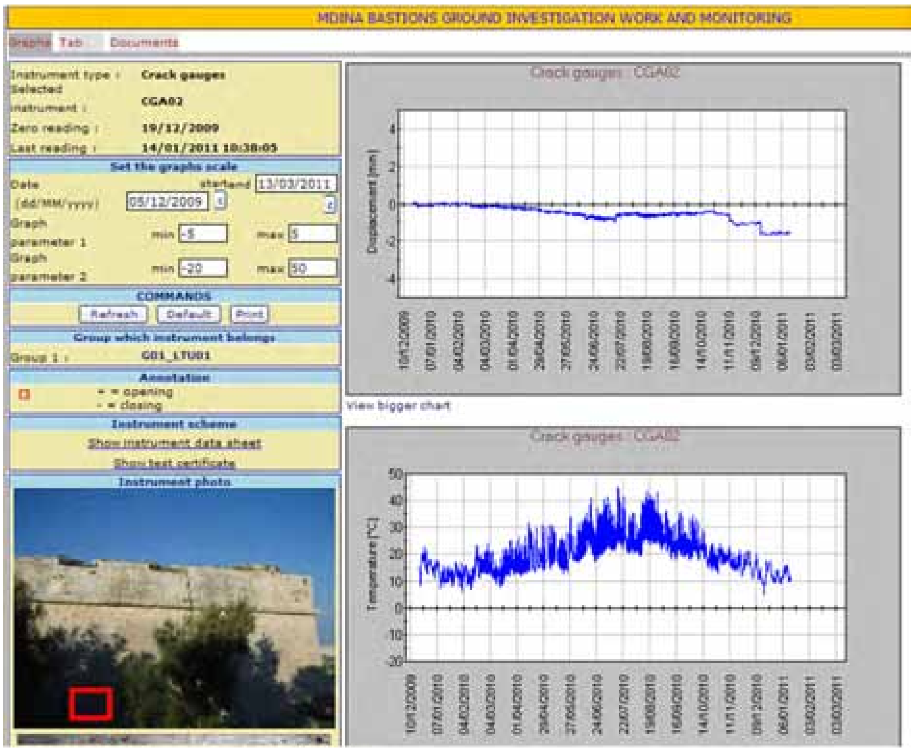

Figure 4.46: Web interface, chart views. A separate page for each instrument installed in Mdina and Gozo (Malta) can be invoked (provided by [5]).

Data recorded by the sensors are viewable in near-real time, except for piezometer Pz3 because its position is not reachable by a direct connection (nor cable or radio).

For each instrument it's possible to interrogate the recorded data and to plot them on a graphic, or to download them in .csv format.

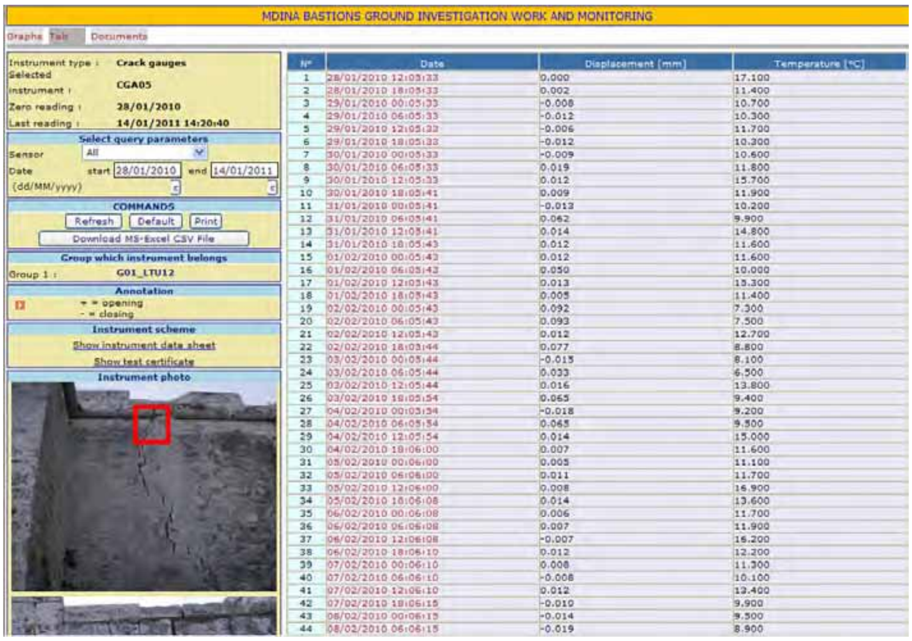

N°	Date	Displacement [mm]	Temperature [°C]
1	28/01/2010 12:05:33	0.000	17.100
2	28/01/2010 18:05:33	0.002	11.400
3	29/01/2010 00:05:33	-0.008	10.700
4	29/01/2010 06:05:33	-0.012	10.300
5	29/01/2010 12:05:32	-0.006	11.700
6	29/01/2010 18:05:32	-0.012	10.300
7	30/01/2010 00:05:33	-0.009	10.600
8	30/01/2010 06:05:33	0.019	11.800
9	30/01/2010 12:05:33	0.012	15.700
10	30/01/2010 18:05:41	0.009	11.900
11	31/01/2010 00:05:41	-0.013	10.200
12	31/01/2010 06:05:41	0.062	9.900
13	31/01/2010 12:05:41	0.014	14.800
14	31/01/2010 18:05:43	0.012	11.600
15	01/02/2010 00:05:42	0.012	11.600
16	01/02/2010 06:05:42	0.050	10.000
17	01/02/2010 12:05:43	0.013	15.300
18	01/02/2010 18:05:43	0.005	11.400
19	02/02/2010 00:05:43	0.092	7.300
20	02/02/2010 06:05:43	0.093	7.500
21	02/02/2010 12:05:43	0.012	12.700
22	02/02/2010 18:05:44	0.077	8.800
23	03/02/2010 00:05:44	-0.015	8.100
24	03/02/2010 06:05:44	0.033	6.500
25	03/02/2010 12:05:44	0.016	13.800
26	03/02/2010 18:05:54	0.065	9.400
27	04/02/2010 00:05:54	-0.018	9.200
28	04/02/2010 06:05:54	0.065	9.500
29	04/02/2010 12:05:54	0.014	15.000
30	04/02/2010 18:06:00	0.007	11.600
31	05/02/2010 00:06:00	0.005	11.100
32	05/02/2010 06:06:00	0.011	11.700
33	05/02/2010 12:06:00	0.008	16.900
34	05/02/2010 18:06:08	0.014	13.600
35	06/02/2010 00:06:08	0.006	11.700
36	06/02/2010 06:06:08	0.007	11.900
37	06/02/2010 12:06:08	-0.007	16.200
38	06/02/2010 18:06:10	0.012	12.200
39	07/02/2010 00:06:10	0.008	11.300
40	07/02/2010 06:06:10	-0.008	10.100
41	07/02/2010 12:06:10	0.012	13.400
42	07/02/2010 18:06:15	-0.010	9.900
43	08/02/2010 00:06:15	-0.014	9.500
44	08/02/2010 06:06:15	-0.019	8.900

Figure 4.47: Web interface, data view . A separate tb page for each instrument installed in Mdina and Gozo (Malta) can be invoked (provided by [5].

Chapter 5

Monitoring activities on the Citadel of Gozo (Malta)

Citadel lies on a hilltop consisting in a limestone formation which shows a high degree of fracturing, and whose rock layers have a different resistance to erosion which leads to the formation of ledges and niches; these factors cause the detachment and fall of rock blocks of various sizes. The instability of the cliff is also affected by the clayey formation underlying the limestone rock cap, which can be subject to flow phenomena or volume variations caused by the seasonal changes of water content. Due to rock falls occurring in the cliff, an accurate geological, geomorphologic and geotechnical investigation was necessary to evaluate the stability of the rock mass underlying the Citadel buildings. The main instability processes were identified and modeled through kinematic analysis and numerical modeling. To ensure safety conditions for the employees involved in the restoration works, a rockfall analysis was also performed.

5.0.9 Geographical setting

The area under investigation is located in the middle of Gozo, a small island measuring 67 km2 in extension, which is the second largest island of the Maltese archipelago, after Malta itself. Other islands forming the archipelago are Comino, plus a small number of uninhabited islets (4.15.1).

The Maltese Archipelago is situated in the Sicily Channel, almost at the center of the Mediterranean Sea, 93 km South of Sicily, 290 km Est of Tunisia and 350 km North of the Libyan coast.

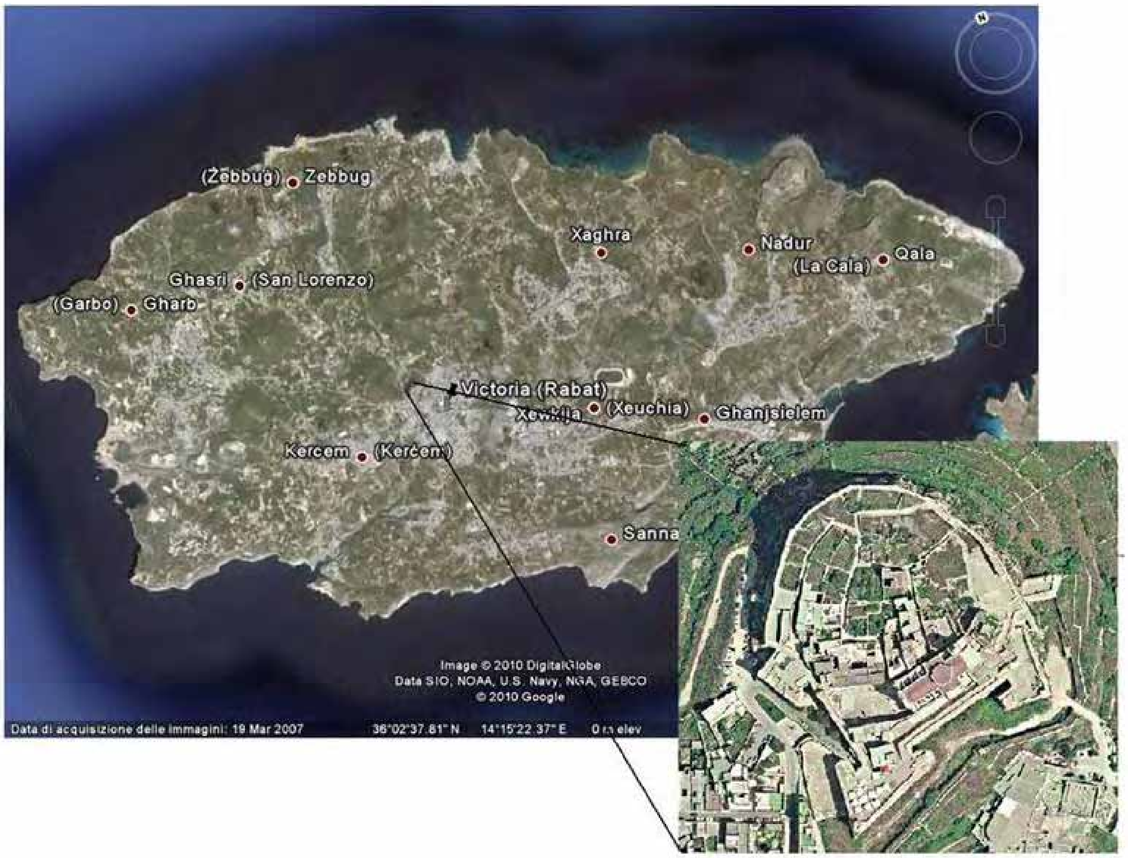

Figure 5.1: Satellite view of Gozo Island, with a zoom on the examined area (modified from [78]).

The Maltese Islands, running NW-SE, stand on a shallow submarine elevation, the Malta plateau, which is part of the "Sicilian-Tunisian Platform", also named "Pelagic Platform" [66]; the latter extends from the Ragusa peninsula of Sicily and continues southwards to the African coasts of Tunisia and Libya 5.2. The sea between the Maltese Islands and Sicily reaches a maximum depth of not more than 200 m and is mostly less than 90 m, although in between the Maltese Islands and the African coast several important submarine deep valleys running NW-SE (termed the Pantelleria Rifts, reaching depths of 1000-1500 m) are present. The great contrast in relief between the mainly shallow seas of the Sicilian-Tunisian Platform and the deep sea areas of the Western and Eastern Mediterranean is particularly shown just to the east of the Maltese Islands; there sea depths fall away over the Malta and Medina Escarpments, within a distance as little as 15 kilometers, from depths less than 200 m to over 3000 m and even over 4000 m across the Ionian Abyssal Plain [66].

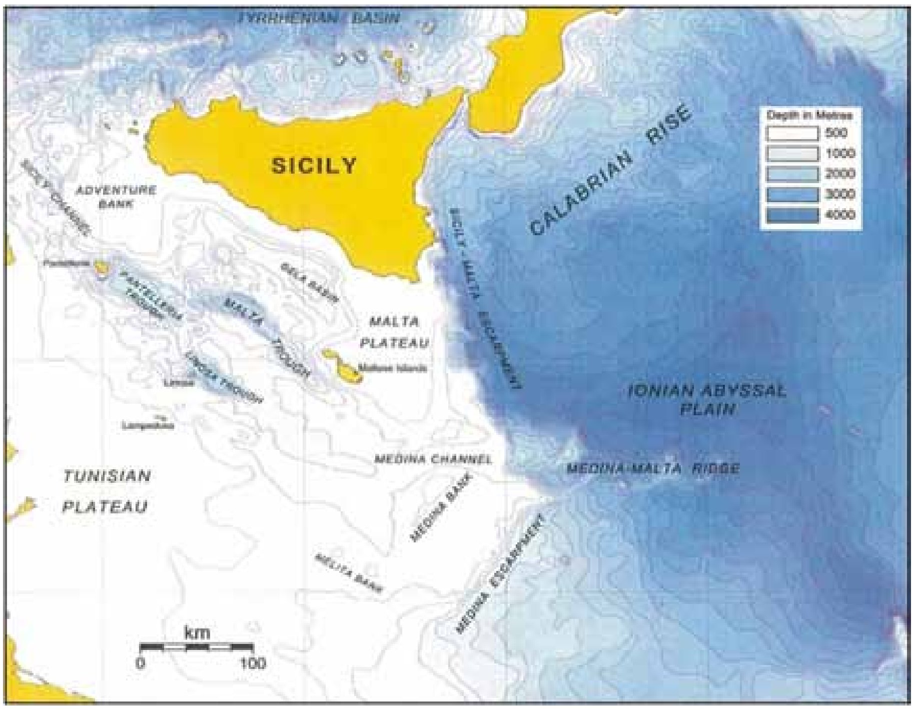

Figure 5.2: Bathymetric Map of the Central Mediterranean around the Maltese Islands (Taken from [66]).

5.0.10 Geological and geomorphological setting

The present landscape of the Maltese Archipelago consists of low hills with terraced fields (the highest point is Ta' Dmejrek, 253m, on Malta Island) 5.3.

Figure 5.3: View of the typical Gozitan landscape (May 2010).

The coastline of the islands is indented and characterized by numerous bays, inlets and promontories. The morphology of Gozo island can be seen in the general context of the Maltese Archipelago: Gozo is essentially a planar table of layered rocks tilted gently towards the north east, the valleys of which have been eroded 5.4 [66]. The layered rocks to be seen on the surface of the Maltese islands are made up of tertiary sediments, mainly limestones, between 50 and 5 My in age, which were originally deposited, from upper Oligocene to upper Miocene, as shallow marine sediments covering all of the Sicily-Tunisian platform. These marine sediments were subsequently uplifted above sea level by a subvertical fault system running in NW-SE and SW-NE, related to the opening of the Pantelleria Rift, during the Pliocene period. The present surface landscape has been modeled by weathering factors such as rain, wind, and around the coast outline by the action of the sea waves. These erosive factors have been further controlled by the internal fabric of the sedimentary rocks, by the alternation of hard and soft beds.

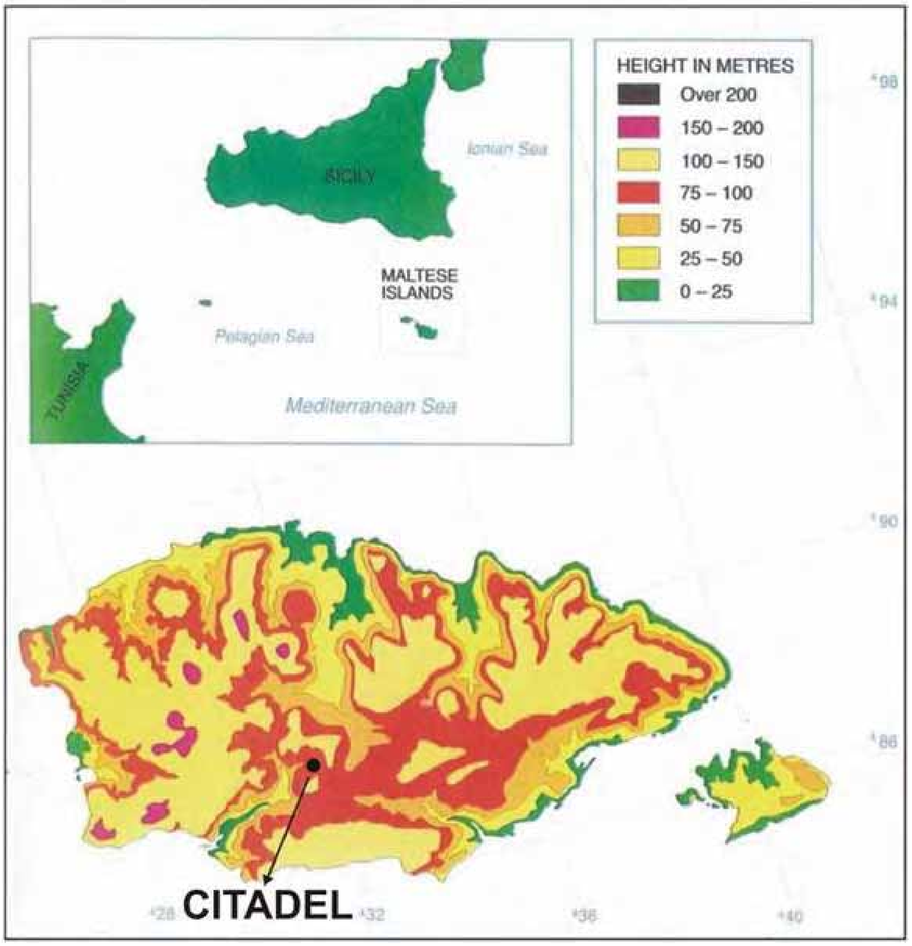

Figure 5.4: Simplified topographic Map of Gozo and Comino (taken from [66]).

The rock formations forming the Maltese Archipelago surface consist mainly in skeletal remains (shells, shell fragments and fine mud-sized debris) rich in calcium carbonate, and secondly in the very finest and lightest components from the distant land sources like water borne clay minerals and volcanic dust. The stratigraphic sequence of rocks seen on the surface of the Maltese islands is essentially very simple, and falls into four distinct layers which, although slightly disturbed by almost vertical fault displacements, lie almost horizontally across the islands [66]. From bottom to the top the four layers are as follows 5.5:

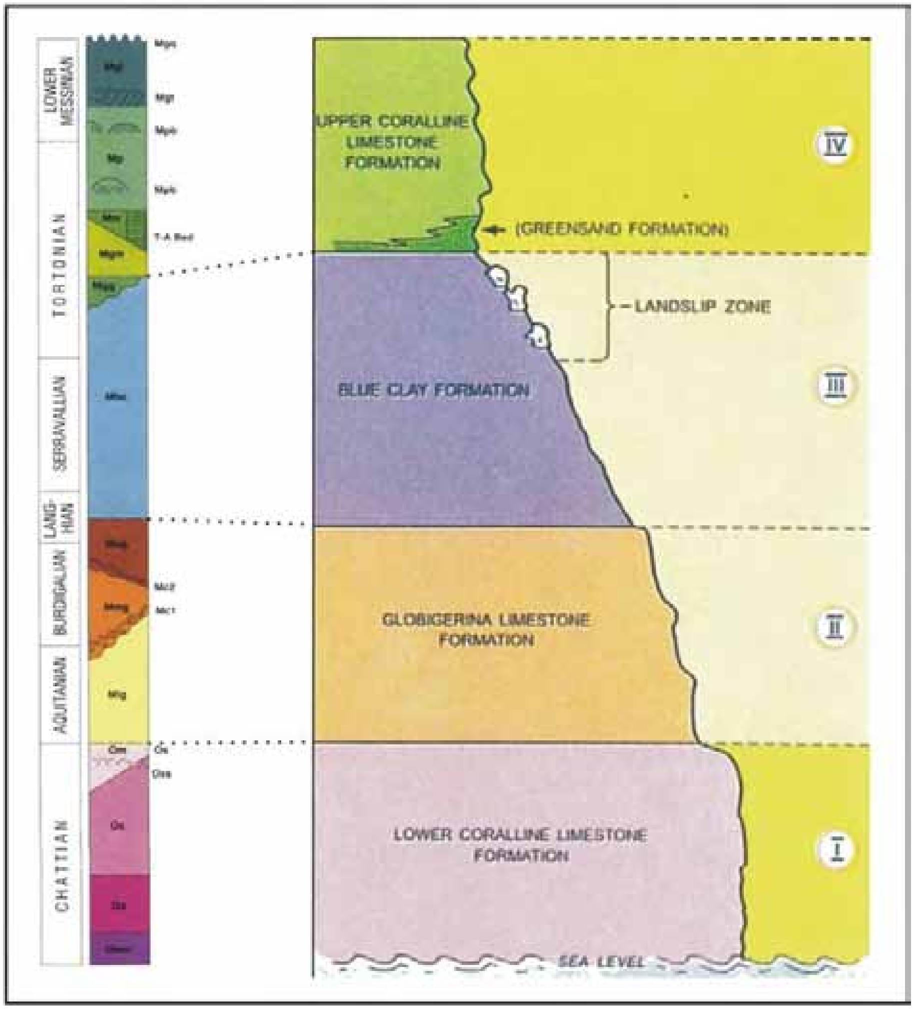

Figure 5.5: Surface schematic stratigraphic sequences of the Maltese Islands (taken from [67, 66]).

1. "Lower Coralline Limestone Formation" (LCL): hard, pale grey limestone unit that forms sheer cliffs from tens to over a hundred meters high, particularly on the south-west coasts of the islands. This unit is named as it contains some beds with fossil corals and common remains of marine calcareous algae. It can be over 140 m in thickness and its base is not seen above sea level; its age falls in upper Oligocene and goes from lower to upper Chattian (28 to 23My) [66]. According to Pedley (1993), it is subdivided in four distinct members:

    - Maghlaq member (Owm): it is poorly exposed and passes transitionally into the overlying member. It consists in massive bedded, pale yellowish-grey carbonate mudstones containing rare benthonic foraminifera.
    - Attard member (Ao): grey limestones (wackestone and packstones) with large coralline algal rhodolit, gastropods and bryozoans fossils (thickness: 10-15m).
    - Xlendi member (Ox): planar to cross-stratified, coarse grained limestones (packstones) with abundant foraminifera fragments. The top contains abundant entire and fragmentary echinoid fossils, in single to multiple beds (Oxs="Scutella bed"; thickness: 0-22 m).

- Mara member (Om): tabular beds of pale-cream to pale-grey carbonate mudstones, wackestones and packstones in 1 to 2 m thick units. Abundant bryozoans fragments and locally important banks of foraminifera algae are present. The top of the member is transitional with the lower Globigerina Limestone Formation, and is taken as the highest bed containing Scutella echinoids (Ms="Scutella bed"; thickness 0-6 m).

2. "Globigerina Limestone Formation" (GL): it's a soft, yellowish fine-grained limestone unit that forms irregular slopes in which small terrace-like steps a few meters high pick out slightly harder bands. This unit takes its name from a type of planktonic foraminifera fossil shell (Globigerina), that is abundant in the limestone. This unit varies from some 20 to over 200 m in thickness; its age is lower-middle miocenic and goes from Acquitanian to Langhian (23 to 13 My) [66]. According to Pedley (1993) it is subdivided in three distinct members:

   - - Lower Globigerina Member (Mlg): pale cream to yellow plancktonic foraminiferal packstones becoming wackestones in a short distance above the base. Pectinid bivalves, fish teeth, solitary corals and echinoid fossils are common. The top of this member is marked by ubiquitous phosphatised hardgrounds (Mc1; thickness 5-40 m).
   - - Medium Globigerina Member (Mmg): a planktonic foraminifera-rich sequence of massive, white, soft carbonate mudstone locally passing into pale-grey marly mudstones. Fine bed laminae are frequent, thin-shelled pectinid bivalves, echinoid and coccoliths fossils are abundant (thickness 0-15 m).
   - - Upper Globigerina Member (Mug): a tripartite, fine grained planktonic foraminiferal limestone sequence comprised of a lower cream coloured wackestone, a central pale grey marl and an upper pale cream coloured limestone. Pectinid bivalves and occasional echinoids are present. Phosphorite conglomerate beds containing fish teeth and other diverse macrofossils occur at he base of the member (Mc2; thickness 2-15 m).

3. "Blue Clay Formation" (BC): this unit is a very soft pelagic medium grey marl and limey clay, mostly with more than 50% calcium carbonate content, that within the islands rarely shows at the surface, forming rolling low slopes that are mostly covered by carbonate raw soil or scattered rubble. Where steep hillsides occur or where sea coast erosion is active, it appears as a banded bluish grey pelagic clay or marl. It contains quartz, augite, hornblende, feldspars, zircon and tormaline grains, while in its upper beds Goethite concretions are common, in association with bivalve molluscs, gasteropods, cephalopods and coral fossils. The thickness of this unit ranges from 18 to 75 m; its age is upper-middle miocenic and goes from Langhian to Tortonian (13 to 7My) [66].

4. "Upper Coralline Limestone Formation" (UCL): the top most unit, a hard, pale grey limestone that appears similar to the lowermost limestone unit. It also forms sheer cliffs of varying height and also contains corals and coralline algal fossils, for which takes its name from. It is over than 150 m thick, however generally forms hill cappings, overlying unconformably the Blue Clay Formation [66]. According to Pedley (1993) it can be subdivided in four distinct members, from bottom to the top:

   - - Ghajn Melel Member (Mgm): this basal member consists in massive bedded dark to pale brown foraminiferal packstones containing glauconite. The rock matrix is largely composed of abraded Heterosegina foraminifer bioclasts with common presence of large Clypeaster echinoids and Macrochlamis pectinid bivalves. It was formed by the marine erosion and reworking of emerged Greensand Formation. Outliers capping hills also contain coral patches. Several boulders composed of this member are found along the slopes arond the Citadel. The reddish color of the sand is attributed to the glauconite in the Ghajn Melel parent rock. This member, upper tortonian in age, goes from 0 to 16 m in thickness. Its formation has to be related to the erosion and reworking of the underlying Greensand formation.

- - Mtarfa Member (Mm): massive to thickly bedded algal carbonate mudstones and wackestones, yellow in their lower layers, white and chalky in the upper ones. The lower beds contain brachiopods, while the upper ones contain gypsum and are characterized by abundant bentonic foraminifera fossils. It can be easily eroded by the weathering to form caves. The blocks falling down the slopes usually crumble to form a white sand. This member shows thickness that vary from 2 to 16 m (generally around 5 m). The age is Late Tortonian.
- - Tal-Pitkal Member (Mp): pale grey and bluish grey coarse grained wackestone and pakestone containing significant coralline algal, molluscs and echinoid bioclasts. Lower parts of the member show abundant large rhodoliths, while the upper part contain patch reef and biostromes (Mpb=Depiru beds). Both parts are dominated by peloidal and molluscan carbonate mudstones, with coralline algae and scattered corals. The age of this member goes from upper Tortonian to lower Messinian, and its thickness ranges from 1 to 30 m (15 to 20 m on the top of plateaus, where erosion doesn't take place).
- - Gebel Imbark Member (Mgi): not common in Gozo, it's a pale grey hard limestone, with sparse faunas, deposits now restricted to erosional outliers synclinal cores, where erosion doesn't take place. Basal beds consist in cross stratified ooidal and peloidal grainstones (Mgt=Tomna Beds). Top beds consist of carbonate mudstones associated with grey marls and paleosols sequences (Mgq=Qammieh Beds). This member reaches thickness from 4 to 20 m. Age: Miocene, EarlyMessinian. Whilst these four rock units suffice to control the surface topography there is another unit, lying between the Upper Coralline and pockets and depressions in the Blue Clay Formations, called the "Greensand Formation" (GS), more than a metre thick, that can occasionally expand to 11 m in Gozo. This formation proved distinctive enough to have deserved a separate name although it is not of sufficient thickness to affect the form of the land surface [66]. It consists in massive, friable brown to greenish glauconite and gypsum grains-rich sand intensely bioturbated bearing bentonic microforaminifera fossils and marine macrofossils. When freshly exposed this formation has a characteristic green colour created by a scattering of dark green sand-sized grains made by a complex potassium-iron-aluminium fillosilicate mineral (Glauconite); this mineral, when altered by weathering, gives this formation a distinctive brown colour. It is rich in benthonic micrforaminifera, sharks teeth, remains of cetaceans, casts of Conus, and encrusting briozoans. It is of Tortonian age in the Miocene (approx. 6 - 10 My) [67]. A simplified geologic map of Gozo island is reported in 5.6.

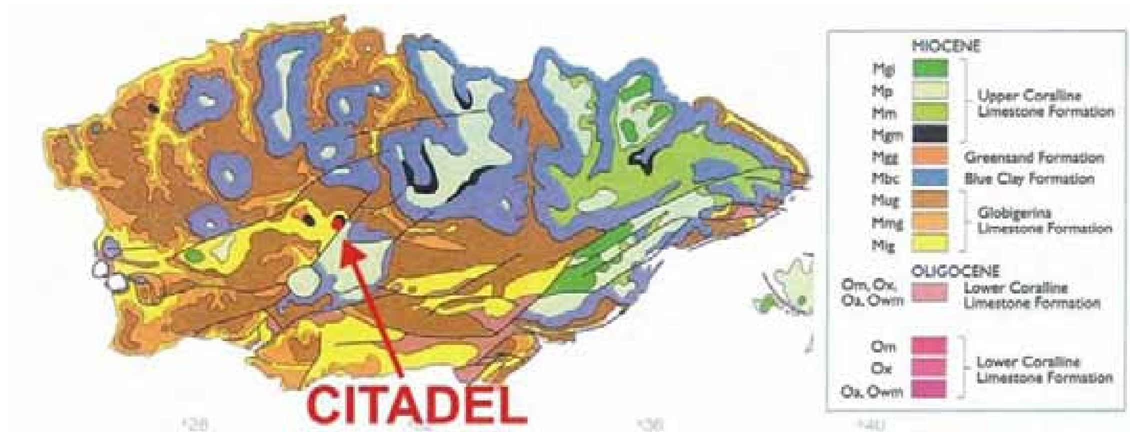

Figure 5.6: Simplified Geological Map of Gozo and Comino with coloured stratigraphic legend (taken from [66]).

The first factor affecting the sculpting of the land surface of the Maltese islands, especially Malta and Gozo, is the different resistance that each of the four above mentioned formations has to erosion. Lower Coralline Limestone is hard and resistant to erosion, but reaches down to sea level where even wave action only slowly undercuts it. It therefore forms high sea cliffs, often with sea caves close to present day sea level. Globigerina Limestone is chalky and fairly soft but has several harder bands, hence it weathers into flat-lying layers which form steps in the landscape at each hard band; additionally these steps have been accentuated in many areas by the human action of building up the natural step into a terrace wall between field levels. The chalky rock is porous, but some of the hard bands are impermeable and so can form minor spring lines as the water percolating from above seeps out sideways where the hard band meets the land surface [66]. Blue clay is easily weathered and the clay minerals in its fabric are easily disaggregated and washed down by either rain or sea water to be the main source of the soils on land or, on the coast, permanently lost to the sea. Clays are also affected by swelling, in fact they increase their volume in relation to water content, expanding when they're dampening and shrinking when drying. Being clays impermeable to water flow, solution caves and contact spring lines can develop along the contact with overlying porous rock formations meets the surface 5.7. The clay is impermeable to water flow and hence acts as a barrier to water percolating down through the overlying fractured and porous Upper Coralline Limestone. Because of this, major spring lines and solution caves develop where the contact of these two units meets the land surface [66].

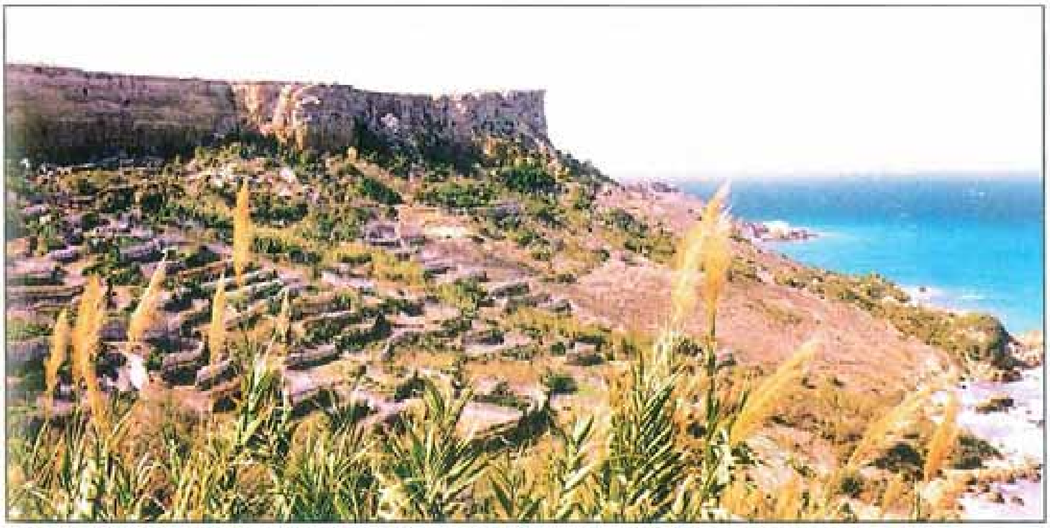

Figure 5.7: Upper Coralline Limestone cliffs overlying Blue Clay hill slopes, above Dahlet Qorrot in Gozo; a line vegetation marks the spring level of the Greensand at the base of the cliff (taken from [66]).

For its limited thickness the Greensand Formation is unable to affect the morphology. Upper Coralline limestone is hard, brittle, resistant to erosion and forms cliffs but, as the Blue Clay beneath it is washed away, it is undercut, breaks away and collapses into progressively smaller blocks that slowly slide away down the clay slopes. Where the Blue Clay Formation is being more rapidly washed away, particularly around the coasts where wave action cuts into it, large Upper Coralline collapsed blocks cover the clay slopes, and even protect them from further erosion [66]. Being at the top of the Maltese Islands stratigraphic pile, the Upper Coralline Limestone overall is subjected to the continuous deluge of rain combined with stress by wind and solar heating/cooling. Rainwater percolates through the hard but porous rock, and then runs sideways when it cannot pass through Blue Clay beneath. The fresh water slowly dissolves the limestone to subsequently form fissures and caves, but also fills wells dug into the upper surface of the limestone [66]. Another frequent geomorphologic process due to this layered stratigraphic sequence is the inversion of topographic relief (5.8).

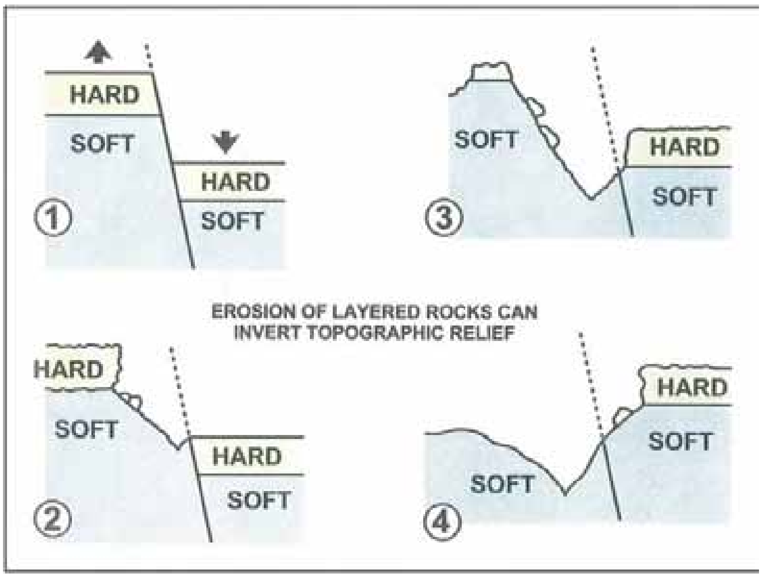

Figure 5.8: Simplified diagram illustrating the inversion of topographic relief (taken from [66]).

5.0.11 Hydrogeological Setting

The geology of the Maltese Islands plays a crucial function in the formation of the hydrological features of the islands. The Maltese stratigraphic sequence has enabled two different types of groundwater bodies to form: the Perched Aquifers, which are limited to the north western extent of the island and, to a lesser extent, in Gozo, and the Mean Sea Level Aquifer, which is located in the southern and central parts of Malta and western part of Gozo . Where the 5 layer rock sequence is still intact and thus the Upper Coralline Limestone lies above the Blue Clay formation, perched aquifers can be found. These groundwater bodies are allowed to form due to the impermeable nature of the Blue Clay lying beneath a permeable layer of Upper Coralline Limestone. On the eastern part of Gozo only the Globigerina and Lower Coralline limestone formation are mainly exposed. Here the Lower Coralline Limestone aquifer or the mean sea level aquifer has formed.

5.0.12 Description of the site

5.0.12.1 Geological and geomorphological setting

The hill of Citadel is one of a number that dot the Gozitan Landscape (il-Gelmus, Il-Jordan, Ghar Ilma) 5.9. These reliefs are described as “destructional hills, which owe their existence to the deeper erosion of the land that surrounds them. All of them are characterized by sub-horizontal or gently inclined Upper Coralline Limestone cap protecting the underlying soft Blue Clay, and by a drainage system presently entrenched in Globigerina Limestone. They represent inter-stream areas or divides which have not yet had enough time for their complete erosion” [68].

The hill consists in a circular Upper Coralline Limestone rock plate, which is 20-25 m thick and 150 m wide, and overlies a level of Greensand Formation on gentle Blue Clay slopes 5.9.

Figure 5.9: The clayey slopes and rock plate on which the Citadel is built (April, 2010).

The rock plate slopes are sub-vertical, sometimes overhanging , while the underlying slopes are mostly characterized by a very gentle to gentle steepness (10 to 18% from the foot of the slope to three quarters uphill), only the upper part, close to the base of the hilltop cliffs, has a steeper gradient (20 to 25%). All around Citadel a widespread flat area where the Globigerina Limestones outcrops extends ; there is a big urbanized area, Victoria, just south of Citadel. Clayey hill slopes have been intensively used for a long time for agricultural purposes. This is particularly evident in the stone walls delimiting plots and retaining earthwork terraces, which are mostly developed on the western, northern and northeastern margins of the hill, and still recognizable in the land structure. At present the Citadel hill slopes are only marginally used for agriculture, most of the area is uncultivated. Terraces are still evident, but the retaining walls show the traces of long-standing neglect [11].

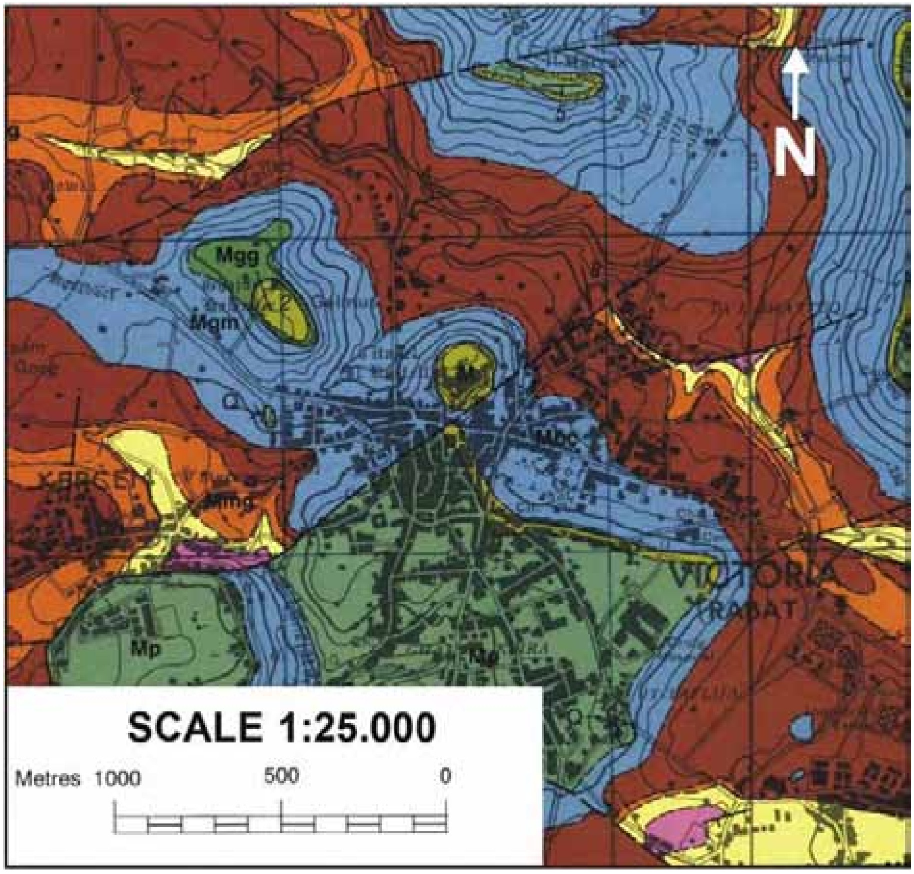

Figure 5.10: Extract from the Geological Map of the Maltese Islands-sheet 2, Gozo and Comino. Mmg=Middle Globigerina Limestone Member Mbc=Blue Clay Formation; Mgg=Greensand Formation; Mgm=Upper Coralline Limestone Formation-Ghajn Melel Member; M=miocenic collapse structure (taken from [67]).

5.0.12.2 Geological model

According to the different geological features of the Citadel rock cap (sedimentary fabric, degree of cementation, geomechanical properties), the geological survey and stratigraphic sections carried out suggested the subdivision within the Ghajn Melel Member of the UCL formation in three distinct sub-members: Upper Bank, Thinly bedded Bank, Lower Bank. This subdivision is particularly evident all along the cliff face perimeter, as shown in 5.11. The different geological features shown by the Ghajn Melel Member are reflected in different degrees of weathering of the cliff face, with large niches or undercuts occurring within the Thinly bedded Bank, which appears to have less resistance to erosion than the Upper and Lower Banks; the latter are both affected by the formation of overhangs and ledges. In an attempt to consolidate and protect these niches from further erosion, and to improve the global stability conditions of the hilltop, in the past several underwalling masonry were built all along the cliff face perimeter 5.12. These underwallings, which have a general bad state of maintenance, often appearing degraded and in several large portions partially collapsed, have a mechanical effect in inhibiting shearing of the overlying ledges which appears of very low efficiency. The strata measures collected at each stratigraphic section show that the bedding planes always dip into the slope from the cliff perimeter towards the centre of the rock plate 5.13, with inclination angles ranging from 10° to 25°.

Figure 5.11: View of the northern sector of the cliff showing the lithological subdivision within the Ghajn Melel member that was adopted (April 2009).

Figure 5.12: Degrated and partially collapsed underwalling masonry (April 2009).

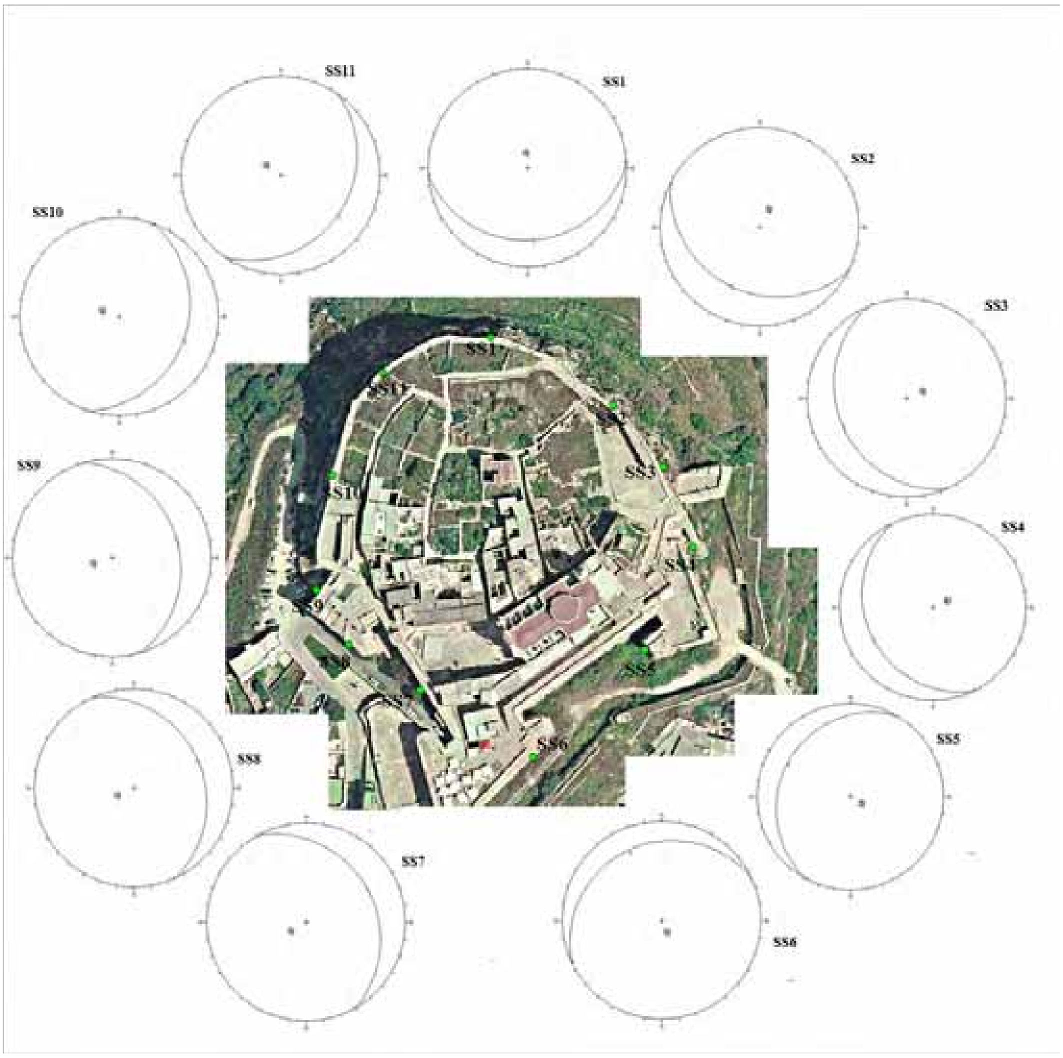

Figure 5.13: Stereographic projections of the Ghajn Melel Member strata dip and dip direction at each surveyed stratigraphic sections along the cliff face perimeter (taken from [106]).

According to Pedley (1974) this structural setting is due to a solution collapse structure late miocenic in age 5.14, like many others scattered all over the Maltese islands. Where the thick Miocene infill is softer then the surrounding materials, an erosional hollow results by recent erosion; instead when the infill is harder than the surrounding materials, because of a higher degree of litification, a circular erosional plateau (mesa) results. Many of these highs and depressions in western Gozo are associated with one of the major faults, on which early movements may have induced the initial collapse. Pedley (1974) and Pedley et al. (2002) postulate that extensive cavern formation in the Lower Coralline Limestone underlying Citadel was accompanied by roof collapse, which led to a higher degree of litification of the overlying Upper Coralline Formation infill. This led to differentiated erosive processes, in which a normal fault striking NE-SW 5.15, and skirting the southeastern border of Citadel, has played an important role, as a result of the uplifting of the Citadel block with respect to the south and southeastern sectors of the examined area. However the throw close to the site appears to be minor [68].

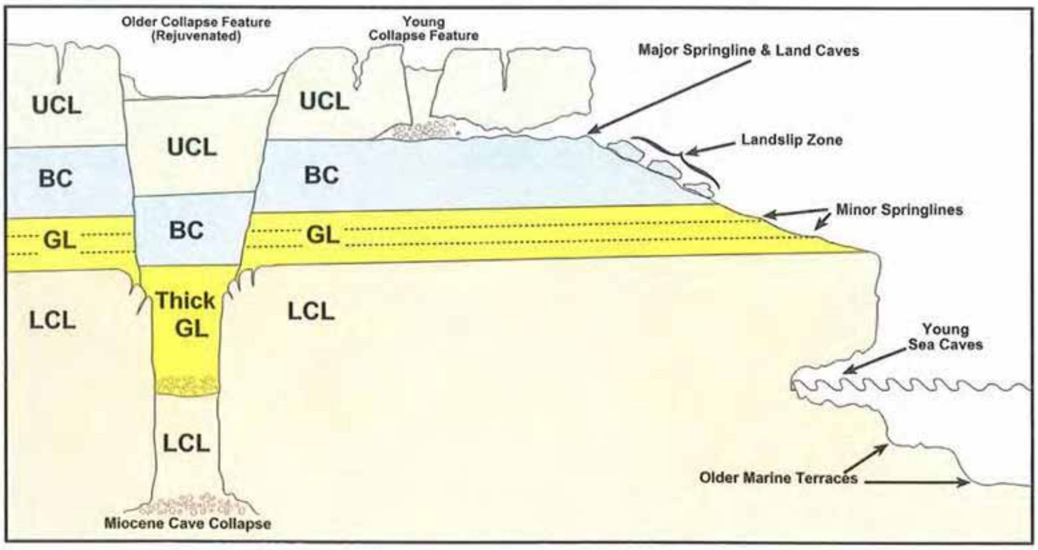

Figure 5.14: Schematic cross section outlining the position of the caves, springs and collapse features in the Maltese Islands (UCL=Upper Coralline Limestone; BC=Blue Clay; GL=Globigerina Limestone; LCL=Lower Coralline Limestone (taken from [7]).

Figure 5.15: Collapse structure at the southern headland of San Dimitri Point, Gozo (taken fro [66]).

The surface of the Maltese Islands also shows the occurrence of numerous caves that have fairly recently collapsed to give a surface depression. These more recent Pliocenic collapse features are essentially from caves formed in the UCL and are in many cases associated with cave systems that developed at the junction between the underlying Blue Clay 5.14, where the archipelago major spring lines form. To give an overview of the underground geology of Citadel, a fence diagram was created based on the data logs of the boreholes 5.16.

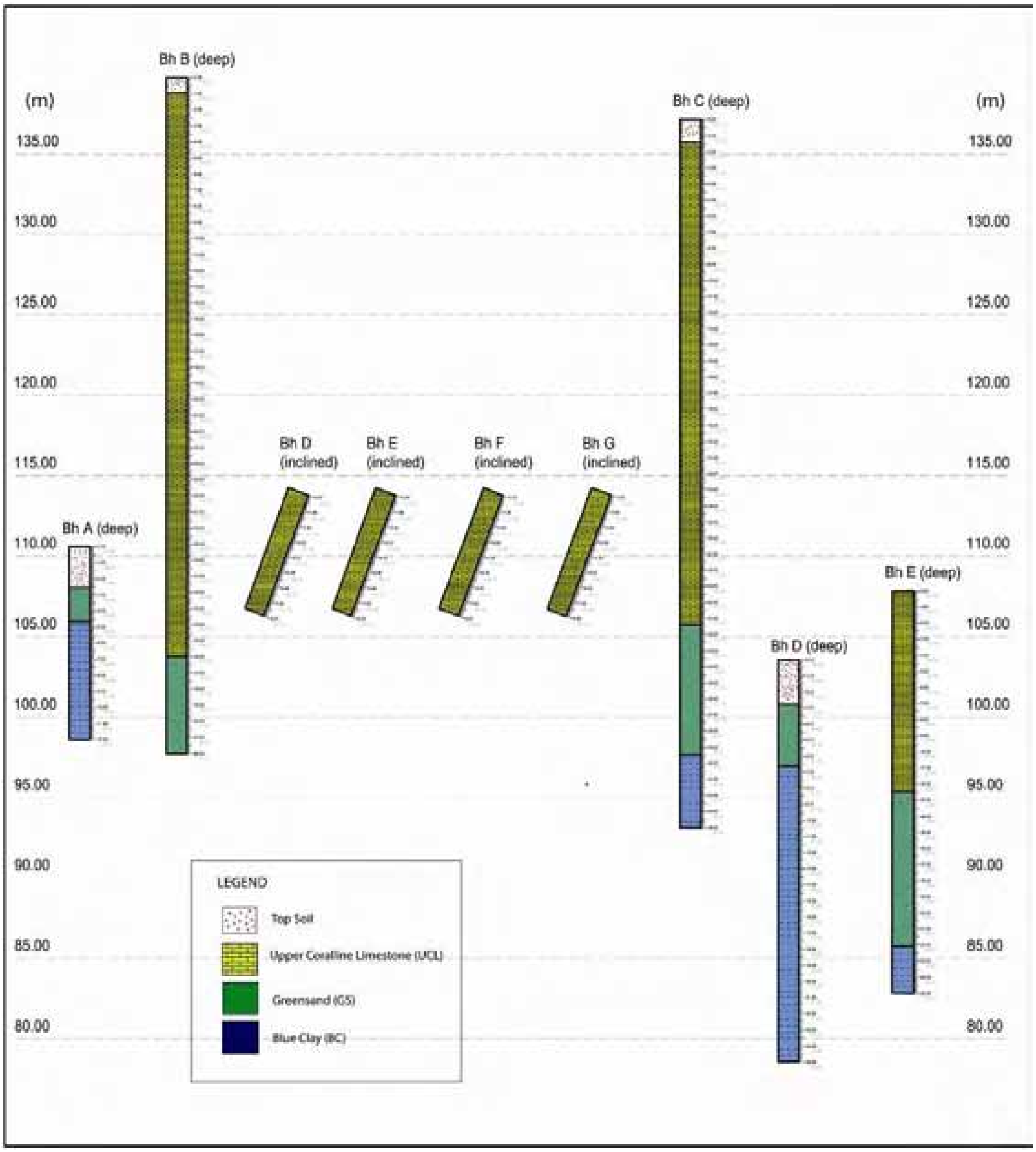

Figure 5.16: Fence diagram through the boreholes (taken from [5]).

This diagram indicates that the rocky plateau is composed entirely of the Ghajn Melel member of the Upper Coralline Limestone formation. This is then underlain by a relatively thin Greensands Layer, followed by the Blue Clay. It is worth noting that, although the borehole logs and the fence diagram indicate distinct boundaries between the different strata, the transition is not so abrupt, both between the Ghajn Melel member and the Greensands, and also between the Greensands and the Blue Clay. The interface would be better described as a gradual transition between the different strata, and therefore the interfaces shown are at best reasonable estimates of the point at which the borehole core can be considered to belong predominantly to one formation rather than to the other [5]. From the analysis of the retrieved borehole cores, the thickness of the Greensand layer is about 10 m; this value is comparable to the thickness of the same formation outcropping at Gelmus hill, less than 1 km WNW from Citadel. All available geological data were put together for the realization of geological maps and related cross-sections 9.115.19.

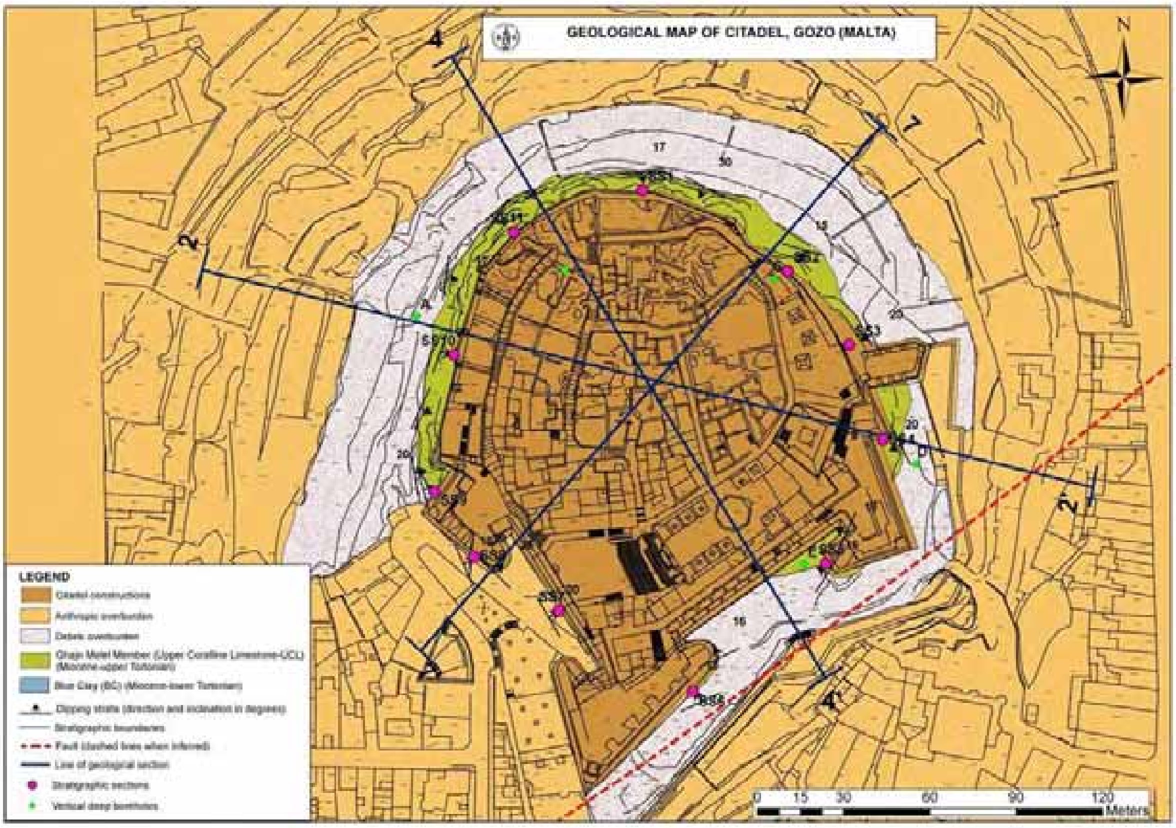

Figure 5.17: Geological map of the outcropping materials within the Citadel area.

The geological map in 9.11 shows the outcropping materials within the Citadel area, while 5.18 reports the inferred position of the contacts between the lithological formations.

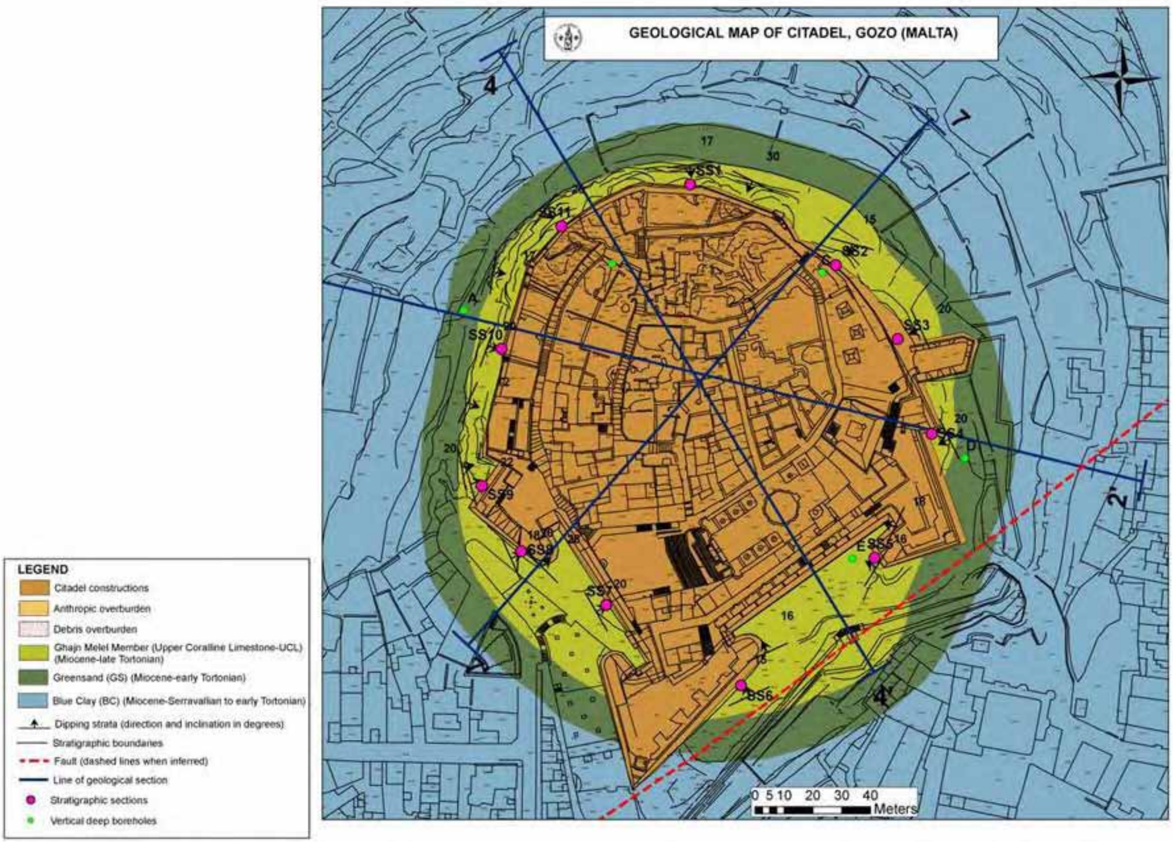

Figure 5.18: Inferred geological map of the Citadel area.

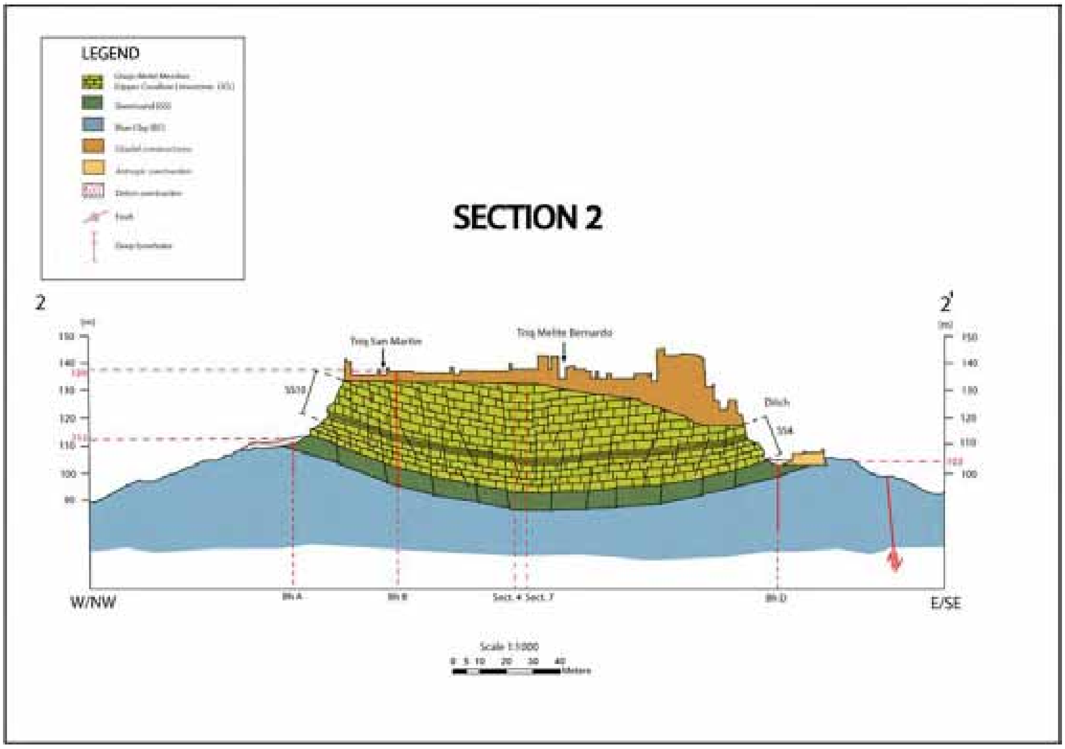

Figure 5.19: Geological cross-sections. .

5.0.12.3 Slope instability processes

The geological setting of the investigated area shows the superimposition of a relatively stiff and brittle limestone plate (made of UCL), on a thick Blue Clay layer. The overlying of rock types with marked contrasts in their geotechnical properties is one of the most critical geological environments for the stability of slopes 5.20. The mechanical characteristics of the materials comprising the rock slab – soft substratum systems are very different in terms of strength, stiffness and brittleness; this leads to typical geomorphological processes, such as flow phenomena in the underlying ductile units and brittle ruptures involving the overlying rock masses. The latter are often affected by huge sub-vertical joints that isolate large blocks 5.24.

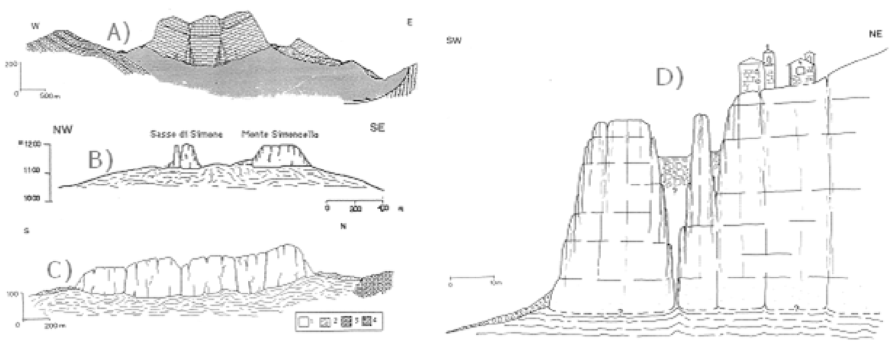

Figure 5.20: Examples of rock slab – soft substratum systems from Northern Appenines – Italy. A) Mt. Fumaiolo; B) Sasso di Simone – Mt. Simoncello; C) La Verna; D) Detail of La Verna relief, beneath the Monastery (Taken from [100]).

According to Scerri (2003) there are four main causes for Citadel hill instability:

- - Differential weathering and erosion produced by the action of the wind, temperature and seasonal saturation changes are the basic elements which trigger instability processes along the hill slopes, affecting the less resistant beds. As a result the cliff face assumes an irregular vertical profile with frequent protruding ledges and niches 5.21. Overhang rock failure at any level may take place by shearing.
- - Citadel cliff face is dissected by an important system of sub-vertical joints running into or nearly parallel to its margin 5.22. This joint system generates vertical rock prisms or slabs in the main limestone body, the stability of which depends mostly on the stability of the underlying Greensand and Blue Clay Formations.
- - A set of local joints and fissures, mostly restricted to the top layers of the cliff face, produced by stress relief, diurnal temperature changes and seasonal climatic changes also dissects the cliff face, skirts the top margin of the hill cap **??**. These joints and fissures have a dip which follows the cap's morphology, having a low dip at the top and steepening to near-vertical a few meters below its edge. These variably dipping joints give form to rock wedges of irregular form that could fail due to the underlying Greensand or Blue Clay instability or simply due to low frictional resistance.
- - Greensand and Blue Clay weathering accompanied by softening undermines the Upper Coralline Limestone cliff producing shearing along the above mentioned joint systems, and detachment of large rock blocks. These resulting detached blocks will gradually drift down hill and may also rotate or topple continuing their movement along the hill slopes. Once a block has slumped down, the relaxation of pressure on the newly exposed face results in the gradual development of a new joint system. The process is therefore ongoing. Slope failure is resisted by sliding, friction and cohesion through intact rock bridges between joints. Additional friction resistance to sliding is provided by the irregularities on the potential sliding surface.

Such factors stabilize blocks which otherwise look precarious. On the other hand fracture opening is enhanced by percolating water and by plant roots. Given the clayey nature of the formation forming the hillslopes, minor solifluxive movements are diffused along the hillslopes themselves.

(a) (b)

Figure 5.21: Gozo autcrops. a) Ledges and niches on the cliff due to differential erosion. b) High persistence joints within the rock mass (April 2009).

On the northern sector of the cliff, a huge rockfall event took place in December 2001 5.22. The resulting debris is still evident.

Figure 5.22: Rockfall debris from the 2001 event (May, 2010).

Evidence of a previous rockfall is also visible slightly east to the one occurring in 2001; this rockfall can be noticed by some blocks located on the slope used to sustain some retaining walls 5.22. To avoid these rockfalls in the past several underwalling masonry structures were built, with the purpose of protecting the niches which are the most eroded portions of the cap-rock outcrops, and to improve the global stability 5.23. These underwallings, widely present on the northern and eastern side of the cliff face, were built in different periods, and many of them are now in a bad state of maintenance 5.23. They show good effects in inhibiting erosion of the niches, but with regard to avoiding the shearing of the overlying ledges, they generally show very low efficiency.

Figure 5.23: Detail showing the conditions of underwalling masonry structures (May, 2010).

Man made terraces also play an important role protecting the Blue Clay hill slopes from instability processes. These terraces, at present abandoned, are located along the hillslopes from West to North and North-East, except for a tight slice located in the northern part of the hill, right below the 2001 rock fall area, possibly as a result of past clay slips [68]. The stone walls delimitating the terraces suffer from lack of maintenance 5.24.

Figure 5.24: Abandoned terrace protecting walls partially built on rockfall debris (May, 2010) .

5.0.12.4 Conditions of the buildings and bastion walls

The buildings and bastion walls, being made of stone (UCL or Globigerina Limestone), are affected by weathering and alteration patterns 5.23 that can be observed on single stones, due mainly to thermal expansion, haloclasty and wind action.

From a structural point of view, although extensive evidence around the enceinte shows rebuilding of structures due to cliff face retreat 5.25, the only evident signs of deformation are related to differential displacement of structures built on the contact between different materials. .

(a)

(b)

Figure 5.25: Identified structural damages on boundaries city walls: a) Evidence of enceinte rectification due to rock mass retreat. b) Structural deformation on the armery bastion (April, 2009).

5.0.13 Monitoring system

The network design We have developed the monitoring project as a result of a collaboration with the Politecnica Ingegneria e Architettura. The monitoring system is designed to be installed within a city environment. He must therefore have a low visual impact and yet be widely disseminated in the ravines, roads, walls and gardens. The choice was therefore directed to the use of a network of wireless sensor network placed inside a prototype monitoring platform for structural instability in urbanized environments with hydrogeological problems.

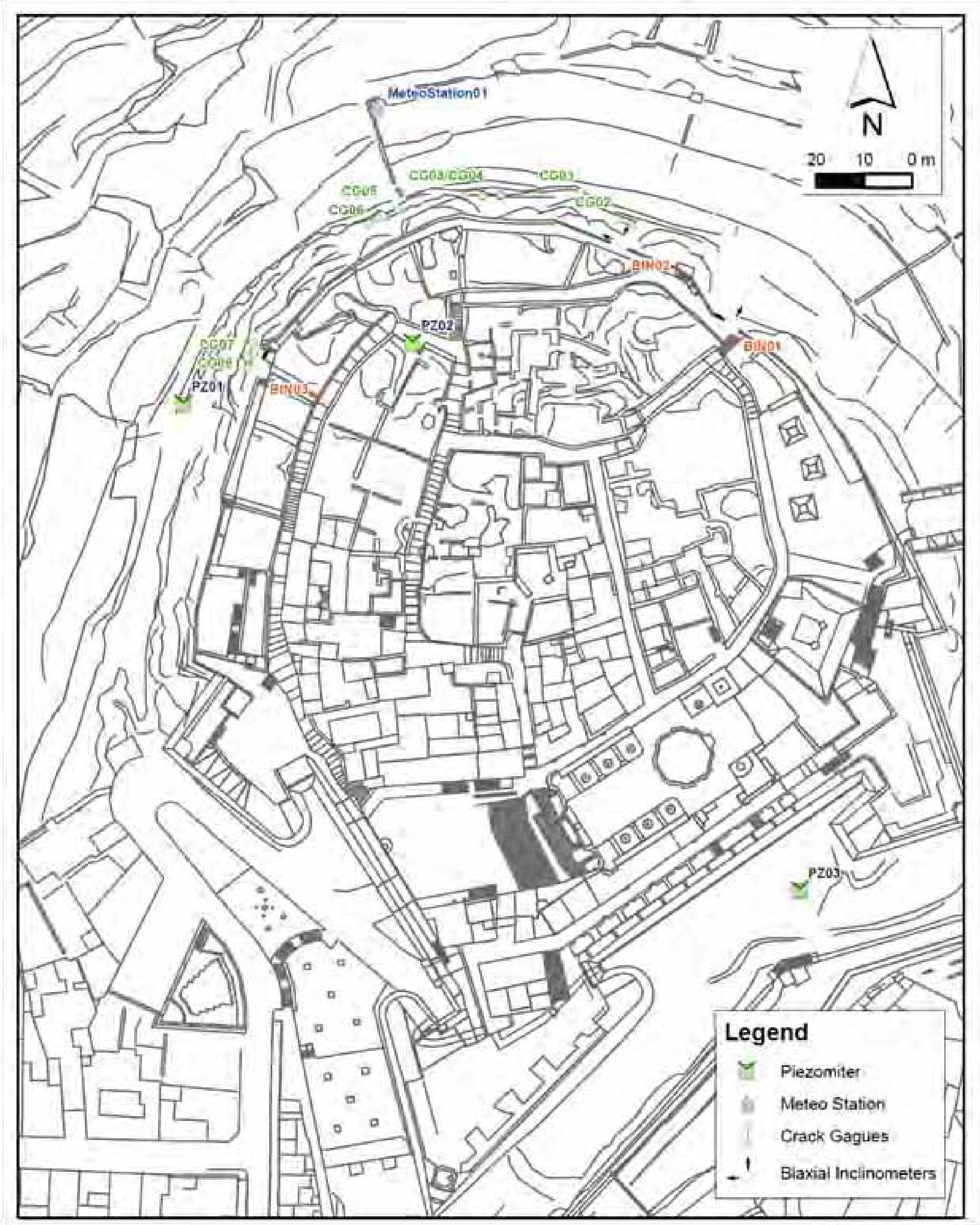

Figure 5.26: Location Map of instruments installed in Citadel (Gozo).

Chapter 6

Integrated systems for the monitoring of Torgiovannetto rock slide.

Introduction Torgiovannetto landslide is located at a former quarry on the southward facing slope of Mount Subasio, 2km NE of the city of Assisi (PG, Umbria Region), Central Italy . It was first observed on May 2003 and, while there is no evidence of correlation between the mass movement and the quarry, it is probable that the extracting activities caused further instability to the whole area. Mount Subasio is part of the Umbria-Marche Apennines, whose geological formations represent the progressive sinking of a marine environment. It consists in a SSE-NNW trending anticline [71, 70, 69] with layers dipping almost vertically in the NE side of the mountain and with several NO-SE striking normal faults on the eastern and western flanks. At the quarry area micritic limestone, belonging to the Maiolica formation (Upper Jurassic – Lower Cretaceous), outcrops. The pureness of this rock (95-99.5% of $CaCO_3$ content) explains the installation of the quarry. The average thickness of the layers ranges between 10 cm and 1 m and sporadically thin clayey fillings may occur [72]. The strike and the dip may vary respectively from 350° to 5° and from 25° to 35°, which means that, in general, the layers dip in the same direction of the slope but with a gentler angle

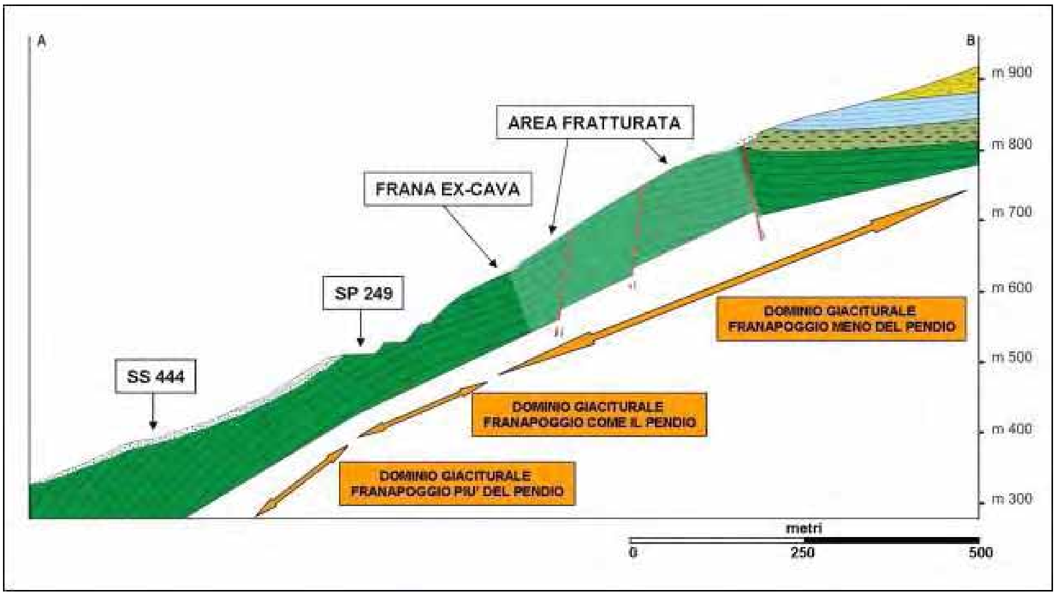

Figure 6.1: Geological cross-section of the northern slope of Mount Subasio (taken from [72]).

The landslide, classified as a rockslide [73], has a rough triangular shape (6.2). The back fracture is a tension crack with an E-W strike, which in some places displays a width up to 1 m. The downhill boundary is represented by a layer that acts as sliding surface and cuts obliquely the quarry front. On the western side the landslide is delimited by a tectonic fracture having a N-S strike.

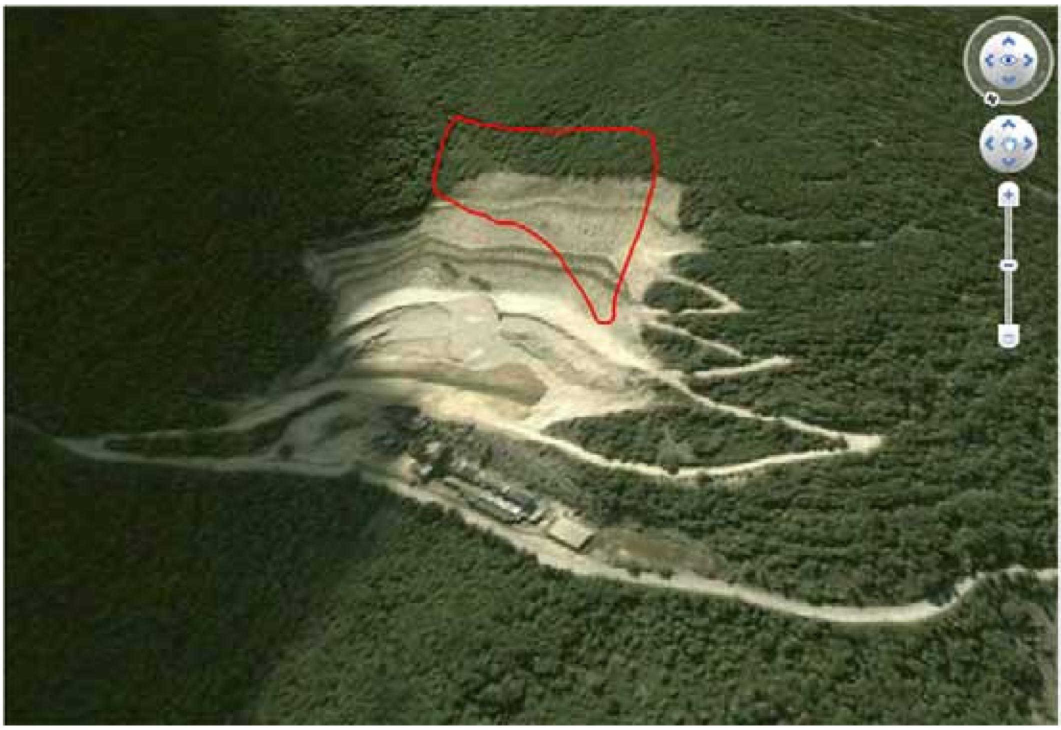

Figure 6.2: Photograph of the quarry and delimitation of the landslide (modified from [78]).

The whole moving mass has an estimated volume of 182.000 m3 [74] Two minor landslides detached during spring 2004 [75] and December 2005 [76] with a volume of respectively few tens and 2500 m3, providing some hints for the mechanical behaviour of the whole slope movement.

Movement pattern and monitoring system The first monitoring campaign had been carried out by Alta Scuola [102], which performed a topographic monitoring and installed several wire extensometers as well as few inclinometers on the landslide. Measurements obtained from the topographic benchmarks from spring 2004 to spring 2007 show that the fastest moving part is the eastern one, close to the back fracture, and as moving westward the displacements decrease. This is possibly due to the friction wielded by the lateral crack, not fully developed yet [74]; Moreover the benchmarks located on the eastern side reveal that the vertical displacements prevail upon the horizontal ones, while the contrary occurs on the western side. The extensometers gave similar results and during the period March 2005 - May 2007 recorded a highest velocity of 1.2 mm/day nearby the eastern end of the back fracture and 0.1 mm/day on the western end. The displacements measured by extensometers here represent the 50-65% of the displacements recorded via the topographic monitoring; this can be due to several reasons, especially that extensometers measured deeper movements and that the benchmarks could be affected by external factors, such as small rock falls. Of the five inclinometers that were installed only one gave useful information. In particular it showed that the sliding surface is 10-12 m deep. In addition it measured that the movement direction creates an azimuth angle of 7° with respect to the north and dips 25°-28°. This datum is in accordance with the topographic measurements and so it appears that the whole landslide moves along the same direction. All these monitoring systems showed a certain degree of seasonal fluctuation. The month that displayed the highest velocities was April, while the minimum was recorded between July and September; the winter season usually presents a new acceleration phase. It can also be stated that the landslide is more sensitive to long rainy periods (and therefore to 30 and 60 days antecedent rainfalls) rather than short intense events [75, 74].

6.1 Multi parametric platform

Here, the WSN, the rain gauge, and the accelerometer work together and change their settings in real time, depending on the intensity and variation of the measured parameter.

In particular, the accelerometer helps WSN to conserve energy while maintaining high measurement accuracy, especially in moments when you could do the most important recordings, such as rapid impulsive movements of the landslide.

The previous monitoring period has shown that we can appreciate intermittent movements of the landslide, however occurred only two paroxysm events from 2003 to these days.

The landslide was noted in May 2003, since then there have been two relatively small paroxysmal events within the landslide body that have occurred in the spring of 2004 and in December 2005 6.3, the first involving a volume of rock as a few tens of m3 and the second approximately 2500 m3.

Figure 6.3: Landslide of December 2005 (taken from [76]).

Installing a monitoring system that runs continuously would be the best way to monitor a continuous process, the higher the sampling rate and the higher the amount of information that I have acquired. However powering on a monitoring system only when there is movement would be more than enough to monitor processes that have an intermittent behavior. For the natural processes that have a periodic behavior is easier to schedule a time tracking, but for those processes that behave in a seemingly random is not possible. However some of these processes are luckily linked to other processes that are often the trigger. They can then be used to control the sequencing of the monitoring activities and the acquisition frequency.

Normally, the sensors of the WSN make an acquisition every 60 seconds, but are sent to the gateway data averaged every 5 minutes. The proper operation of WSN is closely linked to the consumption of energy. Every time I run a measurement every node must activate the radio processor, the AD converter and the transducer. Therefore, the higher the frequency with which you perform the steps the higher energy consumption. The slope has an unfavorable orientation for solar power, as it is exposed to the north.

6.2 Wireless sensor Network

The idea of installing a wireless sensor network is of Prof. Casagli, this type of solution has many positive features. Having to identify a "new" product, until then we only worked with traditional methods, we was looking for a solution that was as much as possible standard, open and documented. From an architectural perspective, the choice to use as Tiny OS operating environment was absolutely appropriate and successful. The problem was to choose which radio processors to use. At the time of the project only two brands were available, or at least accessible, in Europe: a product that was somehow related to INTEL and one sold by Crossbow. For that type of application we chose crossbow, because it was marketed in Italy.

(a)

(b)

Figure 6.4: The schelter contains the gateway, batteries, and central recording unit. a) View of the shelter from west. b) Inside view of the schelter (February, 2010).

The sensor network is based on four sets of macro-components: ·

- Radio processors
- Analog-digital converter
- Transducers
- Gateway

Radio processors We used MICA2 MPR400CB processors. The limitation of this type of objects is that when a problem occurs, managing the data in total autonomy, the only chance of recovery is a classic turn off and on again. Another significant problem is that of consumption. In fact, when the processors are in an X-MESH they are almost always active transmission and therefore consumption are high.

6.2.1 A/D Converter

One of the reasons because of the choice fell on CrossBow was also the availability of three different A / D converter:

- Built in with a resolution of 10 bit;
- MDA 300 with 12 bit resolution (the one we used);
- MDA 320 with 16 bit resolution;

However, after only three months of using the model with 16bit resolution was removed from the list and then we had to use all 12-bit. In any case, the input of the converter is very little robust and consequently we had a remarkable loss of these objects.

6.2.2 Sensors

The first installation was done with sensors Celeschi PT8101-0060 model, with measuring range of 1500mm, in October 2007. The sensors themselves are good products, however I would have to take into account the fact that I used a 12bit AD converter and then a bit would come to weigh almost 4 / 10. For this reason, strain E11-E14 yielded highly unstable measures. The choice of the range of measurement is influenced by wanting to avoid intervention of "repositioning". The behavior of the landslide and the velocity of movement was not yet clear at the beginning of the activity! Subsequently, the network has been integrated with the sensors installed by the previous supplier, model JX-PA-20. These sensors have a measuring range of 500mm, are much less expensive, even if they must be better protected from the elements but with hindsight, however, perform their work admirably.

6.2.3 Gateway

We used the RS232 gateway MIB 510 as collector of data. we have created an application that acquires data from the network and stores them in a DB, using the protocol documentation.

The gateway 232 is connected:

- to a GPRS device that transmitted transparently data as coming from the network (Initially);
- two redundant PCs are used for data acquisition, processing and dispatch of alarms (during the initial installation period);
- to a data-logger that captures locally and transmit them via GPRS (Currently).

6.2.4 Challenges

During the first period of use we found some problems with wireless communications, multi-path and energy consumption were the main problems, some time they were insurmountable, so we adapted the project. We created a "mixed" WSN in which there are both wireless components and traditional wiring.

Another real criticism of the system was the difficulty of having enough energy in the period from November to February. The dorsal power that we created in the upper part of the fractures at the top of the slope becomes a perfect system to collect any discharge which was passing nearby. So much so that they are actually spoiled three charge controllers. The first five years of countless uses. To keep the wireless system I had to work a lot on the cleanliness of food and the surge protection but I'm pretty sure that the levels of signal processors is disturbing that the converters are below the thresholds (30 V) of normal protections. In support of this theory the fact that the radio processors inside the landslide body and having an independent power supply is much less spoiled son (perhaps even only one time following a significant event) than those placed under control of the fractures of the mountain. The data had problems when the devices were connected to the PC, but with both the direct RS232-GPRS gateway that now with the modem connected to a data-logger works fine.

6.3 Accelerometer

An accelerometer Mod. BASALT produced by Kinemetrics [77] was installed in 2010 in the quarry near the road n ° 25. It is used to monitoring mechanical energies, both those coming from seismic events and those from the movement of local surface such as rock falls or opening cracks.

Figure 6.5: Bird View of Torgiovannetto landslide, accelerometer is installed at roadside (modified from [78]).

(a)

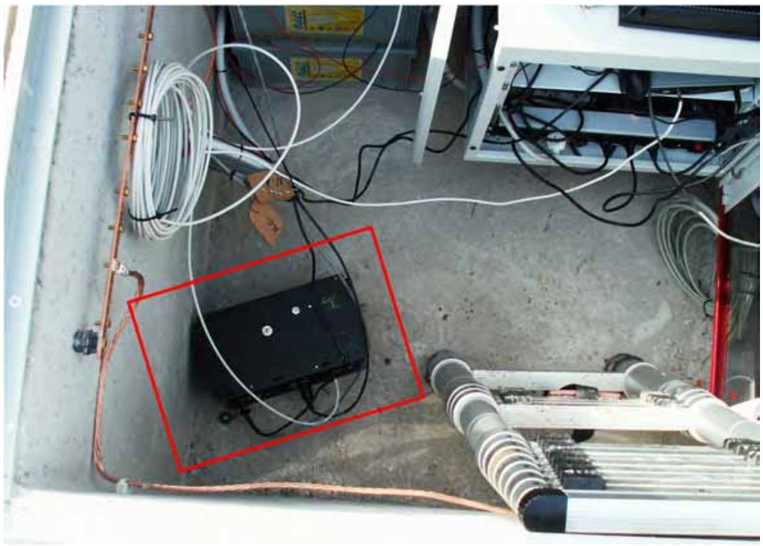

(b)

Figure 6.6: Accelerometer installed at Torgiovannetto landslide: a) Front view (taken from [77] b) Top view in the shelter (February, 2010).

Synchronization tool	GPS
Data Acquisition Type	Individual 24-bit Delta Sigma converter per channel with Black Fin DSP
Anti-alias filter	Double Precision FIR Filter Causal/Acausal; >140 dB attenuation at output Nyquist
Dynamic range	200 sps ~127 dB (RMS noise to RMS clip - Typical) 100 sps ~130 dB (RMS noise to RMS clip - Typical)
Frequency response	DC to 80 Hz @ 200 sps
Sampling rates	1, 10, 50, 100, 200, 250, 500, 1000, 2000 sps
Communications	Modem, RS-232, Ethernet interface
Acquisition modes	Continuous, triggered, time windows

Table 6.1: Main features of the accelerometer (modified from [77].

For our purposes this instrument is used as a switch.

Figure 6.7: Real time web interface.

6.3.1 Self-adaptive configuration

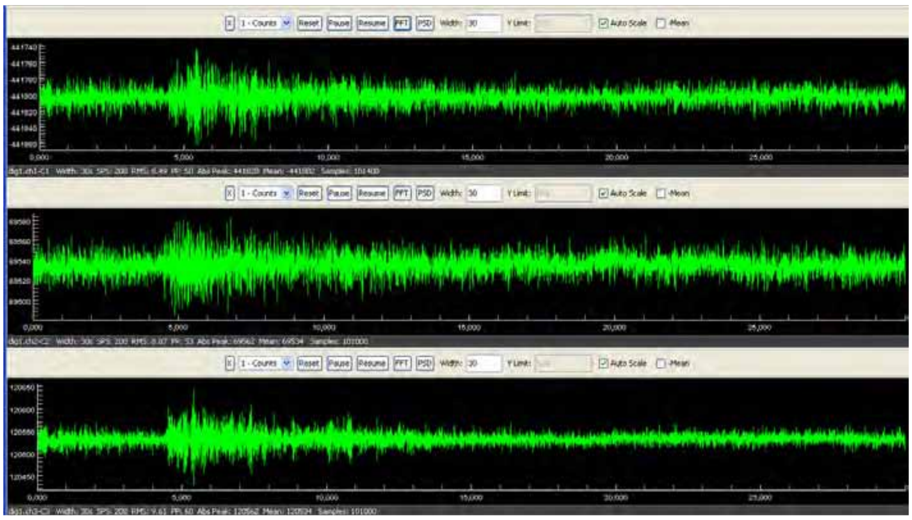

Figure 6.8: Real time wave visualizzation.

During a period of 6 months we created a signal library (Annex 2), we discriminated those from vehicles from those from earthquakes.

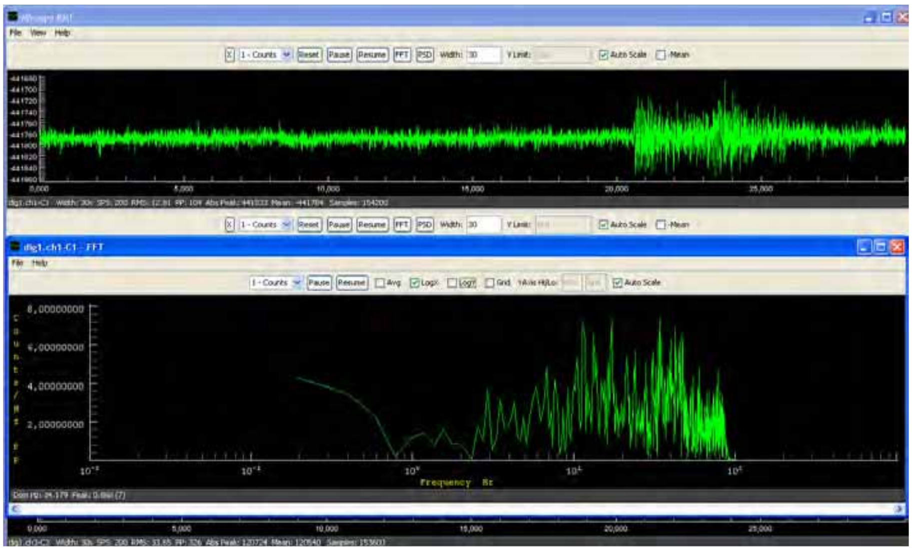

Figure 6.9: Real time FFT analysis of recorded signal.

When acceleration exceed threshold value the system store the recorded signal. Then, a signal FFT analysis is carried out. If the signal is can be correlated to a seismic event, the monitoring system is alerted and the acquisition frequency of the WSN increases.

From this moment, the instruments perform a measurement once per second and, the recorded row data are composed without mediate measurements but one by one.

In this manner we intend to investigate short but rapid movements (mm/ss), that would be invisible to a monitoring system with low measurement frequencies. According to Jibson (1993), an Earthquake can produce impulsive movements. This type of data would provide key information for early warning activities and landslide forecasting [112].

At the time the seismic events recognition is manually executed, but a Matlab program is under construction for this purpose .

The simultaneous use of both systems increases the WSN effectiveness without actually implement in any way the original monitoring system structure.

6.4 Interferometric campaigns

In addition to the traditional measurements, two short-term monitoring campaigns were carried out by University of Firenze, Earth Science Department (UNIFI-DST) by using two different ground-based interferometric radars (GB-InSAR); the first one was performed in collaboration with LiSALab-Ellegi from March 29th to April 14th 2006, while the second one with Ingegneria Dei Sistemi (IDS) from April 11th to April 18th 2008 [79]. The systems adopted are different but share the same basic principles [81, 80]. Two microwave signals are emitted in two different times; the waves reach the target (e.g. the landslide) and are backscattered to the radar, where their amplitude and phase are measured. If, between the two acquisitions, any movement occurred, a phase difference is hence measured. Then from the phase difference it is possible to calculate the actual superficial displacement with millimeter accuracy. If the radar acquires data while moving along a rail (synthetic aperture radar) displacement maps can be computed. Many applications of this technique to monitoring of unstable slopes can be found in literature [83, 82]. 6.10 shows a comparison between an optical image of the landslide and the corresponding power image, function of the backscattering of the microwave signal. This is necessary to correctly interpret the following displacement maps.

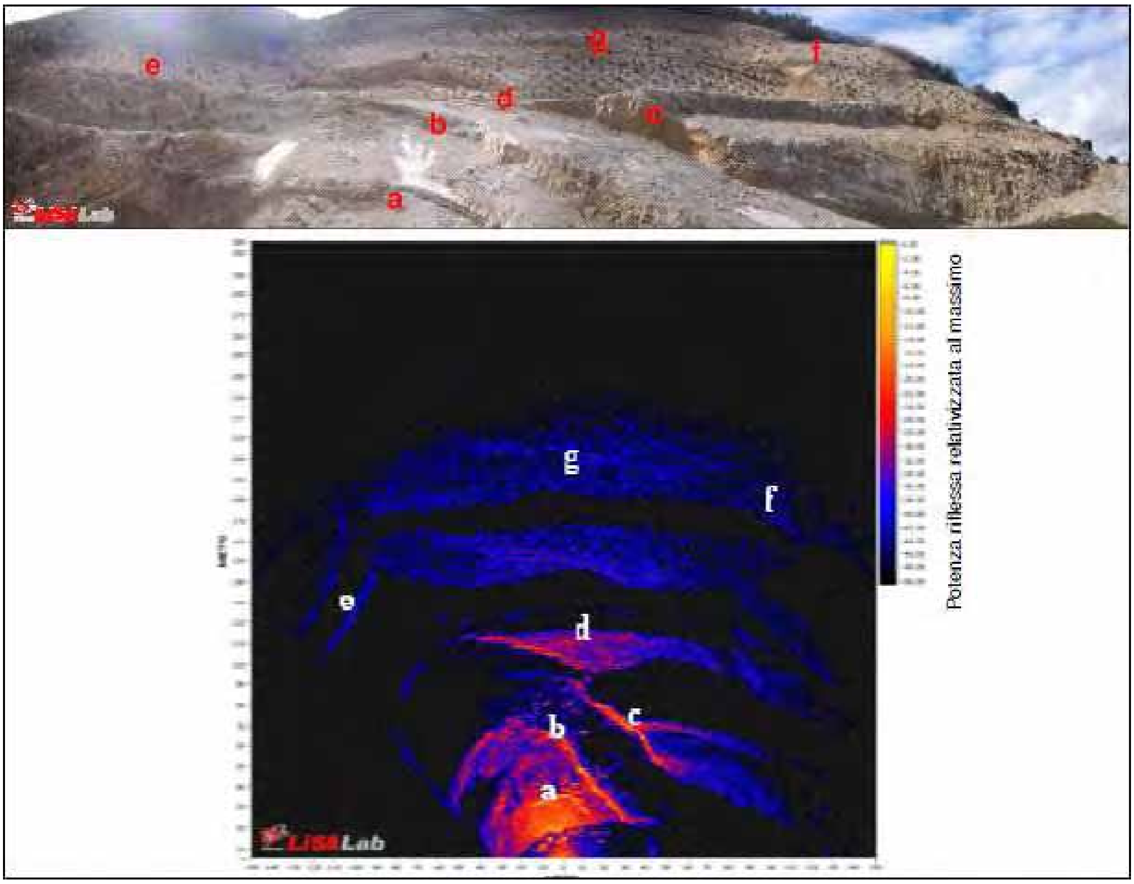

Figure 6.10: Photograph of Torgiovannetto landslide (top) compared to a power image (bottom) both acquired from the radar position during the 2006 campaign (taken from [79]).

The results from the 2006 campaign confirm the picture obtained from the traditional instrumentation 6.11. The whole moving area is clearly detectable, as the surrounding zones (in green) are completely stable. The fastest moving spot is the one at the left side (east), corresponding to region 1, where the average velocity is nearly 1.5 mm/day. The velocity decreases while moving toward the up-right corner (south-west) and reaches the minimum nearby point B (0.4 mm/day). Downhill, all along the basal discontinuity the velocity ranges from almost 1.3 mm/day in region 2 to almost 0.8 mm/day in region 4, while in region 3 it reaches 0.9 mm/day. Between regions 2 and 3 a thin yellow line (0.4 mm/day) bordering the landslide can be noted. This last feature is more remarkably clear from a displacement map obtained from the 2008 campaign 6.12 where a blue line (0.6 mm/day) indicating a slower movement corresponding to the sliding band is visible. The presence of this slow moving layer can be related to the existence of a clayey filling, as described above. This layer detaches the unstable mass from the stable rock, making the passage between the moving and the unmoving zone so neat.

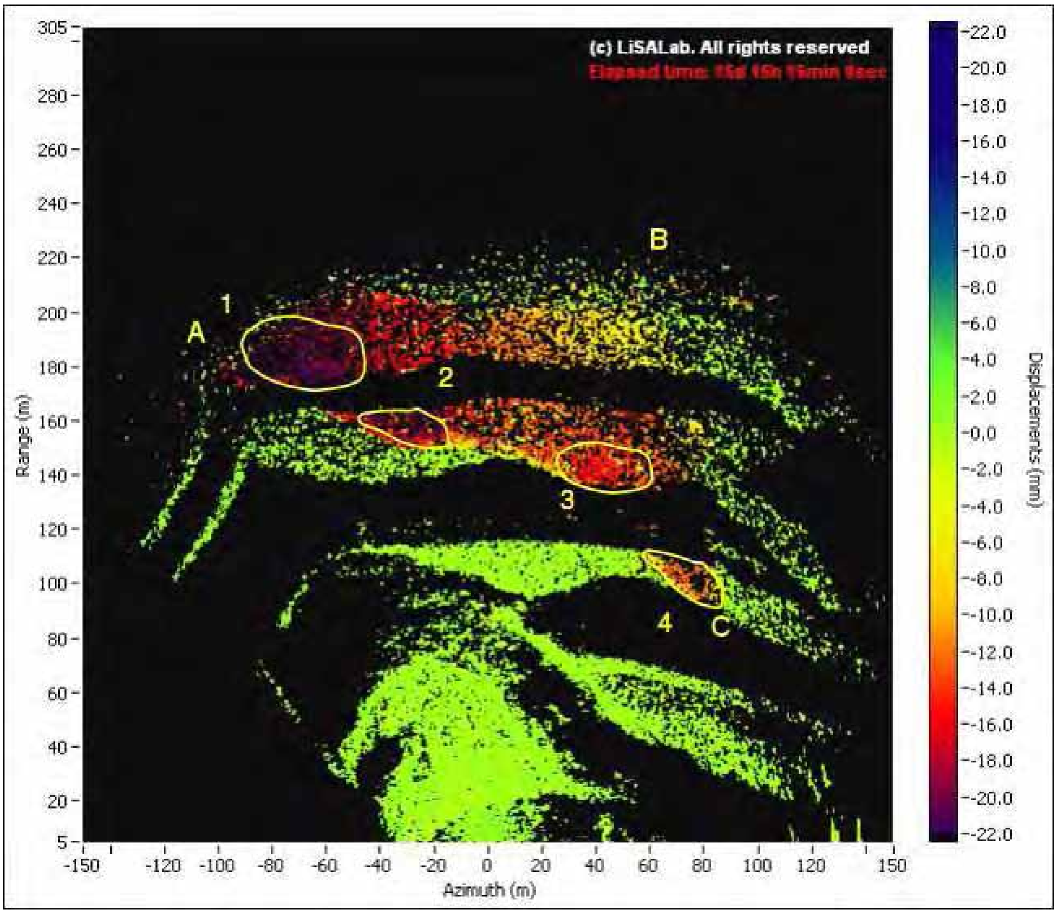

Figure 6.11: Displacement map referred to the time interval from March 29th to April 14th 2006. The letters indicate the vertices of the landslide, while the numbers denote the four areas that showed the highest movements (taken from [79]).

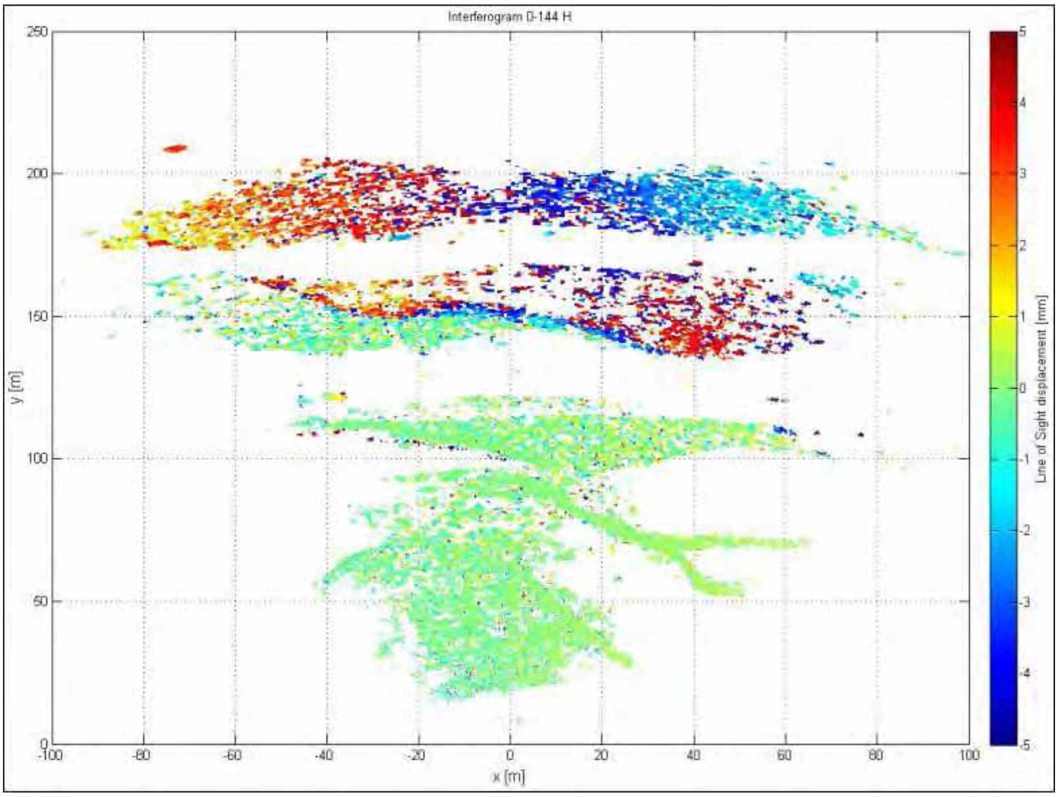

Figure 6.12: Displacement map referred to the time interval from April 11th to April 17th 2008. (taken from [79])

The comparison with 2008 campaign shows that the geometry and kinematics of the landslide remained almost the same during 2 years, with some minor differences in the average velocities (0.3 mm/day for corner B, 1.1 mm/day for region 3 and 1.4 mm/day for region 1). This means that, except for the seasonal variations, Torgiovannetto landslide displayed quite a constant behavior during this period. Another important result obtained by the GB-InSAR campaign is the precise assessing of the unstable area and so a reasonable estimation of the volume involved, necessary for developing models.

6.5 Current monitoring

At present 13 extensometers and a thermometer - rain gauge station are installed on the landslide. The location of each instrument is showed in 6.13, together with the main fractures.

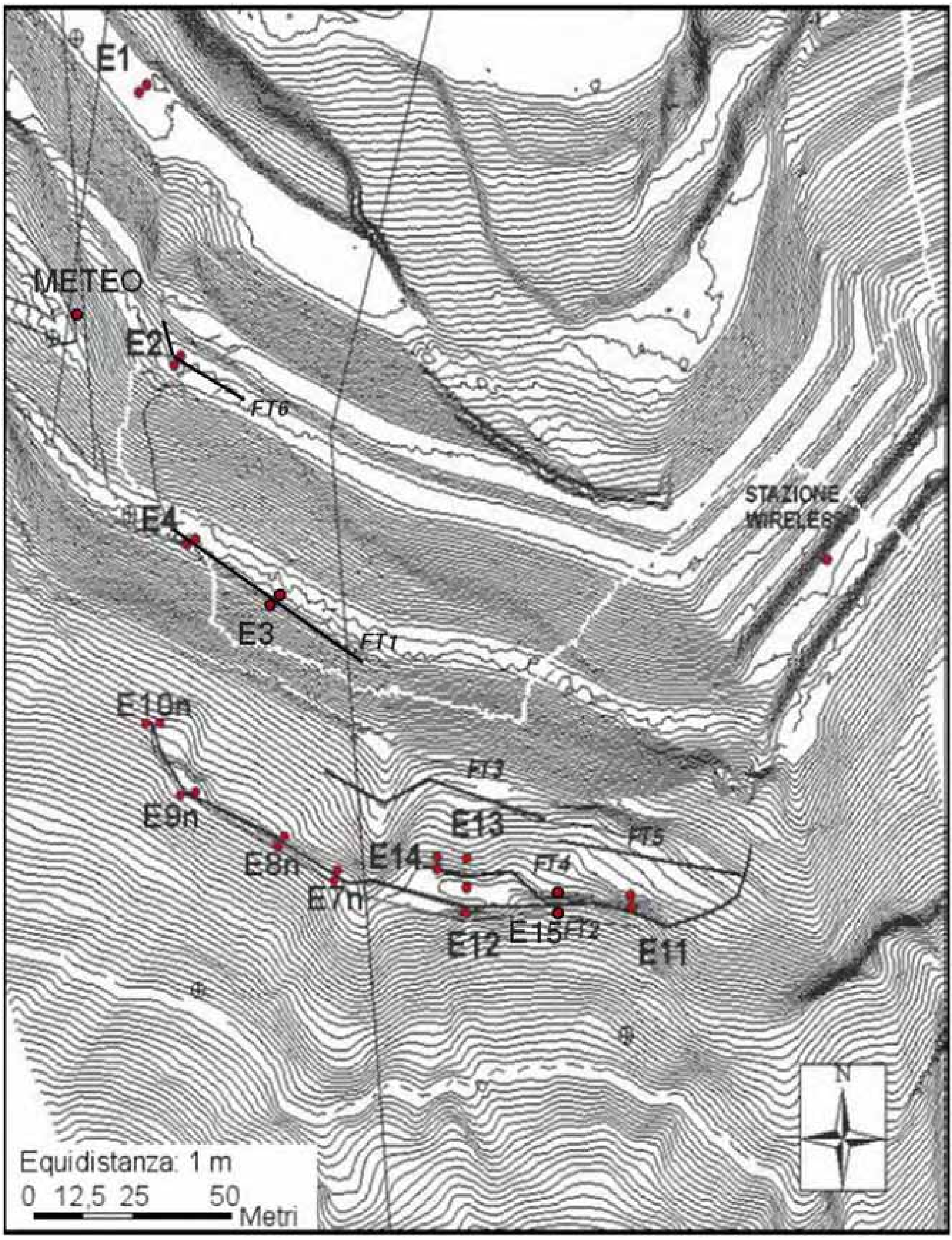

Figure 6.13: Location of the instrument installed at Torgiovannetto landslide. The main fractures are also shown.

Extensometers E10n, E9n, E8n, E7n, E12, E15 and E11 are all located in correspondence with the back fracture (called here FT2). E14 and E13 measure the aperture of the fracture named FT4, just below the previous one. FT1, within the body of the landslide, is monitored by extensometers E4 and E3, while the fracture FT6 by E2. The extensometer E1 is positioned at the NW corner of the landslide and the meteorological station outside the unstable mass. The extensometers consist in an aluminum or stainless steel box with inside and array of sensors and a stainless steel wire, sheathed in nylon or thermoplastic. They can endure extreme temperatures, from -20 °C to 100 °C. The instruments collect a history of around 3 years of data, even if a few interruptions have been occurred to some of them.

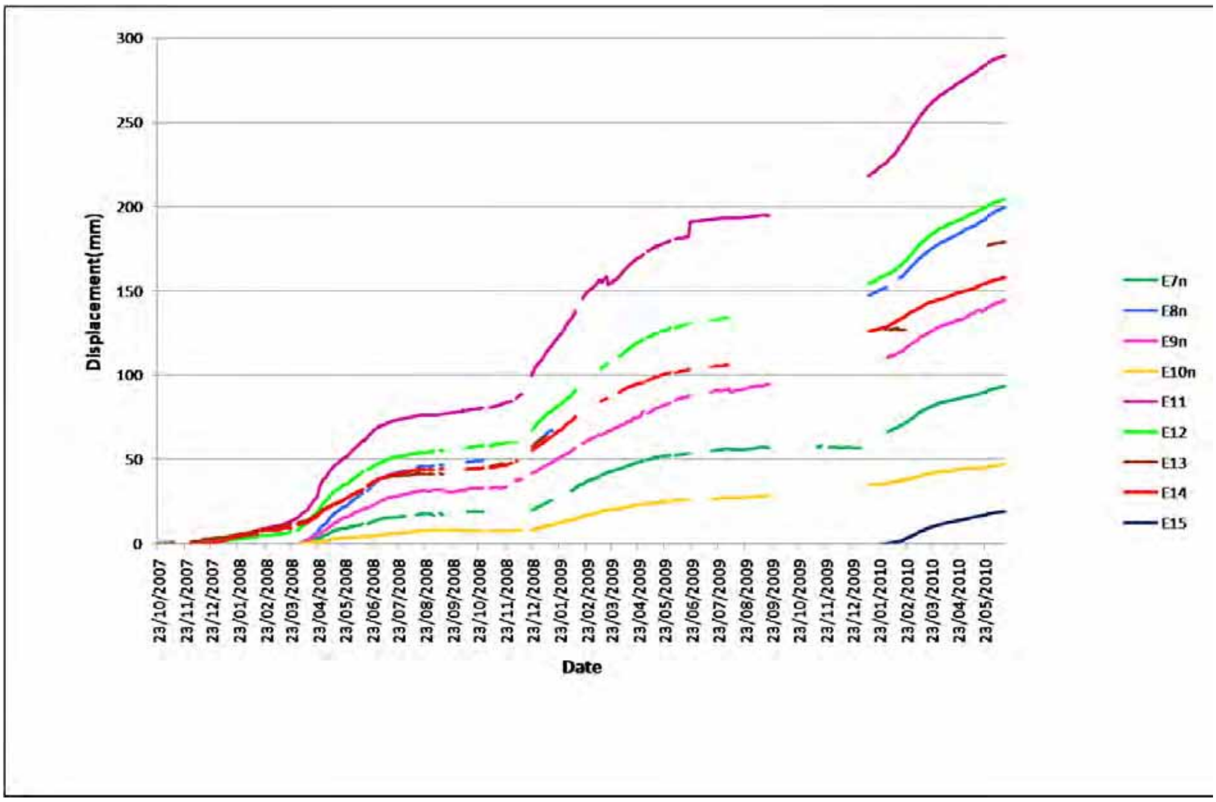

Figure 6.14: Chart of movements recorded by extensimeters at the top of the landslide (taken from [4]).

Since the second half of 2007 to October 2010 the periods showing the highest movements were April 2008 (when E11 measured a daily velocity up to 2.77 mm/day), December 2008 – February 2009 (with a maximum daily velocity of 1.39 mm/day recorded by E11) and February 2010 (during which the highest velocity has been 1.02 mm/day, measured by E11) [4]. Generally the most active seasons proved to be spring and winter, while during summer and autumn the landslide usually experiences low to null movements. This behavior is in accordance with the previously discussed results and it can be related respectively to the presence or lack of extended rainfalls. The highest velocities are still found in the eastern end of the back fracture (E11) and they regularly decrease as moving to the western end until E10n, with the only exception represented by E7n which, even though being in the middle of the fracture, displays low movement rates. The instruments placed at the fracture FT2 show lower displacements, similar to those of E8n. Fractures FT1, monitored by E3 and E4, and FT6, monitored by E2, measure even slower movements, although a daily velocity of 1.63 mm/day was reached by E2 in April 2010 and 1.65 mm/day by E4 in April 2008. E1 has always been almost still. By comparing these data with the ones obtained from Alta Scuola a general slowdown is assessed. For example E11 measured nearly 290 mm in the last 2 years and half, while the corresponding instrument during the previous campaign (E5) recorded up to 250 mm from March 2005 to April 2006. The main exception to this behavior is represented by E10n which maintained a similar velocity.

Chapter 7

Elba Island

The investigated road section is located on the southwest coast of the island, in the town of Punta Timone (Chiessi, 42 ° 45’48 N - 10 ° 06’24 E) 7.1. The area is located within a sector of high natural value and, therefore, with the approval of the Plan of the Tuscan Archipelago National Park (Regional Board resolution No. 87 of December 23, 2009) was placed in the conservation area (Tuscan Archipelago National Park, 2010). Furthermore, the entire area was bounded under P. A. I. This sector of Island is classified as very high hazard geomorphological area (PFMEA).

7.1 Geological and geomorphological setting

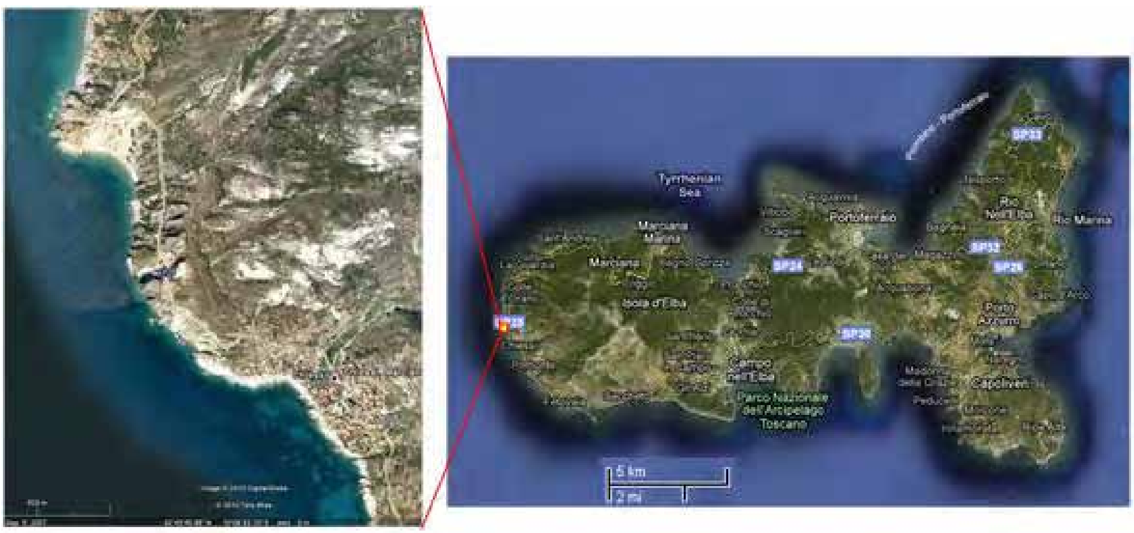

Figure 7.1: Geographical Location (modified from [74]).

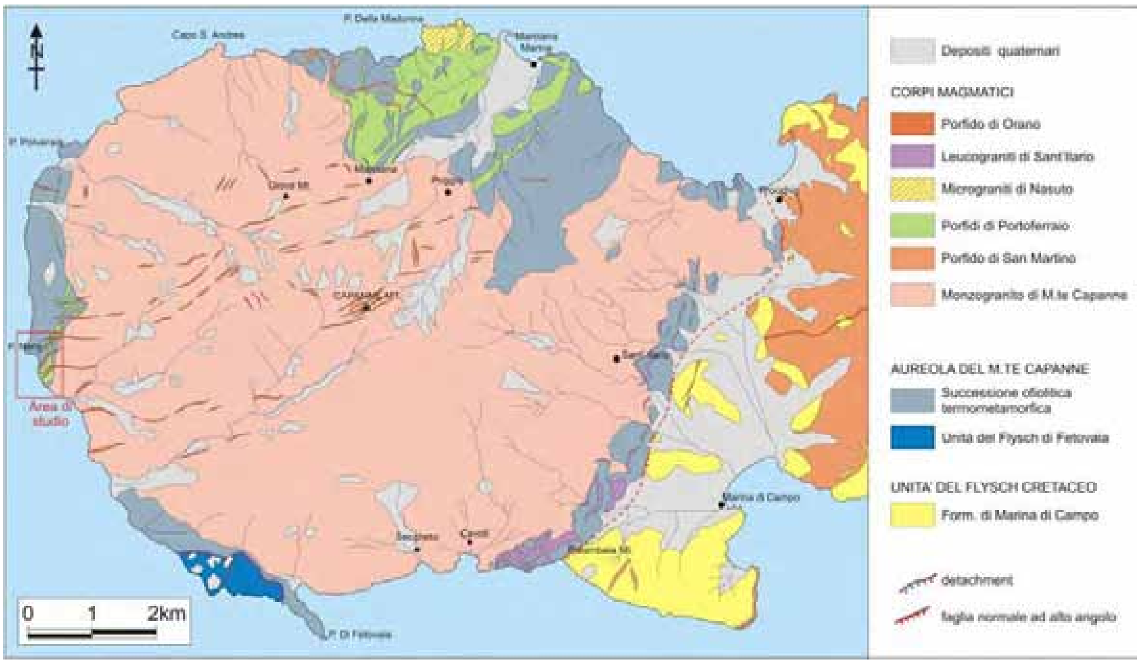

Figure 7.2: Schematic geological map of Mount Capanne (modified from [107]).

In the study area 7.2, the ophyolitic unit lies above the ophiolitic intrusive body, which produced a clear thermo-metamorphic imprint on rocks of oceanic origin, in other medium-facies grades (from cornubianiti to hornblende in a cornubianiti pyroxene: [84, 85]. In the sector of Punta del Timone 7.3it is represented by the ophiolitic sequence Metabasalti and schists and clayey schists 7.4a, resulting from metasomatism of "clay Palombini" Unità di Punta Nera-Punta Fetovaia [86].

This formation can be observed in good outcrops along the coast and the scenic road, it constitute the stratigraphic higher term of the succession. And well represented by metapelites biotitic, sometimes silty, dark gray, black and gray with dark reddish-scaly fracture plates, which are interspersed with layers of meta-gray siliceous limestone, the latter have a thickness from centimeters up to nearly a meter and a laterally discontinuous pattern7.4b.

Bouillin (1983) has found planktonic microforaminiferi of Cretaceous age (hedbergelle, rotalipore, and perhaps even Planomalina Buxtorf) in the limestone promontory of Fetovaia rock. Their presence is in line with age-aptiana cenomaniana age defined for this formation in the Northern Apennines.

As mentioned above in the study area there are also masses of basalt, which rose up directly to Palombini Shales, like almost all sequences outcropping around the M. Huts. This is massive faneritic metabasalti , but with tiny or micro-crystalline crystals. This crystals are mesocrati, dark green, sometimes greenish, and reddish-brown to alteration.

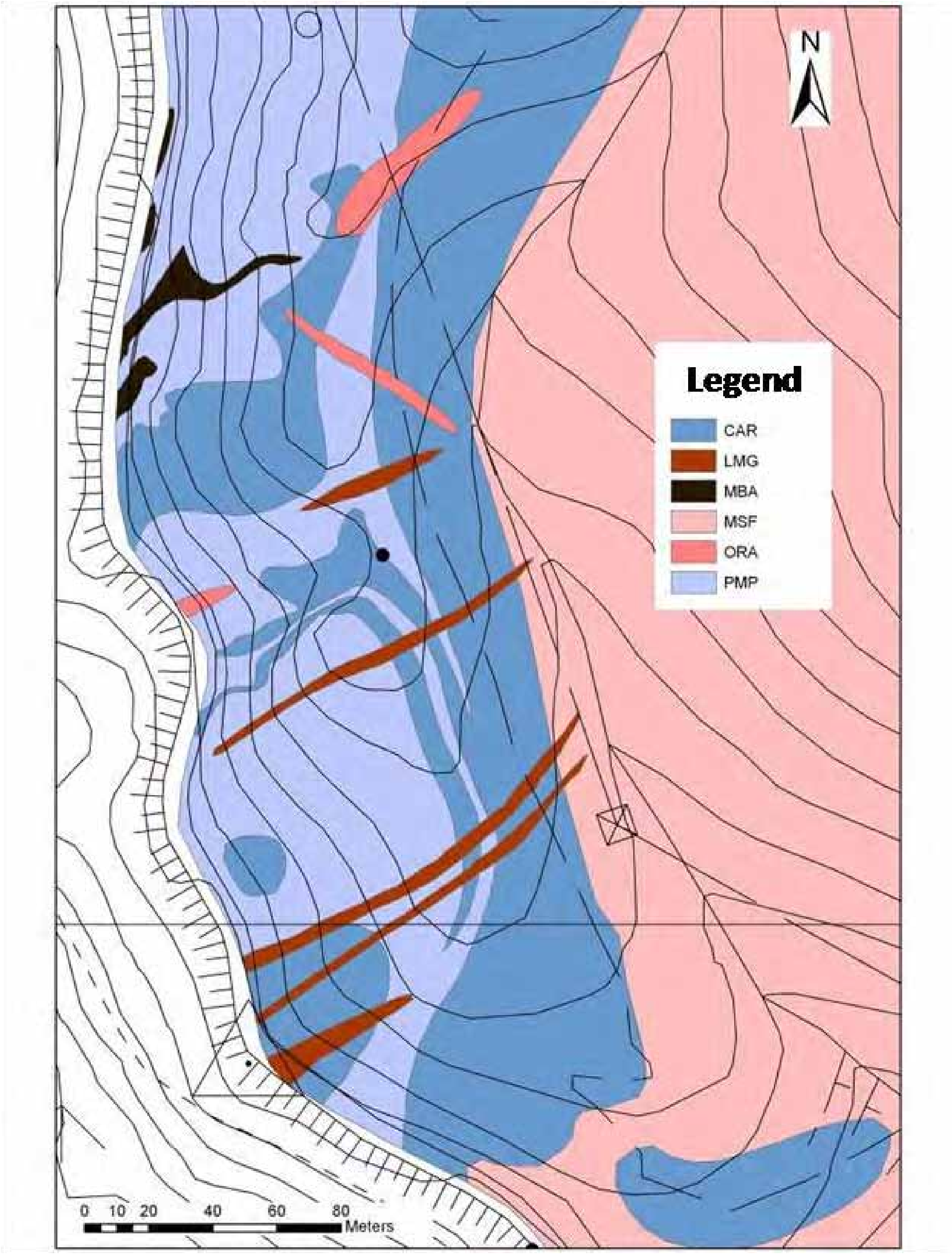

Figure 7.3: Geological Map of the study area elaborated by geological detailed survey. (CAR: schists and clayey schists; LMG: Leucograniti and Micrograin; MBA: Metabasalti; MSF: Monzogranito del Capanne TIME: Porfidi di Orano; PMP: porphyry of Portoferraio).

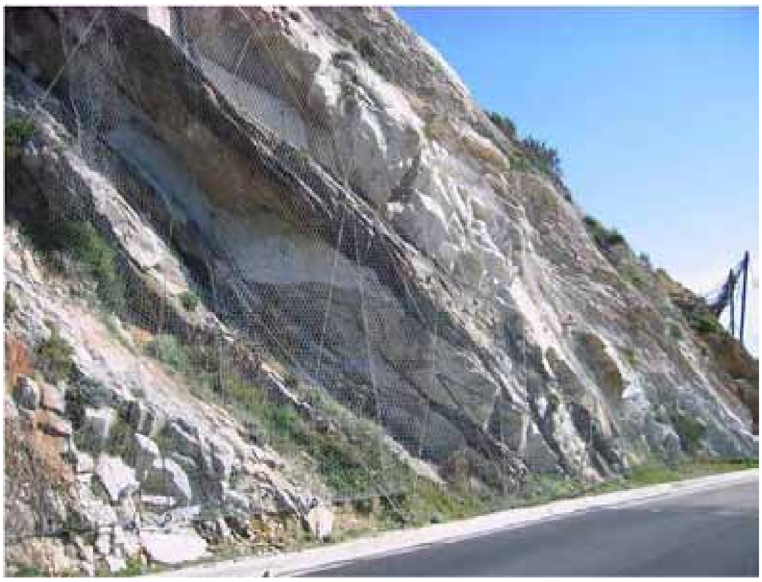

(a)

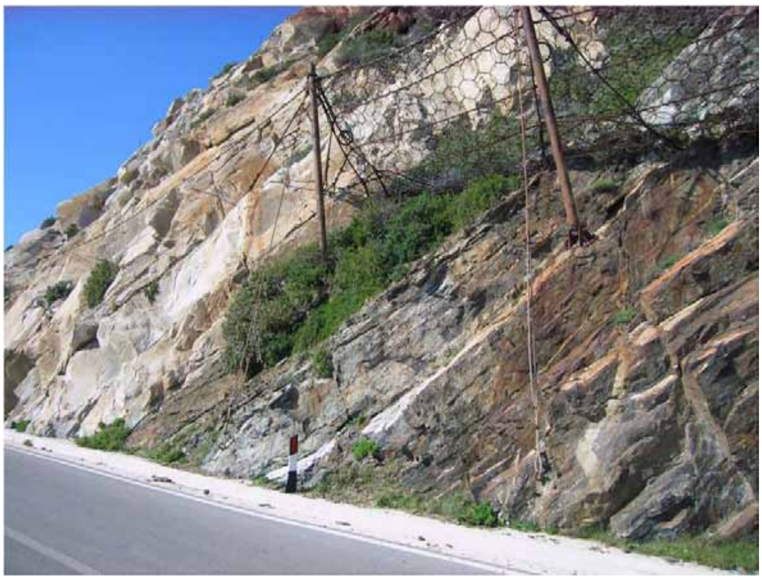

(b)

Figure 7.4: Outcrops along the road N°25 (April, 2010). a) Level of schists and clayey schists in the Porphyry of Portoferraio. b) Contact between the schists and clayey schists and Porphyry of Portoferraio.

The pluton of Mount Capanne corresponds to a monzogranitico and granodiorite mass, locally characterized by large megacristalli of K-feldspar and mafic included. In the study area, the porphyry and porphyry of Portoferraio and the porphyry of Oran, as well as numerous filoncelli leucogranitic and microgranitici, cut the pluton and its coverage with complex geometries (7.57.6).

The Porphyry of Portoferraio (ca. 8 Mya) has monzogranitica-sienogranitica composition and it is characterized by small phenocrysts of quartz, feldspar and biotite 7.5. The swarm of filoncelli leucogranitici appears near the contact with plutonium, and in his coverage. The dikes, with a metric and plurimetric thikness, have sienogranitica composition 7.5. The Porphyry of Orano has monzogranitica and granodioritic composition, with olivine, clinopyroxene and phlogopite and typically dark color [88, 87]. This porphyry results to be the most recent intrusion (6.9-6.8 Mya) [88, 86] and it cuts the entire complex and its aureole .

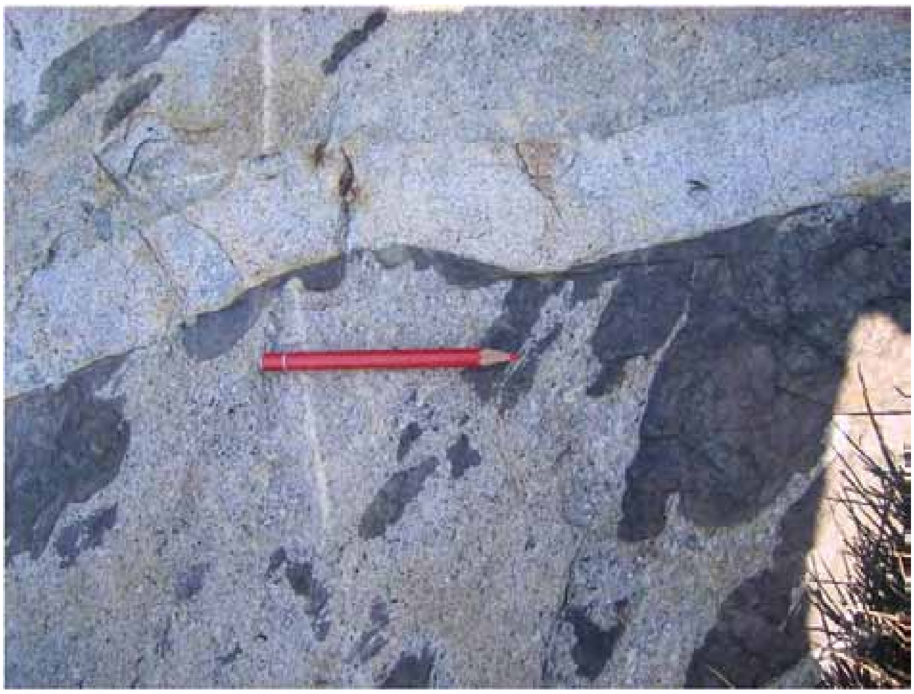

Figure 7.5: Punta del Timone: contact between the schists and clayey schists and Portoferraio porphyry, cut by a filoncello leucogranitico (April, 2010).

The concerned sequence is characterized by widespread phenomena of recrystallization, essentially static, linked to the Tertiary magmatic intrusion of Monte Capanne. Thermo-metamorphic events are locally clearly associated with ductile structures (eg. folds, shear bands milonitiche), referring to two different deformation events[89], followed by a ductile / fragile event. This last event is linked to the discharge phenomena of the d Monzogranito shell of Monte Capanne during his lift [90] and to a late brittle fracture, given by stress phenomena related to the cooling of the pluton.

In Punta del Timone outcrops the most prominent element of the fabric of the schists and clayey schists is a medium / high angle dipping penetrative foliation to the predominantly westerly. The foliation is spaced at the millimeter / sub-millimeter scale and locally it is cut by faults and fractures at high angle. These faults are sometimes characterized by planes streaked with south / southwest dipping .The porphyry of Portoferraio is locally (in Punta del Timone outcrops) involved in the ductile deformation structures observed in ophiolitic metamorphic sequence.

These porphyries, especially when they are of small thickness, have a clear tectonic foliation, consistent with the casing rock, .

Figure 7.6: Filoncelli leucogranitici in the porphyry of Portoferraio (April, 2010).

From a geomorphological point of view extremely steep slopes with intensely altered and poor vegetated soil are found. This kind of soil n the have the same mechanical behavior of detritic material. This alternates with portions of rock mass outcrops of considerable size, that because of their fracture and their franapoggio outcropping tend to release blocks of various sizes downstream .

Over time this activity has resulted in the isolation of three big mass of rock. These mega-bocks (which are designated as a 1st, 2nd and 3rd Mass from North to South along the slope under consideration) are elongated along the direction of maximum slope, 7.7. The Masses 1 and 2 are currently lent against the substrate only along the foliation basal plane. The third mass is laterally constrained also.

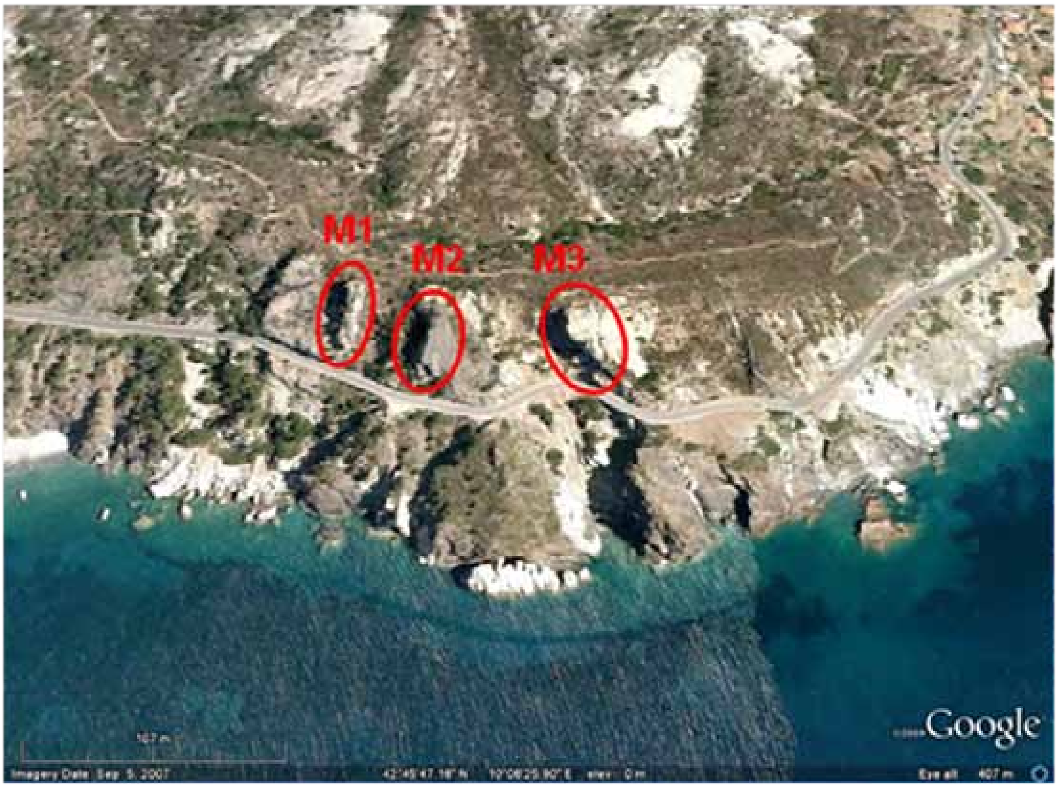

Figure 7.7: Portions of the rock mass, which overhang provincial road N° 25. Highlighted masses: mass 1 = M1, M2 = 2 mass, mass 3 = M3 (taken from [78]).

7.2 Elements at risk

These landslides have resulted in serious security problems for the viability of the SP No 25. The road, called "Ring West" of the island, run within some villages (Pomonte Fetovaia Chiessi, Marciana). The greatest risk road sections were identified in correspondence of Ciglio Rosso, Ogliera, Colle d'Orano, Punta Nera – Punta del Timone (Tuscan Archipelago National Park, 2010). At Punta del Timone, a few meters above the roadway, there are those rock masses, that are the main source of risk relation to partial or total gravitational movements of rock. The local criticity is more likely associated with the individual blocks fall , while the worst scenario for the area is related to the detachment of large clusters with significant risk for the existing infrastructure 7.8 and passing vehicles, especially during the summer.

Figure 7.8: Section of provincial road N° 25 within the study area (March, 2010).

7.2.1 Protection works

Considering the importance of road SP No 25 various works of protection were progressively done and monitoring system were installed. The monitoring system was active, with interruptions and subsequent additions, from the late '80s until 1998, when it was finally abandoned. Here a non-exhaustive list of protective structures in the area concerned, following the temporal order of their installation is provided:

- 1986: rockfall protection located in the portion of the slope behind the SP No 25, in the field consists of the downstream portions of the Ground 37.12.
- 1988-'89: surface nailing located in the portion of the slope behind the SP No 25, downstream of a mass 7.12. Active rods made of steel bars of a 38-42mm diameter located in the upstream portion of the mass 3 (most of them are rusty, others are broken or brittle due to corrosion) (7.10). Underpin and curbs, both studs and bolts, they have been installed from the central area to the area beneath the Mass 3 (7.11).
- 1997-'98: Boulder net installed downstream of mass 1 (7.12); scattered nails (7.12) and tied underpin, both installed within the southern part of mass 2 (7.13).
- 1999-'01: New Rockfall nets with aluminum supports were installed in the portion located downstream of a mass 1, a result of new calculations of the trajectories of falling boulders. The nets were placed at right angles to the slope than the safety nets of the previous intervention of the '97-'98 (7.13). Not pre load boulder net with circular mesh have been located in the upstream portion of the ground 2 (7.14).

Adherents boulder net with pre-tensioned reinforcement and cables with hexagonal mesh of 16mm in diameter, installed in the downstream portion of the Masses 1 and 2 (7.15).

- 2009-‘10: hereinafter the collapse of the debris 26/12/2008 new rockfall barriers were placed at separating the mass 2 from the mass 3 (7.16).

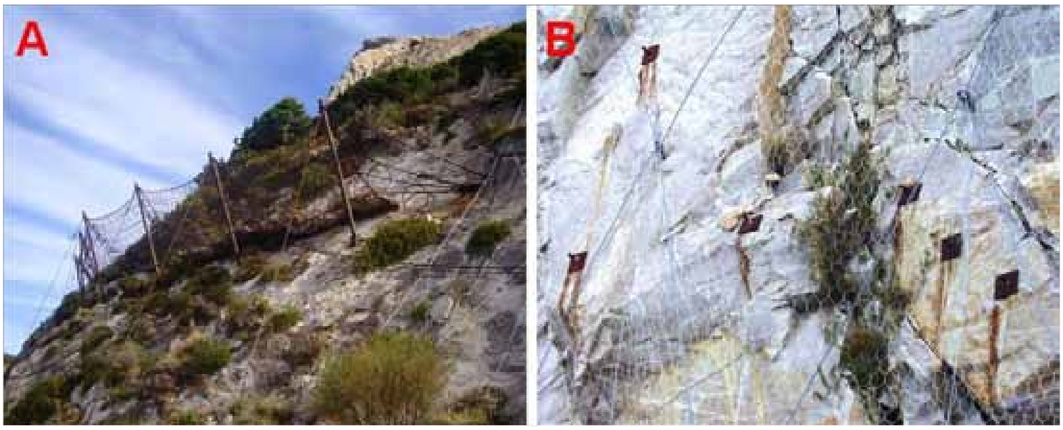

Figure 7.9: Rockfall protection installed in 1986 A-B); nailing surface.s ’88-’89 (April, 2010).

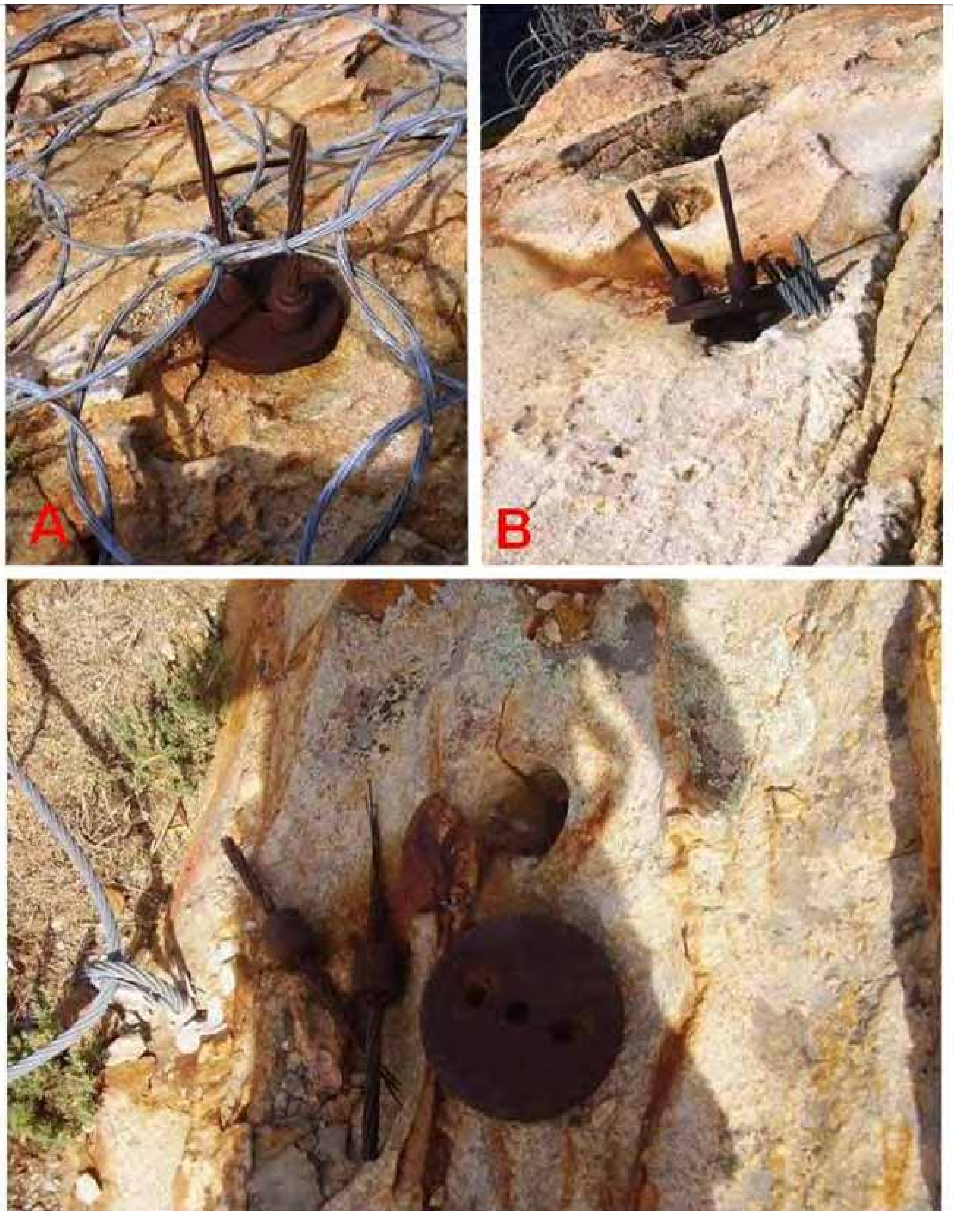

Figure 7.10: Tie-in mounted during two-year '88-'89 A-B-C): broken rods (April, 2010).

Figure 7.11: Underpinned structures (A) and beads (B) relating to the intervention of 88-’89 (April, 2010).

Figure 7.12: Rockfall protection installed in 1986 (A); nailing surface installed during the years (B) ’97-’98 (April, 2010).

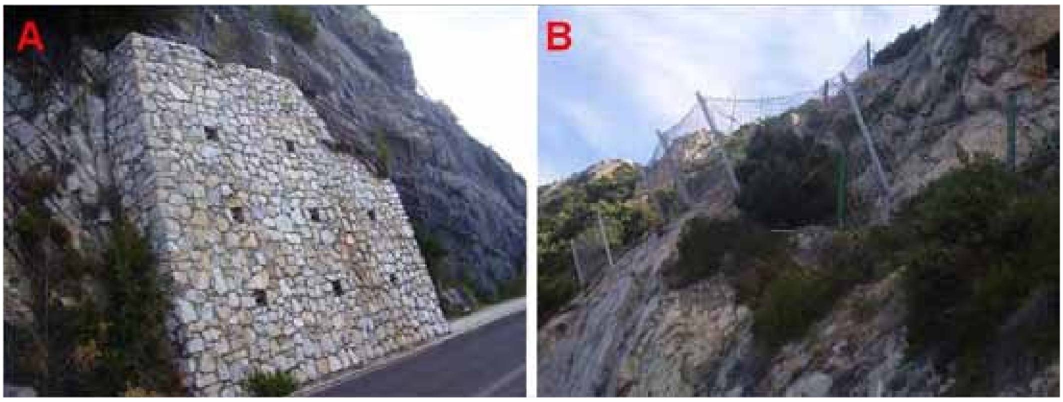

Figure 7.13: Tied underpinned structure with bars installed in '97-'98 (A) and rockfall barriers for (B) the intervention of the three years '99-'01 (April, 2010).

Figure 7.14: Boulder net with cilcular mesh installed in the period '99-'01 (April, 2010).

Figure 7.15: Pretensioned boulder net with hexagonal mesh installed in the intervention of '99-'01 (April, 2010).

Figure 7.16: Rockfall barriers relating to the intervention of the '09-'10 (April, 2010).

7.3 Geomechanical characterization

The mechanical properties of the rock mass was derived from data obtained from geomechanical observations. The rock mass characterization and the quantitative description of the properties of discontinuities were carried out according to the recommendations of the International Society of Rock Mechanics [15].

7.4 Risk scenarios

We identified the main hydro-geological hazards on the basis of field observations and measurement data and geomechanical laser scanning.

They are, in descending order of probability:

- collapse of single blocks of rock;
- collapse of surface debris;
- detachment of portions of the rock mass and slip along (on) the foliation planes (family JN3).

The three types of phenomena are listed below in detail.

7.4.1 Collapse of single block of rock

The possibility of separation of individual blocks of rock bounded by planes of discontinuity is very high because of the intense fracturation pattern of the rock mass. These phenomena can be developed in all outcropping lithology, particularly at clusters of porphyry and granite, where they may reach a maximum size of some cubic meters (7.177.18).

Figure 7.17: View of an unstable block within a located in the central portion of the rock mass 3 (May, 2010).

Figure 7.18: Unstable porphiry block located within the lover part of the rock mass 1 (May, 2010).

Blocks can achieve considerable energy because of the high tilt of the slopes, but the blocks can be contained by the barriers built over the years to protect the roadway.

7.4.2 Surface debris collapse.

it is possible, that detachments of debris slid down the slope or channel , and may reach the roadway, especially during intense weather events. These debris flows are in fact characterized by high energy and strong inhomogeneity of the material, thanks to these features they may be able to break down rockfall barriers, or to cross in with the fine material. The event of 26^{th}December 2008 (7.19) belongs to this category and leads to the slaughter of protective structures and to the occupation of the roadway. New rockfall barriers and some debris barriers were installed to laminate the amount of material along the impluvium, in case of similar events will occur.

Figure 7.19: Debris flow along the impluvium separating rockmass 2 and rockmass event of 26^{th}December 2008 (May, 2010).

7.4.3 Detachment of the rock mass portions

A family of discontinuities (JN3) is produced by the foliation of the outcropping materials and has an inclination comparable to the average of slopes (franapoggio).

The presence of this important discontinuities family, implies the presence of preferred floors slip-angle medium-high (45 ° -50 °), along which significant rock masses can be mobilized (7.20).

An event of this magnitude would lead to the destruction of protective structures installed along the path of the falling mass, in addition a huge amount of material will reach the road, with a probable damage to this one. Since we believe that this is the maximum credible scenario for the concerned area a detailed geomorphological survey was carried out in order to identify the main masses unstable which could lead to a mechanism of this type. we consider three rock masses to be most at risk. These masses have already been the subject of structural repairs and of installation of monitoring systems over the years. The volume those portions of rock slope was calculated through the laser scanning survey of the area.

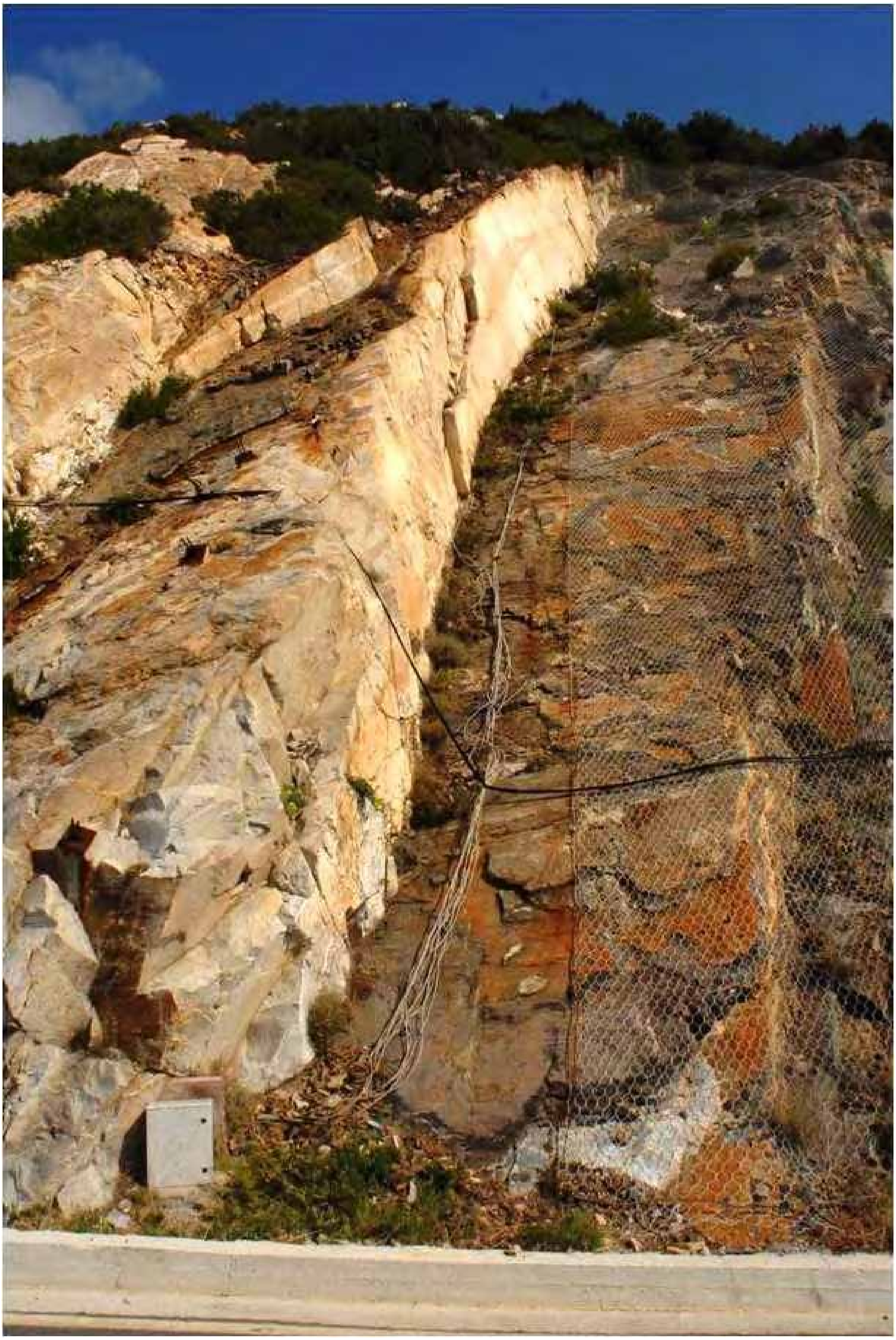

Figure 7.20: Detachment area of a portion of the porfidic rockmass along a well defined basal slip surface (April, 2010).

The rockmass 1 7.24 is an elongated portion of a porphidic rock slope, this portion is completely free along the lateral sides and it relies on the bad-rock only through the basal plane 7.20. The Rockmass 1 does not appear to be the subject of works of structural reinforcement or support in the past. The calculated volume is equal to 3706 m3.

The Mass 2 7.23 is formed by schists and clayey schists, is a body 'smeared' on the porphyry substrate end it is more extensive and 'flattened' with respect to mass 1, it is also free on all sides.

Figure 7.21: Panormic view of Rock mass 1 (April, 2010).

Figure 7.22: View of rock mass 1 from the provincial road n° 25 (April, 2010).

Figure 7.23: View of rock mass 2 from the provincial road N° 25 (April, 2010).

Figure 7.24: View of rock mass 3 from the provincial road N° 25 (April, 2010).

Figure 7.25: Bird eye view of rock mass 3 (April, 2010).

7.5 Stability analysis

Some analysis were performed to assess the degree of stability of these masses. Two different software prduced by Rockscience were used for the analysis of planar mechanisms of slipping and wedges, respectively. The software were chosen to take into account the different geometries of the bodies. The presence of any reinforcing or supporting structures was neglected, because it was not possible to verify their condition and therefore their effectiveness. The software Rocplane was used regarding the masses M1 and M2, which are subject to a planar slip mechanism. The geometry was reconstructed taking into account the slope of the basal sliding plane (48.8 °), the thickness and length of the portions of considered rockmass (7.26). The safety factor was calculated by assigning to the discontinuity the parameters derived from the geomechanical survey . The value is equal to Fs = 1.14. The mass of M3 (7.27) is instead formed by the intersection of two planes (7.28), the first is a basal plane (inclination 50.9 °), belonging to the JN3 family, the other is a lateral plane, and it is conditioned by the presence of a loaf leuco-granite. The software Swedge was used to perform the stability analysis of the wedge (7.29). The obtained security factor is Fs = 1.27. This value is a little higher than the previous one despite the greater inclination of basal plane. Indeed the sliding occurs along the line of intersection between the two plans because of the lateral discontinuity opposes the sliding of lateral discontinuity.

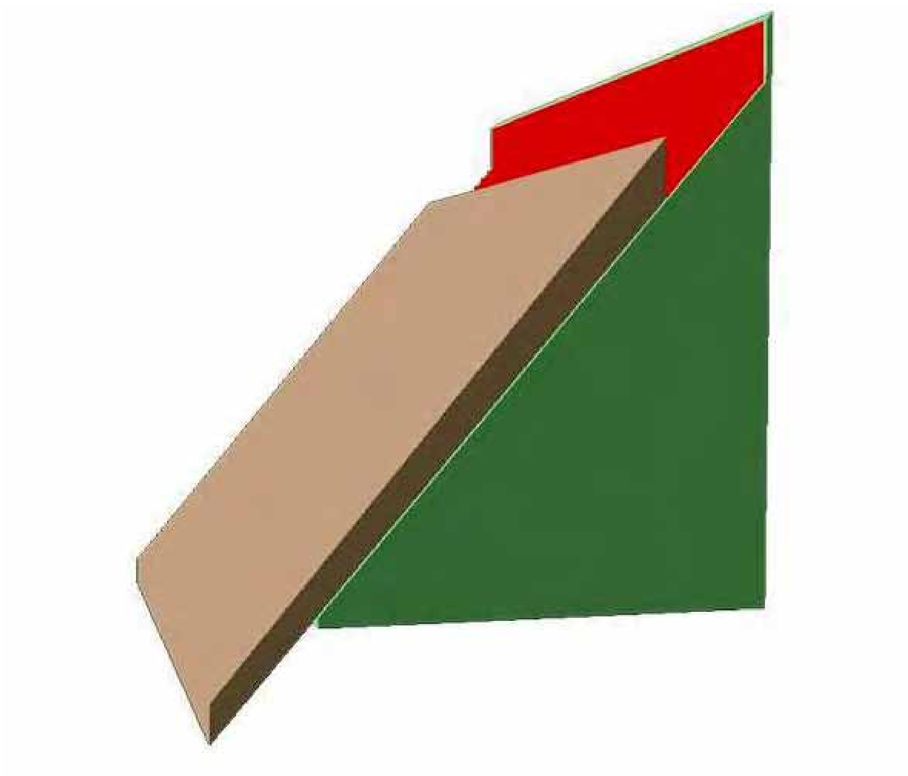

Figure 7.26: Stability analysis, rock-masses 1 e 2.

Figure 7.27: High resolution point cloud of rockmass 3.

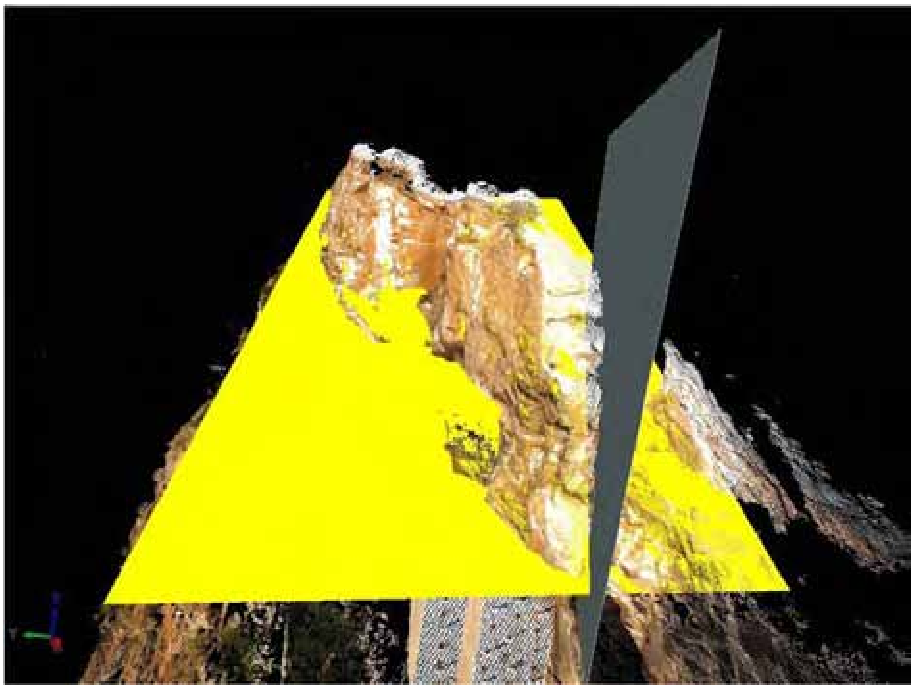

Figure 7.28: Reconstruction of discontinuity planes delimiting the Mass 3.

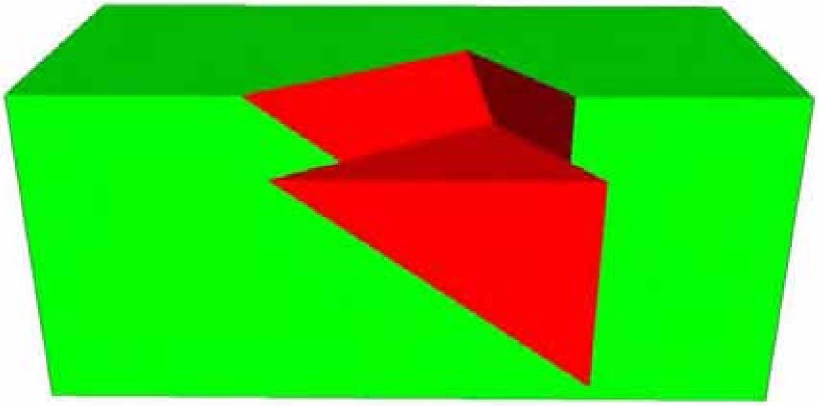

Figure 7.29: Mass 3 Stability analysis.

The analysis results show therefore a precarious stability of the entire masses investigated. The calculated safety factors would suffer a further reduction in case of earthquakes, considering the size of the masses and the types of failure, however earthquakes have a low probability of occurrence in this area. Indeed, the value of stiff soil maximum acceleration with 10% probability of occurrence in 50 years, for the Island of Elba is 0.025g - 0.05g. **??** We obtain a reduction in safety factors to 1.04 and 1.16, respectively for the masses M1, M2 and M3. by applying a horizontal seismic coefficient of 0.05g in the model. We point out that the results of stability analysis necessarily have a qualitative value, considering the level of simplification of the models, the uncertainties on the mechanical characteristics of the discontinuity surfaces (due both to the heterogeneity of materials, the difficulties in assessing the scale effect) (7.30) and the effectiveness of structural interventions. The area in question consists of intensely fractured rock masses, slipping phenomena may occur along the planes of foliation oriented in an unfavorable manner along the slope. Even if we identified portions of the rock mass as high-risk, the occurrence of similar phenomena, even minor, can not be excluded in other areas of the investigated slope.

Figure 7.30: Basal surface of rock mass 1. It is located at the contact between Calcescisti e Argilloscisti and Porfidi di Portoferraio (April, 2010).

7.6 Monitoring system

An automatic monitoring system with remote data transfer was installed in a short time to risk mitigation purpose. It partially replaces the old one installed in the study area since the late 80s.

This system consisted of a set of transducers (crack gauges, strain gauges and load cells).The system was operational until 1992, when it was implemented by a new unit with a modem, so it worked remotely, then it was permanently disabled in 1998.

The monitoring system installed at the Punta Timone (Chiessi, Elba Island) by the company Hortus Ltd., has been designed following the results obtained from the analysis carried out on the slope. The strain gauge sensors position and orientation have been evaluated taking into account the evidence obtained by the geomechanical characterization of the rock mass (7.31).

To limit the cost to build a new system it has been partially implemented on the basis of the existing system, in particular, some constituent elements of the old system have been recovered , others have been replaced, and a meteo station was inserted into .

7.6.1 Wireless sensor network

Through morphological analysis it was considered necessary to use wireless communication systems rather than wired.

The weaknesses of an extensive monitoring system, with many sensors scattered throughout the territory, is the durability of the connections for data transmission.

It was necessary covers distances of tens of meters, and not of kilometers, nevertheless the durability of electrical wires may be very short in a rocky environment, moreover in a coastal one.

To be honest, the durability of any kind of electronic and mechanical tools is short in coastal environment, because of the saline corrosion, however it is better to reduce the corrodible elements like cables.

From the first application of WSN installed in Torgiovannetto, to the last one in Elba Island the view that a monitoring system using WSN is to be preferred to a wired one took field.

This idea has gained even more strength in the city of Mdina (Malta), in which were installed more than 70 nodes, each of which has at least 2 sensors.

The choice of using a wired system would have required the use of about 18.000 meters of wire, instead of 200 meters.

The location of the sensors was due to logistical reasons and to a scale of priorities defined on the basis of carried out investigations and the state of preservation of structural works and existing protection.

The extensimeters E1, E2, E3 are located at the top of a mass, while the E4 sensor was installed at the level of basal sliding of the Rock mass n° 27.32.

However, the installed equipment is, for budgetary reasons, only a first base which would be needed to deeply control the evolution of the unstable masses.

For this reason we chosen to configure the system like an open system, which is able to accommodate any additional equipment.

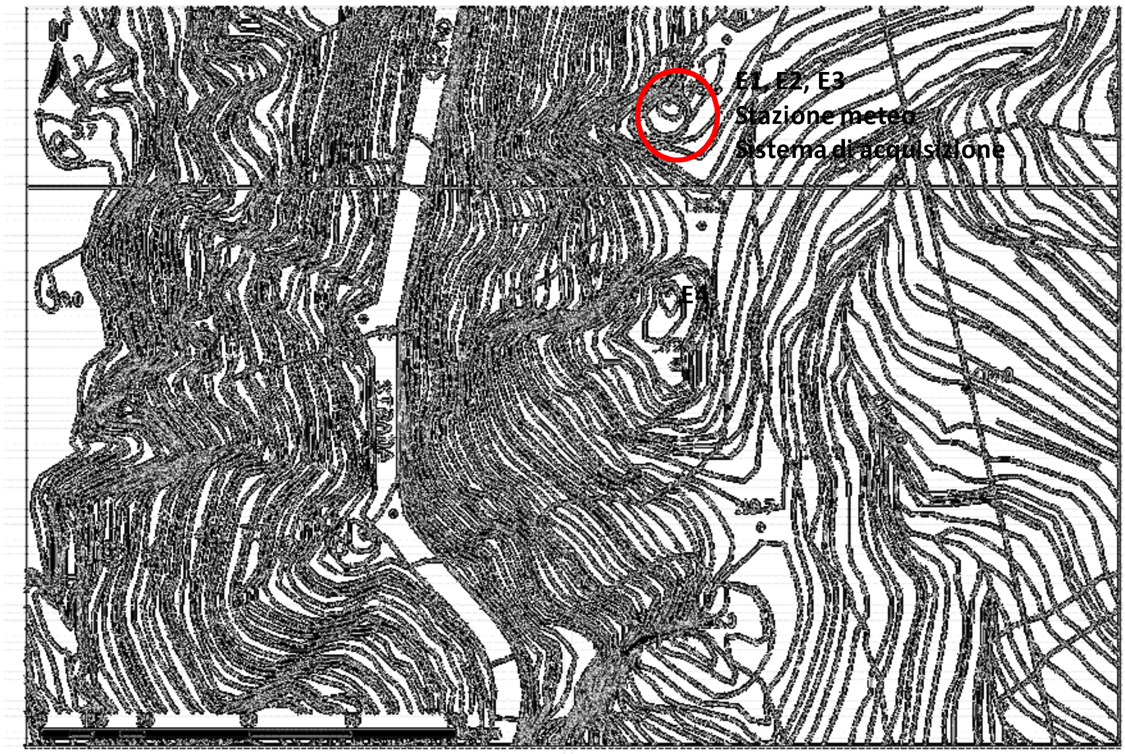

Figure 7.31: Location Map of Sensors and data-logger.

Figure 7.32: Pictures of the components of the Monitoring system installed at Punta del Timone, Elba Island (May, 2010). a) Datalogger and Gateway b) Extensimeter E3 c) Extensimeter E1. d) Extensimeter E2 e) Extensimeter E4 f) Pluviometer.

The measurement frequency and the updating frequency of the databases were established on the basis of geomechanical setting and the magnitude of the expected shifts, but also taking into account the risk level of the provincial road No. 25. The meteorological sensors are running a sample every 60 seconds and record the averaged data every 5 min. The extensimeters E1, E2, E3 and E4 are running a sample every 150 seconds, and record the averaged value every 5 minutes.

7.6.2 Communication and Web interface.

The GPRS transmission system automatically updates data in to the website every 10 minutes. 7.33. The web interface provides charts of the acquired values by the individual sensors in the 72 hours preceding the last update, in the last 60 days and for the whole series available. The graph of rainfall is also reported and it shows the cumulative value. All collected data are also available in ASCII format on a special FTP site, to perform further analysis and processing.

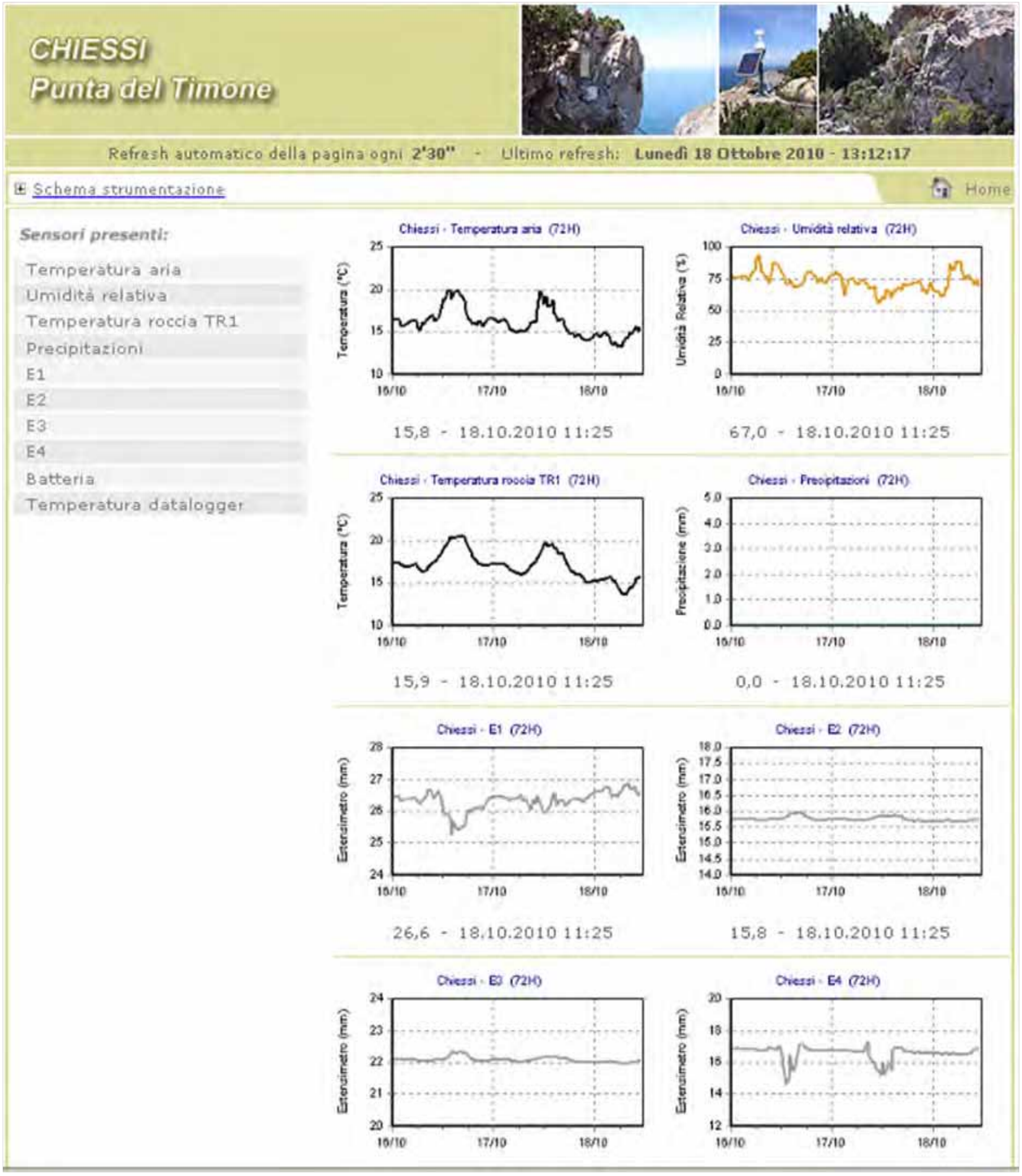

Figure 7.33: Screen shot of web interface (dowered by [113]) .

Part III

Data processing and results

Chapter 8

Platform for landslide monitoring.

The more information is retrieved the more accurate environmental monitoring activities will be performed. The opportunity of measuring different parameters confers unique properties to the multi-parametric monitoring platform. Monitoring tools have acquired over time features of automation and computerization, these features provide the ability to integrate tools into platforms. More instruments, very different to each other, can be controlled from a single location, from a single control panel. A strain gauge and an accelerometer can be driven from the same computer, and the results of the recordings can be viewed in the same Web interface This happens so much easier since the digitization of the data and signal become widely used.

If monitoring is done by way of deferred time you do not need centralized monitoring platforms. In this case the installation of the instruments, reading and interpretation of data, identification of tools that keeps track of movements out of the ordinary or abnormal signals are all activities that may be made at any time.

The monitoring system is then designed based only on the quality of the data to be recorded, not the time to acquire it and return it. Who uses the monitoring system must be adapted to the needs of that system, and to its time for action. Therefore, the traditional monitoring systems are not suited to the needs of real-time applications.

According to www.businnesdictionary.com the term *real time* include those processes which give response that appears to take place instantaneously or in the same time-frame as its real world counterpart action.

However the term real time may assume different means, and it change his stretch depending on the sphere of application:

- Computer modeling - Animations that correspond to real life situations such as an auto accident or a structure under stresses and strains.
- Data processing - Instant updating of information as opposed to delayed updating as in batch processing.
- Data transmission - Simultaneous transfer of data such as in a telephone conversation or video conferencing as opposed to time-shifting where data is first stored and then transmitted.
- Electronic commerce - Immediate (usually under a minute) verification and authorization of a credit card transaction.

In the applications described in this thesis, the concept of real-time must be applied taking into account activities for the monitoring of high risk natural processes. Within the Italian legislation there is the Directive P.C.M. 2004 which discipline the activity of civil protection in real-time end in delayed-time [114].

The term *real-time* corresponds to a period of some months within which an effective and generally temporary action of Civil Protection must be performed. Contrary the term *delayed time* corresponds to a longer period which goes from years up to centuries where the actions of study and estimates, including planning, programming and implementation of operations, are designed to ensure permanent and uniform conditions of human life and property safety, and protection and sustainable use of environmental resources.

In particular, the real-time includes:

- predicting the occurrence of an event, even if complex, be it natural and / or anthropogenic;
- the contrast and the containment of the resulting effects on population and especially on its property;
- management of the emergency state;
- rehabilitation of living conditions existing prior to the event, also pursuing the reduction of hazard where possible through appropriate intervention.

Thus it is noticeable that there is two different way to apply the definition of real-time, the first one take into consideration the process that carry on data acquisition and elaboration processes, the second must satisfy the requirements of rules of Civil Protection . Anyhow, within our study cases, the real time monitoring systems are often employing within Civil Protection issues, therefore both ways have to be kept under consideration.

8.1 Multi-parametric Approach

In previous chapters we have shown monitoring systems applied to different contexts. The different measurement tools have been integrated into complete monitoring system, thus it was possible to observe in detail the activity of the different instability processes.

8.1.1 Data acquisition and compatibility

As the applied systems were built by different companies or work groups, then the output data are structured according to different codes. The first step to develop a multi-parametric monitoring platform is just to decode the data acquired by different instruments and re-encode them to a standard that can be as uniform as possible.

You should be able to compare a rainfall event with surface movements of a landslide or with the seismic energy produced by a seismic event or with the measure of the inclination of a structure and the groundwater level of an aquifer.

Basically it is to synchronize and re-sample the acquired signals.

We have made consistent time series and make them readable by a prototype reader of the various types of data. To do this we have mainly used the software Matlab.

Trying to encode a text file that I think is rather boring task, one must understand the type of encoding the original, then it must be subjected to some process of handling repetitive. However, once you reach a well manageable is of great satisfaction to be able to graph all sorts of time series acquired by means other than through the same script Matlab.

For istance, the tiltmeter measurement files are stored with .lvm extension, ownership of LabView, the software developed by National Instruments [92]. The files are structured according to the example shown in . The design of the LabView control panel for managing tiltmeter was the first programming experience I've had, and thus suffers from all the little mistakes of inexperience own. Such as using the same separator both for the decimal values measured and for time.

The extensimeter, thermometer and piezometers sensor data files are those that come from monitoring nodes in Malta. Since the number of instruments in use, both for the system to Mdina is one installed in the citadel were used the same type of transducers. Consequently, the encoding of a single .txt file is applicable to all others.

8.1.2 Implementation of Self-adaptive procedure

Being able to change your ability to observe an environment as the environment changes is a good way to accurately track its changes. The monitoring of an environment is performed with specific tools. The used instrument must be able to ensure the largest number of "effective" information as possible. As a landslide is an evolving process, as a landslide is an ongoing process even the parameters that are measured change. Instruments that measure with a frequency of on record per week or per day may be used when there is a slow movement. Instead quick movements need higher measurement frequency, from one record per day to several record per minute or per second.

As the conditions of instability change we have to change the 'activities of the monitoring system. Or, when the boundary conditions (such as a heavy rain event) become influential on the mechanism that generates instability then the rain should be record.

Inappropriate measurement frequencies can make the monitoring system useless. Use high frequencies to monitor slow movements make the system slower and heavier to handle than is necessary. On the contrary, recording rapid processes with low measurement frequencies would make the system useless, important information will probably be lost.

Logical processes were applied to optimize the monitoring systems at Torgiovannetto and Malta. Both triggers and the current behavior of the instability process were taken into account. In particular the system on Mdina is changing its recording frequency as a function of velocity measured by the strain gauges and the inclinometers. The higher the recrded velocity, the greater the recording frequency.

The value of recording frequency increases even if some triggering events of high intensity occur. In the case of Malta there were no rainfall events that triggered or accelerated ongoing processes of stability untill date. As the meteorological station has been operating for a short time, it has entered into activity on April 2010, we believe this period to be not sufficient to draw a correct relation between rainfall and surface movements.

A certain correlation was instead found between movements and restoration works. In the monitored sites where there have been restoration works of the walls, some instruments recorded anomalous values of linear and angular deformation.

Inside the A in particular, the renovation works of Vilhena Palace have produced little deformations recorded by the instruments.

8.2 Constraints to the use of Platform

Leave out characteristics of durability of individual elements of the station installed on a specific environment, which will include consideration of the Protection Index (IP).

Once the sensors and all elements of the network were installed in the area of interest, it is necessary to ensure the presence of 2 essential elements: power supply and data supply.

The areas affected by a catastrophic event, or otherwise in which there are conditions of natural hazard, are often characterized by poor quality of primary public services provided, including the provision of electricity and wired communications equipment. In some cases, such as in urban environments, the electrical grid and communications are easier to reach, in other cases they are more difficult to find, such as in large landslides.

However, with a high motivation and especially with a good budget, you can create monitoring platforms under very extreme environmental conditions.

The Stromboli volcano is a striking example of how you can always manage to deliver the two elements mentioned above. The GbInSAR, an interferometric radar, was installed on a flank of the volcano in the 2003 and it's still working.

To connect the platform to the Advanced Operation Centre (COA) of civil protection were hung and buried two kilometers of cable.

In particular, they used a shielded cable and grounded to the power-supply and fiber optic data transmission

Figure 8.1: Buried-electrical and data transmission cables (May, 2007).

Figure 8.2: Path of electrical and optical-fiber cables (Modified from [78]).

8.2.1 Data Provisioning

A monitoring system can also be a closed system that has its dedicated storage devices, such as dataloggers. However, in case of monitoring in an open field, a methodology which provides for the removal of data gathered from monitoring site to a collection protected center is to be preferred.

In the specific case of systems that belong to a monitoring platform is necessary to ensure the exchange of measurement results with other systems belonging to the same platform.

Even in cases where a platform extends for hundreds or thousands of miles, you should be able to ensure a highly efficient data transmission system, both in order to receive real-time data captured by monitoring systems located both to improve the robustness of the platform.

Any monitoring system, if placed inside a monitoring platform, must be able to deliver the measures taken to control and processing center (Head Quarter), even thousands of miles away.

8.2.1.1 Satellite and GSM communication systems.

There are several communication systems that can be used to transmit data with global reach, ground base communication systems and by satellite.

However, the ground based ones are more accessible, both from an economic point of view and ease of use, furthermore, the data GSM networks GSM have reached a very extensive global coverage in a few years Figure 8.3 on page 170.

Instead Satellite networks can cover up to 100% of the planet, such as the IRIDIUM system, and they ensure communication capabilities even desert areas, it is sufficient that a wide and unobstructed sky there is Figure 8.5 on page 171.

However satellite systems are extremely expensive compared to the terrestrial GSM systems, for the same amount of data exchanged and the same transmission speed. Taking into account the normal fee of two major data service providers, one terrestrial and one satellite, we can appreciate differences of two orders of magnitude. These differences are to be considered for the hardware needed as well. So, if a GSM data connection needs just under 100 € per month, a satellite connection needs just under 10.000 € .

Figure 8.3: GSM world coverage (modified from [94]).

Figure 8.4: GSM world coverage Vs global landslide related casualties (modified from [94, 93]) .

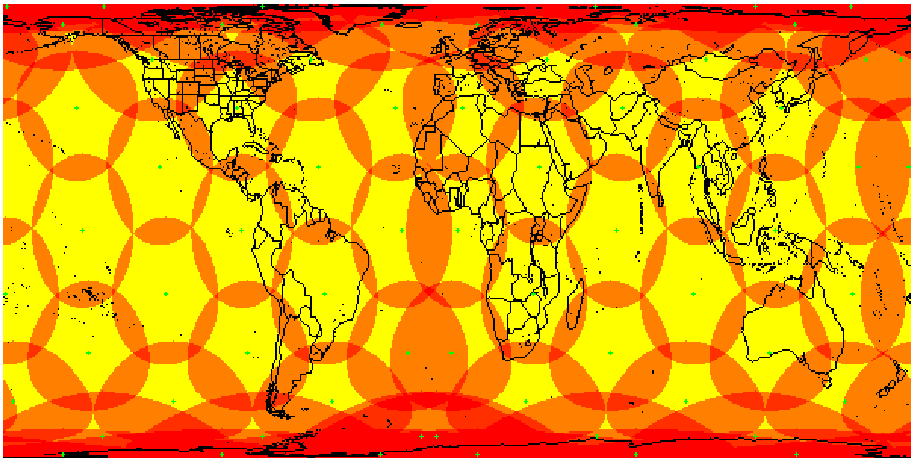

Figure 8.5: Map of IRIDIUM satellite coverage (modified from [105]).

However, the installation of monitoring platforms do not need full global coverage, it is sufficient that there is coverage where monitoring activities are necessary.

In the particular case of platforms used for monitoring of landslide risk, planet's areas of interest will be those that are subject to specific conditions of slope, lithology, moisture, and the frequency and intensity of precipitating factors such as rainfall and seismic events [93]. But especially in areas where the risk associated with landslides is higher.

The figure 8.4 shows the distribution of global landslide related casualties plotted on the GSM global coverage [94].

The comparison shows that the high-risk areas are covered by more than 95%.

In cases where 5% is the master it may be necessary to rely on a satellite transmission system. However, the implementation of a system of local communication hardware that can overcome the distance that separates our platform from a global terrestrial communication system like GSM it is often decisive.

The case of Stromboli is an example; thanks to the efforts of national civil protection, hardware tools are used to connect the local communication with the national network without relying on communications systems satellite.

The areas that are not covered by the GSM communication system are mostly desert areas, both land and sea. In these areas, satellite systems are certainly necessary and are the only means of worldwide communication, but the risk related to landslides is often nil.

8.3 Correction of extensimetric measurements affected by temperature contribution

It is important to keep in mind that the instrumentation, like all natural materials, suffers from deformations due to temperature changes.

The time-series analysis (refer charts) has Confirmed That the relation Between deformation and temperature recorded by the instrument is linear Figure 8.8 on page 173 further, an hysteresis loop Figure 8.10 on page 174 that shows the permanent measured crack deformation, was obtained through a moving average elaboration, respectively 50 and 200 time steps .

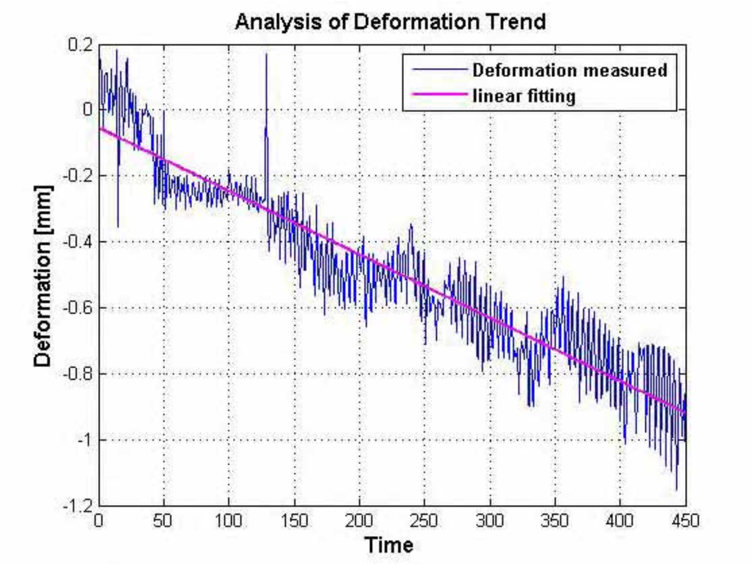

Figure 8.6: Deformation trend obtained by data linear interpolation.

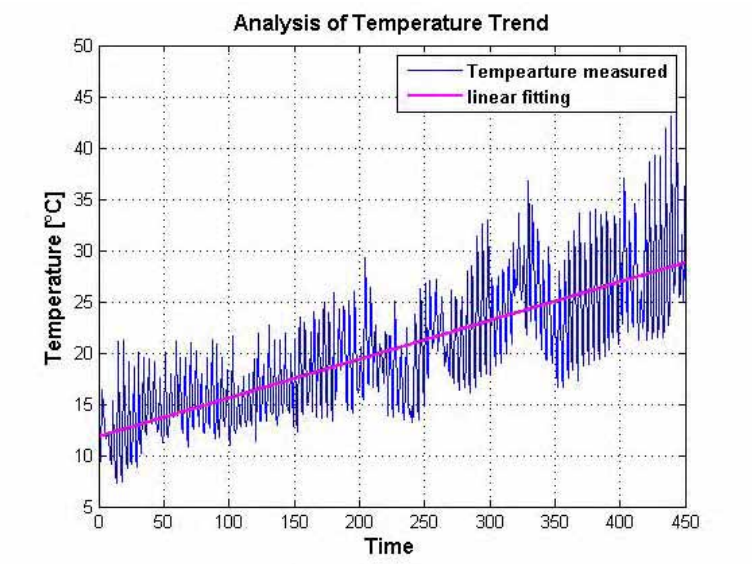

Figure 8.7: Temperature trend obtained by data linear interpolation .

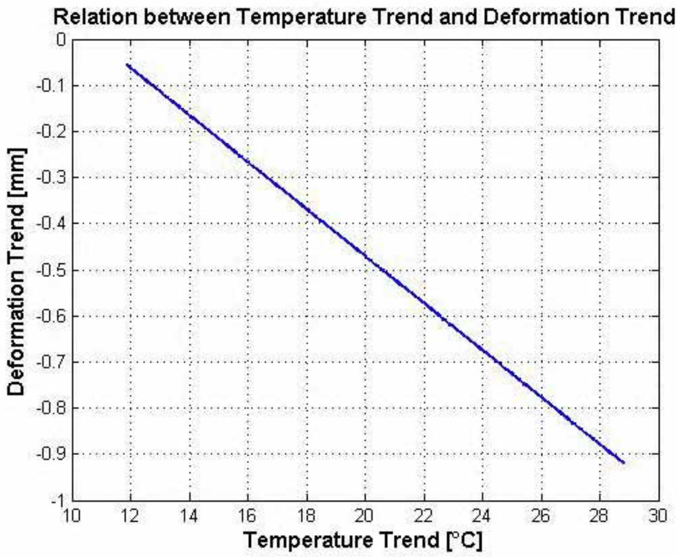

Figure 8.8: Linear relation between trend deformation and trend temperature.

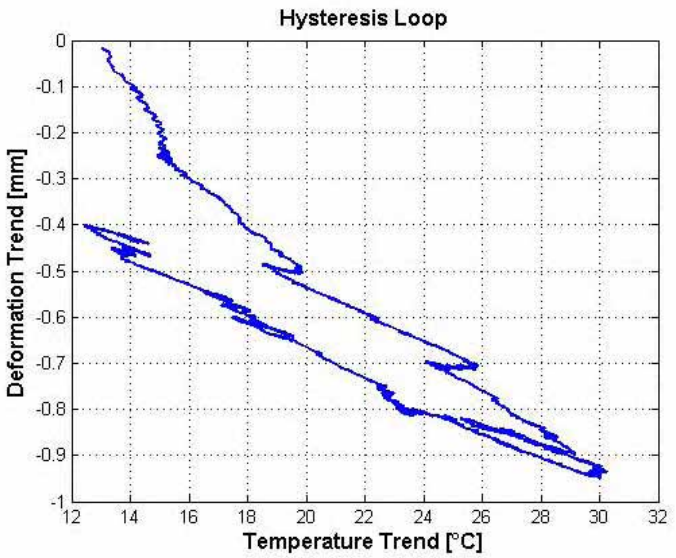

Figure 8.9: Histeresys loop elaborated on data recorded by instrument CGA08.

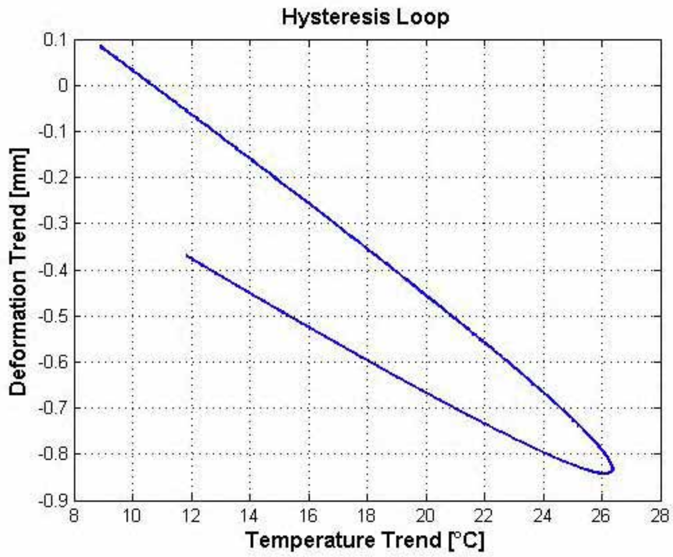

Figure 8.10: Histeresys loop elaborated by polinomial fitting of 3 degree.

The measures recorded by some type of instruments such as rod extensometer must be corrected must before being interpreted. The values must be properly treated to separate the component relating to instrument thermal deformations.

The corrections are essentially based on the principle that for small changes in temperature, with constant pressure value, linear deformation is directly proportional to temperature, to the length of the bar and to the initial temperature to a specific factor K for each material:

$\Delta L = \lambda L_0 \Delta T$

To characterize the influence of temperature on the results of instrumental readings is a challenging task, and at least an annual cycle of temperature readings must be recorded.

At the moment some instruments (e.g. Those which are installed in Mdina & Gozo) have been recording measurements for a period of almost a year, others only for a few months.

The thermometer of the meteo station, which is the more accurate, started his measurements from April.

Hence, the characterization of the temperature influence on deformation records is not yet completely achievable, even if it is already possible to guess some general trends.

To better understand this behavior, a dummy gauge Figure 8.11 on page 175 was installed at the end of November on a block of intact rock, in order to identify and isolate the deformative component related to temperature variations. The dummy gauge was installed in the B Area, taking care to ensure sun daily exposure Figure 8.12 on page 176. It is assumed that all deformation values Figure 8.13 on page 177 recorded by this sensor are to be attributed to variations in temperature Figure 8.14 on page 178, Figure 8.15 on page 179 since no fracture is located between the two extremes of the instrument.

Figure 8.11: Picture of the dummy Gauge installed on an intact rock block (November, 2010).

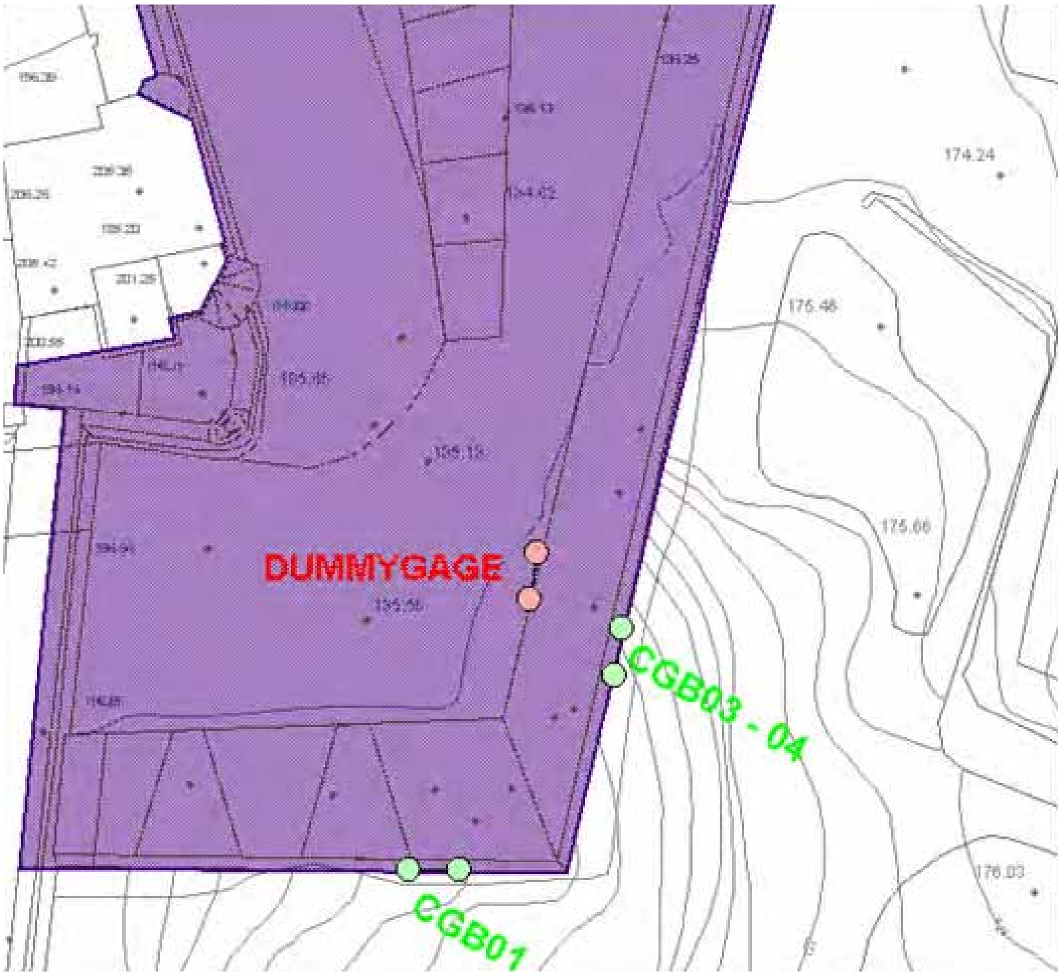

Figure 8.12: Location map of the dummy gauge in Area A (Mdina).

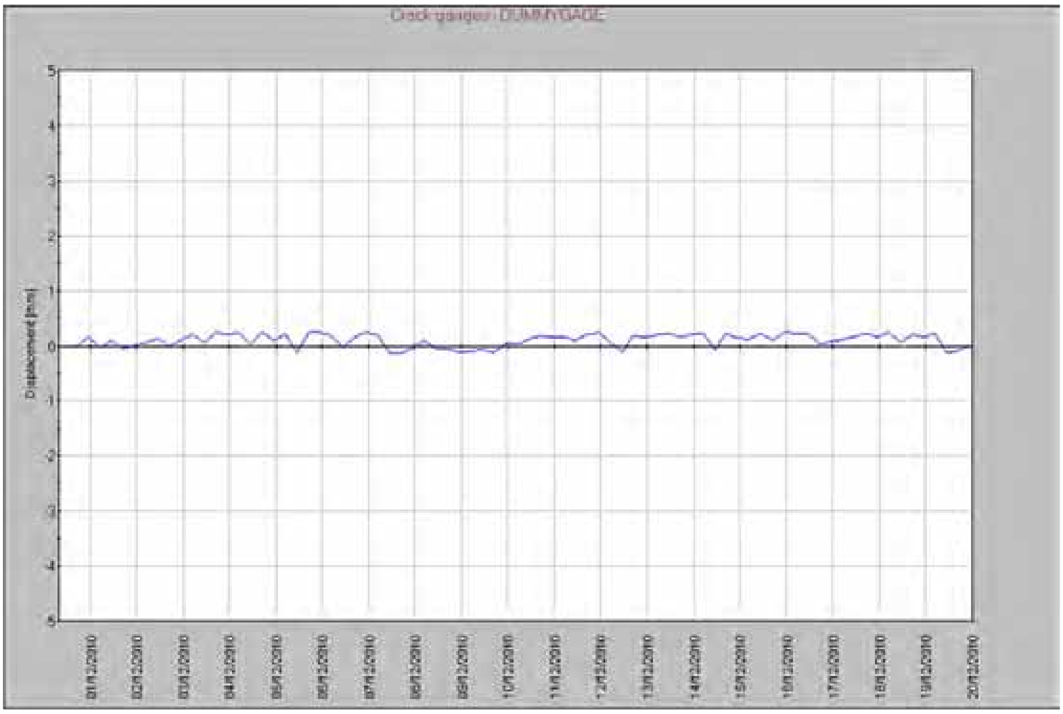

Figure 8.13: Chart of displacements recorded at the Dummy gauge.

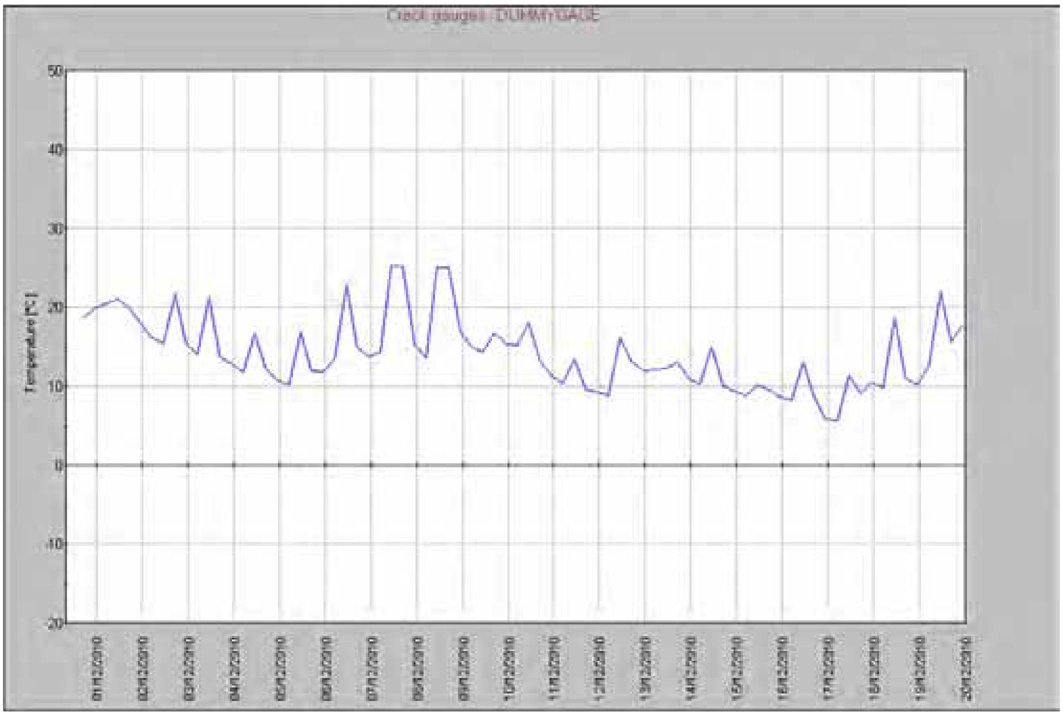

Figure 8.14: Chart of temperature recorded at the Dummy gauge.

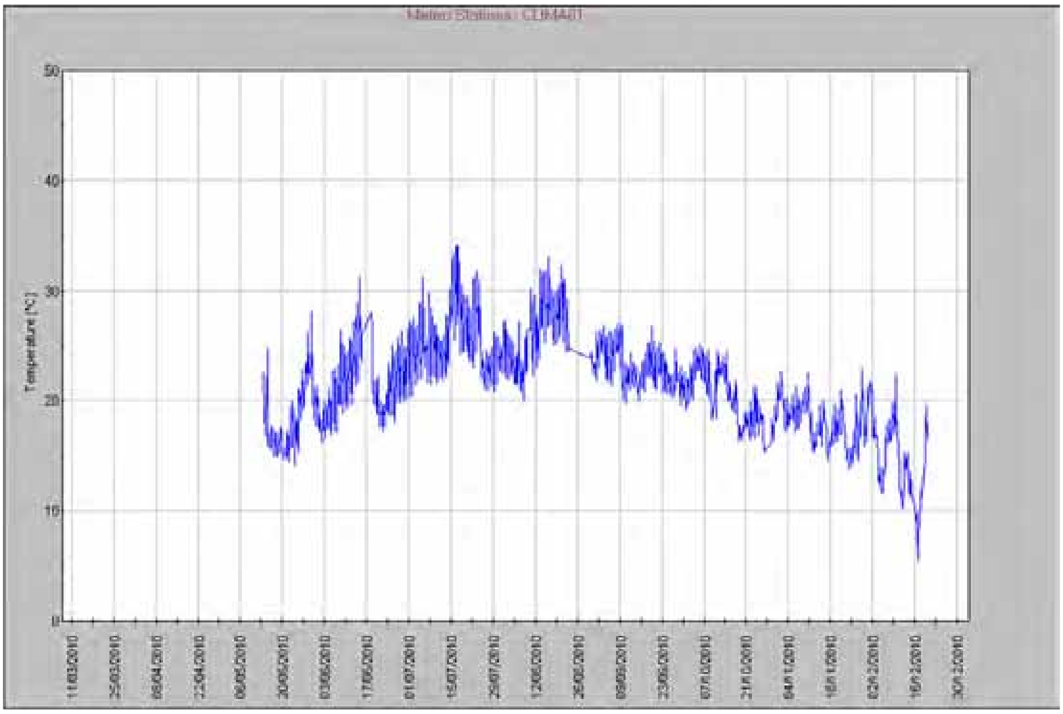

Figure 8.15: Chart of temperature recorded by thermometer of meteo station CLIMA01.

Chapter 9

Integration of Laser Scanner and WSN

We achieved interesting results when we tried to use the point clouds results from laser scanning to design the positioning WSNs. In particular the integration of laser scanner with WSN allowed us to locate the best points were to install instruments and what type of instrument would be more appropriate.

9.1 Identification of optimal zones/points for instrument positioning

In the previous presented aplications we designed the installed WSN after many considerations. Geological, social and economical factors were acting during the monitoring systems design. Rock mass characterization, geological end geomorfological surveys, laser scanning survey and RADAR monitoring were carried out. The WSN were installed several month later the first field observation. It is quite strange, moreover if we think that during the period of survey geologists, ingineers and others working people are exposed in a high hazard area without any monitoring activities. We used the Laser Scanner products to develop a rapid instrument positioning technique, in case of necessity to carried out scientific activities on high risk area without pre-existing alert systems. For an expeditious scenario analysis the Laser Scanner is an effective tool.

During the Gozo monitoring system designing, we deal with few economical disponibilities. The system optimization was very significant. The system was installed after that all survey and analysis activities were carried out. At the and, the positions of installed tools were coincident with the results of kinematic analysis. The kinematic analysis was carried out only using Laser Scanner point clouds. We tried to use the Laser Scanner products to identify optimal zones/point for instrument positioning in all the others case studies. We chose to use the WSN as a monitoring tool considering its relatively low cost, its rapid installation and scalability of systems based on this technology.

9.2 Semi automatic method for nodes positioning optimizaztion

Wireless and wired sensor networks need to be installed in accordance with geometry and distance between nodes.

The choice of system configuration is crucial for his proper functioning. To design an extended monitoring system Mdina takes a long time.

We used the 3D point cloud generated by the laser scanner survey to define the areas of installation of the instruments. The choice was made based on the maximum allowable radio communication distance (taking as a communication mode system peer to peer configuration), but at the same time the geo mechanicalobserved structures were considered.

9.2.1 Distance calculation and node positioning

A mesh of nodes with non-deformable sides is constructed with the distances calculated from the line of sight of the instruments. Software tries to place nodes on the struture created on the basis of the 3D point cloud. Then, considering the crack pattern tries to find the best compromise between distance, number of nodes and geometry of the structure monitored.

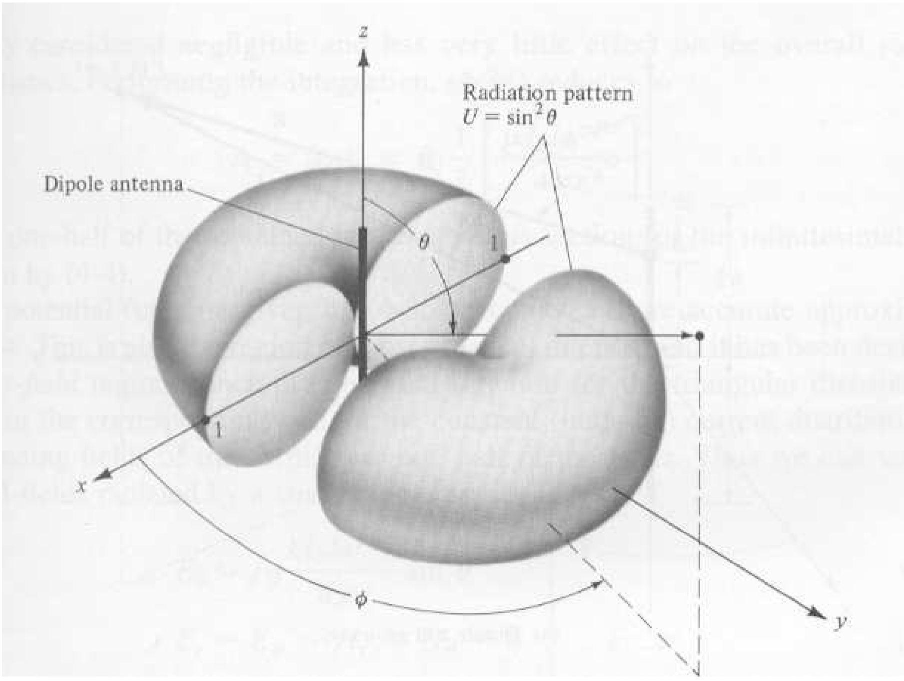

Figure 9.1: Magnetic field generated by a bar antenna.

A magnetic field generated by an antenna with a cilindrical shape can be approximated to a sphere if two conditions occur:

- The antennas must be much smaller than the wavelength;
- the distance between the antennas must be large compared to the wavelength.

The frequencies used by the radio modules applied in the systems of the case studies are 800 MHz ±70Hz.

According to the equation:

$\lambda = \frac{\nu}{v}$

The wavelength is about 35 cm.

Considering that the antennas are of sub-decimetre dimensions and the distances between the nodes are on the order of tens of meters, the two conditions are satisfied.

Once we have considered the magnetic field as a spherical, we can also treat the maximum distance of radio communication such as the radius of a sphere centered in the center of the antenna Figure 9.2 on page 182.

We constructed an ad-hoc created Matlab routine to calculate the minimum distance between the sensor nodes and create a grid. The vertex of the grid representing the communication nodes Figure 9.3 on page 183.

The maximum transmission distance depends on the wireless module used. The maximum communication distance of the sensors installed in Malta is about 100 meters.

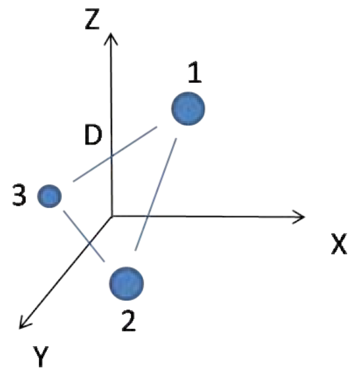

Figure 9.2: Example of distance calculation between nodes.

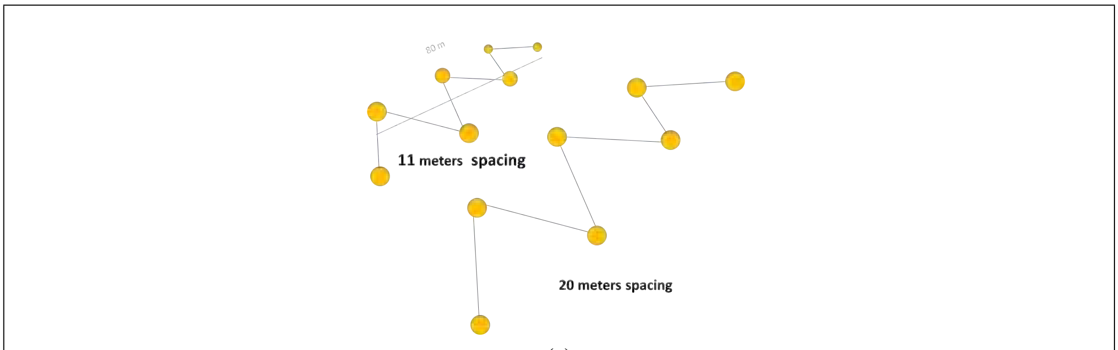

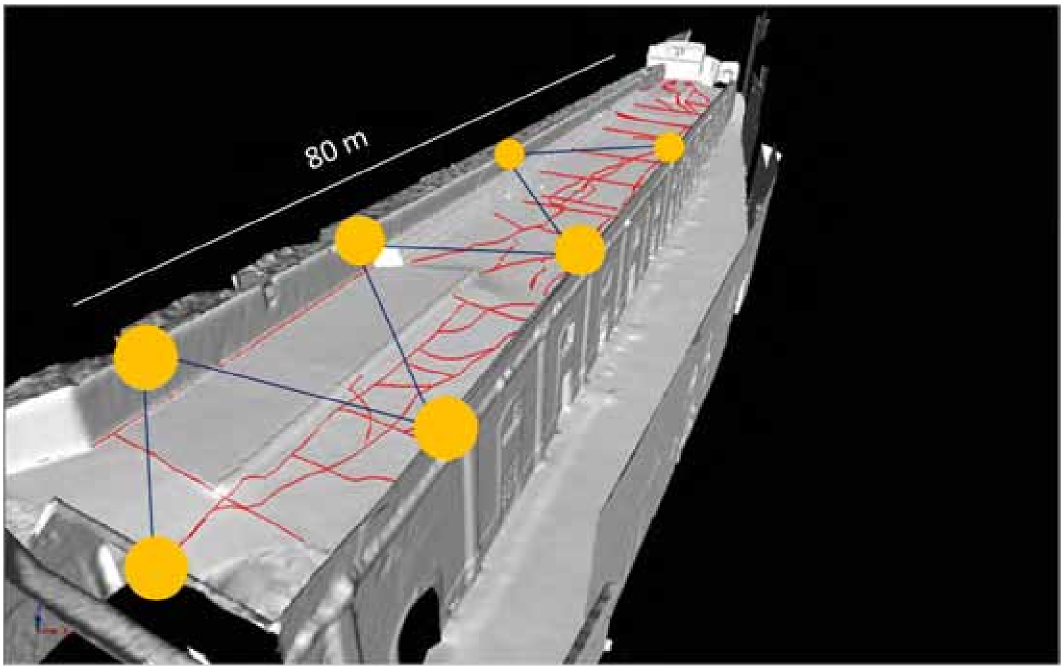

Figure 9.3: Node positioning on 3D surface of structures (modified from [19]). a) Node mesh b) Node mesh on 3D surface with cracks localizzation.

9.2.2 Cracks identification

The method described above requires that the low resistence areas and points, represented by structural cracks on the walls of Mdina, were identified.

Cracks are localized through an in situ (manual) survey and subsequently set on 3D surfaces Figure 9.7 on page 185,Figure 9.8 on page 185,Figure 9.9 on page 185.

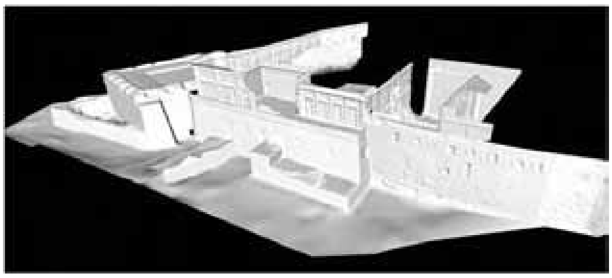

Figure 9.4: Reconstructed 3D surface from point cloud, Area A.

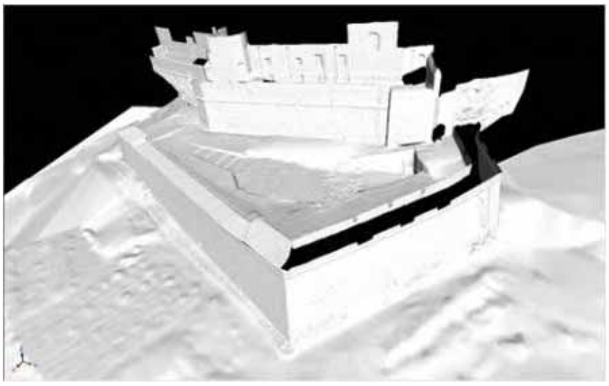

Figure 9.5: Reconstructed 3D surface from point cloud, Area B.

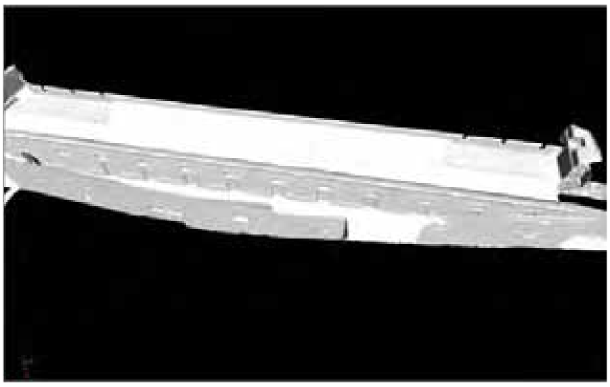

Figure 9.6: Reconstructed 3D surface from point cloud, Area C.

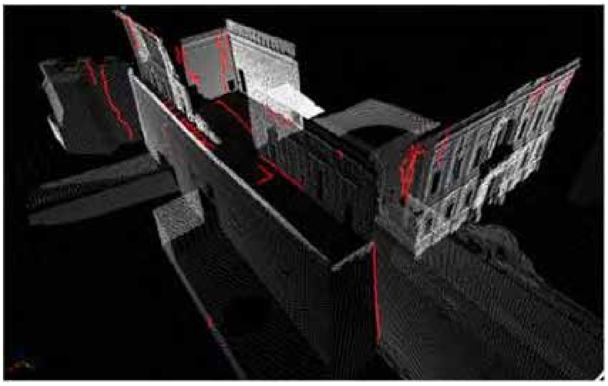

Figure 9.7: Identified cracks plotted on the point cloud, Area A.

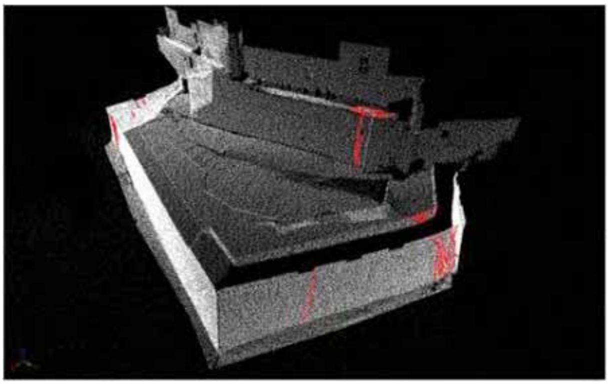

Figure 9.8: Identified cracks plotted on the point cloud, Area B.

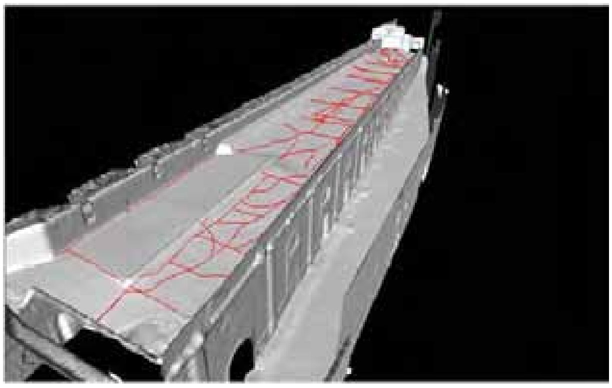

Figure 9.9: Identified cracks plotted on point cloud, Area C.

9.2.3 Displacement vectors calculation.

The laser scanning survey has been performed with the aim of constructing a 3-D digital model of both the damaged structures and the slopes of the study areas Figure 9.10 on page 186. The employed instrument is a long range 3-D laser scanner (RIEGL LMSZ410-i). To completely cover the areas of interest, a total of 56 surveys from diverse positions have been performed.

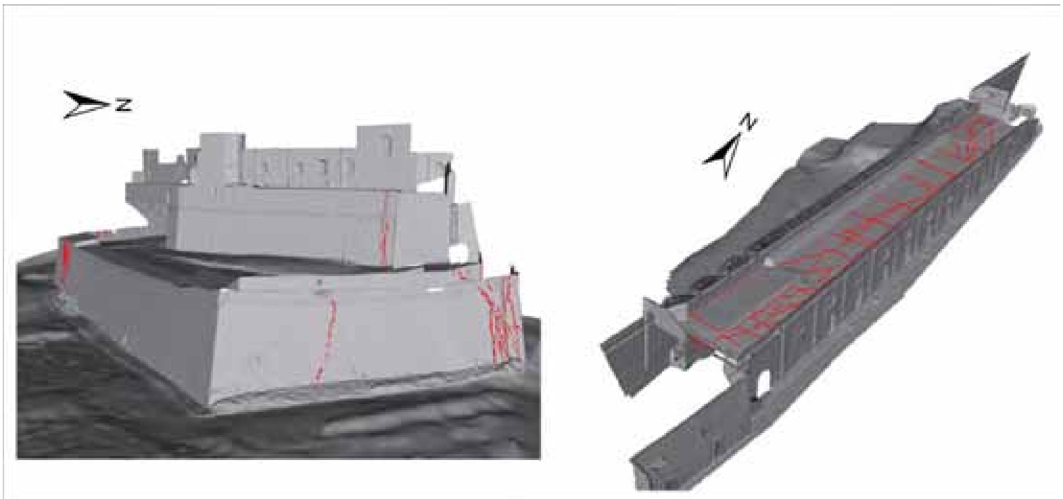

Figure 9.10: Crack distribution on 3-D models obtained from TLS data. Left: Despuig Bastion; right: Curtain Magazines (taken from [19]).

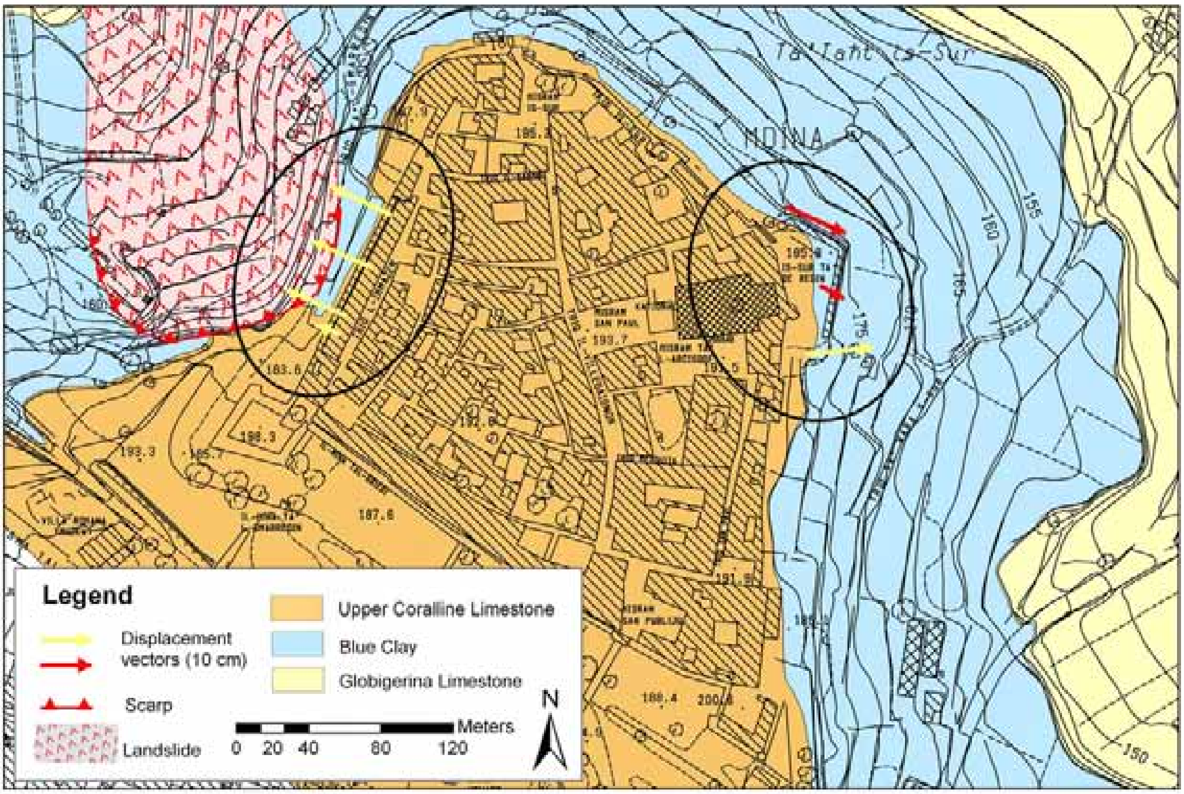

Figure 9.11: Geological map of Mdina and displacement vectors (scaled to the length in legend). Yellow arrows indicate sub-horizontal displacement (dip <15); red arrows represent vectors dipping >15. Left circle: Curtain Magazines; right circle: Despuig Bastion and Cathedral (taken from [19]).

The different point clouds have been linked to a project reference system with the aid of reference points, the coordinates of which were defined by differential GPS. The high detail of the point clouds, integrated with high resolution digital images acquired by the camera mounted over the instrument, allowed the construction of a 3-D map of the main cracks affecting the structures by digitizing 3-D polylines over the crack traces Figure 9.11 on page 187. Displacement vectors have been calculated for the main cracks, with the aim of identifying the structural deformation patterns. Each vector has been drawn by joining two homologue points selected from the 3-D point cloud. These were supposed to be occupying the same location before displacement has occurred Figure 9.12 on page 188. Displacement vectors have been thus calculated from the director cosines and plotted on the map.

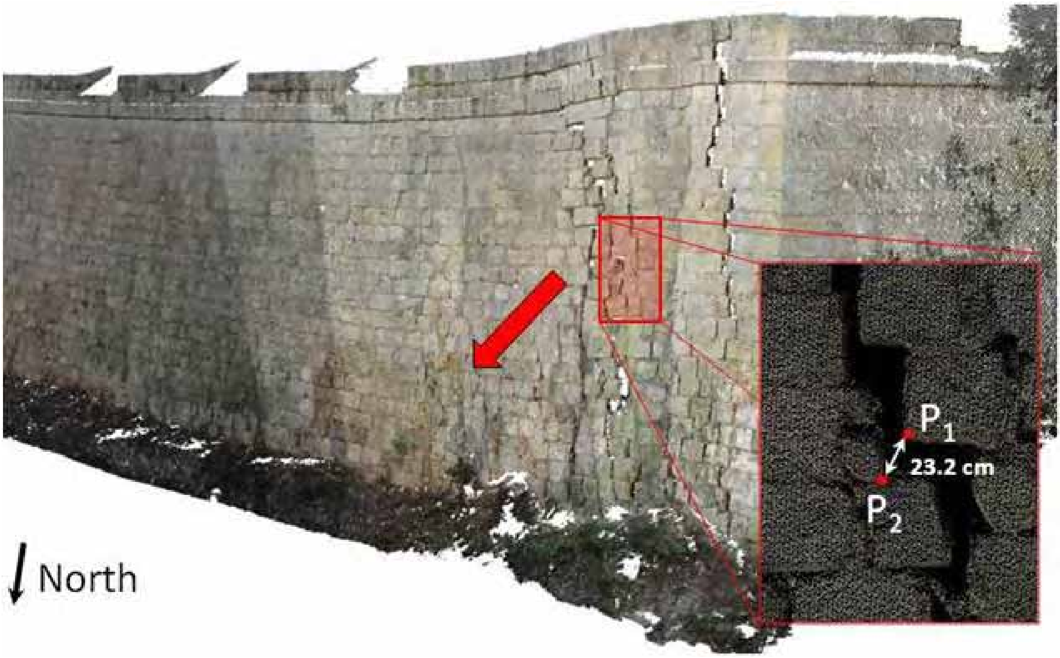

Figure 9.12: Displacement vector calculation on true colored point cloud of the NE wall of the Despuig Bastion . The red arrow on the wall indicates the movement direction (taken from [19]).

The integration of displacement data, 3-D distribution of cracks, and geologic, geomorphologic, and geo-mechanical surveys, allowed us to understand the basic kinematic behavior of the structures in the study area. The proposed methodology can be applied in areas with lack of data and it allows to quickly extract the required geometrical information by post-processing remotely acquired data.

9.3 Rapid rock mass diagnosis method

The laser scanner survey provides very rapid characterization of the observed scenario. Volumes, shapes and some of the structural characteristics of the observed rock slope were calculated on the rock masses either on the anthropic structures as well as in the case of the fortified city of Mdina and Gozo.

9.3.1 Volume, boundary and shape identification.

Laser scanning allowed us to identify the shape and volume of the sliding wedge in the case study of Torgiovannetto. In particular we have compared two point clouds acquired at two different times, a time span of 400 days.

The shows the slope and found the reconstructed 3D surface. The areas of the side who have suffered deformities have been recolored according to the magnitude of deformation.

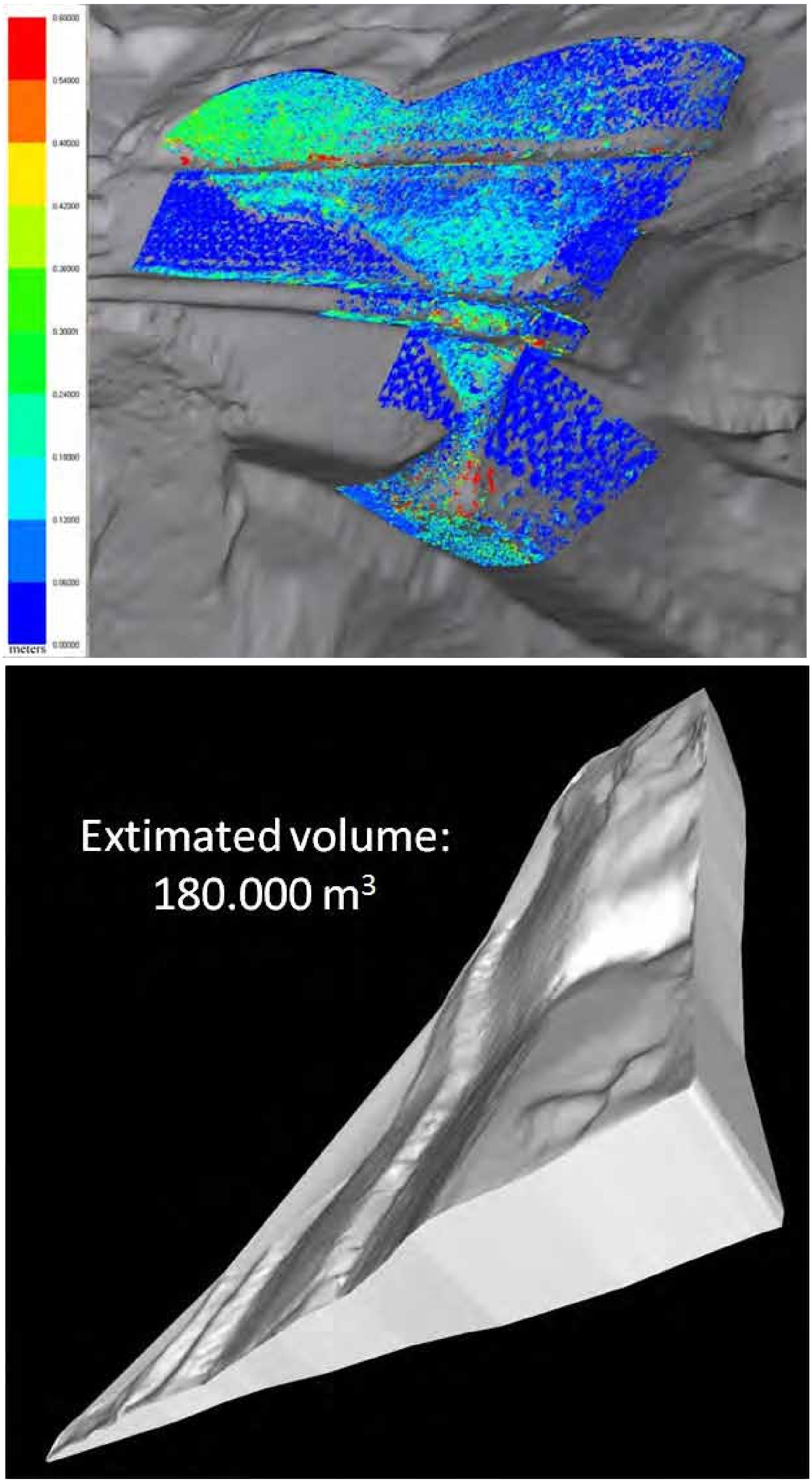

Figure 9.13: 3D reconstructed surface. a) Recolored surface according to the calculated deformation. b) 3D surface of wedge calculated volume.

9.3.2 Cinematic analisys on Walled city borders, Citadel (Malta)

Local slope orientation data were evaluated by analyzing the 3D model produced by the "Consorzio Ferrara Ricerche of the University of Ferrara", within the Service Tender for the documentation of the Citadel Fortifications, Gozo, Malta. It is important to point out that this analysis only takes into account those discontinuities intersected by the scanline geomechanical surveys carried out at the base of the cliff, and does not consider minor and irregular fractures originating in local stress concentrations , thus underestimating the probability of occurrence of instability phenomena in those areas.

The main instability mechanisms investigated with this approach are 4.1.5.6,Figure 4.20 on page 68.

9.3.3 Quantitative Kinematic analysis

The analysis was performed for each triangle of the 3D surface. In order to reduce the number of the triangle and to make the computational time acceptable, the original surface was resampled (9.14) with a total of 23631 triangles instead of 475527. Due to the circular shape of the rock plate, the kinematic analysis result are presented according to the two sectors of Figure 9.15 on page 192. The analysis imput parameters are the slope dip Figure 9.16 on page 193 and dip direction Figure **??** on page **??**-rockwall:, and the discontinuity surface orientation. The discontinuity shear strength has been set to frictional, with $\varphi = 48°$, according to the mean peack friction angle .

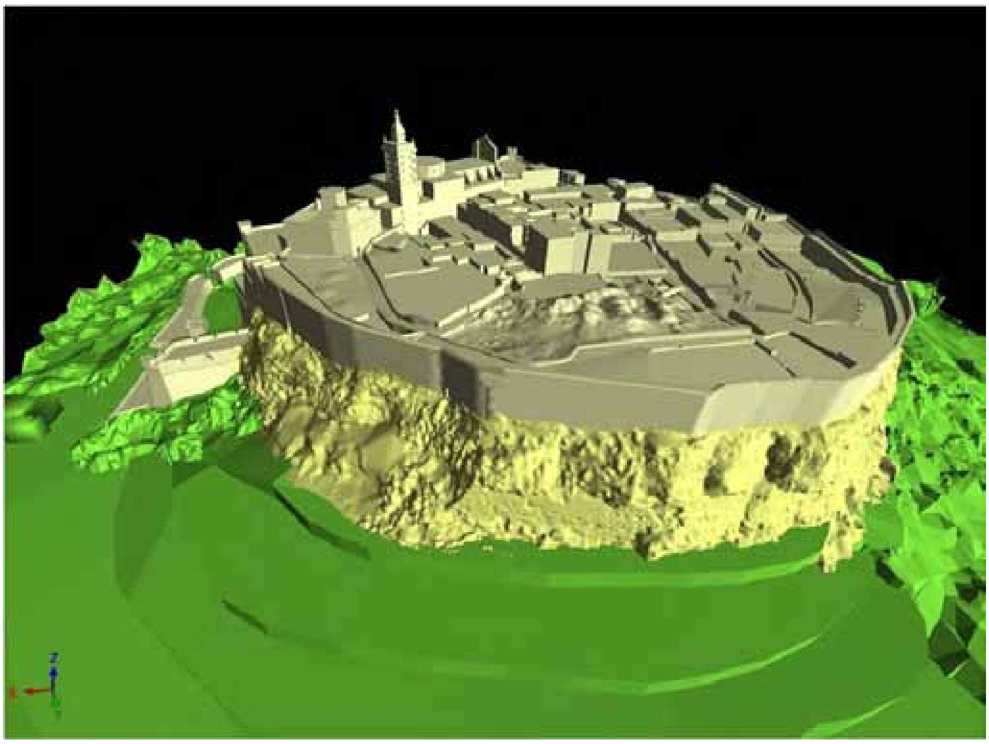

(a)

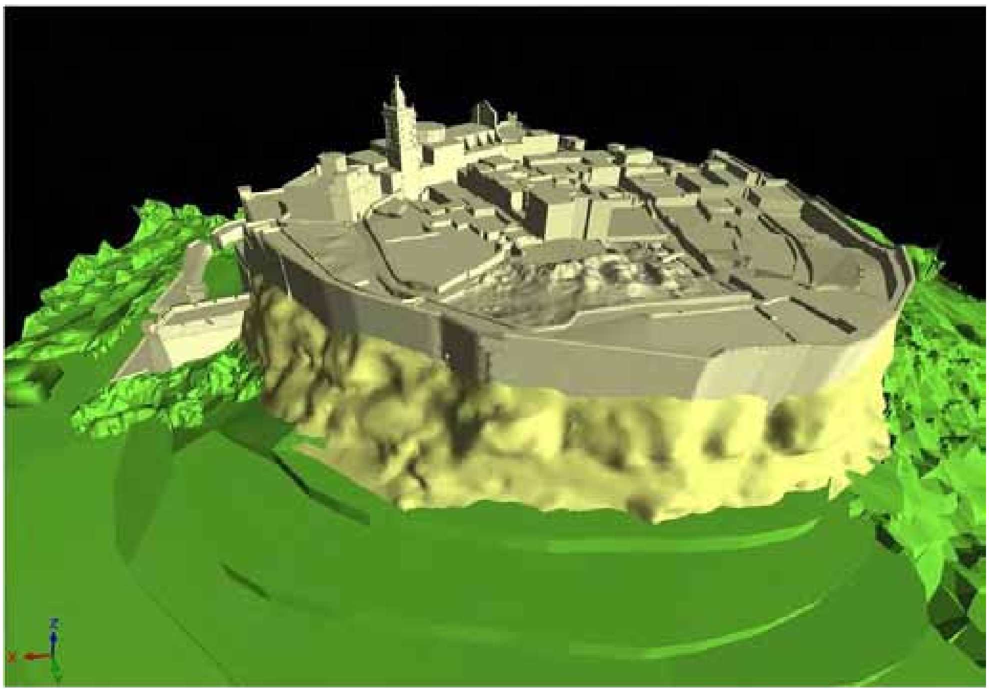

(b)

Figure 9.14: a) 3d model obtained from point cloud. b) Resampled 3d model employed in the kinematic analysis.

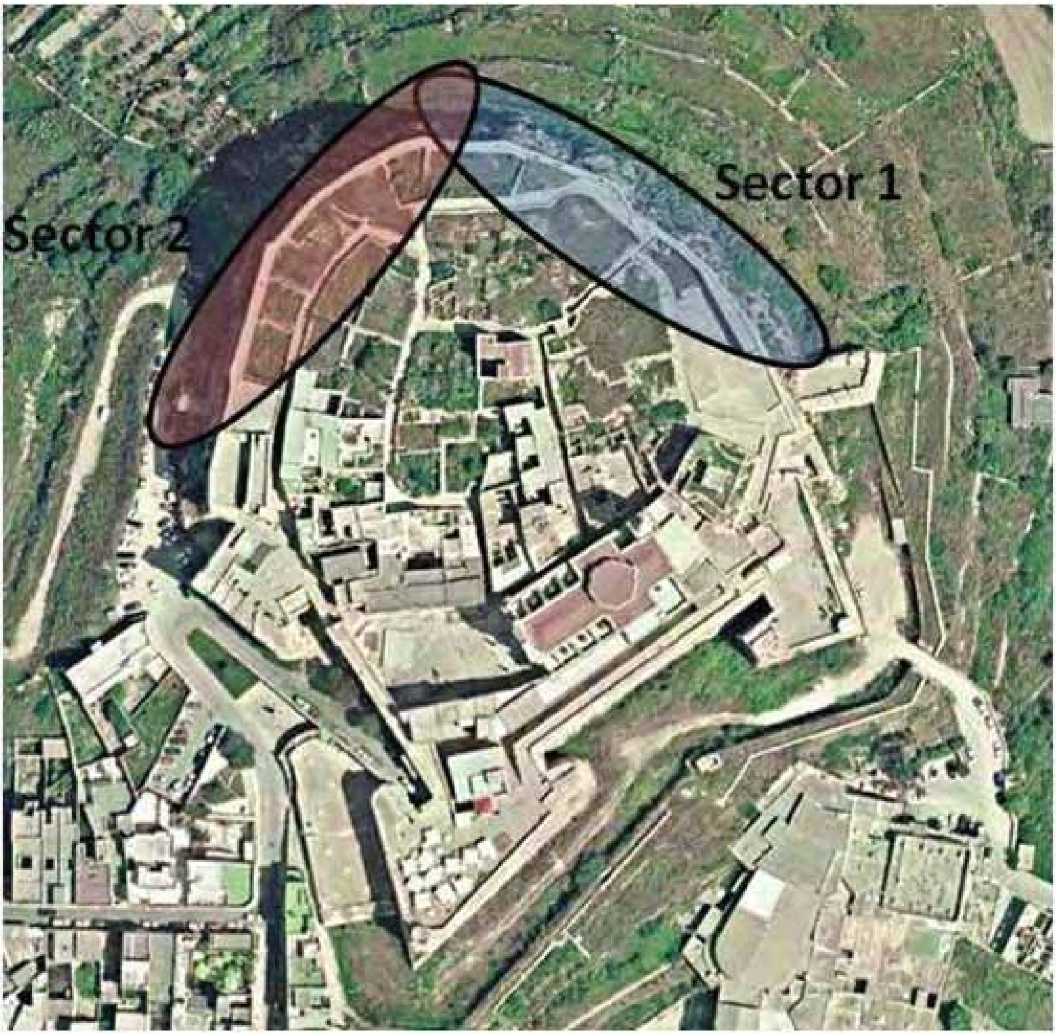

Figure 9.15: Location of the sectors presented in the following images.

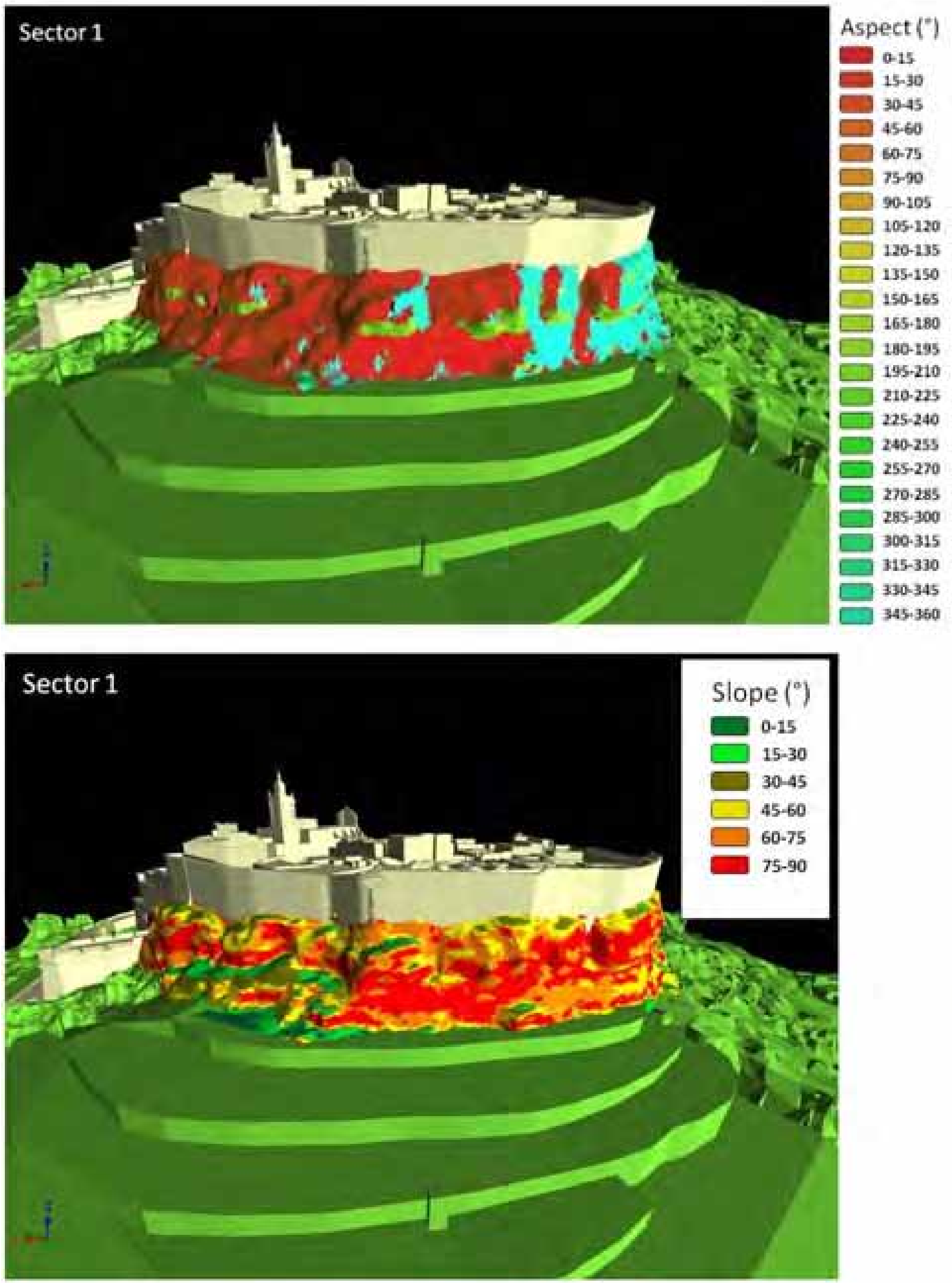

Figure 9.16: Sector 1: Rockwall steepness and rockwall aspect.

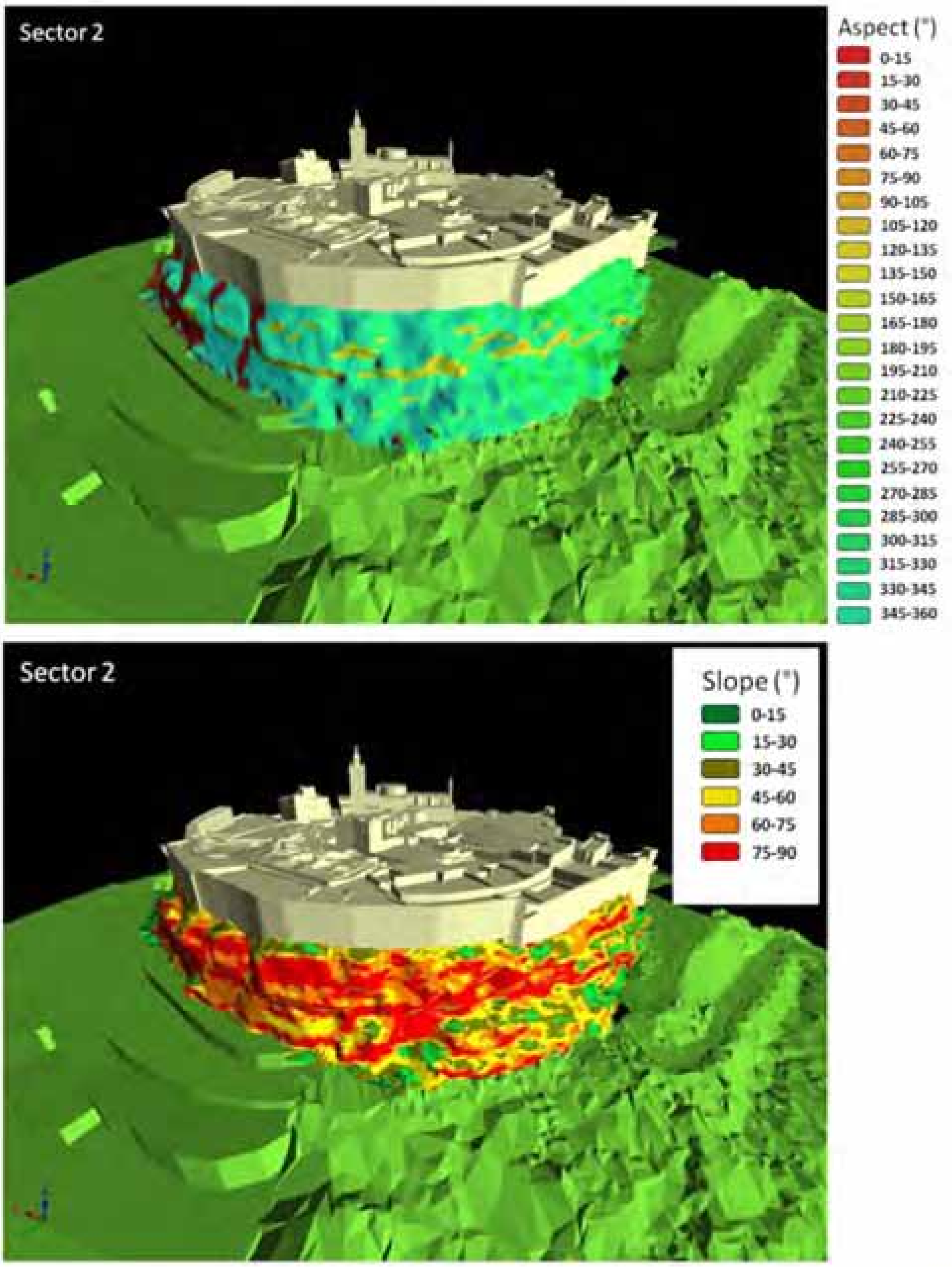

Figure 9.17: Sector 2: Rockwall steepness and rockwall aspect.

The results of the analysis presented in the following images (9.18),(9.19) for the two sectors reported in figure9.15.

For each sector, the kinematic index for the following instability mechanisms are plotted:

plane failure (PF)

wedge failure (WF)

block toppling (BT)

block toppling + sliding (BTS)

flexural toppling (FT)

The kinematic index were plotted with a common legend, scaled according to the maximum values (30%).

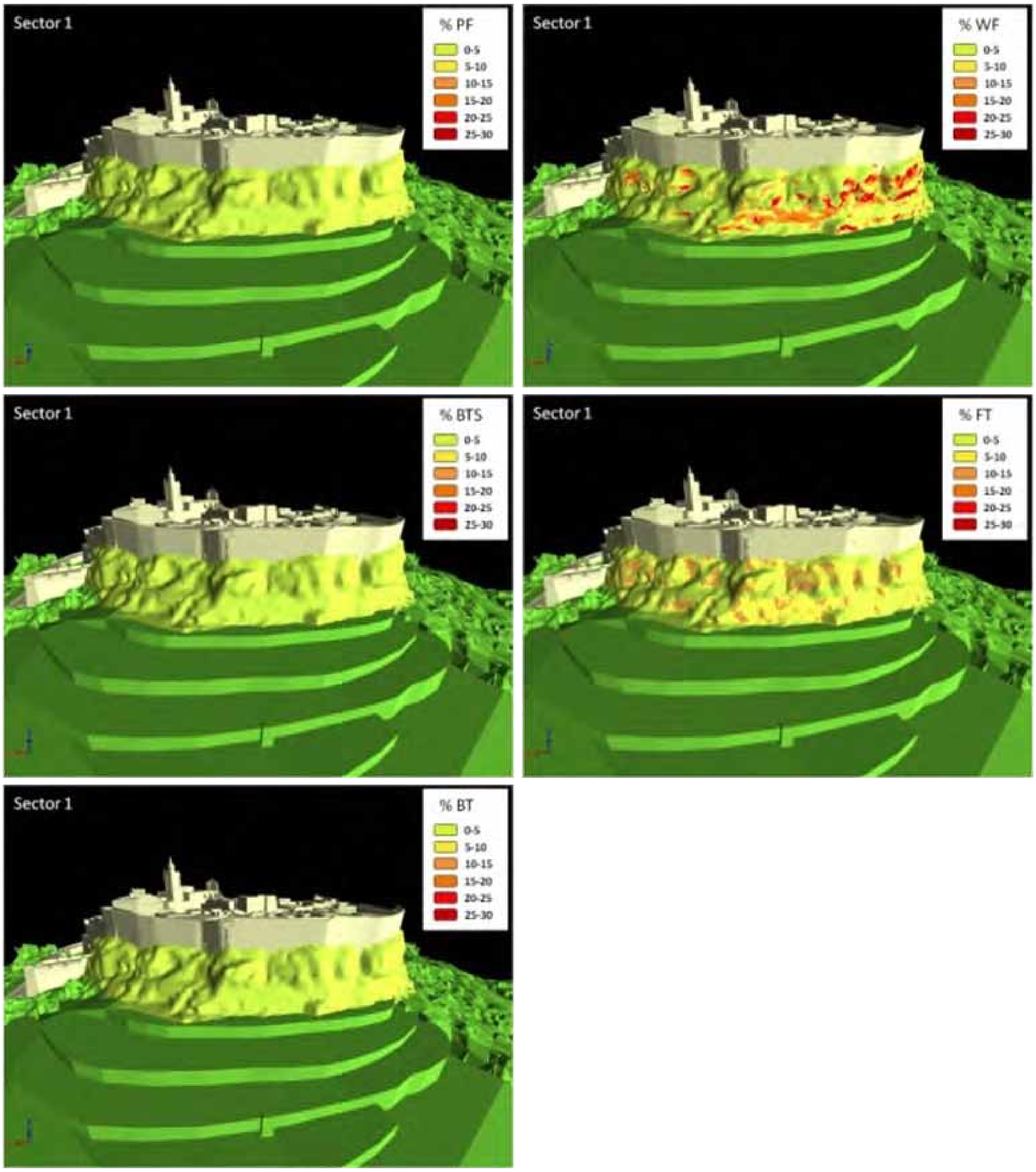

Figure 9.18: Sector 1: kinematic index a) plane failure b) wedge failure c) block toppling d) block toppling + sliding e) flexural toppling.

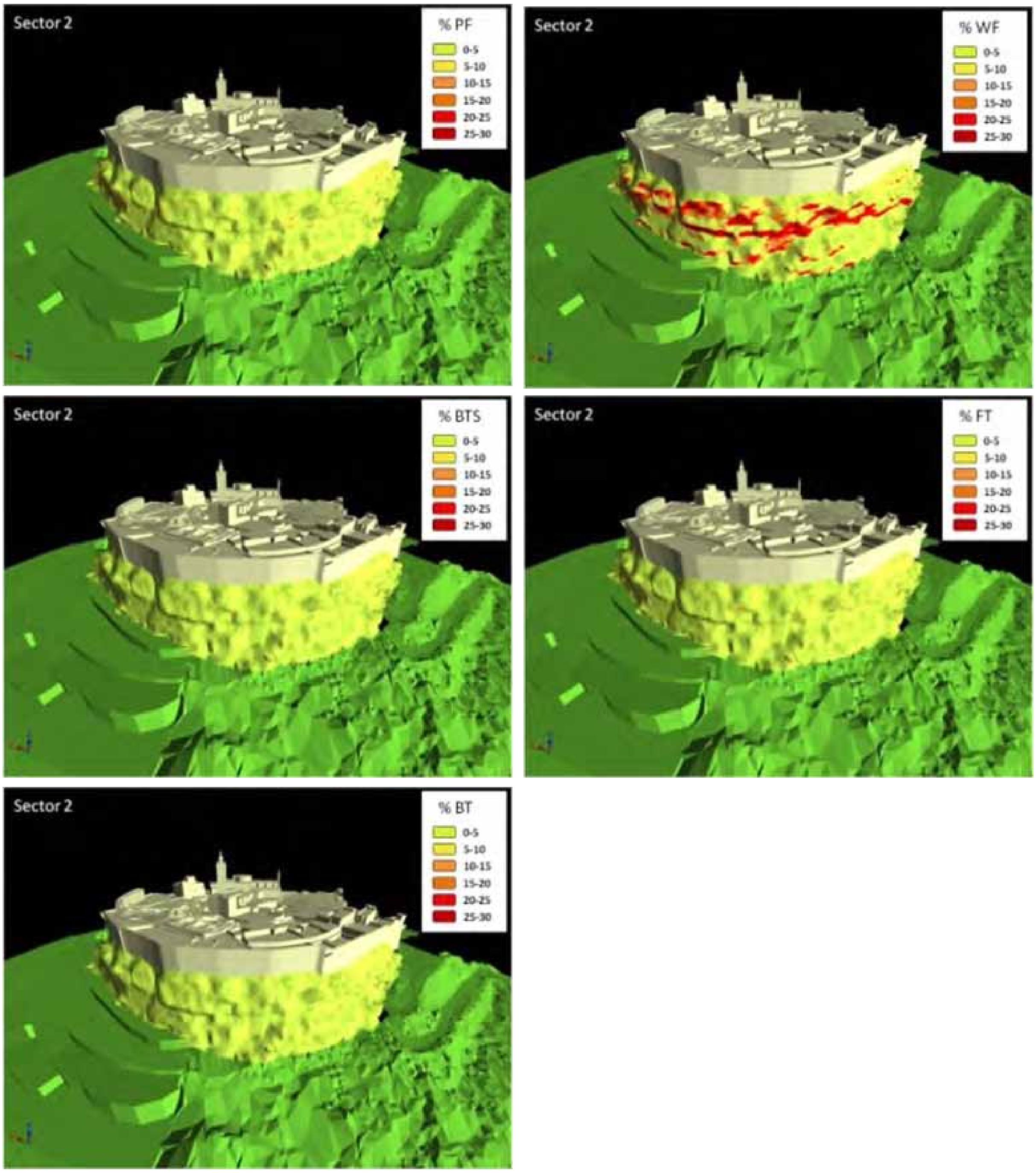

Figure 9.19: Sector 2: kinematic index a) plane failure b) wedge failure c) block toppling d) block toppling + sliding e) flexural toppling.

By analyzing results of the kinematic analysis we can observe that the mechanism associated to the highest index is the wedge failure (WF max=30%), followed by the flexural toppling (FT max=17%). All the other mechanism seem to be irrelevant, probably due to the fact that the bedding plane everywhere gently deep into the slope. All the Northern sector is intensively interested by wedge failure, especially where the wedge formation is favored by the cliff overhangs. The results of this analysis are confirmed by field evidences, which show signs of a number of niches and potential wedge detachment.

9.4 Identification of Optimal zones for instrument Positioning in Elba Island

Gigli and Casagli, developed a Matlab tool called DiAna (Discontinuity Analysis) for the 2D and 3D semi-automatic extraction of rock mass structural information from high resolution point clouds obtained from a terrestrial Laser Scanner [13]. In articular six of the ten ISRM parameters can be evaluated (orientation, numberofsets, spacing/frequency, persistence, block size andscaledependentroughness). In chapter 6 was described the rock slope sctructural set of a metamorphic outcrop on Elba Island.

We used DiAna to obtain geometrical characterization of the main rock mass main discontinuity plane from point cloud. Then, after 3D reconstruction of the rock mass surface, we integrated them and some superficial main cracks were obtained.

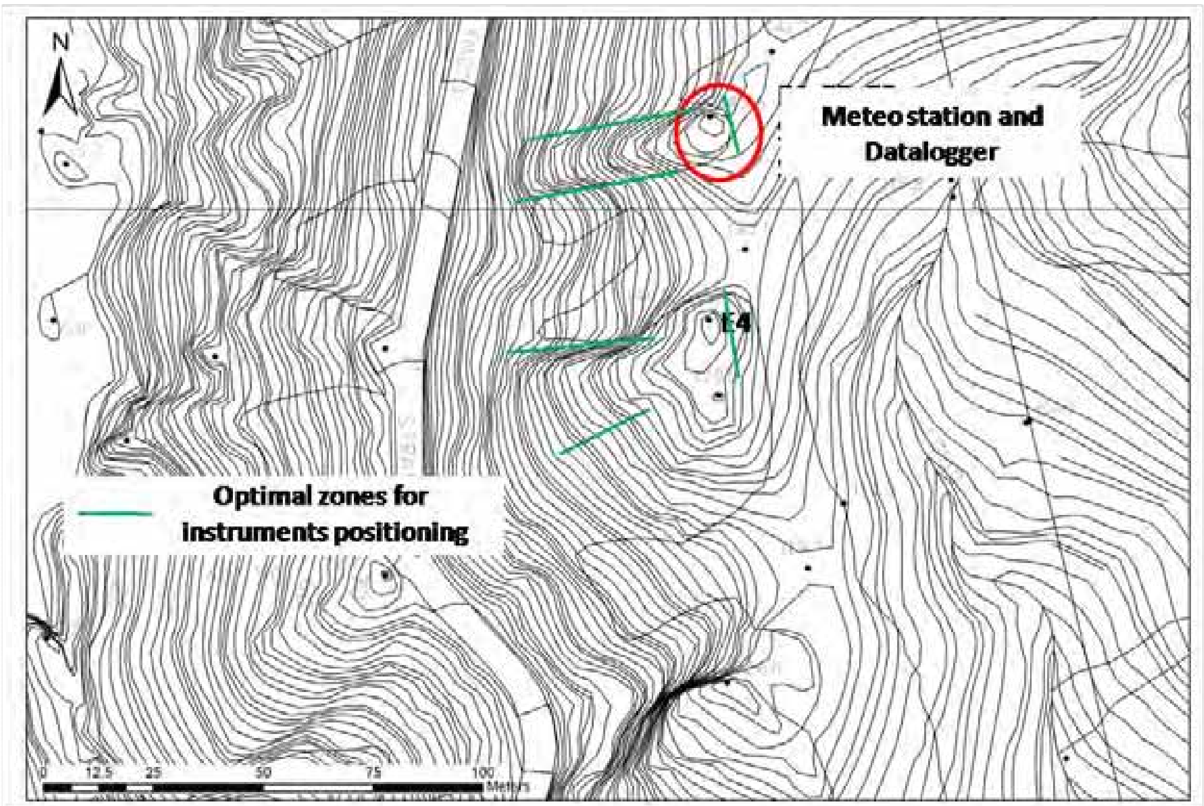

Figure 9.20: Topographic map of Punta del Timone. Location of optimal zones for instruments positioning.

The procedure is not yet automatic, and the choice of the main fracture is still done manually, but it remains a useful tool for rapid characterization of a rock mass.

Chapter 10

Applications' results

10.0.1 System installed at Mdina and Citadel

In order to front high and unexpected local accelerations, a warning system is currently managed by in cooperation with GDtest. This system, which is still under test, is based on velocity thresholds recorded at crack gauges, selected on the base of historical data. The selected threshold value is 0.5 mm of deformation within six hours; the system generates an internal alert event each time the threshold is exceed. The system switches to alarm mode if two alert events occur in succession at the same sensor. This double check of the event was chosen in order to eliminate many of the peaks due to instrumental errors and to reduce false alarms. During the test, the alarm dispatches will be notified only to the staff of the Department of Earth Sciences; then, after a check of data reliability, these will be dispatched to all the personnel concerned.

In the following sections a summary of the main outcomes from the monitoring data is presented; for each area under investigation a location map of the sensors is presented, and a histogram summarizing the mean velocity recorded for the whole monitoring period. Data recorded at significant instruments are also reported and commented.

10.0.1.1 Area A:

Most of the instruments within the A area Figure 8.12 on page 176have been acquiring since December 2009 to January 2011; thus an annual cycle of readings is now available. From the histogram of Figure 10.1 on page 200 it is possible to observe that quite high mean velocities have locally been recorded, with peak values of 0.01 mm/day (CGA 101, CGA 102), that correspond to a total displacement of more than 2.5 mm.

Other instruments showing appreciable deformation rates are: CGA03, CGA05, CGA06, CGA11, CGA12, CGA18. As a general rule, the most unstable sectors seem to be associated with those areas were the restoration works have been more intense, such as the St. Paul Bastion, or under the Vilhena Palace. However, not only the mean velocity (that is based on the first and last considered readings only) is important, but also the general deformation trend. Very often, regular closing movements were recorded up to middle august, followed by an opposite opening behavior. Sometimes the initial closing has been completed recovered with an almost symmetric trend CGA01, Figure 10.2 on page 200 sometimes this trend is unbalanced, resulting in an additional opening which gives the graph an asymmetric aspect CGA11, Figure 10.4 on page 201. Some crack gauges also experience a markedly stepped behavior, with periods of sharp displacements alternated to stable phases CGA101, CGA102, CGA03, Figure 10.5 on page 202Figure 10.6 on page 202Figure 10.23 on page 215. Thus, we can evaluate possible influences of the restoration activities on the recorded displacements, by comparing the occurrence of these steps with the working plan. The onset of the closing behavior and the main accelerating phases seem to be more correlated with the mean daily temperature Figure 8.15 on page 179or with the restoration works than with rainfall Figure 10.3 on page 201or pore water pressures. It is important to remark that most of the crack gauges are located outdoors, and are, therefore, more prone to suffer expansion or contraction due to temperature changes. Some useful information can also be extracted from the biaxial inclinometer readings. For example BINA02 Figure 10.10 on page 205 show a tilting of the St.Paul bastion wall on both axes, with a maximum inclination of 1.5 mm/m. By comparing biaxial inclinometer data with those arising from the topographic survey performed during the restoration works Figure 10.11 on page 206, we can find a fair agreement, as regards both the general trend, and the displacements. For example, inclinometer BINA03 Figure 10.9 on page 204 must be compared to benchmark G3, where axis B (inclinometer) corresponds to axis E (benchmark) and axis A (inclinometer) to axis N (benchmark). To facilitate the comparison, inclinometer data have been plotted with the same time interval of the topographic survey Figure 10.11 on page 206.

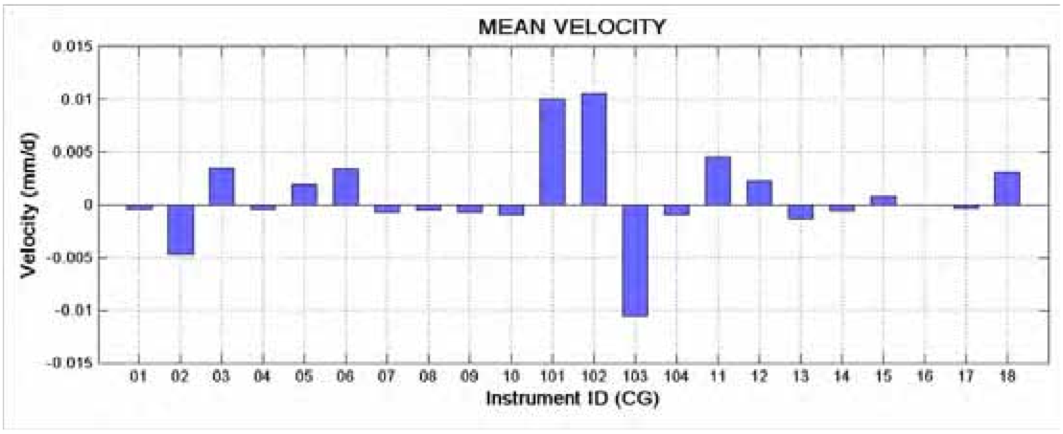

Figure 10.1: Histogram of mean velocity recorded at crack gauges – Area A.

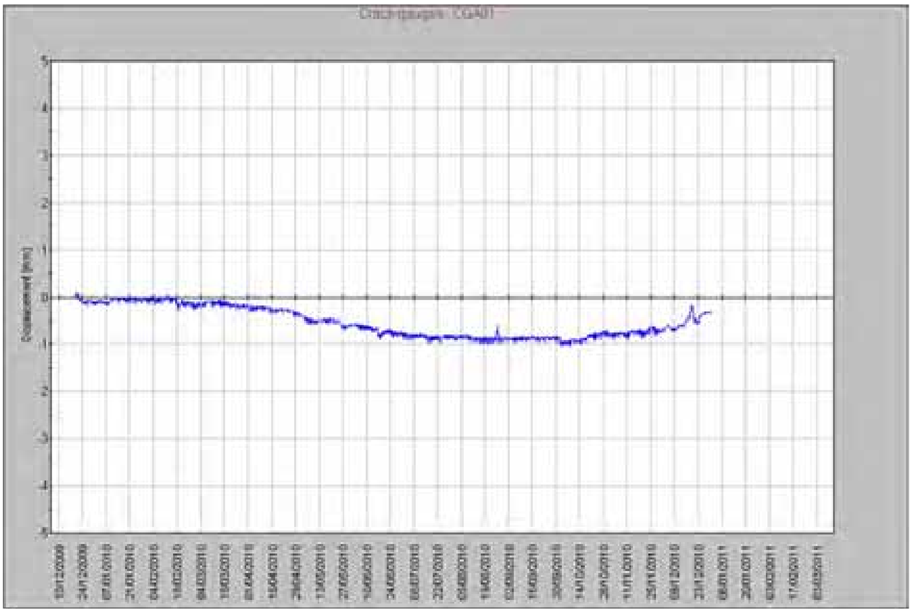

Figure 10.2: Recorded displacements at CGA01.

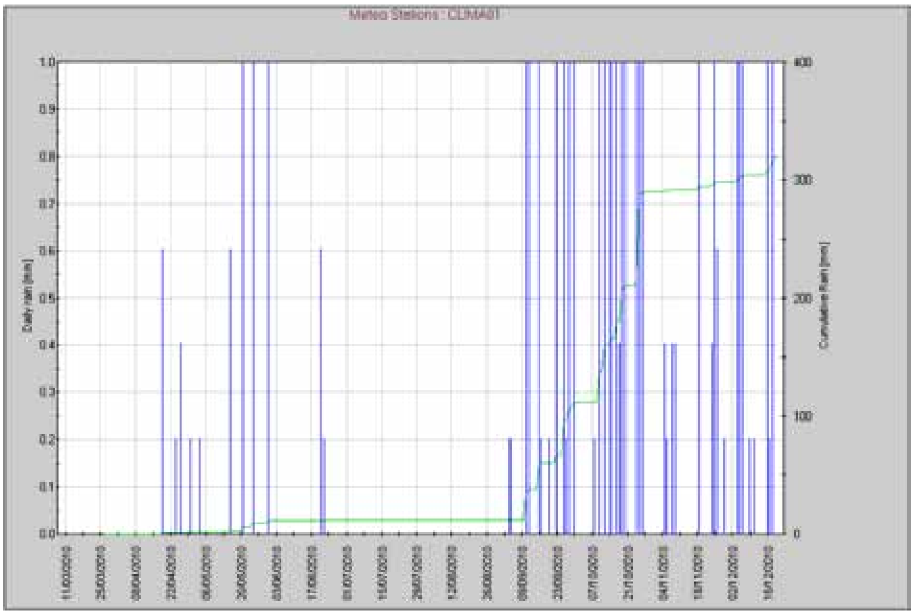

Figure 10.3: Chart of rainfall, daily and cumulative records.

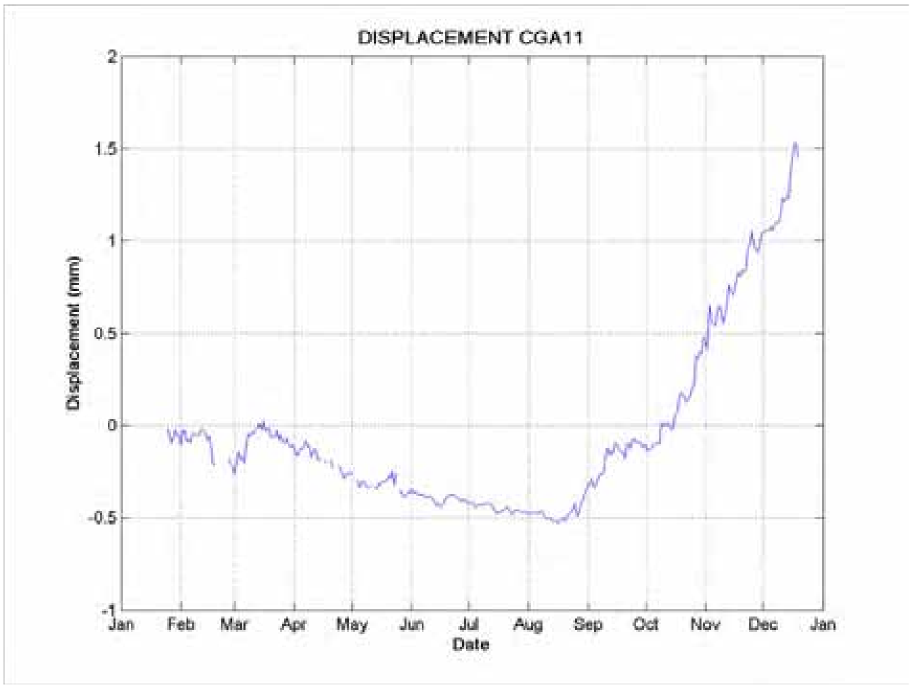

Figure 10.4: Daily displacements at CGA11.

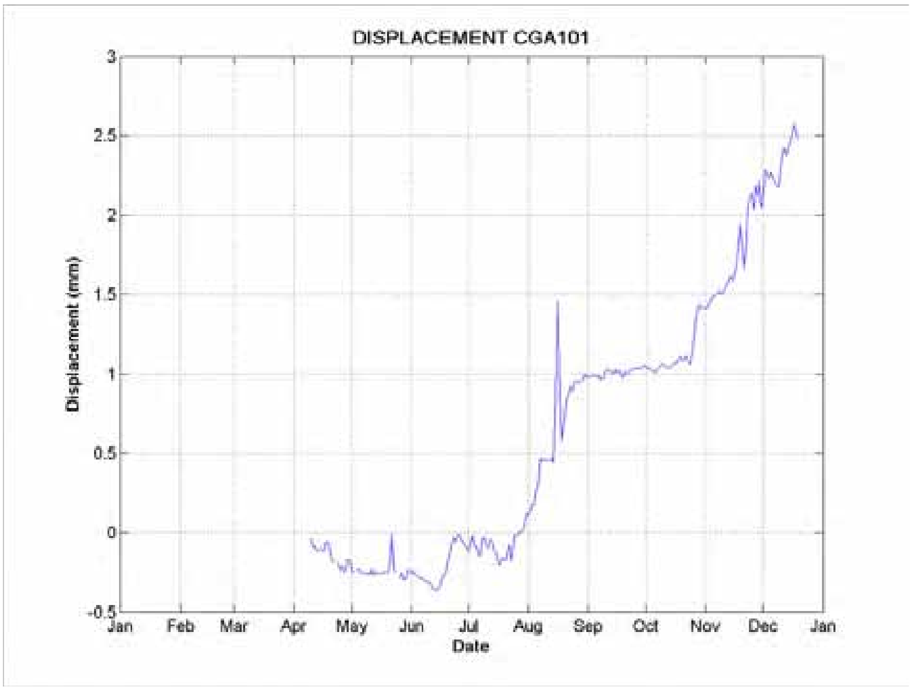

Figure 10.5: Daily displacements at CGA101.

Figure 10.6: Daily displacements at CGA102.

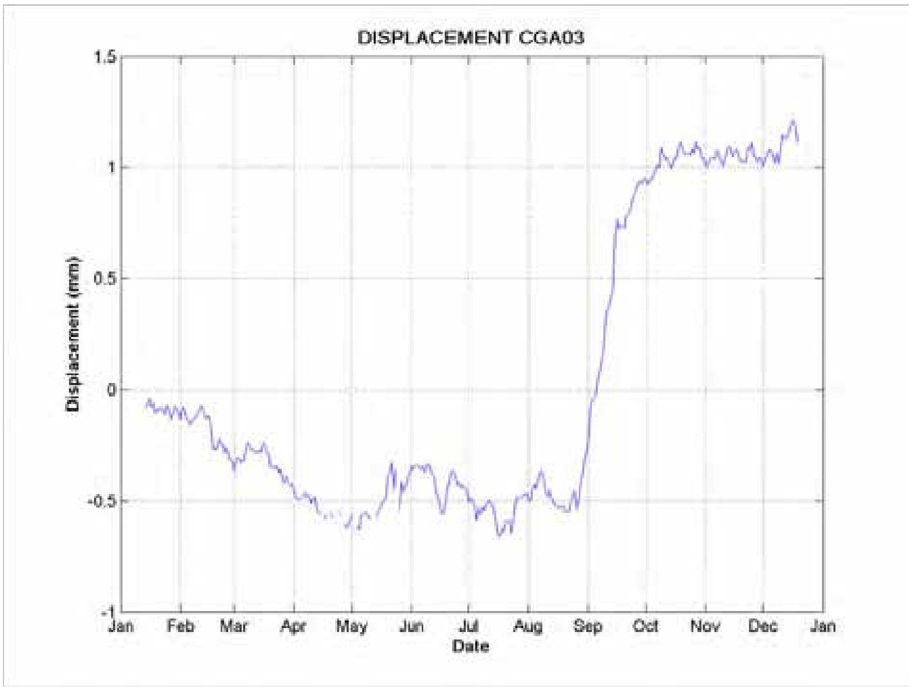

Figure 10.7: Daily displacements at CGA03.

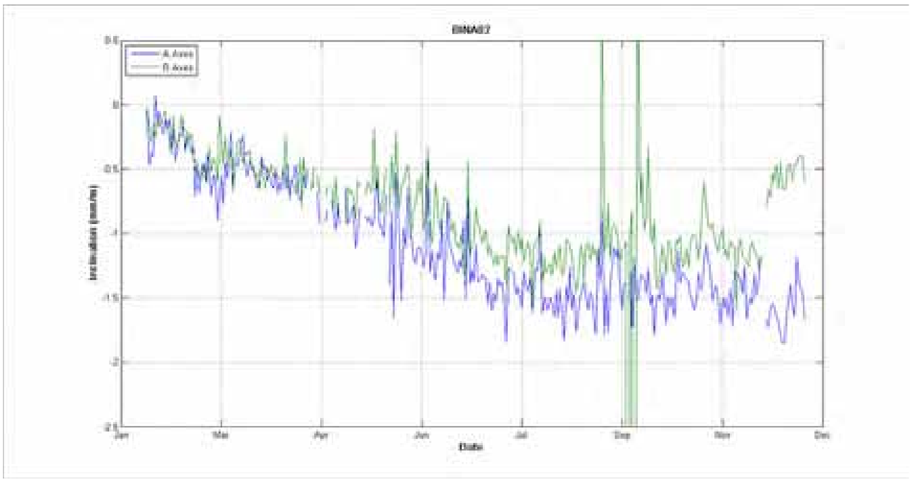

Figure 10.8: Inclinometric data at BINA02.

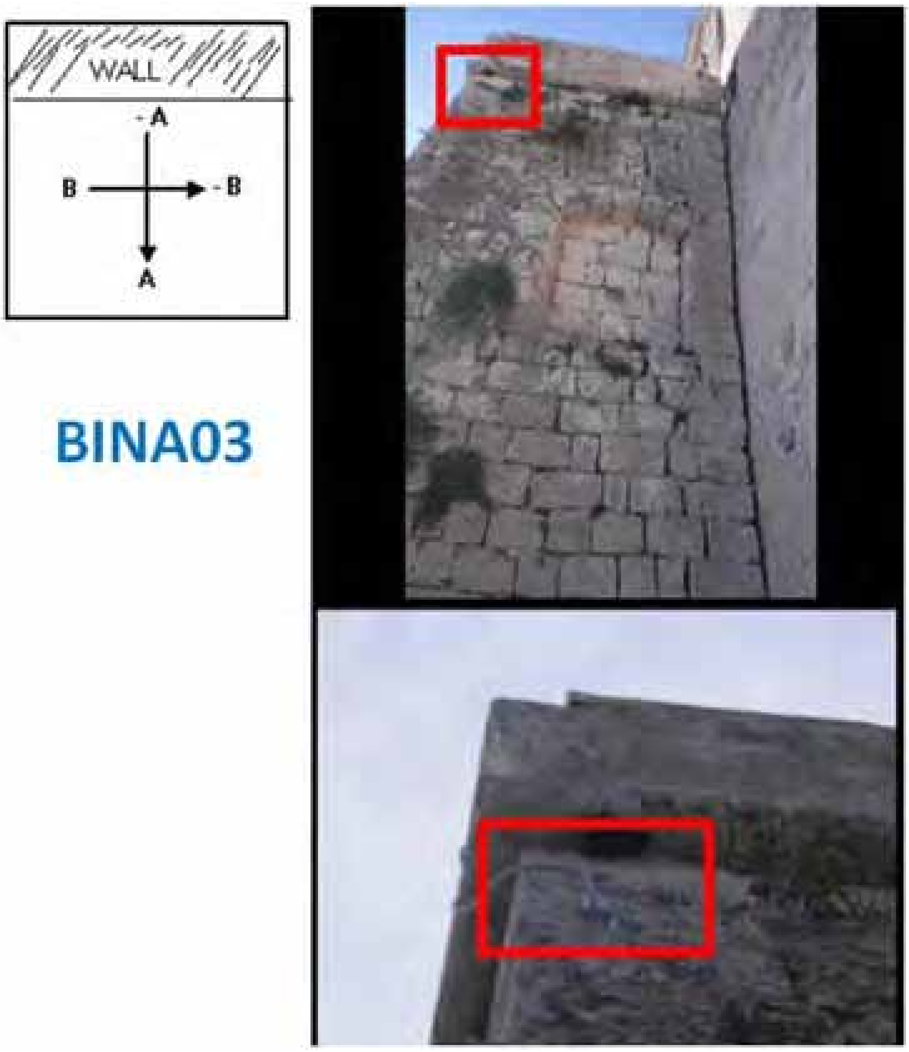

Figure 10.9: Location of biaxial inclinometer BINA03 (Area A, Mdina).

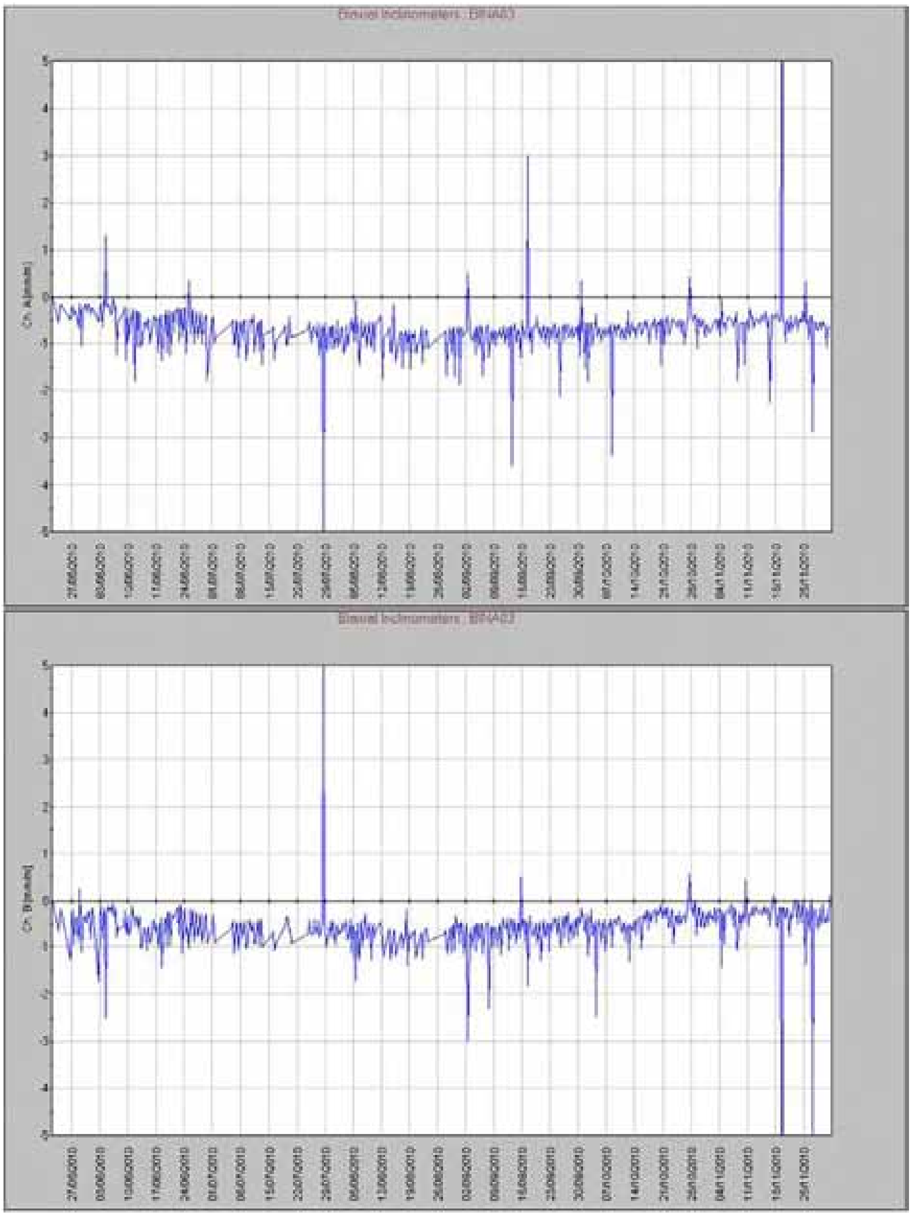

Figure 10.10: Inclinometric data at BINA03.

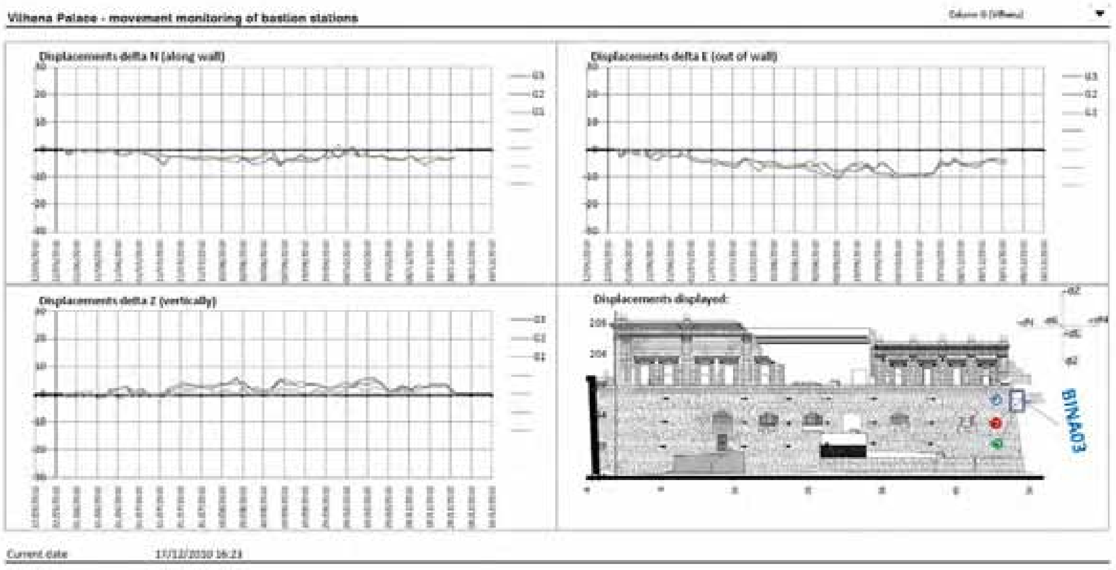

Figure 10.11: Topographic survey (Taken from [12]).

10.0.1.2 Area B

Since instrumental readings at area B Figure 4.40 on page 86 started some months later than area A, an annual cycle of measurements is not yet available. From Figure 10.12 on page 207 we can observe that mean velocities recorded at crack gauges are generally lower than those from the A area. The southern corner seems to be the more unstable during the monitoring period, where CGB02 Figure 10.13 on page 207 and Figure 10.14 on page 208 recorded total displacements of 1.8 mm and 0.8 mm. CGB02 shows the more interesting behavior, where a marked stepped opening is superimposed to a regular closing. The first main step (6^{th} September) cannot be correlated to the onset of rainfall (10^{th} September). The major crack located on the wall over the Despuig Bastion, next to the Cathedral shows a general opening, with values up to 0.7 mm CGB14Figure 10.15 on page 209, but an annual cycle of measures have still to be completed. An anomalous behavior has been recorded on the Northern sector of the Despuig Bastion, where, at the beginning of August, 2010, an increase of pore water pressure at piezometer PZB01 Figure 10.16 on page 210 has been recorded, followed by an instantaneous tilting of axis B of inclinometer Figure 10.17 on page 211. The displacements were not confirmed by the crack gauges, and seem to be associated to anthropic activities. Some deformations were recorded by the borehole inclinometer INC02Figure 10.18 on page 212 at a depth of 9-11 m, but the direction of movement are not completely consistent with the probable true direction, suggesting to wait the next measurements.

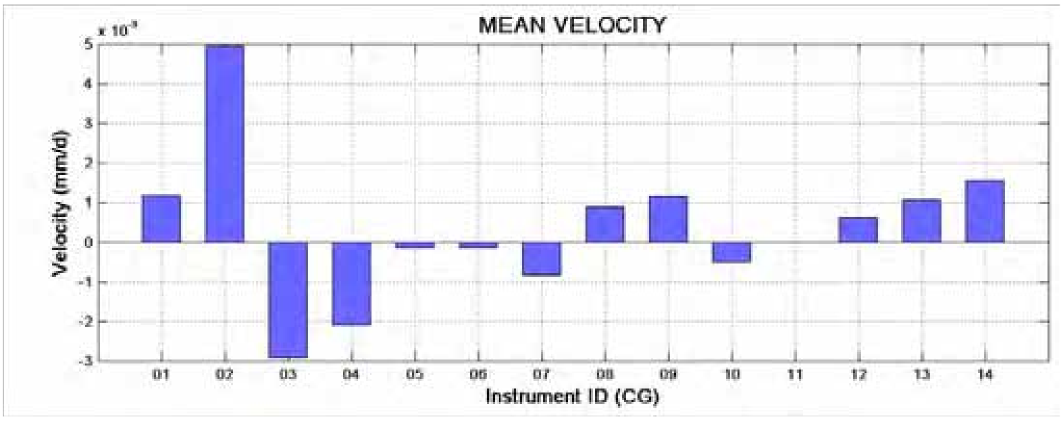

Figure 10.12: Histogram of mean velocity recorded at crack gauges – Area B.

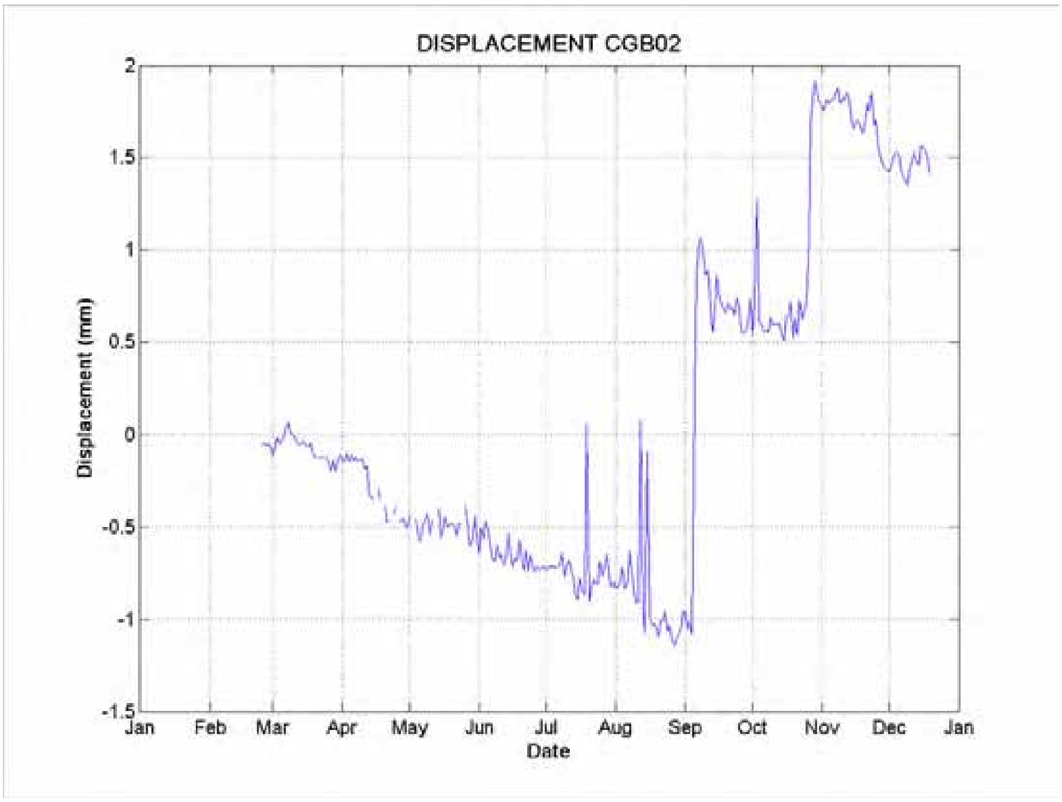

Figure 10.13: Daily displacements at CGB02.

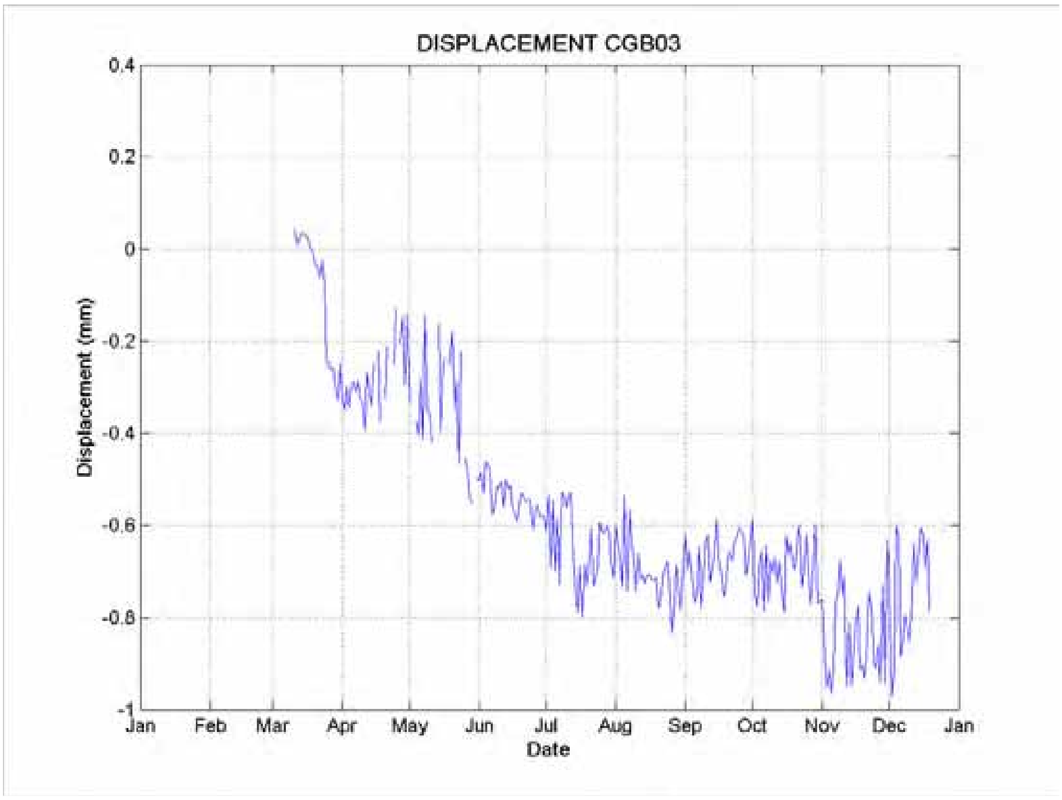

Figure 10.14: Daily displacements at CGB03.

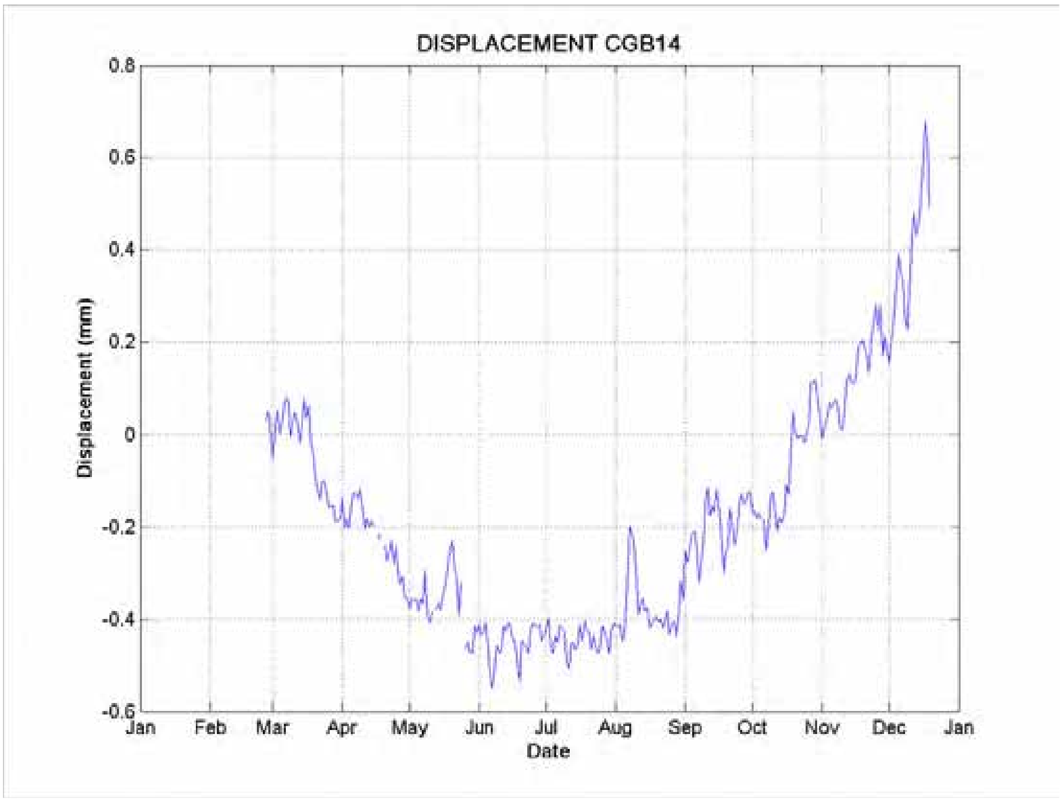

Figure 10.15: Daily displacements at CGB14.

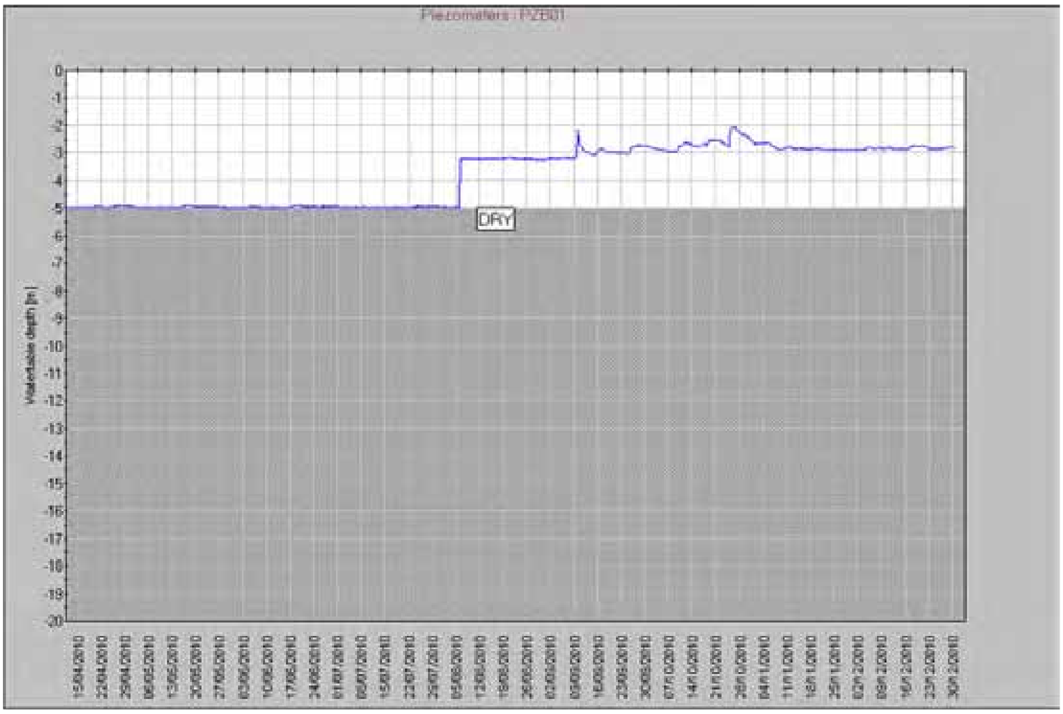

Figure 10.16: Piezometric data at PZB01.

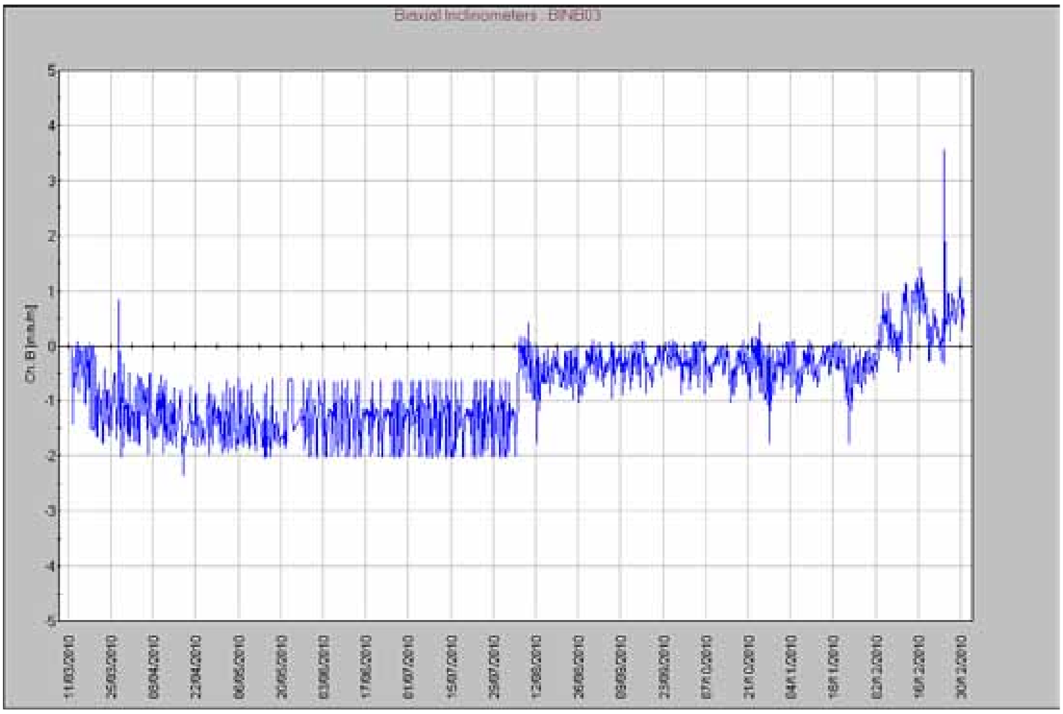

Figure 10.17: Inclinometric data at BINB03 (axis B).

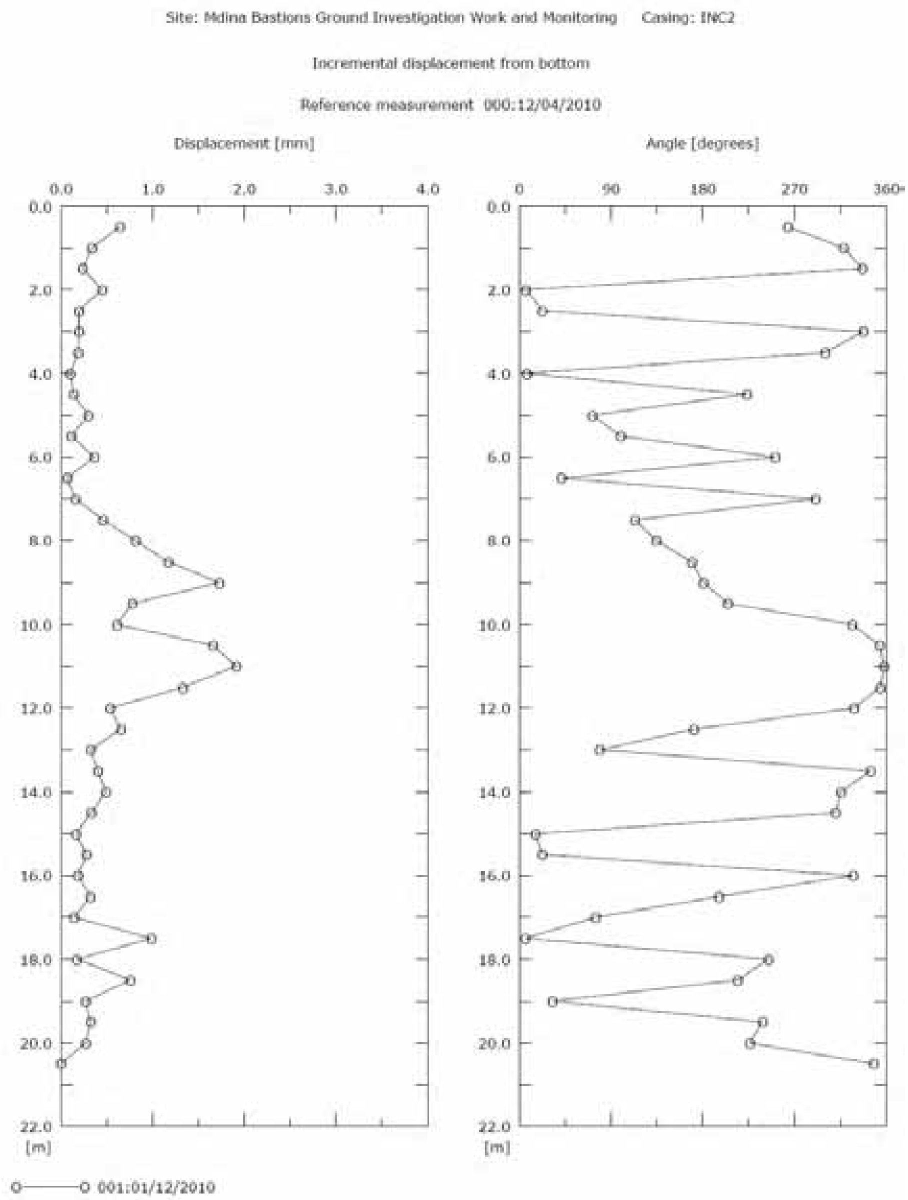

Figure 10.18: Inclinometric data from borehole inclinometer installed in Mdina, INC02 (taken from [5]).

10.0.1.3 Area C

Since instrumental readings at area C Figure 4.41 on page 87started some months later than those at area A, an annual cycle of measurements is not yet available. By observing Figure 10.19 on page 213 a general instability is evident, with almost all crack gauges experiencing opening. The highest mean velocities were recorded at the sensors located along the eastern wall (CGC05, CGC08, CGC10, CGC15, CGC17, CGC19) Figure 10.20 on page 213,Figure 10.23 on page 215. Biaxial inclinometers show the same behavior, with the highest tilting displacements along the eastern wall BINC04 Figure 10.24 on page 215, with respect to the western one BINC03 Figure 10.25 on page 216. The borehole inclinometer INC01 shows a clear surface at

8.5 m depth, with direction consistent with the slope dip direction. This surface was not clear on the data from the first reading, thus it's important to wait for the next reading to confirm the occurrence of a possible failure surface.

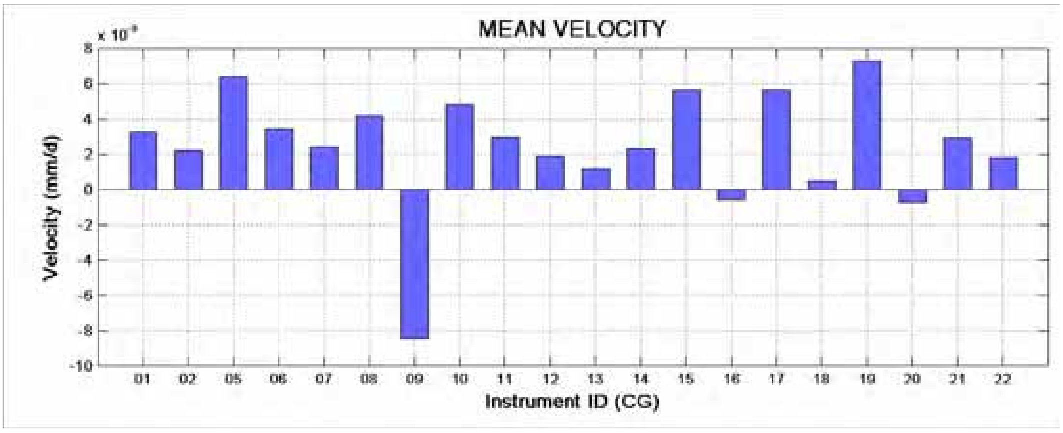

Figure 10.19: Histogram of mean velocity recorded at crack gauges – Area C.

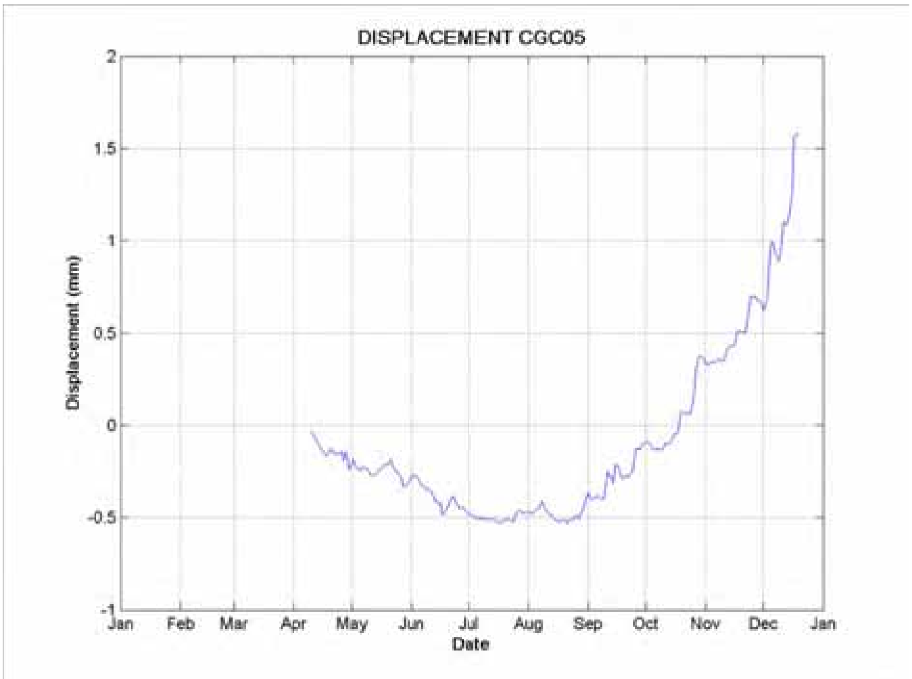

Figure 10.20: Daily displacements at CGC05.

Figure 10.21: Daily displacements at CGC15.

Figure 10.22: Daily displacements at CGC17.

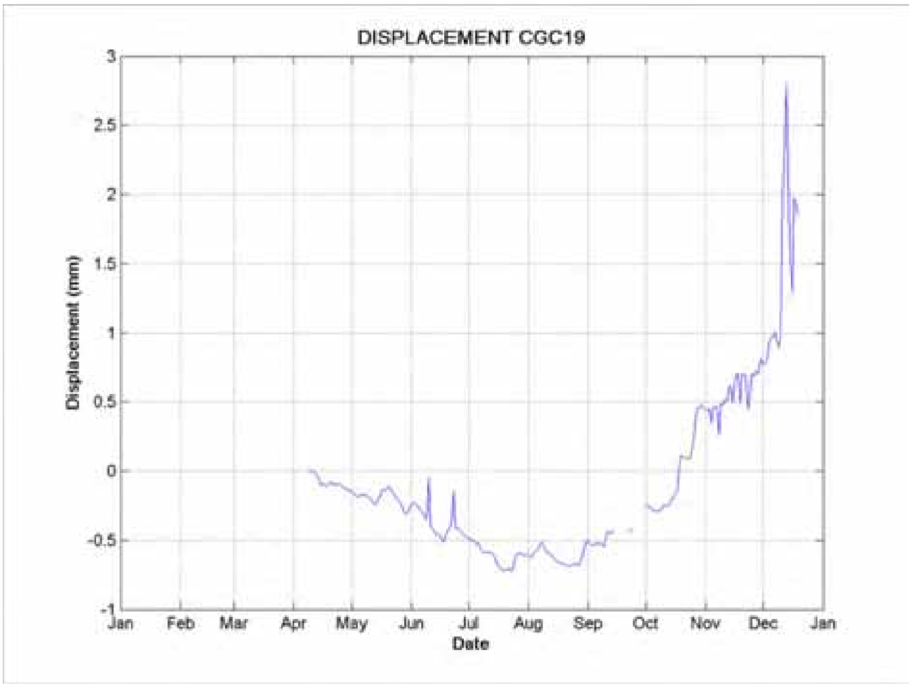

Figure 10.23: Daily displacements at CGC19.

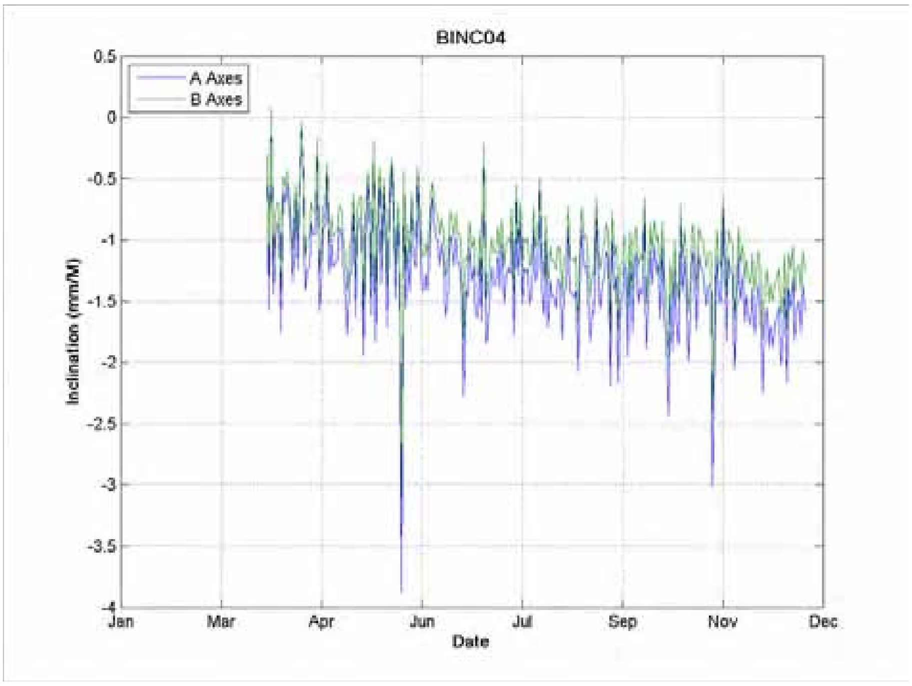

Figure 10.24: Inclinometric data at BINC04.

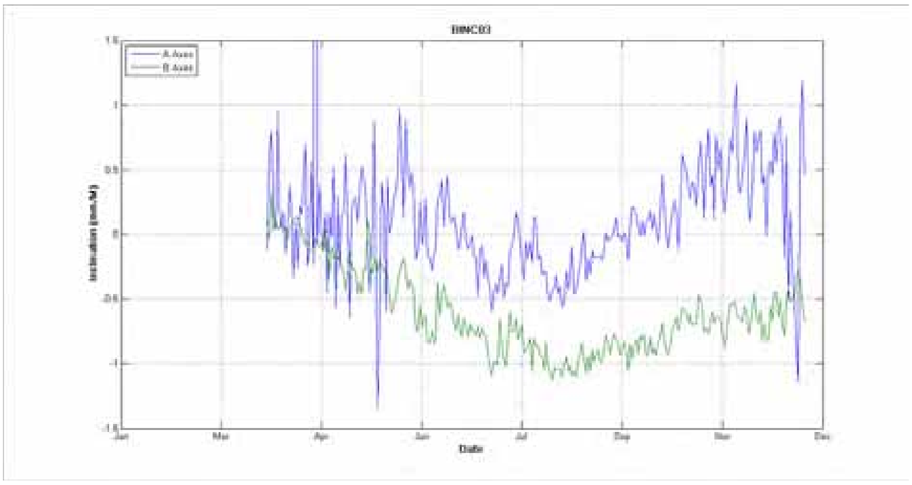

Figure 10.25: Inclinometric data at BINC03.

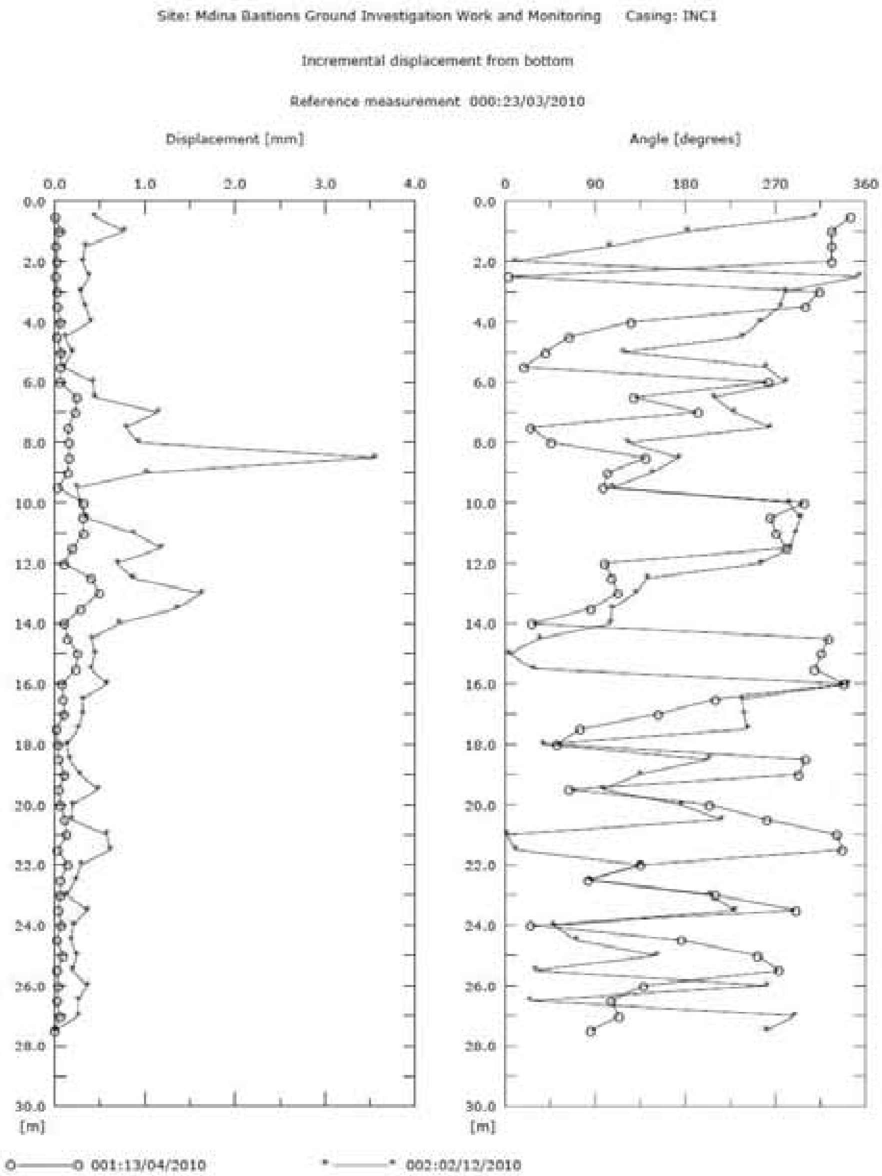

Figure 10.26: Inclinometric data from borehole inclinometer installed in Mdina, INC01 (taken from [5]).

10.1 Early warning activities and self-adptive procedures.

10.1.1 System installed at Torgiovannetto

In March 2009 University of Firenze, Earth Science Department, has been commissioned by Umbria Region to furnish scientific support to the monitoring activities at Torgiovannetto landslide. In fact, even after the construction of the retaining wall, the area is still affected by residual risk, especially in the case of a total collapse of the mass movement. For this reason an early warning system has been specifically designed.

Before starting with the actual design of the EWS, few design criteria have been pointed out. This methodological approach is recommended since it permits to come up with a coherent system that aims at few, well determined objectives. Sometimes, in order to achieve a certain goal, some choices must be done and some other goals must be discarded; for this reason defining the working criteria since the early stages will help to choose which direction to follow and to give the early warning system a role. The main criterion adopted here was simplicity. In fact in emergency conditions everything must be simple and straight-forward; the action to be taken must be clear and fast and misunderstandings or errors are not tolerable. Furthermore, trying to forecast the imminent failure of a landslide and to alert people is a very complicated task, for this reason some simplifications must be done anyway. Creating an early warning system that reflects all the possible features of a landslide can bring very little improvements and instead compromise the whole system. Simplicity can be implemented in many different ways within an EWS, as in the choice of few warning levels, of schematic thresholds etc; this will be discussed more in detail further on. Another criterion, more site-specific, was the avoidance of false alarms. Adopting counter-measures against false alarms can make the EWS less conservative. However, in this case the presence of the retaining wall and the absence of houses among the elements at risk made this solution possible. Moreover, as stated by Lacasse and Nadim (2009), an automatic early warning system generating a false alarm may cause more severe consequences than the landslide itself, inducing additionally a loss of credibility in the population. An important thing considered during the design phase was that the landslide is expected to show an accelerating trend a few days before the failure. This will give some time to the emergency procedures and the EWS has been designed accordingly. This piece of information demonstrates once more the importance of the geological knowledge of the mass wasting.

10.1.1.1 Data processing

10.1.1.2 Description of the early warning system

The system, managed by UNIFI-DST, has 3 warning levels

- Ordinary level: no emergency. Data collected by extensometers are checked daily by UNIFI-DST and a monthly monitoring bulletin is released. Other activities involve: maintenance (by UNIFI-DST); constant communication between stakeholders and daily weather forecasting (by Umbria Region); support in instruments maintenance (by Assisi municipality).

- Attention level: when entering the attention level UNIFI-DST immediately notifies all the other stakeholders (namely Umbria Region, Perugia Province, Assisi Municipality, h24 personnel on duty). Data are checked more frequently and a daily bulletin is released. In this level every stakeholder prepares for a possible alarm and personnel are activated. No public communication is made yet. In addition to the activities carried out during ordinary level, estimations of ground saturation will be executed by Umbria Region.

- Alarm level: when entering the alarm level UNIFI-DST immediately notifies all the other stakeholders. Data checking frequency is further increased and 2 bulletins are emitted every day. The Provincial Street 249/1 is manually closed and fences are installed to close the road. Municipal emergency plan is activated. Ground saturation data are involved in the forecasting of future landslide developments.

For each extensometer a velocity (mm/day) threshold has been assigned Table 10.1 on page 219. The velocity is obtained by averaging the values of the previous 24 hours, in order to reduce the noise of measurements and so to improve the reliability of the system. These thresholds have been obtained empirically by analyzing the most critical periods of the last years of monitoring.

Extensometer	Threshold
E1	0.50 mm/day
E2	0.50 mm/day
E3	0.50 mm/day
E4	0.50 mm/day
E10n	0.50 mm/day
E7n	1.00 mm/day
E8n	1.00 mm/day
E9n	1.00 mm/day
E11	1.00 mm/day
E12	1.00 mm/day
E13	1.00 mm/day
E14	1.00 mm/day
E15	1.00 mm/day

Table 10.1: Velocity threshold values assigned to each extensometer.

Velocity is manually checked every day; in addition, an automatic check is executed every 8 hours. Whenever two or more sensors exceed their respective threshold an automatic notification is sent to the UNIFI-DST personnel who verify the reliability of the information. If it is confirmed, UNIFI-DST will communicate to the other stakeholders that the attention level has been reached. The level will return to ordinary when the conditions for the triggering of the attention level no longer exist. The reliability of the thresholds has been verified by performing a back analysis which showed that during the previous 2 years and half of monitoring attention level would have been entered only 7 times, due to heavy rains or, in few occurrences, due to instrumental errors. This has been considered a good result also because the cases due to instrumental errors can be filtered out by UNIFI-DST personnel. After the implementation of the system, attention level occurred only once, after a rainy period, and it lasted only one day. During the rest of the time the landslide showed no worrying behavior. The triggering of alarm level is not connected with any threshold. Instead it makes use of expert judgment and interpretation mainly based on the application of the empirical forecasting methods by Saito (1965) and Fukuzono (1985). Successful applications of these methods can be found in [98] [97]; For each sensor the forecasting methods mentioned above will be applied. If an upcoming failure is hinted either by using this approach or by a remarkable acceleration suggesting that the landslide entered the tertiary creep, the alarm level will be declared and all the actions previously described will be taken. Also the revocation of the alarm level is subject to expert judgment. So far alarm level has never been reached. Bulletins mark every phase of activity; they indicate the present warning level, the current status of the monitoring system and any notes and comments. Extraordinary bulletins are emitted whenever the current warning level changes or in case of significant malfunctioning of the instruments. Finally, to visually assess the conditions of the landslide, of the retaining wall and of the street, 3 cameras have been installed 10.27.

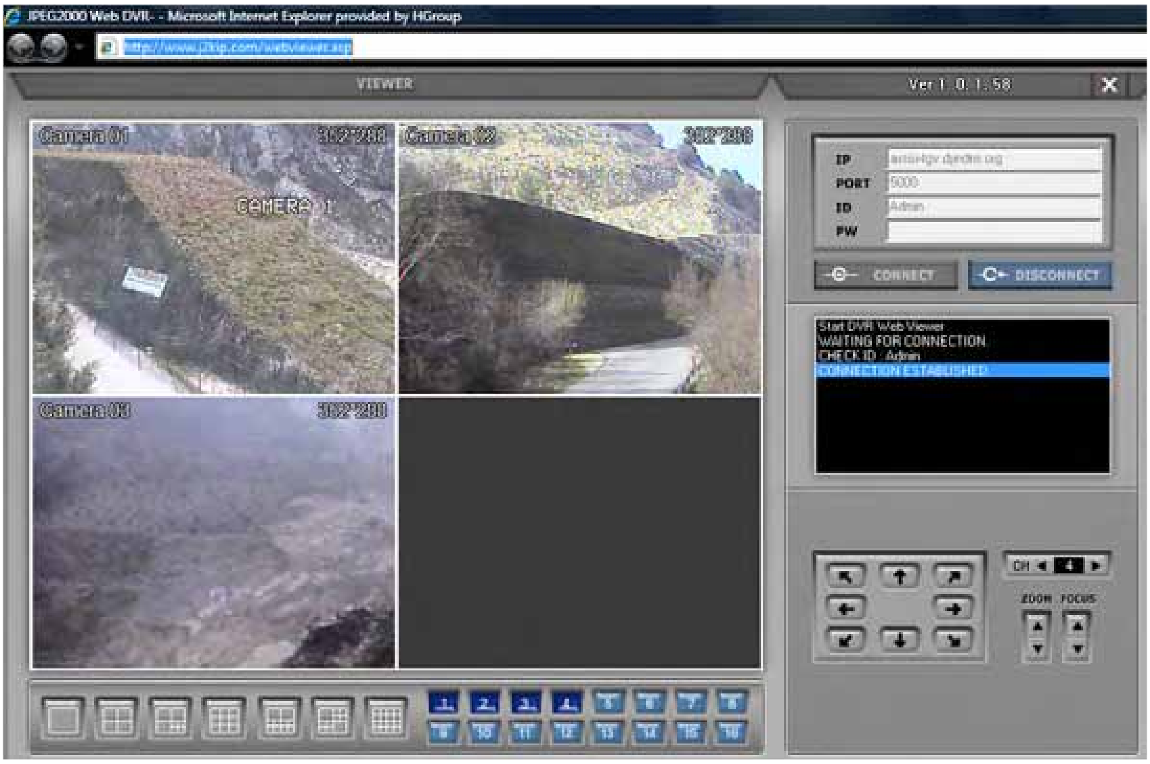

Figure 10.27: Screen shot of the video recording system for the control of different views of the landslide.

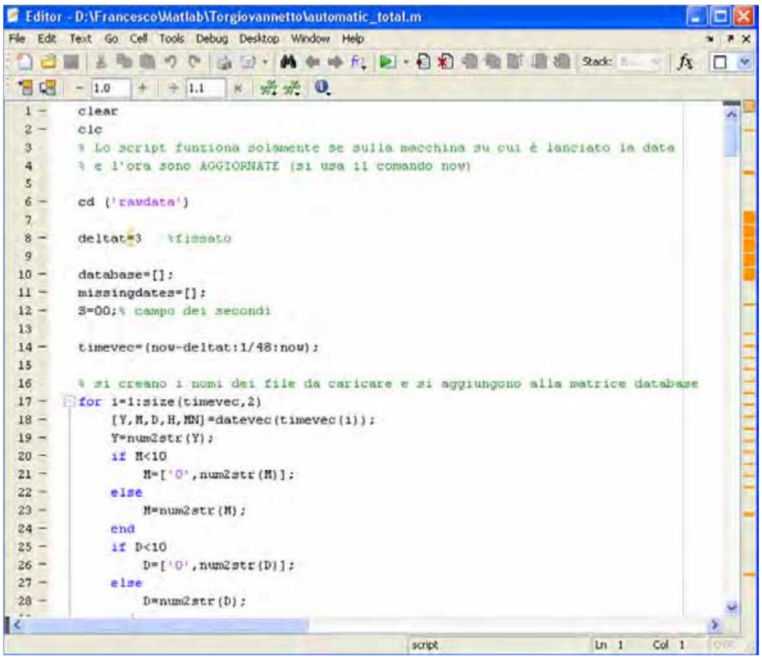

Figure 10.28: Screen shot of Matlab routine.

10.1.2 System installed at Mdina and Citadel

In order to front high and unexpected local accelerations, a warning system is currently managed by in cooperation with GDtest. This system, which is still under test, is based on velocity thresholds recorded at crack gauges, selected on the base of historical data. The selected threshold value is 0.5 mm of deformation within six hours; the system generates an internal alert event each time the threshold is exceeded. The system switches to alarm mode if two alert events occur in succession at the same sensor. This double check of the event was chosen in order to eliminate many of the peaks due to instrumental errors and to reduce false alarms. During the test, the alarm dispatches will be notified only to the staff of the Department of Earth Sciences; then, after a check of data reliability, these will be dispatched to all the personnel concerned.

In the following sections a summary of the main outcomes from the monitoring data is presented; for each area under investigation a location map of the sensors is presented, and a histogram summarizing the mean velocity recorded for the whole monitoring period. Data recorded at significant instruments are also reported and commented.

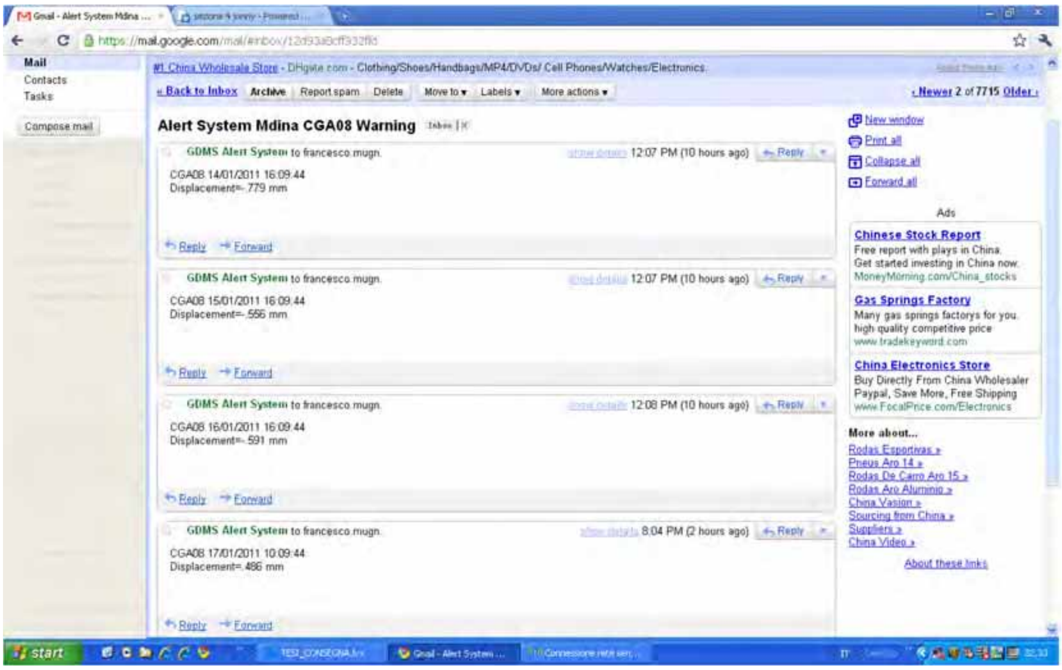

Figure 10.29: Screenshot of alarm message dispatched by automatic e-mail function. The instrument number, velocity and time of measurement is reported in the e-mail body.

10.1.3 System installed at Elba Island

10.1.3.1 Data analysis

Analysis of monitoring data relating to a monitoring period span from March 18 to October 4, 2010. The difference in behavior of the different strain gauges installed is to be highlight, in particular sensors E1 and E4 are characterized by a values recorded oscillation much stronger than the tools E2 and E3. Such behavior does not depend on the movements of the masses along the planes of slipping, but it is related to the geometric configuration of installation, since the iron bars of the instruments E1 and E4 have a length over 200cm. The temperature therefore influence the system in a decisive manner, mainly because of the large size of some constituent parts of the inductive strain. These consist of three parts, a metal rod, an electromagnetic transmitter and an electromagnetic steel plate targets.

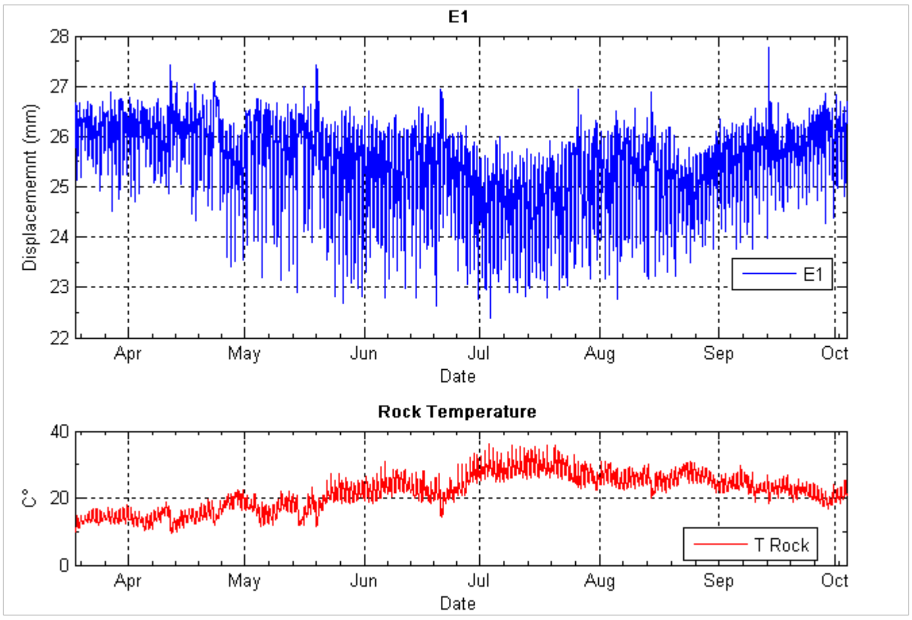

Figure 10.30: Chart of displacement and Temperature measured in E1.

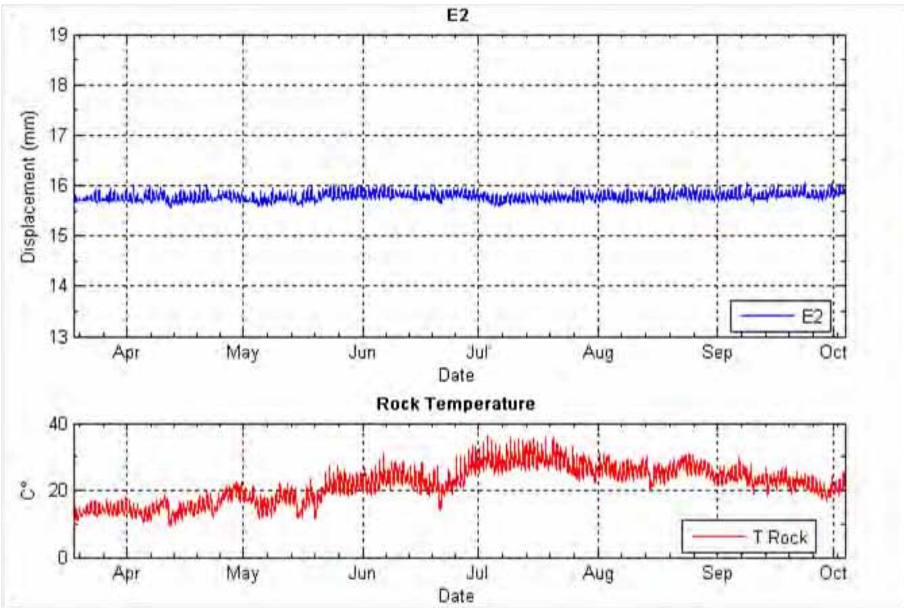

Figure 10.31: Chart of displacement and Temperature measured in E2.

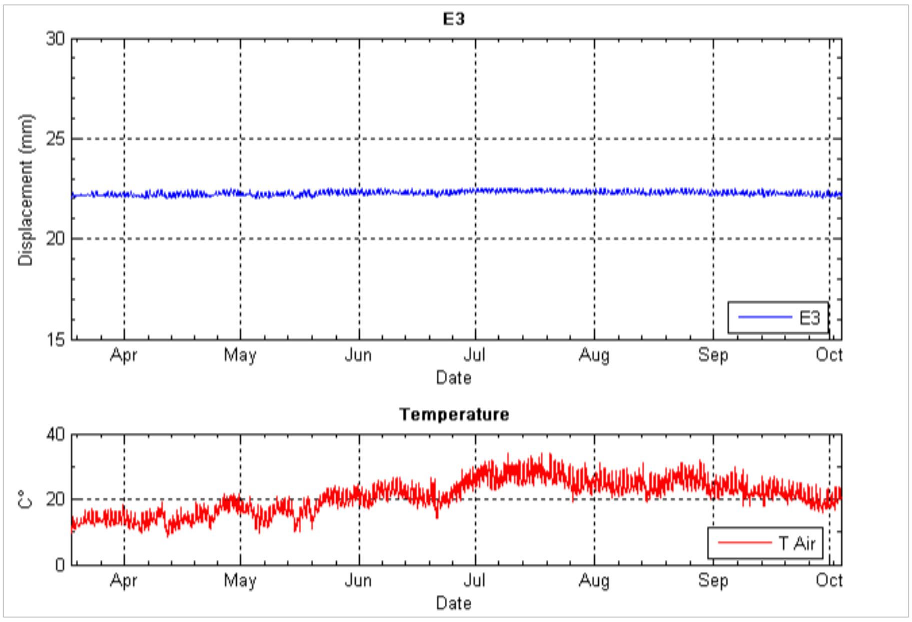

Figure 10.32: Chart of displacement and Temperature measured in E3.

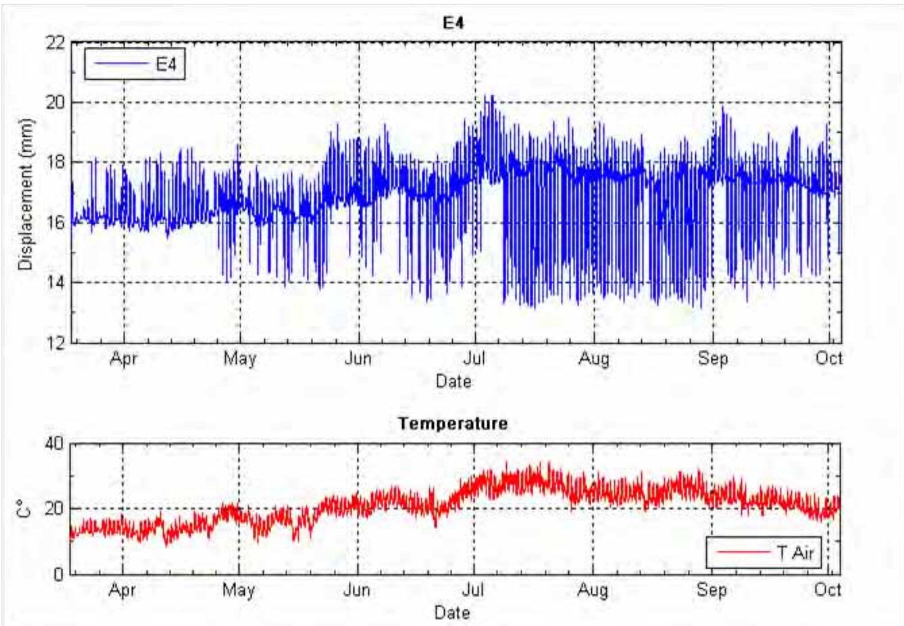

Figure 10.33: Chart of displacement and Temperature measured in E4.

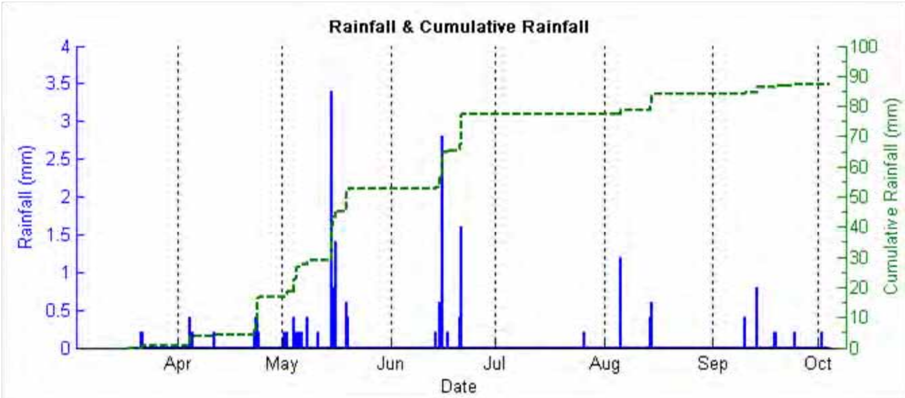

Figure 10.34: Rainfall chart, single event, blue. Cumulative curve for the considered period ,green.

Measures accuracy and errors correction. When we are looking for a periodicity in the signals it is useful to perform the Fast Fourier Transform.

FFT Analysis Inductive sensors capable of measuring displacements with accuracies of about 0.5 mm (1% FS) are used in the monitoring system, but the measures are affected by background noise quite high. The noise is largely attributable to the deformation of metal bar caused by temperature variation.

As mentioned above, thermal deformation is negligible for the E2 and E3 sensors, but it becomes more significant at the E1 and E4, in which the metal bar is over 2 meters in length.

Figure 101 and Figure 102 shows the graphs of the frequency spectrum calculated for displacement and temperature by Fast Fourier transform (FFT).

A peak on intensity values at a frequency of 1.12e-005 Hz (corresponding to a period of approximately 24 hours) on both signals was detected. This shows that the measured deformations are directly related to the temperature trend.

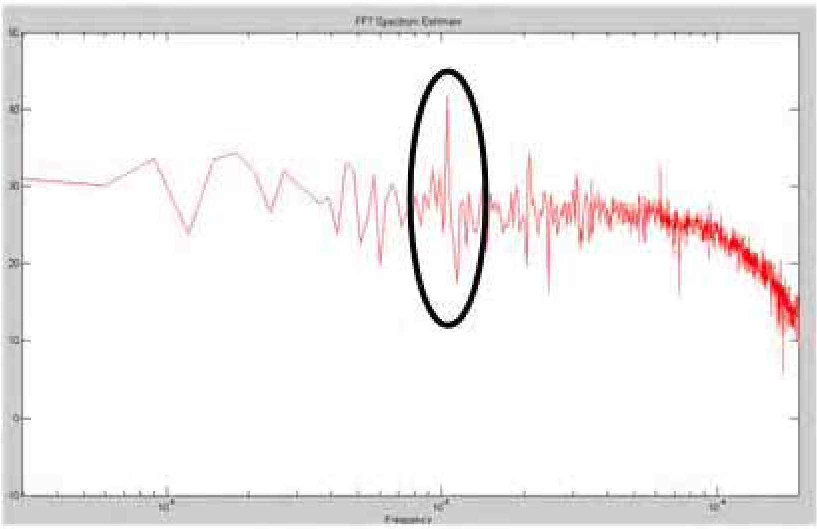

Figure 10.35: Frequency spectrum of E1 signal.

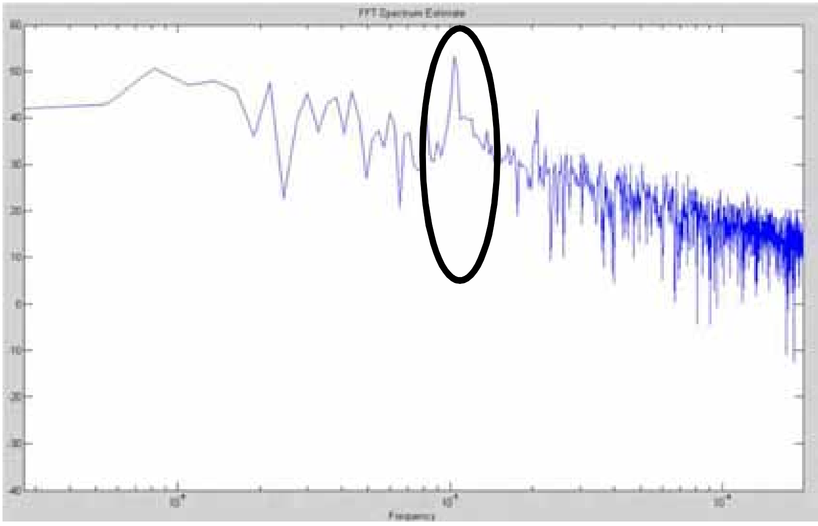

Figure 10.36: Frequency spectrum of T-air signal.

You can generally apply certain procedures to correct the calculation error due to temperature.

The length change ΔL of one dimension solid body is proportional to ΔT, if the pressure is constant and if temperature variations are small enough. We can write the relation

$\Delta L = \lambda$ LTD

The coefficient of linear expansion \lambda is characteristic of each material and varies depending on the geometry of the body.

To filter the component of deformation related to temperature we tried to correct the distortion of the E1 signal according to a correction factor. This factor was determined according to the length of the metal, the type of material that constitutes it, and the temperature measured by thermometers installed in-situ.

However, this correction has not produced satisfactory results.

An explanation of the ineffectiveness of the corrections made can be found in the temperature values used for the correction. In fact we used air and rock temperature rather than the one of metal bar.

The shows the trend of air and rock measured temperature for a period of 3 days. Since the thermal coefficients of the rock and the air are different, the measured values differ, in a more intense manner during the hours of more intense inoculation. To make more accurate correction of measured values of displacement is therefore necessary to have the value of temperature of the metal bar; for this purpose has been scheduled for next month a session to measure the temperature of the metal bar with a temperature probe. For a successful correction of the data we need a fairly long period of measurement, including at least two seasonal thermal cycles, equivalent to a calendar year.

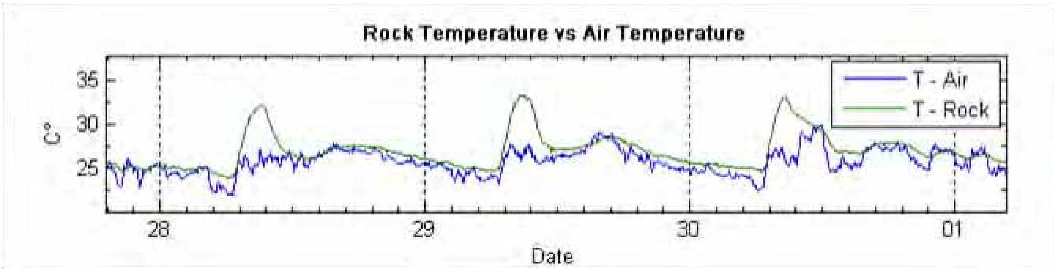

Figure 10.37: Air Vs Rock Temperature in a 3 days period.

It is considered that the metal bar which is anchored on the ferrite core is the weak link of the measurement system, as a result of evidence collected during this first period of monitoring. The thermal expansion and deformation for bending under the force of its own weight and under the pressure of the wind becomes not negligible when the bar reaches considerable lengths (> 1 m).

10.1.3.2 Threshold values

Threshold of attention were established based on the results of field surveys and observations made during this first reporting period. For extensimeters E1 and E4, deformation greater than 1 mm per day are considered to be the threshold that separates the ordinary state of attention from the alert state, while for the extensimeters E2 and E3 this value is reduced to 0.25 mm / day. It should also be noted that the threshold values are more significant the longer the period analyzed, so we will update the values when we have a longer time series.

10.1.3.3 Relation between water-table and movements

The monitoring sistems working in Mdina and Citadel have also Piezometer sensors.

In chapter 4 has shown that structures based on the plate may be affected by subsidence caused by deep movements of the soft clay substrate.

However few correlation seems to exist between the piezometric level and surface movements.

In the B area one Piezometer only , the PZB01, is able to measure relevant variation in water table level.

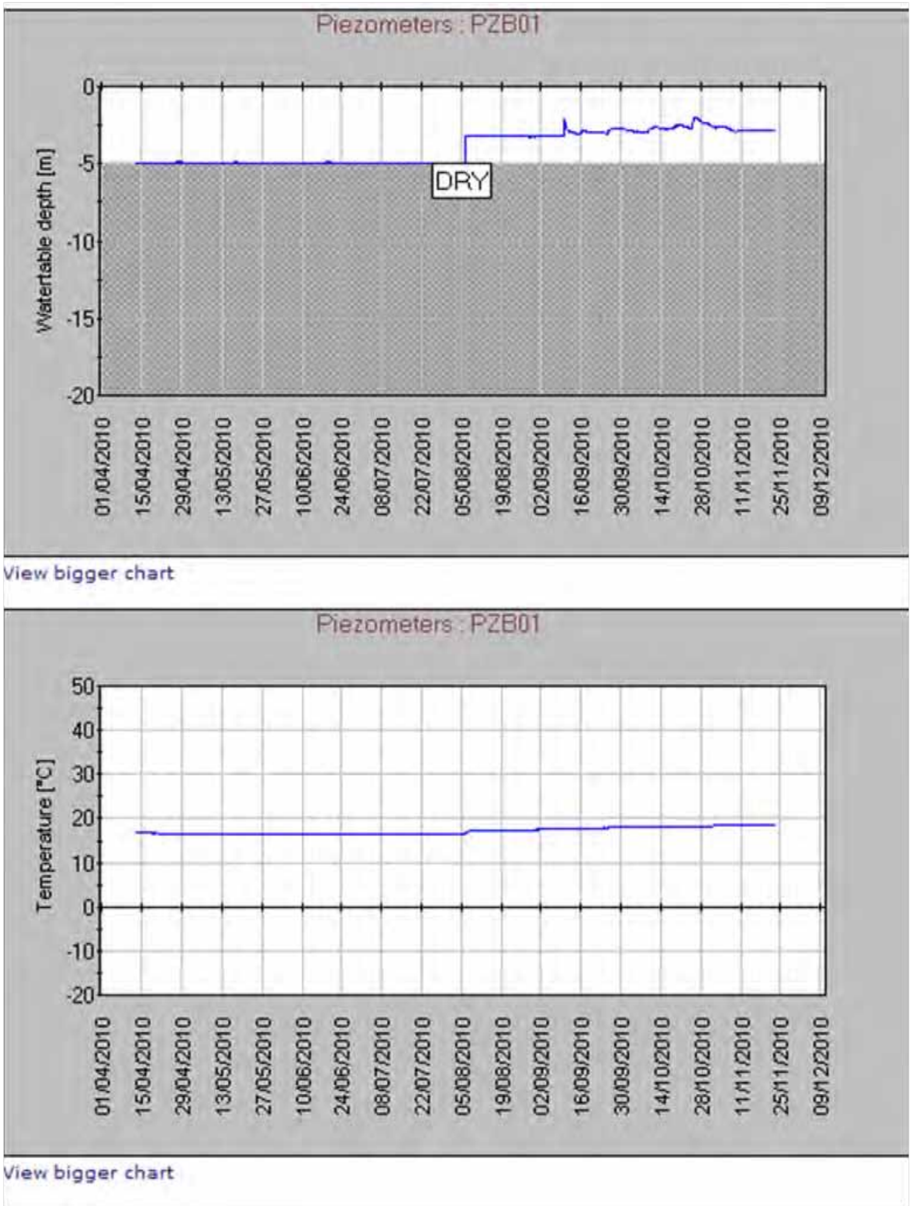

Figure 10.38: Chart of PZB01 Piezometric level and Temperature.

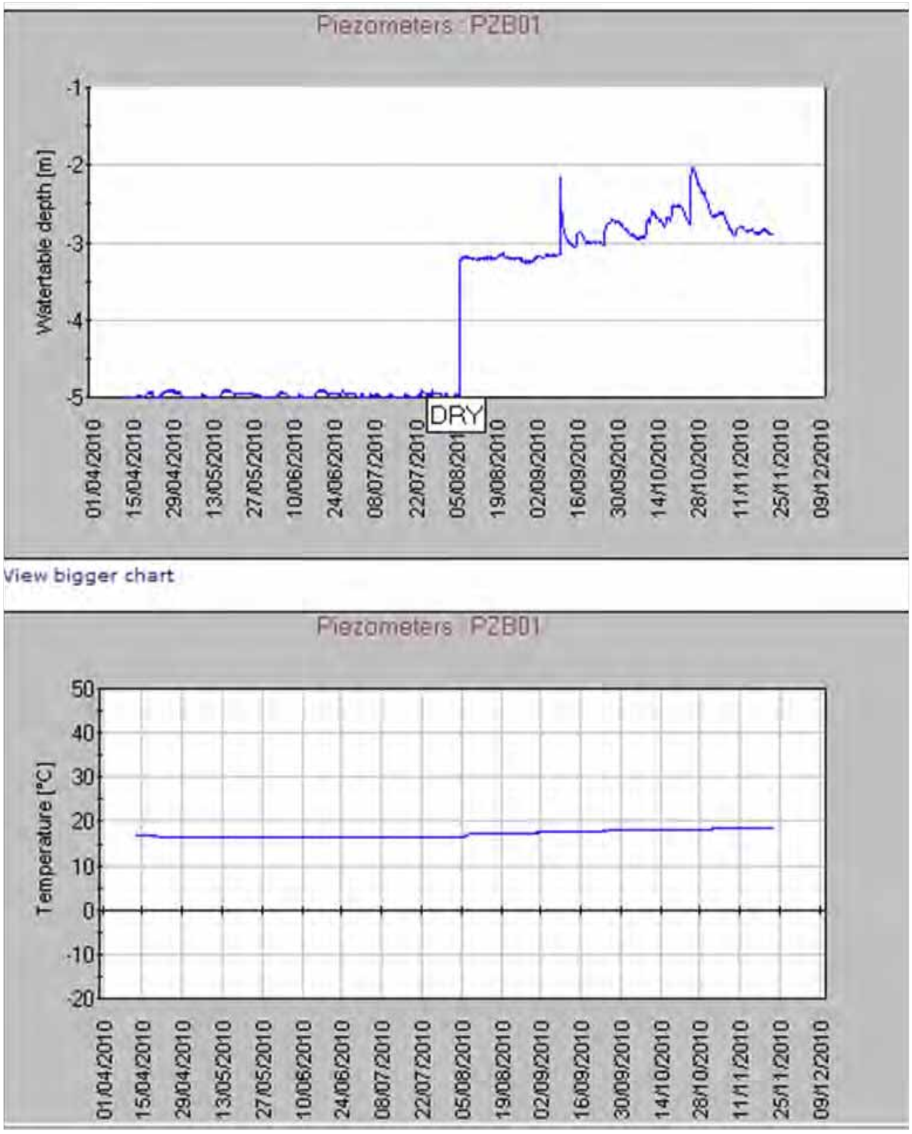

Figure 10.39: Zoom view of PZB01 - Piezometric level

A comparison with measurements made by neighbors instruments (CGB05, CGB06, CGB07, CGB08, CGB09, CGB10, CGB11, CGB12) in the same period, shows that only the BINB03 biaxial inclinometer detects a change in inclunation value.

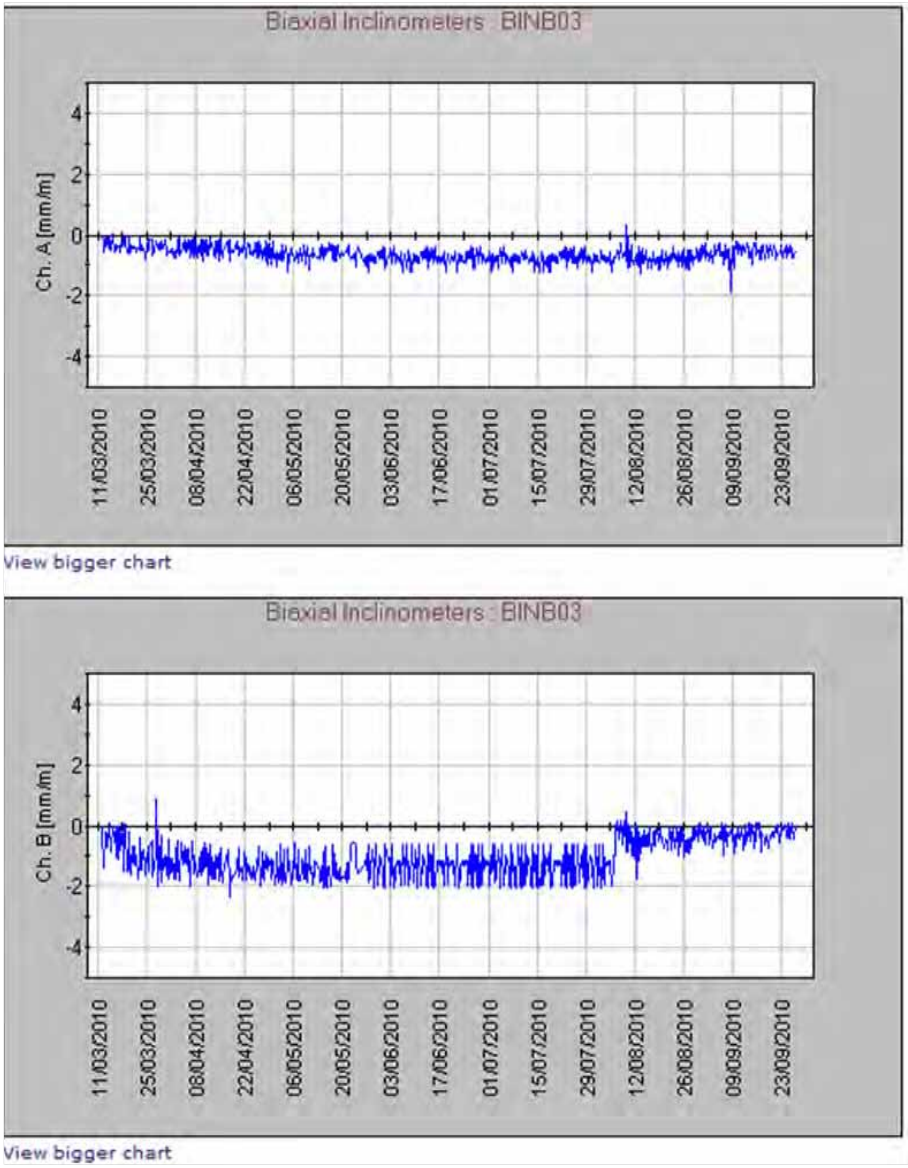

Figure 10.40: Tilt variation measured by BINB03 Biaxial inclinometer.

10.1.3.4 Relation between water table level and water temperature.

The graph in the figure shows that the temperature remains stable over time, despite the fact that the sensors are installed a few meters deep, instead of the temperature measured at the surface that varies considerably with time.

One of the reasons could be the presence of very isolated pockets of water.

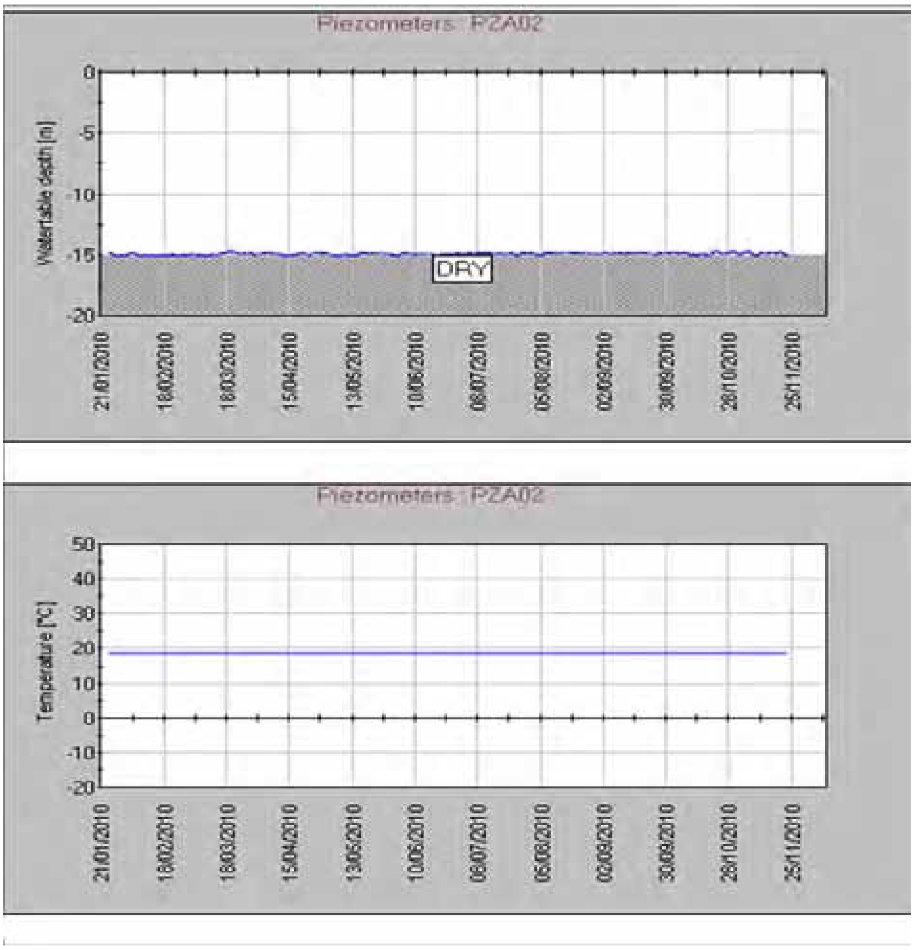

Figure 10.41: Temperature chart of PZA01.

Chapter 11

Conclusions

Monitoring data were used to achieve a higher degree of understanding of complex phenomena such as landslides, also trying to give faillure predictions through the application of experimental forecasting methods. Analysis of activities and data processing, together with those of surveying, monitoring and studying of the different examined instability processes, were performed to verify the effectiveness of an integrated use of different kinds of monitoring systems. In an attempt to pursue the main objective of this thesis we tried to trace a guide line, in which sometimes effective choices were done, even though expensive in terms of time spent, giving satisfactory results, and being fully in line with expectations. In other cases, on the opposite, the same amount of time spent was not just enough to deepen some aspect, and a big effort was invested in analysis and calculations that did not return the desired result. In other circumstances we had to deal with unexpected problems, some of which requested access to research areas beyond the background knowledge of our ordinary course of study in geology, like the correction of signals from the influence of temperature on strain gauge measurements, or the construction of communication equipments and remote control. However, thanks to the effectiveness and versatility shown by the systems and the measuring instruments used, the possibilities of wider applications of monitoring tools and the integration of multi-type measures to provide complementary information, were also outlined. For some aspects the simultaneous application of technologically advanced monitoring tools can be used not only to increase the quality of measurements (in terms of accuracy and precision) but also to give additional properties to the monitoring system. Hence it can be used by an operational structure of emergency, both in public and private areas, for ordinary applications use, as it was shown by the case study in the archipelago of Malta, regarding the sites of Mdina and Citadel. The awareness of having, at least in part, achieved the goal was set up on the correspondence observed between the developed models and the measurements obtained through monitoring campaigns. The models have reached a much higher index of validation as the entered data were acquired through measurements taken at sampling rates congruent with variation of their real-world observed phenomenon. Some analysis on how the reliability of a forecasting model varies as a function of frequency acquisition were carried out; in all the examined cases the instruments of last generation are to be preferred, being fully satisfying considering the rapidity of measuring, the high sampling rate and automation. Even in those cases where the studied phenomenon was characterized by few slow movements, it was still subject to change in velocity without speed precursors or anyway with notice periods shorter than the acquisition period. With the work going on the need to re-size the objective purpose was often felt, and we tried to align the expectations to the results. In the case study of Torgiovannetto in particular, radar interferometry was used during a short time span, and hence it was not able to incorporate a continuous flow of data within the automated phases of data acquisition, filtering and control. However, thanks to an extensive range vision and to the high measurement accuracy, the development of a failure prediction model would be needed. On the contrary, the attempt to produce a prediction model of rupture has not borne fruit so further research would be needed in this particular field. Among the successes of this work certainly we highlight the suggestions and the considerations which lead to an effective integrated monitoring system, obtained by analyzing the results of an integrated monitoring campaign, and by the comparison between the capabilities of the instrumentation verified through the intensive use of multiple tools. The project for the creation and the installation of monitoring facilities of Mdina and Gozo, is the result of the considerations and knowledge gained during this PhD experience. The monitoring systems set in Mdina and Gozo, described in detail in Chapters 2-3-4-5, are rather complex wireless monitoring systems, whose acquired data were usable by the personnel involved through the use of web platforms. As further developments the central controller must be improved so that it can manage remote sensing tools and wireless sensor networks all together; in this way platforms like those presented in this work could yield better results if applied to adverse environments. The platforms may be installed and managed far away thanks to their characteristics of remote control and self-adaptive capabilities. It must be certainly improved in some technical characteristics, both with regard to the longevity of the system without human maintenance, and without a stable link with electrical and communication delivers. For example there are places in the world where there are not structures with enough specialized staff to directly manage advanced monitoring systems; on the other hand many of this areas are characterized by high risk natural contexts. Nowadays there are many autonomous power-supply systems, some of which are powered by alternative energy and are equipped with high performance batteries or accumulator systems. A WSN monitoring system like those installed in Mdina may work more than six months without draining the batteries; however, in order to ready a real-time monitoring system, the communication between the instrumentation installed in the field and the operation room located in analysis and elaboration centres must to be ensured. Comparing the two maps in 8.4 it is quite evident that most areas affected by landslide risk in the world have a good GSM coverage. This let us think that it is possible to install and use self-adaptive and multi-parametric platforms in many world areas affected by instability processes, assuming that power supply is not a real problem.

Bibliography

[1] Varnes D.J. (1978) - Slope movements types and processes. In: Schuster R.L. & Krizeck R.J. (Eds.). Landslides: analysis and control. Washington Transp. Res. Board, Spec. Rep., 176, Nat. Sci. Acad., pp. 11-33.

[2] Giani G.P. (1992) - Rock Slope Stability Analysis. , A.A. Balkema, Rotterdam .

[3] Schuster R.L., Wieczorek G.F. (2002) - Landslides triggers and types. In: Ryba´ r, Stemberk, Wagner (eds) Proceedings of the 1st European conference on landslides, Prague. Balkema, Rotterdam, pp 59–78

[4] Dotta G. (2010). "Studio dei processi di instabilità sulla frana di Torgiovannetto. Junior Degree Thesis, Università degli Studi di Firenze, A.A. 2009-2010.

[5] GDTest, Geodesign and test. (2010) - home page /http://www.gdtest.it (accessed August 2010)

[6] Akyildiz I.F., Su, W.Y. (2002) - Sankarasubramaniam, and Cayirci E. , - A survey on sensor networks," IEEE Commun. Mag., vol. 40, no. 8, pp. 102-114, Aug. 2002.

[7] Tubaishatand M., Madria S. (2003) - Sensor networks: an overview," IEEE Potentials, vol. 22, no. 2, pp. 20-23, Apr./May 2003.

[8] Verdone R., Dardari D., Mazzini G., and Conti A. (2008) - Wireless Sensor and Actuator Networks: technologies, analysis and design. Elsevier, 2008.

[9] Karl H. and Willig A. (2003) - A short survey of wireless sensor net- works," Technical University Berlin, Telecommunication Networks Group, Tech. Rep., Oct. 2003.

[10] Chong C.Y. and Kumar S.P. (2003) - Sensor networks: evolution, opportunities and challenges," Proceedings of the IEEE, vol. 91, no. 8, pp. 1247-1256, Aug. 2003.

[11] Lucchi M. (2007) - Cooperative Communication and Distributed Detection in Wireless Sensor Networks. PhD Thesis.

[12] Smolnikar M., Platiše U., Mohorčič1M. (2010) - Versatile Sensor Node: A Platform for Connecting Sensors with the Internet. Conference Sensors and Actuators in Ljubljana 21^{th} October 2010.

[13] Gigli G, Casagli N. (2011) - Semi-automatic extraction of rock mass structural data from high resolution LIDAR point clouds. Int J Rock Mech Mining Sci,doi:10.1016/j.ijrmms. 2010.11.009

[14] Priest SD. (2003) - Discontinuity analysis for rock engineering. London:Chapman& Hall.

[15] ISRM. (1978) - Suggested methods for the quantitative description of discontinuities in rock masses. International Journal of Rock Mechanics and Mining Sciences & Geomechanics Abstracts ;15:319–68

[16] Chandler J. (1999) - Effective application of automated digital photogrammetry for geomorphological research. Earth Surface Processes and Landforms; 24: 51–63.

[17] Lane SN, James TD, Crowell MD. (2000) - Application of digital photogrammetry to complex topography for geomorphological research. Photogrammetric Record ;16:793–821

[18] Kraus K, Pfeifer N. (1998) - Determination of terrain models in wooded areas with airborne laser scanner data. ISPRS Journal of Photogrammetry and Remote Sensing ; 53:193–203.

[19] Gigli G, Mugnai F, Leoni L, Casagli N. (2009) - Analysis of deformations in historic urban areas using terrestrial laserscanning. Natural Hazards and Earth System Science 9:1759–61.

[20] Ferretti A, Prati C, Rocca F. (1999) - Multibaseline InSAR D.E.M. reconstruction : the wavelet approach. IEEE Transactions on Geoscience and RemoteSensing ;37:705–15.

[21] Oppikofer T., Jaboyedoff M., Blikra L.H., Derron M.H. (2008) - Characterization and monitoring of the Åknes rockslide using terrestrial laserscanning. In: Proceedings of the 4th Canadian conference on geohazards: from causesto management. p.211–18.

[22] Oppikofer T, Jaboyedoff M, Keusen HR. (2008) - Collapse at the eastern Eiger flank in the Swiss Alps. NatureGeoscience. 1:531–5.

[23] Abellan A., Vilaplana J.M., Martınez J. (2006) - Application of a long-range terrestrial laser scanner to a detailed rockfall study at Vall de Nu´ria (Eastern Pyrenees, Spain). Engineering Geology;88:136–48.

[24] Lombardi L., Casagli N., Gigli G., Nocentini M. (2006) - Verifica delle condizioni di sicurezza della S.P. Lodovica in seguito ai fenomeni di crollo nella cava di Sesto di Moriano (Lucca). Giornale di Geologia Applicata, AIGA2006;3: 249–56. [In Italian]

[25] Jaboyedoff M., Couture R., Locat P. (2009) -Structural analysis of Turtle Mountain (Alberta) using digital elevation model: toward a progressive failure. Geo- morphology 2009;103:5–16

[26] Ferretti, A., Prati, C., and Rocca, F. - (2001) Permanent Scatterers InSAR Interferometry, IEEE T. Geosci. Remote, 39(1), 8–20.

[27] Kenyi, L.W., Kaufmann, V. (2003) - Estimation of rock glacier surface deformation using SAR interferometry data, IEEE Trans. Geosci. Remote Sensing, vol. 41, pp. 1512-1515.

[28] Casagli, N., Del Ventisette, C., Farina, P., Guerri, L., Antonello, G., Fortuny-Guasch, J., Tarchi, D., Leva, D., Rivolta, C., 2007. - Monitoraggio della frana del Ruinon mediante tecniche interferometriche radar – Final Report.

[29] Tarchi, D., Leva, D., Farina, P., Basso, M., Casagli, N., Del Piccolo, A., Moretti, S., Mannucci, G., Tavelli, S. (2002) - Applicazione dell'interferometria radar da terra per il controllo dei movimenti franosi: la frana del Ruinon in Valfurva (SO). CNR-GNDCI no. 2543, Regione Lombardia, Tipolitografia Grifo, Perugia, 79 pp.

[30] Leva, D., Nico, G., Tarchi, D., Fortuny-Guasch, J., Sieber, A. J. (2003a) - Temporal analysis of a landslide, by means of a ground-based SAR interferometer. IEEE Trans. Geosci. Remote Sensing, vol. 41, pp. 633-636.

[31] Luzi C, Verna C, Melsen B. (2007) - A prospective clinical investigation of the failure rate of immediately loaded mini-implants used for orthodontic anchorage. Prog Orthod. 8:192–201

[32] Burgmann, R., Rosen, P. A., Fielding, E. J. (2000) - Synthetic Aperature Radar Interferometry to Measure Earth's Surface Topography and its Deformation, Ann. Rev. Earth and Plan. Sci. 28,169–209. CHESTER,

[33] Loxdale, H.D., Massonnet, B., Weisser, W.W. (2010) - Why are there so few aphid clones? Bulletin of Entomological Research, in press.

[34] J. Askne, M.Santoro, G. Smith and J.E.S. Fransson. (2003) - Multi-temporal repeat-pass SAR interferometry of boreal forest," IEEE Transactions on Geoscience and Remote Sensing, vol. 41, 7, pp. 1540-1550.

[35] Massonnet D., Thatcher W., Vadon H. (1996) - Detection of postseismic fault-zone collapse following the Landers earthquake", Nature, vol. 382, no. 6592, pp. 612 - 616, .

[36] Massonnet D., et al. (1993) - The displacement field of the landers earthquake mapped by radar interferometry. Nature, vol. 364, pp. 138 - 142.

[37] Lanari R., Mora O., Manunta M., Mallorquí J.J., Berardino P., and Sansosti E. (2004) - A small baseline approach for investigating deformations on full resolution differential SAR interferograms. IEEE Trans. Geosci. Remote Sens., vol. 42, pp. 1377 .

[38] M. Crosetto , B. Crippa and E. Biescas (2005) - Early detection and in-depth analysis of deformation phenomena by radar interferometry, Eng. Geol., vol. 79, pp. 81.

[39] Goldstein R.M., Zebker H.A., and Werner C.L. (1988) - Satellite radar interferometry: Two-dimensional phase unwrapping. Radio Sci., vol. 23, no. 4, pp. 713 - 720, .

[40] Reigber A., Scheiberand R. (2003) - Airborne differential SAR interferometry: First results at L-band, IEEE Trans. Geosci. Remote Sensing, vol. 41 , pp. 1516 - 1520, .

[41] Strozzi T., Farina P., Corsini A., Ambrosi C., Thüring M., Zilger J., Wiesmann A., Wegmüller U., and Werner C. (2005) - Survey and monitoring of landslide displacements by means of L-band satellite SAR interferometry, Landslides 2 (3), pp. 193–201.

[42] Rudolf H., Leva D., Tarchi D., Sieber A. J. (1999) - A mobile and versatile SAR system. Proceedings of Geoscience and Remote Sensing Symposium, IGARSS 1999, Hamburg, pp. 592-594.

[43] Noferini L., Pieraccini M., Mecatti D., Luzi G., Atzeni C., Tamburini A. and Broccolato M. (2005) Permanent scatterers analysis for atmospheric correction in ground-based SAR interferometry. IEEE Trans. Geosci. Remote Sens., vol. 43, pp. 1459.

[44] Pipia L., Fabregas X., Aguasca A., Lopez-Martinez C., Duque S., Mallorqui J.J., Marturia J. - (2009) Polarimetric Differential SAR Interferometry. First Results With Ground-Based Measurements, Geoscience and Remote Sensing Letters, IEEE On page(s): 167 - 171 , Volume: 6 Issue: 1, Jan.

[45] Fortuny J., Ohlmer E., Sieber A. J., Pasquali P., Prati C., and Rocca F. (1994) - Validating SAR interferometry applications by using EMSL. Proc. IEEE Int. Geosci. Remote Sensing Symp. (IGARSS) , vol. 2, pp. 736 - 738, .

[46] Mensa D. L. (1991) - High Resolution Radar Cross-Section Imaging, pg. 16, Artech House, Boston.

[47] Ferretti A., Prati C., Rocca F. (2000) - Non-linear Subsidence Rate Estimation Using Permanent Scatterers in Differential SAR Interferometry. IEEE Trans. On Geoscience and Remote Sensing, 38: 2202-2212.

[48] Casagli N. (1992) - Slope instability in rock masses overlying a soft substratum some analyses in the italian northern appennine. Master of Science in engineering rock mechanics, Imperial College, London.

[49] Pedley H.M. (1993) - Geological Maps of the Maltese Islands. Scale, 1:25 000, 2 sheets, Oil Exploration Directorate, British Geological Survey, Keyworth.

[50] Galea, P.(2007) - Seismic history of the Maltese islands and considerations on seismic risk, Ann. Geophys.-Italy, 50(6), 725–740.

[51] De Lucca, D. (1993) - Architectural interventions in Mdina following the earthquake of 1693, in: Mdina and the Earthquake of 1693, edited by: Azzopardi, C. J., Heritage Books, Malta, 49 pp.

[52] Baratin L., Bitelli G., Bonnici H., Unguendoli M., and Zanutta A. (2001) - Traditional and modern methods of surveying architectural heritage: a few examples in the fortified island of Malta, in: Proceedings of the 18th International Symposium of CIPA, Potsdam, Germany, 18–21 September .

[53] Bonnici H., Gatt N., Spiteri S. C., and Valentino J. (2008) - Vilhena palace and underlying bastions (Mdina, Malta) – A multidisciplinary approach in defining a consolidation intervention, Geografia Fisica e Dinamica Quaternaria, 31(2), 99–105.

[54] Dipartimento di architettura e pianificazione territoriale università di Bologna (2003) – Consolidamento del palazzo Vilhena – Mdina (Malta).

[55] Barton N.R., Choubey V. (1977) - The shear strenght of rock joints in theory and practice. Rock Mechanics, 10, 1-54.

[56] Bieniawski Z.T. (1989) - Engineering Rock Mass classification. Wiley, New York. 251 pages.

[57] Barton N.R., Lien R., Lunde J. (1974) - Engineering classification of rock masses for the design of tunnel support. Rock Mech., 6 (4), 189-239.

[58] Marinos P., Hoek E. (2001) - Estimating the geotechnical properties of heterogeneous rock masses such as flysch. Bull. Enginng Geol. & the Environment (IAEG), 60, 85-92.

[59] Goodman R.E., Bray J.W. (1976) - Toppling of rock slopes. Proc. Special Conf. on Rock Engineering for Foundations & Slopes. ASCE, Boulder (Colorado), 2, 201-234.

[60] Casagli N., Pini G. (1993) - Analisi cinematica della stabilità in versanti naturali e fronti di scavo in roccia. Atti 3° Convegno Nazionale dei Giovani Ricercatori in Geologia Applicata, Potenza.

[61] Arayici, Y. (2007) - An approach for real world data modelling with the 3-D terrestrial laser scanner for built environment, Automat. Constr., 16, 816–829.

[62] Lambers, K., Eisenbeiss, H., Sauerbier, M., Kupferschmidt, D., Gaisecker, T., Sotoodeh, S., and Hanusch, T. (2007) - Combining photogrammetry and laser scanning for the recording and modelling of the Late Intermediate Period site of Pinchango Alto, Palpa, Peru, J. Archaeol. Sci., 34, 1702–1712, .

[63] Yastikli, N. (2007) - Documentation of cultural heritage using digital photogrammetry and laser scanning, J. Cult. Herit., 8, 423–427.

[64] Al-kheder, S., Al-shawabkeh, Y., and Haala, N. (2009) -Developing a documentation system for desert palaces in Jordan using 3-D laser scanning and digital photogrammetry, J. Archaeol. Sci., 36, 537–546.

[65] Ribes Technologies (2010) - home page http://www.grupporibes.it (accessed January 2010)

[66] Pedley M., Hughes Clarke M., Galea P. (2002) – Limestone isles in a crystal sea. The geology of the Maltese islands. Publisher Enterprises Group Ltd. 109 pp.

[67] Pedley M. (1974) - Pedley M. (1993) – Geological map of the Maltese islands. Sheet n. 2: Gozo and Comino. Oil exploration Directorate, Office of the Prime Minister, Valletta, Malta.

[68] Scerri, S. (2003) – IC – Cittadella, Victoria, Gozo. Structural stability of the cliff margin.

[69] Lavecchia G., Minelli G., Pialli G., (1988) - The Umbria-Marche arcuate fold belt (Italy), Tectonophysics, vol. 18, pp. 108-118.

[70] Tavarnelli E., (1997) - Structural evolution of a foreland fold-and-thrust belt: the Umbria-Marche Apennines, Italy", Journ. Strict. Geol., vol. 7, pp. 751-754.

[71] Mirabella F., Pucci, S. (2002) - Integration of geological and geophysical data along a section crossing the region of the 1997-98 Umbria-Marche earthquakes (Italy)", Boll. Soc. Geol. It., vol. spec. 1, no. 8, pp. 891-900.

[72] I.R.P.I. (Istituto di Ricerca per la Protezione Idrogeologica, CNR, Perugia) (2006) - Caratteristiche litologiche, strutturali e geomorfologiche del versante nel quale ricade l'area della ex-cava in prossimità di casa Tor Giovanetto, Comune di Assisi", dati non pubblicati.

[73] Cruden D.M. & Varnes D.J. (1994) - Landslides Types and Processes. In: "Landslides: Investigation and Mitigation". Transportation Research Board. National Academy of Sciences.

[74] Casagli N., Gigli G., Lombardi L., Mattiangeli L., Nocentini M., Vannocci P. (2008) - Indagini geofisiche e geotecniche e modellazione dinamica della frana di Torgiovannetto (PG) - Rapporto finale. Convenzione fra il Dipartimento di Scienze della Terra dell'Università di Firenze e la Provincia di Perugia, fonte non pubblicata.

[75] Alta Scuola (2005a) - Studio del fenomeno franoso interessante la cava di Torgiovannetto di Assisi (PG) - Relazione di prima fase. fonte non pubblicata.

[76] Casagli N., Gigli G., Lombardi L., Nocentini M. (2006) - Valutazione delle distanze di propagazione relative ai fenomeni franosi presenti sul fronte della cava di Torgiovannetto (PG) - Relazione 2.0", fonte non pubblicata.

[77] Kinemetrics (2010) - home page http://www.kinemetrics.com (December, 2010)

[78] Google Earth (2010) - home page http://www.google.com (January, 2010)

[79] Intrieri E. (2008). "Applicazione dell'inteferometria radar da terra al monitoraggio e alla mappatura rapida delle frane". Master Degree Thesis, Università degli Studi di Firenze, A.A. 2007-2008.

[80] Luzi G., Pieraccini M., Mecatti D., Noferini L., Guidi G., Moia F., Atzeni C., (2004b) - Ground-based radar interferometry for landslides monitoring: atmospheric and instrumental decorrelation sources on experimental data", IEEE Trans. Geosci. Remote Sensing, vol. 42, no. 11, pp. 2454-2466.

[81] Rudolf H., Leva D., Tarchi D., Sieber A. J., (1999) - A mobile and versatile SAR system", Proceedings of Geoscience and Remote Sensing Symposium, IGARSS 1999, Hamburg, pp. 592-594.

[82] Atzeni C., Basso M., Canuti P., Casagli N., Leva D., Luzi G., Moretti S., Pieraccini M., Sieber A. J., Tarchi D. (2001) - Ground-based SAR interferometry for landslide monitoring and control", Proceedings of 15th Int. Conf. Soil Mechanics & Geotechnical Engeneering. ATG9 Field Workshop on Landslides and Natural/Cultural Heritages. Trabzon, Turkey, 23-24 August, 2001, pp. 195-209.

[83] Barla G., Borri-Brunetto M., Devin P., Zaninetti A. (1995) - Validation of a distinct element model for toppling rock slopes. Proceedings of the Eighth International Congress on Rock Mechanics, Tokyo, vol. 1, pp. 417-421. T. Fujii, Ed. Rotterdam: A. A. Balkema.

[84] Barberi F., Innocenti F. (1965) - Le rocce cornubianitico-calcaree dell'anello termometamorfico del Monte Capanne (Isola d'Elba). Atti Soc. Tosc. Sci. Nat., Mem., Ser. A, 72: 306-398.

[85] Spohn A., (1981) - Die ophiolitführenden Gesteine von West-Elba: Stratigraphie, Tektonik, Metamorphose. Berliner Geowiss. Abh., Reihe A, 37: 124 pp.

[86] Bortolotti V., Fazzuoli M., Pandeli E., Principi G., Babbini A., Corti S. (2001) - Geology of Central and Eastern Elba Island, Italy. Ofioliti, 26 (2a), 97-150.

[87] Dini A., Innocenti F., Rocchi S., Tonarini S., Westerman D.S., (2002)- The magmatic evolution of the late Miocene laccolith-pluton-dyke granitic complex of Elba Island, Italy. Geological Magazine, 139, 257-279.

[88] Rocchi S, Dini A, Innocenti F, Tonarini S, Westerman D.S., (2003) - Elba Island: intrusive magmatism. In: Poli G, Perugini D, Rocchi S, Dini A (eds). Miocene to Recent Plutonism and Volcanism in the Tuscan Magmatic Province (Central Italy), Periodico di Mineralogia 72:73-104 Special Issue no. 2.

[89] Principi G., Fanucci F., Bortolotti V., Chiari M., Dini A., Fazzuoli M., F. Menna F., Moretti S., Nirta G., Pandeli E., Reale V.. Note illustrative della Carta Geologica d'Italia alla scala 1:50.000 - foglio 316, 328, 329 ISOLA D'ELBA. In stampa.

[90] Coli M., Conticelli S., Pandeli E., Moratti G., Papini P., Tommasini S., (2001) - Meeting EL.I.C.A. 97. Pre-meeting transect Corsica - Elba - Southern Tuscany Guidebook. 2. C. Western Elba. Ofioliti, 26 (2a): 347-356.

[91] Directive of the President of Ministry of Council (2004) - PCM 27^{th} February 2004.

[92] National Instruments (2009) - Home page, http://www.ni.com (acessed January, 2011)

[93] Nadim F, Kjekstad O, Domaas U, Rafat R, Peduzzi P (2006a) Global landslide risk case study. In: Arnold M, Chen RS, Deichemann U, Dilley M (eds) Natural disaster hotspots. Case studies. The World Bank, Washington, DC, p 204

[94] Mobile World Live - Home page, http://www.mobileworldlive.com (accessed January, 2011)

[95] Hoek E., Bray J.W. (1981) - Rock Slope Engineering. Revised Third Edition. Istitution of Mining and Metallurgy, London.

[96] Hudson J.A., Harrison J.P. (1997) – Engineering rock mechanics. Pergamon ed.

[97] Casagli N., Proietti C., Righini G., Cigna F., Pancioli V. (2009) - Linee guida per l'analisi di dati interferometrici satellitari in aree soggette a dissesti idrogeologici. Ministero dell'Ambiente e della Tutela del Territorio e del Mare, Direzione Generale per la Difesa del Suolo.

[98] Rose N. D, Hungr O. (2006) - Forecasting potential rock slope failure in open pit mines using the inverse-velocity method", International Journal of Rock Mechanics and Mining Science, vol. 44, no. 2, pp. 308-320.

[99] Geokon (2009) Home page, http://www.geokon.com (accessed January, 2011)

[100] Encardio-rite (2009) Home page, fttp://www.encardio.com (accessed January, 2011)

[101] Ripepe M., Marchetti E., Ulivieri G. (2007) - Infrasonic monitoring at Stromboli volcano during the 2003 effusive eruption: Insights on the explosive and degassing process of an open conduit system, J. Geophys. Res., 112, B09207, doi:10.1029/2006JB004613

[102] Mugnai F. (2006). - Studio dei processi di instabilità sulla Rupe di Canossa. Master Degree Thesis, Università degli Studi di Firenze, A.A. 2005-2006.

[103] EMWIS (2008) - Euro-Mediterranean Water Information System. homepage http://www.emwis.org

[104] Roclab Software, Rocscience (2004) - homepage, http://www.rocscience.com (acceded December, 2010)

[105] Iridium communication (2010) - Home page, http://www.geoborders.com (accessed January, 2011)

[106] Salvatici T. (2010) - Analisi di dati geotecnici per lo studio dell'instabilità della Cittadella di Gozo (Malta). Università degli Studi di Firenze, A.A. 2007-2008

[107] Garfagnoli F., Menna F., Nirta G., Pandeli E., Principi G. (2010) - The contact metamorphic aureole of the Mt. Capanne pluton: new data from the CARG project. Abstract volume. 85° Congresso della Società Geologica Italiana. Pisa, 6-8 Settembre 2010.

[108] Tarchi D., Rudolf H., Luzi G., Chiarantini L., Coppo P., Sieber A. J. (1999) - SAR interferometry for structural change detection: a demonstration test on a dam", Proc. of Geoscience and Remote Sensing Symposium, IGARSS, vol. 3, pp. 1525-1527.

[109] Luzi, G., Macaluso, G., Mecatti, D., Noferini, L., Pieraccini, M., Atzeni, C., 2004a, "Ground-based radar interferometry: results of experimental campaigns for landslides monitoring in Italy", Proceedings of 24th EARSeL (European Advanced Remote Sensing Laboratoires) Symposium, Dubrovnik (Croatia), 25-27 May 2004.

[110] Hoek E., Brown E.T., 1980. Empirical strength criterion for rock masses. J. Geotech. Engng Div., ASCE 106 (GT9), 1013-1035.

[111] Hoek, E., Carranza-Torres, C.T., Corkum, B., 2002. Hoek-Brown failure criterion – 2002 edition. Proc. North American Rock Mechanics Society meeting in Toronto in July 2002.

[112] Jibson R.W., and Keefer D.K. (1993) - Analysis of the seismic origin of landslides examples from the New Madrid seismic zone. Geological Society of American Bulletin 105, pp. 521–536.

[113] Hortus srl, Piattaforme web per la gestione di dati di monitoraggio, Sistemi di monitoraggio idrogeologico Home page http://www.hortus.it/ (accessed January, 2011)

[114] Hoek E., 1999. Rock Engineering. Course notes. University of Toronto. Disponibile presso il sito: www.rocscience.com.

Acknowledgements

First of all I give thanks to my parents who helped me in everything, sustained me in my several journeys and, above all, always gave me their unparalleled love.

Then I am thankful to Giovanni Gigli, great both in stature and in his heart, always able to go beyond especially in front of a problem; the “best” I have met so far.

Thank you especially to Guido Luzi, who offered me the right words and ideas to go on without anxiety in my times of need, and most of all who set an example, always.

I want to dedicate a thought to my friends in Terranuova who often found the time to exchange some words and a hug among my several journeys, my thousands of departures and my many returns. The same words are for Massimo, Serena and my fantastic nephew Carlotta; every one of them made me feel important.

And how not to thank Emanuele for his one thousand ideas offered to me.

William, for his precious help in carrying out the cartography of Mdina and Gozo. And then Riccardo, Veronica, Giacomo, Luca, Deodato e Francesca, Lorenzo, Paolo, Sandro, Gabriele, Melania, Pasquale, Patrizia, Gianluca, Giovanni, Samuele, Goffredo, George, Ping, Filippo, Remo, Gabriele, Pietro, Stefano, Chiara, Luca, Massimiliano, Giorgio, Francesca, Silvia, Federico, Maurizio, Chiara... they all gave me an idea, a suggestion or a useful obstacle to give strength to my activities.

I would also like to thank Renzo, Flavia, Elisa, Irene and their incredible hospitality.

Thanks also to Alexander who guided me among the wonderful mountains of Kyrgyzstan and thank you to all my companions during that unforgettable journey.

Thank you to Nicola who believed in me and provided me with part of his time and with this efficient structure that he was able to build during these years.

I give thanks also to the personnel of the Department of the National Civil Protection I had the pleasure to work with and with whom I shared emergency periods and unique scientific experiences.

A thank also to Mauro Reguzzoni, man of great capabilities and force of will, always available to furnish data and information… real-time!

Thank you also to Davide and all LisaLab-Ellegi… they are always in real-time mode too!

I am finally thankful to Eng. Richard Sansom and Arch. Norbert Gatt for their availability and for furnishing data from the monitoring systems in Mdina, acquired and elaborated within the project: “Service Contract for the provision of geotechnical engineering consultancy and project management services in relation with the consolidation of the terrain underlying the bastion walls and historic places of the city of Mdina”, funded by the ERDF for Malta and carried out by a consortium led by Politecnica Ingegneria e Architettura for the MRRA, Works Division, Restoration Unit, Floriana, Malta.

Ringraziamenti

Per prima cosa ringrazio i miei genitori, che mi hanno aiutato in tutto, mi hanno sostenuto nei miei tanti viaggi, ma soprattutto mi hanno dato sempre il loro mai eguagliabile amore.

Poi ringrazio Giovanni Gigli, grande sia di statura che di cuore. . . .capace sempre di andare oltre, soprattutto nei problemi. . . il più "bravo" che abbia conosciuto fino ad ora.

Voglio ringraziare in modo particolare Guido Luzi, che nel momento del bisogno mi ha offerto le parole e le idee giuste per continuare senza timore, ma più di tutto mi ha dato l'esempio, sempre.

Un pensiero lo voglio dedicare agli amici di Terranuova che tra i tanti viaggi che ho fatto, le mie mille partenze ed i miei tanti ritorni, hanno trovato spesso il tempo di scambiare due parole ed un abbraccio. Stesse parole sono per Massimo, Serena e per la mia mitica nipote Carlotta. . . .tutti mi hanno fatto sempre sentire importante.

E come non ringraziare Emanuele per le mille idee in regalo, e William, per il prezioso aiuto nella messa a punto della cartografia di Mdina e Gozo.

E poi Riccardo, Veronica, Giacomo, Luca, Deodato e Francesca, Lorenzo, Paolo, Sandro, Gabriele, Melania, Pasquale, Patrizia, Gianluca, Giovanni, Samuele, Goffredo, George, Ping, Filippo, Remo, Gabriele, Pietro, Stefano, Chiara, Luca, Massimiliano, Giorgio, Francesca, Silvia, Federico, Maurizio, Chiara. . . .ognuno mi ha offerto uno spunto, un consiglio o un utile ostacolo per dare vigore nuovo alle mie attività.

Vorrei ringraziare anche Renzo, Flavia, Elisa, Irene e la loro incredibile ospitalità.

Grazie anche ad Alexander che mi ha guidato tra le bellissime montagne del Kyrgyzstan. . . e grazie a tutti i compagni di quell'indimenticabile viaggio.

Grazie al Prof. Nicola Casagli, che ha creduto in me ed ha messo a disposizione parte del suo tempo e di questa struttura così efficiente che con il tempo è riuscito a costruire.

Ringrazio anche il personale del Dipartimento della Protezione Civile Nazionale con il quale ho avuto il piacere di condividere periodi di emergenza ed esperienze scientifiche uniche.

Un grazie anche a Mauro Reguzzoni, uomo di grandi capacità e volontà, sempre disponibile a fornire dati ed informazioni. . . ..in real-time!

Grazie anche a Davide ed a tutta la LisaLab-Ellegi....anche loro sempre in modalità real-time!

Grazie all'ingegnere Richard Sansom ed all'architetto Norbert Gatt per la loro disponibilità e per aver messo a disposizione i dati dei sistemi di monitoraggio di Mdina, acquisiti ed elaborati nell'ambito del progetto: "Service Contract for the provision of geotechnical engineering consultancy and project management services in relation with the consolidation of the terrain underlying the bastion walls and historic places of the city of Mdina", funded by the ERDF for Malta and carried out by a consortium led by Politecnica Ingegneria e Architettura for the MRRA, Works Division, Restoration Unit, Floriana, Malta.

Grazie infine a GDtest, a Massimo ed a Celalettin, per le competenze e la passione che hanno profuso tra le mura delle città fortificate maltesi.

Ognuna delle persone che ho incontrato in questi 4 anni, con le quali ho condiviso momenti di lavoro e di riposo, ognuno ha lasciato dentro questo lavoro di tesi un seme ed in me un ricordo, . . . nella speranza di aver fatto altrettanto vi ringrazio con affetto.

.

"If I have the gift of prophecy and can fathom all mysteries and all knowledge [. . .] but have not love, I am nothing. [. . .] Love never fails. But where there are prophecies, they will cease; where there are tongues, they will be stilled; where there is knowledge, it will pass away. [. . .]. And now these three remain: faith, hope and love. But the greatest of these is love."

Saint Paul (1Cor 13,1-13)